Dun 830.H-15

NAS 1.60:1468

JUL 18 1979

COMPLETED

NASA Technical Paper 1468

Effect of Several Geometric Parameters on the Static Internal Performance of Three Nonaxisymmetric Nozzle Concepts

ORIGINAL

Bobby L. Berrier and Richard J. Re

JULY 1979

NASA

137

NASA Technical Paper 1468

Effect of Several Geometric Parameters on the Static Internal Performance of Three Nonaxisymmetric Nozzle Concepts

Bobby L. Berrier and Richard J. Re
Langley Research Center
Hampton, Virginia

National Aeronautics
and Space Administration

**Scientific and Technical
Information Branch**

1979

SUMMARY

An investigation has been conducted at static conditions (wind off) in the static-test facility of the Langley 16-foot transonic tunnel. The effects of several geometric parameters on the internal performance of nonaxisymmetric convergent-divergent, single-ramp expansion, and wedge nozzles were investigated at nozzle pressure ratios up to approximately 10. In addition, two different thrust-vectoring schemes were investigated with the wedge nozzle.

The results of this investigation indicate that as with conventional round nozzles, peak nonaxisymmetric-nozzle internal performance occurs near the nozzle pressure ratio required for fully expanded exhaust flow. Nozzle sidewall length or area generally had little effect on the internal performance of the nozzles investigated. Cutting the sidewalls back from the exit plane on the nonaxisymmetric convergent-divergent nozzles helped to alleviate problems associated with unsymmetric internal flow separation on the divergent flap surfaces for overexpanded flow conditions.

INTRODUCTION

Since the advent of the turbojet engine, exhaust nozzles have traditionally been circular in cross section to facilitate integration with the engine. Extensive development of the "round" nozzle concept has resulted in structurally and thermally efficient exhaust systems with high internal performance. However, experimental investigations (refs. 1 to 3) on current, twin-engine fighter aircraft have shown that sizable airplane performance penalties are associated with the installation of the exhaust system into the airframe. Most of the external installation penalty, for multiengine aircraft, probably results from the integration of "round" nozzles into a "rectangular" afterbody. (See ref. 4.) These configurations inherently have boattailed "gutter" interfairings or base regions on the afterbody.

Recent studies on twin-engine fighter airplanes (refs. 5 to 13) have identified potential benefits for a new nozzle concept, the nonaxisymmetric or two-dimensional nozzle. This unique nozzle concept is geometrically amenable to improved capability in the areas of improved integration for installed drag reduction; thrust vectoring for maneuver enhancement and short-field take-off and landing; and thrust reversing for improved agility, ground handling, and reduced landing ground roll. Development of the nonaxisymmetric nozzle has concentrated primarily on three nozzle types, the convergent-divergent (refs. 7, 10 to 12, and 14), single-ramp expansion (refs. 8 and 13 to 18), and wedge (refs. 4, 7, 10 to 12, 14, and 19 to 24). Most of the experimental investigations conducted on these three nozzle types have concentrated on quantifying the uninstalled and installed performance of specific nozzle designs at various nozzle power settings during cruise, vectored thrust, and reverse-thrust operating modes. Currently, little effort has been expended on providing parametric data on nozzle internal design geometric variables which could

lead to improved nonaxisymmetric nozzle designs with higher performance and/or lower structural weight. One of the obvious geometry design parameters, which is unique to nonaxisymmetric nozzles and requires design consideration, is nozzle sidewall geometry. If nozzle sidewall area could be decreased without substantial loss in performance, nozzle structural weight and nozzle cooling requirements could probably be reduced. In addition, utilization of a simple wedge flap for providing a thrust-vectoring capability could reduce weight from vectoring schemes currently under consideration for wedge-type nozzles.

This paper presents the internal performance of three different nonaxisymmetric nozzle types, namely, convergent-divergent, single-ramp expansion, and wedge. The effects on internal performance of nozzle sidewall geometry are presented for all three types of nozzles. In addition, for the convergent-divergent type nozzle, the effects on internal performance of varying divergent flap length, divergence angle, and expansion ratio are presented. For the wedge-type nozzle, the effects on internal performance of varying external flap length (external expansion ratio) and vectoring scheme are presented. This investigation was conducted in the static-test facility of the Langley 16-foot transonic tunnel at a Mach number of 0 and at nozzle pressure ratios up to approximately 10.

SYMBOLS

All forces (with the exception of resultant gross thrust) and angles are referred to the model centerline (body axis). A detailed discussion of the data-reduction and calibration procedures as well as definitions of forces, angles, and propulsion relationships used herein can be found in reference 14.

AR nozzle-throat aspect ratio, $\frac{w_t}{h_t}$

A_e nozzle-exit area, cm^2

$A_{e,e}$ external exit area for fully expanded flow (exit area at end of external exhaust flow expansion), cm^2

$A_{e,i}$ internal exit area (exit area at end of internal exhaust flow expansion), cm^2

A_t nozzle-throat area, cm^2

F measured thrust along body axis, N

F_i ideal isentropic gross thrust, $w_p\sqrt{RT_{t,j}\frac{2\gamma}{\gamma-1}\left[1-\left(\frac{p_\infty}{p_{t,j}}\right)^{\frac{\gamma-1}{\gamma}}\right]}$, N

F_r resultant gross thrust, $\sqrt{F^2 + N^2}$, N

h_e nozzle-exit height, cm

h_t nozzle-throat height, cm

h_w wedge height, cm

N measured normal force, N

p local static pressure, Pa

$p_{t,j}$ jet total pressure, Pa

p_∞ ambient pressure, Pa

R gas constant (for $\gamma = 1.3997$), 287.3 J/kg-K

$T_{t,j}$ jet total temperature, K

w_i ideal mass-flow rate, kg/sec

w_p measured mass-flow rate, kg/sec

w_t nozzle-throat width, 10.157 cm

x axial distance measured from nozzle connect station, positive downstream, cm

x_e length from nozzle connect station to nozzle-exit station, cm

x_f length from nozzle connect station to hinge of wedge vector flap, cm

x_s length from nozzle connect station to end of nozzle sidewall, cm

x_t length from nozzle connect station to nozzle-throat station, cm

y lateral distance measured from model centerline, positive to left looking upstream, cm

z vertical distance measured from model centerline, positive up, cm

γ ratio of specific heats, 1.3997 for air

ρ divergence angle of nozzle divergent flap, deg

δ_{static} resultant thrust vector angle, $\tan^{-1} \frac{N}{F}$, deg

δ_v geometric vector angle measured from horizontal reference line, deg

Subscripts:

d	design point
e	external
i	internal
l	lower
max	maximum
u	upper

Configuration designations:

2-D C-D	two-dimensional convergent-divergent nozzles
C1. . .C13	convergent-divergent nozzles
SR1. . .SR5	single-ramp expansion nozzles
W1. . .W4	wedge nozzles
G	gimbaled
V	vectored
F	forward flap

APPARATUS AND METHODS

Static-Test Facility

This investigation was conducted in the static-test facility of the Langley 16-foot transonic tunnel. Testing is accomplished in a room with a high ceiling where the jet exhausts to atmosphere through a large open doorway. The control room is remotely located from the test area, and a closed-circuit television camera is used to observe the model. This facility utilizes the same clean, dry-air supply as that used in the 16-foot transonic tunnel and a similar air-control system - including valving, filters, and a heat exchanger (to operate the jet flow at constant stagnation temperature). Data are recorded on a 96-channel, magnetic-tape data-acquisition system.

Single-Engine Propulsion Simulation System

A sketch of the single-engine air-powered nacelle model on which various nozzles were mounted is presented in figure 1 with a typical nozzle configuration attached. The body shell forward of station 52.07 was removed for this investigation.

An external high-pressure air system provided a continuous flow of clean, dry air at a controlled temperature of about 300 K. This high-pressure air was varied up to approximately 10 atm (1 atm = 101.3 kPa) and was brought through the dolly-mounted support strut by six tubes which connect to a high-pressure plenum chamber. As shown in figure 1, the air was then discharged perpendicularly into the model low-pressure plenum through eight multiholed sonic nozzles equally spaced around the high-pressure plenum. This method was designed to minimize any forces imposed by the transfer of axial momentum as the air is passed from the nonmetric high-pressure plenum to the metric (mounted to the force balance) low-pressure plenum. Two flexible metal bellows are used as seals and serve to compensate for axial forces caused by pressurization.

The air was then passed from the model low-pressure plenum (circular in cross section) through a transition choke plate and instrumentation section which were common for all nonaxisymmetric nozzles investigated. The transition section provided a smooth flow path for the airflow from the round low-pressure plenum to the rectangular choke plate and instrumentation section. The instrumentation section had a flow path width-height ratio of 1.437 and was identical in geometry to the nozzle airflow entrance. All nozzle configurations were attached to the instrumentation section at model station 104.47.

Nozzle Design

Three different nonaxisymmetric nozzle concepts were investigated for the current study, namely, convergent-divergent, single-ramp expansion, and wedge. Sketches and photographs of the nozzle configurations are shown in figures 2, 3, and 4 for the convergent-divergent, single-ramp expansion, and wedge nozzle concepts, respectively. Parametric geometry changes were obtained by use of interchangeable upper and lower nozzle flaps and sidewalls. All nozzles had a constant exhaust flow path width of 10.157 cm.

For the convergent-divergent nozzle concept (see fig. 2), parametric geometry variations were made to determine the effects of expansion ratio, divergence angle, divergent flap length, and sidewall length on internal performance. With the exception of configurations C7 and C8 (see fig. 2(c)), the sidewall geometries investigated represent fixed sidewalls which would probably result in external fences for variable-geometry nozzles operating at low expansion ratios on an actual aircraft. Configuration C7 represents a fixed sidewall which would not result in external fences when installed on an aircraft but which would result in venting the sidewalls along the divergent flaps during engine operation at high expansion ratios. Configuration C8 represents a variable-geometry sidewall concept where the sidewall is split along the model centerline and each sidewall half is attached rigidly to the nozzle divergent flaps. Thus, as nozzle expansion ratio is increased from low to high values, the sidewall opens in a scissorlike manner to vent the centerline area of the sidewall.

For the single-ramp expansion nozzle concept (see fig. 3), only sidewall geometry effects were investigated. All sidewall geometries for this nozzle concept represent fixed geometry designs.

Parametric geometry variations for the wedge nozzle concept (see fig. 4) were made to determine the effects of external expansion ratio, sidewall length, and vectored thrust operation on internal performance. All wedge nozzle configurations utilized the same centerbody wedge. Two different vector schemes were investigated. Configuration W4(G20) (see fig. 4(c)) represents a vector scheme in which a gimbal mechanism is inserted into the engine tailpipe ahead of the nozzle. This vector scheme incorporates a subsonic flow-turning process to achieve the desired thrust vector angle. All other vectored configurations (see figs. 4(a) and 4(b)) represent a vector scheme in which a simple flap is deflected into the exhaust flow on the wedge lower surface. This vector scheme incorporates a forced deflection of the flow on the wedge lower surface only. The effects of vector angle and vector flap location were investigated.

Instrumentation

A three-component strain-gage balance was used to measure the forces and moments on the model downstream of station 52.07 cm. (See fig. 1.) Jet total pressure was measured at a fixed station in the instrumentation section (see fig. 1) by means of a four-probe rake through the upper surface, a three-probe rake through the side, and a three-probe rake through the corner. A thermocouple, also located in the instrumentation section, was used to measure jet total temperature. An electronic turbine flowmeter was used to measure the mass flow of the high-pressure air in the supply line.

With the exception of several pressure tubes taped to the upper and lower flaps during the first several data runs, the model contained no external pressure instrumentation. Internal static-pressure orifices were located on the nozzle divergent flaps and sidewalls and also on the wedge upper and lower surfaces. The locations of these orifices are given in the appendix.

Data Reduction

All data were recorded simultaneously on magnetic tape. Approximately 11 frames of data, taken at a rate of 2 frames per second, were used for each data point; average values were used in computations. Data were recorded in an ascending order of $p_{t,j}$ with several repeat points being recorded as $p_{t,j}$ was decreased from the maximum value obtained. With the exception of resultant gross thrust F_r, all force data in this report are referenced to the model centerline.

The basic performance parameter used for the presentation of results is the internal thrust ratio F/F_i, which is the ratio of the actual nozzle thrust (along the body axis) to the ideal nozzle thrust. Actual nozzle thrust was obtained from the balance axial-force measurement corrected for weight tares and balance interactions. Although the bellows arrangement was designed to eliminate pressure and momentum interactions with the balance, small bellows tares on axial, normal, and pitch balance components still exist. These tares result from a small pressure difference between the ends of the bellows when internal velocities are high and also small differences in the forward and aft bellows spring constants when the bellows are pressurized. As discussed in

reference 15, these bellows tares were determined by running calibration nozzles with known performance over a range of expected normal forces and pitching moments. The balance data were then corrected in a manner similar to that discussed in reference 14. During the first several data runs, external nozzle pressures were measured on the nozzle upper and lower flaps to determine whether a correction would be required for a "suck down" effect of the jet on external surfaces. Negligible effects of the jet on external pressures were found and no correction was applied to the data.

RESULTS AND DISCUSSION

Basic Data

Basic data for the nonaxisymmetric convergent-divergent, single-ramp expansion, and wedge nozzle concepts are presented in figures 5, 6, and 7, respectively. Nozzle internal thrust ratio F/F_i, resultant thrust ratio F_r/F_i, and discharge coefficient w_p/w_i are presented as a function of nozzle pressure ratio $p_{t,j}/p_\infty$ for each configuration investigated. These basic data are used for the comparisons shown in later sections of this paper. Resultant thrust ratios, shown by the dashed lines in figures 6 and 7, are essentially equal to internal thrust ratio F/F_i, except for those configurations which are unsymmetric above and below the model centerline (single-ramp expansion and vectored-wedge configurations). Significant differences between internal thrust ratio and resultant thrust ratio occur for the unsymmetric configurations, since the jet-exhaust flow is turned from the axial direction.

For the nonaxisymmetric convergent-divergent and single-ramp expansion nozzles operating at nozzle pressure ratios greater than about 2.0, the measured values of discharge coefficient w_p/w_i are less than 1.0 and are relatively independent of nozzle pressure ratio. Discharge coefficients less than 1.0 are caused by viscous effects which reduce the amount of flow passing through the throat because of momentum and vena contracta losses. The sonic flow area is, therefore, proportionately less than the geometric throat area A_t by the ratio of measured mass flow to ideal mass flow w_p/w_i. At nozzle pressure ratios less than about 2.0, values of discharge coefficient greater than 1.0 may be noted for all nozzles investigated. When a convergent-divergent nozzle is choked but at a nozzle pressure ratio less than about 1.9, the Mach number at the throat is 1.0 and the mass flow remains at its peak value. However, the denominator of discharge coefficient is the ideal mass flow of a convergent nozzle having the same throat area. Since a convergent nozzle may be unchoked at these conditions, its mass flow has decreased from the peak value. This decrease in the denominator results in an increase in discharge coefficient and its values may exceed 1.0. This condition does not reflect a physically impossible situation but is a direct result of the definition used for discharge coefficient. For the wedge nozzles, an increasing discharge coefficient with nozzle pressure ratio was measured with values greater than 1.0 being obtained at the highest nozzle pressure ratios. The variation of discharge coefficient with nozzle pressure ratio probably indicates a movement of the actual sonic throat location and area as nozzle pressure ratio varied.

Resultant Thrust Vector Angles

Measured resultant thrust vector angles δ_{static} are presented in figures 8 to 10 as a function of nozzle pressure ratio for the nonaxisymmetric convergent-divergent, single-ramp expansion, and wedge nozzle concepts, respectively.

Since nonaxisymmetric nozzles generally have large flat divergent walls in the nozzle pitch plane, the possibility exists that unsymmetrical internal flow separation will cause unwanted thrust vector angles at certain conditions. Unlike conventional round nozzles, which tend to average out unsymmetric internal flow separation about the pitch and yaw axis, nonaxisymmetric nozzles would tend to act as fluidic valves and produce forces in the pitch plane, since that is the plane in which the flow is being expanded. In addition, the direction of force would be dependent upon which divergent flap (upper or lower) the flow separation occurred on. This phenomenon can be readily observed by examination of the measured resultant thrust vector angles for nonaxisymmetric convergent-divergent (2-D C-D) nozzles shown in figure 8. At nozzle pressure ratios greater than 3.0, small resultant thrust vector angles (less than 1^{o}) were measured and were nearly independent of nozzle pressure ratio. The small negative angles measured probably result from model misalignment during assembly and/or construction. Resultant thrust vector angles of this magnitude would have negligible effects (less than 0.02 percent) on internal performance. However, at typical take-off and landing conditions (low speed, $p_{t,j}/p_{\infty} < 3.0$), where aircraft control is critical and the current data are most applicable, large variations of resultant thrust vector angle (from -8^{o} to 9^{o}) were measured. In addition, the magnitude of the resultant thrust vector angle and its variation with nozzle pressure ratio were unpredictable (i.e., not repeatable). Unpredictable resultant thrust vector angles of this magnitude could cause severe aircraft control problems during take-off and landing. The magnitude of the resultant thrust vector angles, for $p_{t,j}/p_{\infty} < 3.0$, tended to increase with increasing nozzle divergent flap length and/or increasing nozzle flap divergence angle. (See fig. 8(a).) Fortunately, high divergence angles and long divergent flaps are generally associated with high-expansion-ratio nozzles (exemplified by configurations C4, C9, C10, and C12) which are designed to operate at transonic and supersonic speeds at nozzle pressure ratios greater than 3.0. At take-off and landing conditions (low $p_{t,j}/p_{\infty}$), modern variable-geometry nozzles are closed down to operate at low expansion ratios and therefore have low nozzle flap divergence angles and/or short divergent flap lengths (exemplified by configurations C1 and C11). Thus, at take-off and landing conditions, the severity of the problem is not as great as it was initially thought to be. In addition, a potential solution to the internal flow separation problem is suggested by the results shown in figure 8(b). These results indicate that venting the nozzle sidewalls, either by wall truncation or by providing longitudinal slots, significantly reduces the magnitude of the measured resultant thrust vector angles for $p_{t,j}/p_{\infty} < 3.0$. Of course, the effect of venting the nozzle sidewalls on nozzle internal performance, if any, must also be considered.

Measured resultant thrust vector angles for the single-ramp expansion nozzles are presented in figure 9 and, as expected, exhibit large nonlinear variations with nozzle pressure ratio. A resultant thrust vector angle of zero

would be expected only at nozzle pressure ratios near design (fully expanded flow). Similar results are reported in reference 25 for a similar nozzle design. These trends are caused by changing wave patterns impinging upon the expansion ramp as the nozzle pressure ratio varies. At nozzle pressure ratios greater or less than approximately 7.0, an axial-force performance penalty would be associated with the nonzero values of measured resultant thrust vector angles, since the thrust is turned away from the axial direction. The magnitude of this penalty can be assessed by comparing internal thrust ratio with the resultant thrust ratio shown in figure 6 for the single-ramp expansion nozzles. At a nozzle pressure ratio of 4.15, for example, resultant thrust vector angles ranging from -5.5° to -8.7° (see fig. 9) cause from 0.5 to 1.2 percent loss of axial thrust. These data suggest a need for integration of a variable nozzle expansion ramp with an onboard flight computer to eliminate unwanted resultant thrust vector angles. Of course, airplane trim drag and nozzle external drag would also have to be considered in the computer logic.

The effect of nozzle sidewall containment is also addressed by figure 9, and as with the 2-D C-D nozzles, reducing the amount of sidewall containment on single-ramp expansion nozzles tends to reduce the variation of resultant thrust vector angle with nozzle pressure ratio.

Figure 10 presents measured resultant thrust vector angles for the wedge nozzle configurations. In general, nozzle external expansion ratio $(A_e/A_t)_e$ and nozzle sidewall length had no effect on the resultant thrust vector angles. An unrepeatable variation of $\pm 2^{\circ}$ was found near $p_{t,j}/p_{\infty} = 8.5$ for both $(A_e/A_t)_e = 2.982$ (long external flap) configurations; this variation may result from asymmetric shock-induced separation on the wedge.

Jet-exhaust flow-turning capability of a simple hinged flap on the wedge lower surface is shown in figures 10(b) to 10(e). Large variations in resultant thrust vector angle occur with increasing nozzle pressure ratio for all these configurations. These variations probably result from the changing wave patterns in the supersonic exhaust stream as jet total pressure is varied. The results indicate that a simple hinged flap is an effective flow-turning device for small vector angles (approximately 5°) but rapidly loses its effectiveness as flap angle is increased. For example, with the vector flap angle of 5° ($\delta_v = 5^{\circ}$), the values of measured resultant thrust vector angle were generally greater than 5°; however, with $\delta_v = 20^{\circ}$, the measured δ_{static} values were always less than 20°.

The turning capability of a gimbal vectoring scheme is compared with the simple flap vectoring scheme at $\delta_v = 20^{\circ}$ in figure 10(f). As expected, since flow turning is accomplished in subsonic flow ahead of the nozzle throat, the gimbal vectoring scheme is a very effective flow-turning device; measured resultant thrust vector angle δ_{static} generally varied less than 1° about the geometric design vector angle of 20°. In addition, the gimbal scheme has much greater flow-turning capability than a simple flap scheme at high vector angles. It should be noted, however, that the gimbal vectoring scheme may have a large detrimental effect on aircraft aerodynamics during wind-on operation. Results presented in reference 25 on a similar gimbal vectoring scheme installed with a conventional round nozzle show large increases in external drag during wind-on vectored operation.

Internal Static-Pressure Distributions

Internal static-pressure data are presented in tabulated form in the appendix. Typical internal static-pressure distributions for each nonaxisymmetric nozzle type investigated are presented in figures 11 to 14. In general, the measured internal static-pressure distributions are similar to those measured in conventional round nozzles (ref. 26). For $p_{t,j}/p_\infty < 5.0$, for example, the static-pressure distributions on the divergent flap of the 2-D C-D nozzle (see fig. 11) show a typical sudden pressure rise across the exhaust-flow normal shock; this is generally followed by a plateau pressure indicating shock-induced flow separation from the wall.

Figures 12 and 13 show that the effect of venting the nozzle sidewalls is confined to a region close to the sidewall. Thus, one might expect little effect of venting the sidewalls on the nozzle internal performance at static conditions. As expected, since flow turning occurs upstream of the nozzle throat, the effect of gimbaled vectoring on the wedge internal static-pressure distributions (see fig. 14) is negligible. This fact leads one to expect little effect of gimbal thrust vectoring on wedge nozzle internal performance.

Internal Performance Comparisons

Nonaxisymmetric convergent-divergent nozzles.- The effect of several nozzle geometric design parameters on internal performance of 2-D C-D nozzles is presented in figures 15 to 17. The effects of nozzle expansion ratio A_e/A_t, divergence angle ρ, and divergent flap length on internal performance are shown in figure 15. Comparison of parts (a) and (b) with part (c) of figure 15 shows that the major impact on performance is caused by nozzle expansion ratio. For $p_{t,j}/p_\infty > 4.0$, divergence angle and divergent flap length had little effect (less than 1 percent) on internal performance. (See fig. 15(c).) At lower nozzle pressure ratios, divergence angle and flap length affect the internal flow separation characteristics and larger effects on internal performance are observed. The effect of expansion ratio on 2-D C-D nozzle internal performance is similar to that which would be obtained on conventional round nozzles. Peak performance is obtained near the nozzle pressure ratio required for fully expanded exhaust flow. Values of the nozzle pressure ratio required for fully expanded flow $(p_{t,j}/p_\infty)_d$ are listed in table I for all expansion ratios investigated for each type nonaxisymmetric nozzle. The three configurations shown in figure 15(a) are representative of a single, variable-geometry (hinged flap) nozzle operating at a fixed engine power setting (constant A_t). The variable expansion ratio range (1.089 to 1.797) has a corresponding $(p_{t,j}/p_\infty)_d$ range from 2.97 to 8.79, which, for a typical turbofan engine, corresponds to an operating flight Mach number range from 0.3 to 1.6. (See ref. 21.) Since expansion ratio would be continuously variable, nozzle internal performance can be estimated for this Mach range by fairing a line through the peak performance points for each nozzle expansion ratio investigated. For the postulated nozzle under consideration (see fig. 15(a)), this procedure results in excellent nozzle internal performance (F/F_i = 0.987 to 0.996) throughout a Mach number range from 0.3 to 1.6. These results are almost identical to those one would expect to obtain with conventional round nozzles with the same range of variable expansion ratio.

TABLE I.- NOZZLE PRESSURE RATIOS FOR FULLY EXPANDED FLOW

(a) Nonaxisymmetric convergent-divergent nozzles

A_e/A_t	$(p_{t,j}/p_\infty)_d$
1.089	2.97
1.248	4.25
1.397	5.41
1.797	8.79

(b) Nonaxisymmetric single-ramp expansion nozzles

A_e/A_t	$(p_{t,j}/p_\infty)_d$
1.236	4.19
1.529	5.99

(c) Nonaxisymmetric wedge nozzles

A_e/A_t	$(p_{t,j}/p_\infty)_d$
1.220	4.01
2.980	20.90
3.810	31.12

Figure 16 presents the effect of sidewall length on 2-D C-D nozzle internal performance. In general, cutting the nozzle sidewalls back from the exit plane (thus reducing the weight and cooling area) had little effect on nozzle internal performance. It should be noted that these results were obtained at wind-off conditions and that external flow interactions could affect internal performance at forward speeds. Cutting the sidewall back approximately 40 to 50 percent resulted in internal performance variations which were generally within the balance accuracy (1/2 percent of F_i). Cutting the sidewall back approximately 75 percent resulted in only a 1-percent internal performance loss at high nozzle pressure ratios. (See fig. 16(b).)

Sidewall slots or vents had little or no effect on 2-D C-D nozzle internal performance, as shown by figure 17.

Single-ramp expansion nozzles.- The effect of sidewall geometry (sidewall area) on the internal performance of a single-ramp expansion nozzle is presented in figure 18. For these nozzles, the exhaust flow expansion process occurs both internally and externally. Internal expansion occurs from the throat up to the lower flap exit. External expansion occurs downstream of the lower flap exit and between fixed (expansion ramp) and free (free stream/exhaust) upper and lower boundaries, respectively. Thus, internal performance is influenced by internal and external expansion ratios and is generally characterized by two performance peaks. The first peak occurs near the design pressure ratio corresponding to $(A_e/A_t)_i$ and is generally lower than the second peak, which occurs near the design pressure ratio corresponding to $(A_e/A_t)_e$.

Reducing nozzle sidewall area on this type of nonaxisymmetric nozzle generally had a negligible effect on internal performance. A tendency to increase performance at the first performance peak (configurations SR3 and SR5) and decrease performance at high jet total-pressure ratios (configuration SR3) may be noted. It should also be noted that nozzles with free-expansion boundaries will be sensitive to external flow effects at forward speeds.

Wedge nozzles.- The effects of sidewall length and external expansion ratio on wedge nozzle internal performance are presented in figure 19. The wedge nozzles of this investigation have free-expansion boundaries downstream of the flap exits similar to the single-ramp expansion nozzles discussed previously. However, the design nozzle pressure ratios $(p_{t,j}/p_\infty)_d$, corresponding to both external expansion ratios $(A_e/A_t)_e$ investigated, occur well beyond the capability of the test facility used for the current investigation. Therefore, the second performance peak, for the wedge nozzles investigated, is not defined by the data shown in figure 19.

The wedge nozzle performance levels shown in figure 19 are 3 to 4 percent below that measured for the 2-D C-D and single-ramp expansion nozzles. However, peak performance was probably not reached because of the limited nozzle pressure range. In addition, it is expected that external flow interactions will have beneficial effects on internal performance. (See ref. 14.) The effect of wedge nozzle sidewall length on internal performance was generally negligible (less than 1/2 percent of F_i). For $p_{t,j}/p_\infty > 5.0$, the low-external-expansion-ratio wedge nozzles (W3 and W4) had significantly higher performance than the high-external-expansion-ratio nozzles (W1 and W2) over the nozzle pressure ratio range of the tests. One explanation for this result is that the second performance peak for the low $(A_e/A_t)_e$ nozzles will probably occur at a lower nozzle pressure ratio than that for the high $(A_e/A_t)_e$ nozzles.

Figure 20 presents the effect of vector flap angle on internal performance of wedge nozzles. Flow-turning capabilities of the vector flap were discussed in a previous section. As shown by figure 20, large internal performance losses are associated with vectored operation, the losses generally increasing with increasing vector flap angle. For a vector flap angle of 20°, losses up to 6.5 percent of F_i were measured. However, it should be noted that most of the internal performance penalty shown in figure 20 results from turning the resultant force vector away from the body axis (thrust being defined as an axial force) and not from reductions in gross thrust magnitude (nozzle

operating efficiency). Comparison of the resultant gross thrust ratios during vectored operation with the unvectored internal thrust ratio (fig. 7) for each wedge nozzle configuration indicates that the maximum gross thrust loss measured was 4 percent. (Compare parts (a) and (d) of fig. 7 at $p_{t,j}/p_\infty = 4.0$.) For configurations W3 and W4, gross thrust losses due to vectoring were generally less than 2 percent of F_i, which is the criterion of reference 7 for being acceptable performance.

Figure 21 presents the effect of external-expansion ratio on internal performance of vectored thrust wedge nozzles utilizing a vector flap. At $p_{t,j}/p_\infty > 3.0$, larger internal performance losses are incurred with the high-external-expansion-ratio configuration than with the low-external-expansion-ratio configuration, probably because the low-external-expansion-ratio configuration operates closer to its design nozzle pressure ratio. Examination of figure 7 shows that the high-expansion-ratio nozzle (W1) has higher resultant gross thrust losses during vectored operation than the low-expansion-ratio nozzle (W3), as indicated previously.

The effect of sidewall length on the internal performance of vectored flap wedge nozzles is shown in figure 22. In general, sidewall length had little effect on either the unvectored or vectored nozzle internal performance. Figure 23 presents the effect of vector flap location on the internal performance of vectored flap wedge nozzles. At values of $p_{t,j}/p_\infty < 7.0$, which are representative of typical turbofan engines at subsonic Mach numbers, a forward vector flap location improved internal performance during vectored thrust operation. It should be noted however that because the wedge surface was curved, geometric vector angle δ_v decreased as the vector flap moved forward. Thus, it was expected that the forward vector flap location ($\delta_v = 3.5^\circ$) would produce lower performance losses (gross thrust vector closer to body axis) than the aft vector flap location ($\delta_v = 5^\circ$).

A comparison of vectored wedge nozzle performance using two different vectoring schemes for $\delta_v = 20^\circ$ is presented in figure 24. As shown, both vector schemes produce large losses (4 to 7 percent) in internal thrust ratio during vectored ($\delta_v = 20^\circ$) operation. The vector flap scheme appears to be highly competitive with the gimbal vector scheme for $p_{t,j}/p_\infty < 6.0$. However, care should be exercised when using these data since the measured resultant thrust vector angles for these two schemes (fig. 10(f)) were significantly different for the same geometric vector angle. A better measure of vectoring scheme merit for this case would be resultant gross thrust. (See figs. 7(n) and 7(o).) For convenience, performance parameters for the vector flap, gimbal, and unvectored nozzles are given in table II for several nozzle pressure ratios. The $[1 - \cos(\delta_{static})]$ term indicates the loss in internal thrust ratio F/F_i which results from turning the gross thrust vector away from the axial direction an amount equal to the measured resultant thrust vector angle δ_{static}. For $\delta_v = 20^\circ$, the measured resultant thrust vector angle for the vector flap configuration was approximately 14° as compared with approximately 20° for the gimbal configuration. As discussed previously, the gimbal vector scheme is a much more efficient flow-turning device than the vector flap scheme for vector angles greater than 5°. However, because of the larger resultant thrust vector angles, the loss in internal thrust ratio F/F_i resulting from turning the gross thrust vector away from the axial direction is

TABLE II.- PERFORMANCE COMPARISONS OF VECTORED AND UNVECTORED WEDGE NOZZLES

	Configuration W4			Configuration W4(V20)			Configuration W4(G20)		
Vector scheme	None			Flap			Gimbal		
$p_{t,j}/p_\infty$	2.0	4.0	6.0	2.0	4.0	6.0	2.0	4.0	6.0
δ_{static}, deg	-0.6	-0.8	-0.8	14.5	13.9	15.3	20.4	20.2	20.4
$1 - \cos(\delta_{static})$ . . .	0	0	0	0.032	0.029	0.036	0.063	0.062	0.063
F/F_i	0.909	0.959	0.968	0.843	0.923	0.913	0.848	0.901	0.915
F_r/F_i	0.909	0.959	0.968	0.874	0.951	0.952	0.905	0.961	0.973

approximately double for the gimbal configuration as compared with that of the vector flap configuration (6 percent as compared with 3 percent). Comparing the resultant gross thrust ratios F_r/F_i for the gimbal vectoring configuration with the unvectored baseline configuration indicates that the total internal thrust ratio loss for the gimbal vectoring scheme results from the gross thrust vector direction as opposed to a loss in gross thrust (or nozzle efficiency). These data indicate that the gimbal scheme is a very efficient vectoring scheme in terms of flow-turning capability and nozzle efficiency. It should be noted, however, that these data are for static (wind-off) conditions and the gimbal vectoring scheme may have a large detrimental effect on aircraft aerodynamics during wind-on operation. (See ref. 25.) Comparison of the resultant gross thrust ratios F_r/F_i for the vector flap configuration with the unvectored baseline configuration indicates a loss of gross thrust (nozzle efficiency) of about 1 to 3.5 percent for the vector flap scheme at $\delta_v = 20^\circ$. Based on the performance criterion of reference 7 for flow-turning losses and the inefficient flow-turning capability for $\delta_v > 5^\circ$, the simple flap vectoring scheme appears to be a viable design option only for applications with small ($\delta_v < 10^\circ$) vectoring requirements.

CONCLUSIONS

An investigation has been conducted at static conditions (Mach number equal to zero) in the static-test facility of the Langley 16-foot transonic tunnel. The effect of several geometric parameters on the internal performance of three nonaxisymmetric nozzle concepts was investigated. The three nonaxisymmetric nozzle concepts investigated were convergent-divergent, single-ramp expansion, and wedge nozzles. Two different thrust-vectoring schemes were investigated with the wedge nozzle. The nozzle pressure ratio was varied up to approximately 10. Results from this study indicate the following conclusions for each nonaxisymmetric nozzle type.

Nonaxisymmetric Convergent-Divergent Nozzles

1. Nozzle expansion ratio is the predominant design parameter affecting nonaxisymmetric convergent-divergent (2-D C-D) nozzle internal performance. As with conventional round nozzles, peak internal performance occurs near the nozzle pressure ratio required for fully expanded exhaust flow. Peak internal performance was almost identical to that expected for conventional round nozzles.

2. Divergent flap length and flap divergence angle had only minor effects on 2-D C-D nozzle internal performance.

3. Cutting the 2-D C-D nozzle sidewall back to approximately 50 percent of the divergent flap length or venting (slotting) the full length sidewall had little effect on nozzle performance. Cutting the sidewall back approximately 75 percent resulted in only a 1-percent reduction in internal performance.

4. At nozzle pressure ratios typical of take-off and landing speeds, several of the 2-D C-D nozzle configurations (generally those with the higher expansion ratios) exhibited large unpredictable variations in measured resultant thrust vector angle. These variations, which could cause severe control problems at low speeds, were caused by unsymmetrical internal flow separation from the divergent flaps and tended to become larger in magnitude with increasing divergence angle and flap length. This problem was not as severe for nozzles having lower expansion ratios typical of landing and take-off conditions. In addition, cutting the nozzle sidewall back or venting the sidewall significantly reduced the magnitude of the resultant thrust vector angle variation.

Single-Ramp Expansion Nozzles

1. Reducing sidewall area (containment) on the single-ramp expansion nozzles generally had a negligible effect on nozzle internal performance.

2. Although the single-ramp expansion nozzles were designed for no thrust vectoring, they exhibited large nonlinear variations of resultant thrust vector angle with increasing nozzle pressure ratio because of the changing exhaust-flow wave patterns. These variations were reduced somewhat by reducing the amount of sidewall containment area, but a variable expansion ramp would be required to completely cancel resultant thrust vector angles at all conditions.

Wedge Nozzles

1. A gimbal vector scheme proved to be a very efficient thrust-vectoring device at static (wind-off) conditions for the wedge nozzles. This vectoring scheme generally provided measured resultant thrust vector angles equal to the design geometric vector angle over the entire nozzle pressure ratio range tested with no loss in nozzle resultant gross thrust ratio. However, this vector scheme may have a large detrimental effect on aircraft aerodynamics during wind-on operation.

2. The vector flap scheme produced nozzle performance (resultant gross thrust ratio) losses of up to 3.5 percent during vectored operation. In addition, flow-turning capabilities decreased significantly with increasing geometric vector flap angle. These deficiencies will probably limit application of the vector flap scheme to applications with small vectoring requirements.

Langley Research Center
National Aeronautics and Space Administration
Hampton, VA 23665
May 11, 1979

APPENDIX

INTERNAL STATIC-PRESSURE DATA

Internal static-pressure distributions were measured on the nozzle flaps and sidewalls for most of the configurations investigated. Wedge static pressures were also measured on most of the wedge nozzles. Internal static-pressure orifice locations are shown in figures 25, 26, and 27 for the nonaxisymmetric convergent-divergent, single-ramp expansion, and wedge nozzles, respectively. Internal static-pressure data are presented in tables III, IV, and V for the nonaxisymmetric convergent-divergent, single-ramp expansion, and wedge nozzles, respectively. Data are presented as ratios of local static pressure to the jet total pressure $p/p_{t,j}$ at each orifice location over a range of nozzle pressure ratio $p_{t,j}/p_{\infty}$.

APPENDIX

TABLE III.- COMPUTER PRINTOUT OF RATIO OF INTERNAL STATIC PRESSURE TO JET TOTAL PRESSURE FOR NONAXISYMMETRIC CONVERGENT-DIVERGENT NOZZLES

(a) Configuration C1

		Flap static pressure, $p/p_{t,j}$									
		Row 1					Row 2				
		x/x_t					x/x_t				
Point	$p_{t,j}/p_\infty$	0.791	1.011	1.286	1.560	1.890	0.791	1.011	1.286	1.560	1.890
1	1.001	.996	.995	1.000	1.000	.999	1.001	.999	.998	.999	1.000
2	1.528	.798	.413	.404	.397	.434	.801	.417	.417	.395	.636
3	1.753	.795	.412	.404	.399	.404	.800	.418	.415	.393	.508
4	2.004	.795	.413	.404	.398	.364	.801	.418	.415	.392	.359
5	2.257	.794	.414	.404	.397	.365	.801	.419	.418	.393	.358
6	2.518	.794	.415	.404	.397	.365	.800	.419	.419	.392	.358
7	2.987	.794	.415	.403	.396	.365	.796	.417	.418	.391	.357
8	3.528	.794	.415	.403	.395	.365	.797	.417	.418	.390	.357
9	4.114	.794	.415	.402	.395	.365	.797	.416	.417	.389	.356
10	5.144	.793	.414	.402	.395	.365	.798	.415	.415	.387	.354
11	6.243	.794	.413	.402	.395	.365	.798	.415	.414	.386	.353
12	9.756	.794	.412	.402	.396	.366	.798	.415	.413	.385	.352
13	8.229	.794	.413	.402	.395	.365	.798	.415	.414	.386	.353
14	6.134	.794	.414	.402	.395	.365	.797	.415	.415	.386	.354
15	4.685	.795	.415	.402	.395	.365	.796	.417	.416	.388	.355
16	2.972	.795	.416	.403	.397	.366	.794	.418	.417	.390	.357
17	2.002	.797	.415	.403	.398	.366	.797	.417	.415	.392	.357
18	1.001	1.002	1.001	.998	.999	.999	.993	.998	.996	.999	.998

		Sidewall static pressure, $p/p_{t,j}$									
		Row 3					Row 4			Row 5	
		x/x_t					x/x_t			x/x_t	
Point	$p_{t,j}/p_\infty$	0.791	1.011	1.286	1.560	1.890	1.286	1.560	1.890	1.560	1.890
1	1.001	1.001	1.003	.998	.999	.998	1.013	.998	.997	.996	.995
2	1.528	.800	.585	.435	.401	.630	.450	.420	.632	.431	.625
3	1.753	.797	.584	.437	.399	.512	.445	.386	.500	.419	.515
4	2.004	.796	.583	.437	.400	.358	.443	.385	.409	.401	.448
5	2.257	.796	.581	.436	.399	.357	.442	.384	.363	.390	.406
6	2.518	.797	.581	.435	.398	.357	.440	.383	.359	.385	.383
7	2.987	.796	.579	.434	.397	.356	.436	.382	.357	.379	.351
8	3.528	.796	.578	.433	.397	.355	.428	.381	.356	.375	.327
9	4.114	.796	.578	.432	.396	.354	.426	.380	.355	.373	.303
10	5.144	.794	.577	.431	.394	.353	.424	.378	.352	.371	.270
11	6.243	.794	.577	.431	.393	.351	.423	.377	.351	.371	.265
12	9.756	.794	.578	.431	.392	.350	.422	.377	.350	.371	.268
13	8.229	.795	.577	.431	.393	.351	.422	.377	.351	.371	.269
14	6.134	.794	.576	.432	.394	.352	.423	.378	.352	.372	.276
15	4.685	.797	.575	.433	.396	.353	.425	.380	.354	.375	.303
16	2.972	.798	.576	.435	.397	.355	.427	.382	.357	.380	.351
17	2.002	.798	.578	.439	.399	.356	.426	.385	.410	.403	.448
18	1.001	1.000	.993	.999	.998	.998	.994	.996	.999	1.001	1.000

TABLE III.- Continued

(b) Configuration C2

Flap static pressure, $p/p_{t,j}$

Point	$p_{t,j}/p_\infty$	Row 1 x/x_t = 0.791	1.011	1.286	1.560	1.890	Row 2 x/x_t = 0.791	1.011	1.286	1.560	1.890
1	1.001	.998	.998	1.000	1.000	.999	1.000	1.001	1.000	1.004	.998
2	1.445	.800	.417	.490	.643	.684	.803	.419	.528	.647	.673
3	1.735	.799	.414	.465	.400	.587	.802	.419	.421	.462	.581
4	2.008	.798	.415	.405	.400	.369	.805	.420	.423	.395	.496
5	2.221	.797	.416	.405	.399	.368	.804	.421	.424	.396	.450
6	2.488	.797	.417	.405	.399	.366	.804	.421	.424	.393	.399
7	2.957	.797	.417	.404	.398	.366	.795	.419	.422	.392	.337
8	3.472	.797	.417	.404	.397	.366	.797	.419	.422	.391	.288
9	3.986	.798	.416	.403	.397	.366	.798	.418	.421	.390	.250
10	5.469	.797	.415	.403	.397	.366	.800	.418	.420	.388	.194
11	8.008	.798	.415	.403	.398	.366	.801	.417	.418	.387	.192
12	9.588	.798	.414	.403	.398	.366	.800	.417	.417	.387	.191
13	8.036	.799	.415	.403	.398	.366	.801	.417	.418	.387	.192
14	5.969	.799	.416	.404	.398	.367	.801	.418	.419	.389	.194
15	3.473	.799	.417	.403	.397	.367	.797	.419	.420	.390	.250
16	2.954	.799	.417	.404	.399	.367	.795	.419	.421	.391	.339
17	1.988	.799	.416	.404	.400	.369	.805	.420	.420	.394	.502
18	.999	1.000	1.003	1.000	1.000	1.001	1.000	1.001	1.000	1.001	1.002

Sidewall static pressure, $p/p_{t,j}$

Point	$p_{t,j}/p_\infty$	Row 3 x/x_t = 0.791	1.011	1.286	1.560	Row 4 x/x_t = 1.286	1.560	Row 5 x/x_t = 1.560
1	1.001	1.002	1.004	.999	1.000	1.000	1.000	1.001
2	1.445	.804	.586	.534	.644	.536	.649	.663
3	1.735	.802	.584	.445	.503	.436	.524	.537
4	2.008	.801	.584	.445	.400	.436	.433	.480
5	2.221	.800	.583	.445	.399	.439	.401	.438
6	2.488	.799	.582	.444	.398	.439	.394	.461
7	2.957	.800	.581	.443	.396	.438	.388	.342
8	3.472	.799	.581	.441	.396	.437	.387	.293
9	3.986	.799	.580	.441	.395	.437	.385	.258
10	5.469	.795	.580	.441	.395	.435	.383	.209
11	8.008	.796	.580	.441	.394	.433	.382	.208
12	9.588	.797	.580	.441	.393	.432	.382	.223
13	8.036	.797	.580	.441	.394	.434	.382	.223
14	5.969	.798	.579	.442	.395	.435	.383	.224
15	3.473	.802	.578	.442	.396	.437	.384	.269
16	2.954	.803	.579	.444	.396	.437	.388	.345
17	1.988	.804	.581	.446	.400	.436	.439	.481
18	.999	.998	.998	1.000	1.001	1.000	1.000	1.001

TABLE III.- Continued

(c) Configuration C3

		Flap static pressures, $p/p_{t,j}$									
		Row 1					Row 2				
				x/x_t					x/x_t		
Point	$p_{t,j}/p_\infty$	0.791	1.011	1.286	1.560	1.890	0.791	1.011	1.286	1.560	1.890
1	1.000	.997	.999	1.001	.999	1.000	1.000	.999	1.001	.999	1.000
2	1.484	.808	.525	.649	.665	.679	.813	.548	.648	.675	.677
3	1.736	.801	.414	.408	.597	.582	.805	.418	.556	.582	.583
4	1.978	.799	.415	.408	.400	.544	.804	.419	.484	.503	.514
5	2.227	.798	.416	.408	.399	.472	.806	.420	.422	.446	.447
6	2.486	.799	.417	.405	.400	.348	.806	.421	.415	.397	.399
7	2.939	.798	.417	.404	.399	.347	.794	.419	.411	.338	.338
8	3.478	.797	.417	.404	.397	.347	.796	.418	.411	.287	.287
9	3.953	.797	.416	.403	.397	.347	.798	.418	.411	.251	.254
10	5.946	.797	.415	.403	.397	.348	.800	.417	.410	.189	.195
11	8.014	.800	.415	.404	.399	.348	.802	.419	.410	.188	.129
12	9.842	.802	.416	.404	.400	.349	.803	.419	.410	.188	.128
13	8.029	.799	.415	.403	.399	.349	.801	.419	.409	.188	.129
14	6.000	.799	.416	.403	.398	.349	.800	.418	.410	.189	.195
15	3.959	.799	.417	.402	.398	.348	.797	.419	.410	.252	.254
16	2.924	.799	.417	.403	.400	.348	.794	.419	.410	.341	.341
17	1.984	.799	.416	.404	.401	.348	.804	.420	.410	.403	.513
18	1.000	.999	1.002	.999	1.001	1.000	.996	1.001	.999	1.000	1.001

		Sidewall static pressures, $p/p_{t,j}$			
		Row 3			Row 4
			x/x_t		x/x_t
Point	$p_{t,j}/p_\infty$	0.791	1.011	1.220	1.220
1	1.000	.997	1.002	1.001	1.000
2	1.484	.813	.643	.494	.498
3	1.736	.801	.586	.479	.518
4	1.978	.800	.585	.426	.461
5	2.227	.798	.584	.422	.451
6	2.486	.798	.583	.421	.447
7	2.939	.798	.581	.420	.446
8	3.478	.799	.581	.417	.446
9	3.953	.799	.581	.417	.446
10	5.946	.794	.580	.416	.445
11	8.014	.797	.581	.418	.445
12	9.842	.799	.582	.416	.445
13	8.029	.798	.581	.416	.446
14	6.000	.798	.580	.418	.447
15	3.959	.803	.579	.419	.447
16	2.924	.803	.580	.421	.448
17	1.984	.805	.583	.426	.461
18	1.000	1.001	.998	1.000	1.000

APPENDIX

TABLE III.- Continued

(d) Configuration C4

		Flap static pressures, $p/p_{t,j}$									
		Row 1					Row 2				
		x/x_t					x/x_t				
Point	$p_{t,j}/p_\infty$	0.791	1.011	1.286	1.560	1.890	0.791	1.011	1.286	1.560	1.890
1	1.662	.996	.997	.998	.998	.998	.996	.996	.996	.995	.999
2	1.484	.719	.391	.511	.616	.671	.795	.383	.573	.652	.669
3	1.738	.787	.381	.272	.454	.568	.792	.383	.290	.354	.569
4	1.997	.787	.380	.273	.429	.457	.795	.384	.288	.462	.495
5	2.498	.787	.381	.276	.375	.366	.796	.385	.285	.364	.378
6	3.003	.786	.380	.276	.190	.321	.793	.384	.286	.192	.307
7	3.507	.786	.379	.278	.190	.272	.792	.383	.286	.193	.263
8	4.018	.786	.379	.277	.191	.226	.793	.383	.285	.193	.217
9	5.010	.786	.378	.276	.191	.115	.794	.382	.284	.193	.117
10	6.153	.786	.378	.275	.190	.115	.793	.382	.284	.192	.117
11	8.276	.788	.377	.275	.189	.115	.794	.383	.284	.192	.118
12	9.150	.788	.377	.275	.189	.116	.795	.383	.284	.192	.118
13	9.552	.788	.377	.275	.189	.115	.794	.384	.284	.192	.118
14	9.153	.788	.377	.275	.190	.116	.794	.384	.284	.192	.118
15	8.234	.788	.378	.275	.190	.116	.794	.383	.284	.193	.118
16	6.168	.788	.378	.275	.190	.116	.794	.383	.285	.194	.118
17	4.004	.788	.380	.277	.191	.227	.793	.384	.286	.195	.218
18	2.987	.789	.381	.277	.191	.322	.793	.385	.288	.195	.309
19	1.993	.791	.382	.274	.435	.462	.795	.386	.288	.469	.484
20	1.000	1.001	1.003	1.000	1.000	1.000	1.003	.999	1.001	1.001	1.000

		Sidewall static pressures, $p/p_{t,j}$									
		Row 3					Row 4			Row 5	
		x/x_t					x/x_t			x/x_t	
Point	$p_{t,j}/p_\infty$	0.791	1.011	1.286	1.560	1.890	1.286	1.560	1.890	1.560	1.890
1	1.662	.994	1.001	.997	.997	.997	.997	.997	.997	.997	.998
2	1.484	.800	.603	.602	.629	.631	.620	.625	.626	.626	.627
3	1.738	.797	.590	.398	.532	.530	.521	.531	.527	.527	.527
4	1.997	.797	.588	.323	.458	.471	.370	.451	.469	.451	.472
5	2.498	.797	.586	.267	.303	.384	.272	.234	.400	.291	.389
6	3.003	.796	.584	.267	.173	.308	.272	.185	.302	.191	.305
7	3.507	.797	.583	.268	.174	.253	.272	.184	.256	.189	.255
8	4.018	.796	.583	.268	.174	.144	.272	.185	.146	.189	.201
9	5.010	.795	.582	.267	.173	.144	.271	.184	.134	.189	.123
10	6.153	.795	.582	.266	.173	.143	.270	.184	.134	.189	.123
11	8.276	.796	.583	.266	.172	.143	.269	.184	.134	.189	.122
12	9.150	.797	.584	.266	.172	.143	.267	.184	.133	.189	.122
13	9.552	.797	.584	.266	.172	.143	.268	.184	.133	.189	.122
14	9.153	.798	.584	.266	.172	.143	.268	.184	.133	.189	.122
15	8.234	.797	.583	.266	.172	.144	.268	.184	.134	.189	.172
16	6.168	.798	.582	.267	.174	.144	.269	.185	.134	.190	.123
17	4.004	.800	.581	.268	.175	.144	.272	.186	.146	.189	.198
18	2.987	.801	.582	.268	.175	.311	.273	.186	.304	.191	.308
19	1.993	.801	.586	.313	.458	.472	.369	.450	.471	.450	.474
20	1.000	1.000	.997	1.000	1.001	1.001	1.002	1.000	1.001	1.001	1.001

TABLE III.- Continued

(e) Configuration C5

		Flap static pressures, $p/p_{t,j}$									
		Row 1					Row 2				
		x/x_t					x/x_t				
Point	$p_{t,j}/p_\infty$	0.791	1.011	1.286	1.560	1.890	0.791	1.011	1.286	1.560	1.890
1	.999	.997	1.000	1.000	.99[illegible]	1.001	1.007	1.999	.997	.998	1.005
2	1.499	.7[illegible]9	.381	.515	.619	.669	.794	.383	.55[illegible]	.659	.678
3	1.754	.788	.381	.272	.462	.590	.794	.384	.294	.557	.577
4	1.995	.78[illegible]	.381	.274	.439	.462	.796	.385	.290	.483	.512
5	2.562	.787	.381	.276	.36[illegible]	.383	.796	.[illegible]86	.285	.326	.412
6	3.067	.787	.380	.277	.190	.319	.792	.386	.28[illegible]	.193	.345
7	3.499	.787	.380	.278	.191	.271	.792	.384	.286	.193	.277
8	4.024	.787	.379	.278	.191	.225	.793	.384	.285	.193	.235
9	5.067	.787	.378	.276	.191	.115	.792	.384	.285	.193	.183
10	6.117	.786	.378	.276	.190	.115	.794	.384	.284	.193	.144
11	8.220	.788	.377	.275	.190	.115	.793	.384	.284	.192	.095
12	9.697	.788	.377	.275	.190	.115	.793	.384	.284	.192	.088
13	9.559	.788	.377	.275	.190	.115	.793	.384	.284	.192	.086
14	9.122	.788	.377	.275	.190	.115	.793	.384	.284	.192	.089
15	8.220	.788	.377	.275	.190	.116	.793	.384	.284	.193	.095
16	6.133	.788	.378	.276	.191	.115	.792	.384	.285	.194	.144
17	4.060	.788	.379	.277	.191	.220	.789	.384	.286	.195	.233
18	2.998	.788	.381	.277	.191	.323	.787	.386	.287	.195	.349
19	1.993	.790	.382	.279	.491	.462	.787	.385	.233	.487	.465
20	1.062	1.061	1.000	.999	1.000	.999	.987	.998	1.001	1.000	.990

		Sidewall static pressures, $p/p_{t,j}$						
		Row 3				Row 4		Row 5
		x/x_t				x/x_t		x/x_t
Point	$p_{t,j}/p_\infty$	0.791	1.011	1.286	1.560	1.286	1.560	1.560
1	.999	.992	1.001	.997	.997	.99[illegible]	.997	1.000
2	1.499	.799	.59[illegible]	.580	.62[illegible]	.612	.611	.613
3	1.754	.797	.590	.368	.533	.517	.515	.51[illegible]
4	1.995	.798	.589	.353	.474	.404	.47[illegible]	.471
5	2.562	.798	.587	.269	.377	.274	.375	.375
6	3.067	.797	.586	.266	.307	.275	.255	.253
7	3.499	.798	.585	.266	.172	.275	.149	.195
8	4.024	.797	.584	.266	.172	.274	.18[illegible]	.192
9	5.067	.795	.584	.265	.172	.273	.187	.149
10	6.117	.797	.584	.265	.172	.273	.187	.149
11	8.220	.797	.584	.269	.171	.272	.18[illegible]	.149
12	9.697	.798	.585	.269	.170	.272	.186	.149
13	9.559	.798	.585	.269	.170	.272	.18[illegible]	.188
14	9.122	.798	.585	.269	.171	.272	.186	.149
15	8.220	.796	.584	.265	.171	.272	.186	.189
16	6.133	.799	.583	.266	.173	.273	.188	.190
17	4.060	.801	.583	.268	.173	.276	.190	.199
18	2.998	.801	.584	.268	.310	.277	.261	.255
19	1.993	.804	.587	.357	.478	.409	.47[illegible]	.477
20	1.062	1.001	.997	1.061	1.001	1.002	1.002	.993

TABLE III.- Continued

(f) Configuration C6

		Flap static pressures, $p/p_{t,j}$									
		Row 1					Row 2				
		x/x_t					x/x_t				
Point	$p_{t,j}/p_\infty$	0.791	1.011	1.286	1.560	1.890	0.791	1.011	1.286	1.560	1.890
1	1.660	1.000	.997	1.000	1.001	.999	1.005	.999	.997	.999	1.000
2	1.484	.792	.391	.583	.629	.669	.801	.394	.595	.674	.676
3	1.719	.791	.381	.590	.582	.609	.800	.394	.558	.583	.582
4	1.978	.788	.381	.274	.422	.479	.801	.395	.444	.509	.505
5	2.487	.788	.381	.277	.354	.377	.800	.397	.312	.387	.409
6	2.989	.788	.381	.277	.291	.317	.791	.386	.284	.315	.329
7	3.518	.787	.380	.279	.191	.287	.792	.394	.284	.260	.283
8	4.015	.788	.396	.278	.191	.223	.793	.394	.282	.220	.241
9	5.004	.788	.374	.277	.191	.101	.794	.394	.282	.161	.174
10	6.046	.787	.374	.276	.190	.106	.794	.394	.282	.124	.140
11	8.074	.788	.377	.275	.189	.113	.794	.394	.281	.109	.105
12	8.944	.788	.377	.276	.189	.115	.793	.395	.281	.108	.098
13	9.427	.789	.377	.276	.189	.117	.794	.395	.281	.109	.094
14	8.975	.788	.377	.276	.189	.116	.793	.395	.281	.109	.091
15	8.142	.789	.378	.275	.190	.114	.794	.395	.281	.109	.104
16	6.635	.788	.378	.276	.190	.107	.799	.394	.282	.124	.140
17	4.011	.790	.380	.277	.191	.222	.790	.395	.283	.220	.243
18	2.971	.791	.381	.276	.190	.319	.787	.397	.286	.318	.343
19	1.976	.794	.381	.273	.423	.482	.795	.396	.447	.510	.506
20	1.660	1.004	1.001	1.000	1.000	.998	.995	1.001	1.002	.999	1.001

		Sidewall static pressures, $p/p_{t,j}$			
		Row 3			Row 4
		x/x_t			x/x_t
Point	$p_{t,j}/p_\infty$	0.791	1.011	1.220	1.220
1	1.660	1.002	1.000	.995	1.002
2	1.484	.807	.595	.627	.618
3	1.719	.805	.591	.532	.527
4	1.978	.802	.590	.449	.470
5	2.487	.800	.588	.325	.304
6	2.989	.800	.587	.322	.289
7	3.518	.799	.586	.320	.287
8	4.015	.800	.585	.319	.287
9	5.004	.801	.585	.317	.285
10	6.046	.798	.585	.316	.284
11	8.074	.797	.585	.315	.282
12	8.944	.797	.586	.315	.282
13	9.427	.798	.584	.315	.282
14	8.975	.798	.586	.315	.282
15	8.142	.798	.585	.315	.283
16	6.635	.799	.584	.316	.284
17	4.011	.802	.584	.320	.286
18	2.971	.803	.585	.324	.288
19	1.976	.806	.589	.453	.471
20	1.660	.999	.999	1.003	1.002

APPENDIX

TABLE III.- Continued

(g) Configuration C7

Flap static pressures, $p/p_{t,j}$

		Row 1					Row 2				
				x/x_t					x/x_t		
Point	$p_{t,j}/p_\infty$	0.791	1.011	1.286	1.560	1.890	0.791	1.011	1.286	1.560	1.890
1	1.000	1.002	1.001	.999	.999	1.001	1.006	1.001	.999	.999	1.000
2	1.486	.791	.381	.517	.627	.673	.795	.384	.589	.665	.668
3	1.722	.789	.381	.273	.473	.597	.797	.385	.409	.567	.576
4	1.994	.789	.381	.274	.423	.467	.797	.386	.303	.480	.497
5	2.480	.788	.381	.276	.363	.381	.797	.387	.288	.384	.398
6	2.986	.787	.380	.277	.191	.322	.793	.386	.287	.305	.330
7	3.483	.787	.380	.278	.191	.272	.794	.385	.287	.257	.284
8	3.992	.787	.379	.278	.191	.227	.794	.384	.286	.210	.242
9	5.006	.787	.378	.276	.191	.116	.794	.384	.286	.179	.174
10	6.076	.786	.378	.276	.190	.116	.794	.384	.285	.171	.136
11	8.188	.787	.377	.275	.190	.116	.794	.384	.285	.167	.101
12	9.034	.787	.377	.275	.190	.116	.794	.385	.285	.166	.096
13	9.480	.787	.377	.275	.190	.116	.794	.385	.285	.166	.094
14	9.024	.787	.377	.275	.190	.116	.793	.385	.285	.166	.096
15	8.196	.787	.377	.275	.190	.116	.794	.385	.285	.167	.102
16	6.059	.787	.378	.275	.191	.116	.793	.384	.285	.171	.135
17	3.995	.788	.379	.277	.191	.227	.792	.385	.286	.212	.243
18	2.989	.788	.380	.277	.191	.323	.790	.387	.288	.303	.332
19	1.989	.790	.381	.274	.423	.471	.793	.386	.300	.483	.503
20	1.002	1.000	.999	.999	.999	.998	.998	1.000	.999	1.000	.998

Sidewall static pressures, $p/p_{t,j}$

		Row 3					Row 6		
				x/x_t				x/x_t	
Point	$p_{t,j}/p_\infty$	0.791	1.011	1.286	1.560	1.890	1.286	1.560	1.890
1	1.000	1.006	1.002	.998	.998	1.000	.998	.998	.999
2	1.488	.806	.595	.593	.648	.662	.583	.628	.651
3	1.722	.803	.593	.337	.556	.572	.497	.541	.558
4	1.994	.803	.591	.266	.449	.514	.399	.455	.487
5	2.480	.802	.589	.267	.329	.433	.356	.378	.386
6	2.986	.799	.588	.268	.185	.349	.314	.311	.324
7	3.483	.799	.587	.268	.175	.306	.277	.260	.274
8	3.992	.799	.587	.268	.175	.264	.266	.231	.237
9	5.006	.799	.586	.268	.174	.136	.261	.182	.188
10	6.076	.797	.586	.267	.174	.131	.262	.168	.163
11	8.188	.798	.587	.267	.172	.129	.260	.161	.123
12	9.034	.799	.587	.268	.172	.129	.259	.160	.117
13	9.480	.799	.587	.268	.171	.129	.259	.160	.115
14	9.024	.799	.587	.268	.172	.129	.259	.160	.117
15	8.196	.799	.587	.268	.172	.129	.259	.161	.123
16	6.059	.799	.586	.268	.174	.131	.261	.168	.163
17	3.995	.801	.586	.270	.174	.239	.268	.231	.237
18	2.989	.801	.587	.270	.186	.353	.319	.314	.325
19	1.989	.803	.591	.269	.436	.520	.406	.471	.493
20	1.002	.999	.998	1.001	.999	.998	1.000	1.000	.999

TABLE III.- Continued

(h) Configuration C8

Flap static pressures, $p/p_{t,j}$

Point	$p_{t,j}/p_\infty$	Row 1 x/x_t 0.791	1.011	1.286	1.560	1.890	Row 2 x/x_t 0.791	1.011	1.286	1.560	1.890
1	1.000	.996	.998	1.000	.999	1.000	1.002	.999	1.000	1.000	1.000
2	1.482	.789	.380	.493	.600	.665	.798	.382	.517	.653	.673
3	1.725	.787	.380	.272	.432	.581	.795	.384	.285	.572	.576
4	1.983	.787	.381	.274	.421	.465	.798	.385	.285	.500	.509
5	2.486	.786	.380	.277	.371	.384	.799	.386	.286	.313	.422
6	2.982	.785	.380	.277	.191	.323	.793	.385	.286	.194	.306
7	3.480	.786	.379	.278	.191	.273	.794	.384	.286	.194	.299
8	4.025	.787	.379	.278	.191	.225	.793	.383	.284	.193	.169
9	5.034	.786	.378	.276	.191	.115	.794	.383	.284	.193	.119
10	6.093	.786	.377	.275	.190	.115	.794	.383	.283	.193	.113
11	8.240	.787	.377	.275	.190	.116	.794	.384	.283	.191	.111
12	9.068	.788	.377	.275	.190	.115	.794	.384	.283	.191	.111
13	9.471	.788	.377	.275	.190	.115	.794	.384	.283	.191	.111
14	9.030	.788	.377	.275	.190	.116	.794	.384	.283	.191	.111
15	8.174	.787	.377	.275	.190	.116	.794	.384	.283	.192	.111
16	6.119	.787	.378	.275	.191	.116	.793	.384	.283	.193	.113
17	4.015	.786	.379	.277	.191	.225	.792	.384	.285	.194	.169
18	2.983	.788	.380	.277	.191	.323	.791	.387	.286	.194	.307
19	1.988	.789	.380	.274	.424	.467	.793	.387	.285	.504	.511
20	1.001	1.000	.998	.999	.999	.999	.993	1.001	.999	1.000	.999

Sidewall static pressures, $p/p_{t,j}$

Point	$p_{t,j}/p_\infty$	Row 7 x/x_t 0.791	1.011	1.286	1.560	1.890	Row 8 x/x_t 1.286	1.560	1.890
1	1.000	.995	1.001	.998	1.000	1.000	1.000	1.000	.999
2	1.482	.801	.593	.594	.647	.533	.659	.596	.674
3	1.725	.799	.593	.425	.538	.349	.559	.519	.578
4	1.983	.800	.592	.324	.468	.277	.487	.463	.504
5	2.486	.800	.590	.263	.382	.277	.388	.351	.403
6	2.982	.799	.589	.263	.319	.278	.322	.240	.353
7	3.480	.799	.588	.263	.270	.278	.280	.203	.287
8	4.025	.798	.588	.264	.239	.278	.237	.194	.206
9	5.034	.799	.587	.263	.194	.276	.181	.192	.129
10	6.093	.797	.587	.263	.169	.275	.153	.192	.115
11	8.240	.798	.588	.262	.156	.274	.122	.191	.112
12	9.068	.799	.588	.263	.154	.274	.118	.191	.112
13	9.471	.799	.588	.263	.154	.274	.117	.190	.112
14	9.030	.799	.588	.263	.154	.274	.118	.191	.112
15	8.174	.798	.587	.263	.156	.274	.122	.191	.112
16	6.119	.799	.586	.263	.169	.275	.153	.192	.115
17	4.015	.802	.586	.265	.239	.278	.238	.194	.207
18	2.983	.833	.588	.265	.320	.278	.323	.240	.353
19	1.988	.804	.591	.331	.471	.278	.490	.483	.509
20	1.001	1.001	.998	1.002	1.002	1.000	.999	1.000	1.000

APPENDIX

TABLE III.- Continued

(i) Configuration C9

		Flap static pressures, $p/p_{t,j}$				
		Row 1				
		x/x_t				
Point	$p_{t,j}/p_\infty$	0.791	1.011	1.286	1.560	1.890
1	1.041	.997	.997	.999	.998	.998
2	1.535	.520	.381	.342	.498	.643
3	1.715	.560	.383	.344	.424	.517
4	1.994	.749	.384	.346	.459	.478
5	2.519	.797	.385	.346	.233	.373
6	3.015	.796	.385	.346	.234	.206
7	3.496	.796	.385	.345	.234	.206
8	4.040	.796	.385	.345	.234	.209
9	5.010	.796	.384	.345	.234	.209
10	5.575	.796	.384	.344	.233	.209
11	6.140	.796	.384	.345	.233	.208
12	7.181	.796	.384	.345	.233	.208
13	8.233	.796	.384	.345	.233	.207
14	9.743	.797	.383	.344	.233	.207
15	7.180	.797	.384	.344	.233	.208
16	5.554	.797	.384	.344	.234	.209
17	4.643	.797	.385	.344	.235	.208
18	3.033	.796	.386	.345	.235	.207
19	1.971	.966	.388	.344	.483	.479
20	1.061	1.062	1.004	.999	1.001	.999

		Sidewall static pressures, $p/p_{t,j}$									
		Row 3					Row 4			Row 5	
		x/x_t					x/x_t			x/x_t	
Point	$p_{t,j}/p_\infty$	0.791	1.011	1.286	1.560	1.890	1.286	1.560	1.890	1.560	1.890
1	1.041	1.005	1.000	.998	.998	.997	.999	.998	.997	.998	.998
2	1.535	.799	.591	.449	.560	.618	.451	.560	.618	.574	.627
3	1.715	.807	.591	.401	.415	.539	.347	.448	.537	.473	.537
4	1.994	.802	.590	.389	.288	.446	.347	.247	.444	.273	.488
5	2.519	.802	.577	.401	.287	.384	.346	.244	.360	.244	.341
6	3.015	.797	.576	.401	.287	.197	.346	.243	.210	.243	.264
7	3.496	.798	.576	.401	.287	.198	.344	.243	.205	.243	.218
8	4.040	.798	.576	.400	.287	.198	.344	.243	.205	.243	.216
9	5.050	.798	.576	.399	.286	.198	.343	.242	.204	.242	.205
10	5.575	.798	.576	.399	.286	.197	.343	.242	.203	.241	.205
11	6.140	.798	.576	.398	.286	.197	.343	.242	.203	.241	.204
12	7.181	.798	.576	.398	.285	.196	.343	.241	.203	.241	.204
13	8.233	.798	.577	.398	.285	.196	.342	.241	.203	.241	.203
14	9.743	.797	.577	.398	.285	.196	.342	.241	.232	.240	.203
15	7.180	.797	.576	.399	.285	.197	.343	.242	.233	.241	.204
16	5.554	.798	.575	.398	.286	.199	.344	.242	.205	.242	.205
17	4.643	.798	.575	.401	.287	.199	.345	.243	.207	.243	.210
18	3.033	.794	.576	.397	.288	.198	.346	.243	.212	.243	.267
19	1.971	.794	.580	.395	.286	.499	.346	.248	.473	.275	.474
20	1.061	.998	.998	.999	.999	.998	.998	.999	1.001	.999	1.002

APPENDIX

TABLE III.- Continued

(j) Configuration C10

		Flap static pressures, $p/p_{t,j}$			
		Row 1			
		x/x_t			
Point	$p_{t,j}/p_\infty$	0.791	1.011	1.286	1.560
1	1.661	.996	.997	1.000	.997
2	1.562	.791	.418	.580	.617
3	1.770	.784	.378	.436	.504
4	2.003	.783	.379	.424	.456
5	2.533	.779	.380	.226	.378
6	3.027	.777	.380	.227	.363
7	3.512	.776	.379	.227	.161
8	4.036	.776	.378	.228	.161
9	5.089	.774	.378	.227	.161
10	6.213	.773	.378	.226	.161
11	8.347	.773	.378	.225	.160
12	9.272	.774	.378	.225	.160
13	9.646	.774	.378	.225	.160
14	9.230	.774	.378	.225	.160
15	6.223	.774	.378	.226	.161
16	4.023	.777	.379	.227	.161
17	3.061	.780	.381	.226	.308
18	1.995	.786	.381	.417	.453
19	1.661	1.000	1.004	.999	1.001

		Sidewall static pressures, $p/p_{t,j}$			
		Row 3			
		x/x_t			
Point	$p_{t,j}/p_\infty$	0.791	1.011	1.286	1.560
1	1.661	1.002	1.000	.998	.998
2	1.562	.803	.401	.562	.627
3	1.770	.801	.384	.368	.501
4	2.003	.801	.583	.357	.459
5	2.533	.800	.580	.265	.364
6	3.027	.797	.580	.265	.306
7	3.512	.798	.580	.265	.253
8	4.036	.798	.580	.265	.124
9	5.089	.798	.580	.264	.124
10	6.213	.798	.580	.264	.124
11	8.347	.798	.581	.264	.125
12	9.272	.799	.581	.264	.125
13	9.646	.798	.582	.264	.125
14	9.230	.799	.581	.264	.125
15	6.223	.798	.580	.264	.125
16	4.023	.796	.580	.266	.125
17	3.061	.794	.580	.264	.310
18	1.995	.799	.583	.365	.463
19	1.661	.998	1.000	1.001	1.000

TABLE III.- Continued

(k) Configuration C11

		Flap static pressures, $p/p_{t,j}$			
		Row 1			
		x/x_t			
Point	$p_{t,j}/p_\infty$	0.791	1.011	1.286	1.560
1	1.061	.997	.997	1.000	.998
2	1.488	.792	.354	.351	.696
3	1.745	.786	.355	.349	.532
4	1.998	.787	.354	.347	.484
5	2.501	.784	.355	.347	.344
6	3.014	.782	.355	.347	.222
7	3.766	.780	.354	.346	.222
8	4.367	.779	.353	.346	.222
9	4.817	.779	.353	.345	.222
10	6.141	.778	.353	.345	.221
11	9.266	.779	.353	.345	.221
12	9.878	.779	.353	.345	.221
13	6.121	.779	.353	.345	.222
14	4.280	.782	.354	.345	.223
15	3.008	.785	.356	.347	.223
16	2.004	.790	.357	.346	.483
17	.999	1.003	1.004	1.002	1.002

		Sidewall static pressures, $p/p_{t,j}$						
		Row 3				Row 4		Row 5
		x/x_t				x/x_t		x/x_t
Point	$p_{t,j}/p_\infty$	0.791	1.011	1.286	1.560	1.286	1.560	1.560
1	1.001	.998	1.001	.999	.999	.998	.998	.997
2	1.488	.800	.583	.574	.637	.563	.645	.649
3	1.745	.802	.583	.427	.538	.355	.545	.550
4	1.998	.802	.582	.293	.469	.347	.472	.483
5	2.501	.803	.579	.294	.271	.348	.315	.341
6	3.014	.798	.578	.295	.270	.346	.245	.263
7	3.766	.798	.577	.295	.270	.345	.242	.237
8	4.367	.798	.577	.295	.269	.345	.242	.233
9	4.817	.799	.577	.294	.269	.345	.241	.231
10	6.141	.798	.577	.294	.269	.345	.240	.229
11	9.266	.799	.578	.294	.268	.344	.239	.228
12	9.878	.799	.579	.294	.268	.344	.239	.226
13	6.121	.799	.577	.295	.269	.346	.240	.230
14	4.280	.799	.577	.296	.270	.347	.243	.234
15	3.008	.799	.578	.296	.271	.348	.247	.268
16	2.004	.802	.582	.294	.468	.349	.472	.481
17	.999	1.002	1.000	1.002	1.002	1.002	1.003	1.002

TABLE III.- Concluded

(1) Configuration C12

		Flap static pressures, $p/p_{t,j}$						
		Row 1						
		x/x_t						
Point	$p_{t,j}/p_\infty$	0.791	1.011	1.286	1.560	1.890	2.220	2.769
1	1.001	.995	.997	.999	.998	.998	.998	.999
2	1.585	.793	.434	.349	.485	.561	.534	.596
3	1.851	.790	.404	.346	.467	.472	.483	.508
4	1.997	.789	.405	.346	.430	.442	.453	.473
5	2.578	.786	.406	.347	.229	.235	.356	.368
6	3.031	.784	.406	.347	.230	.203	.184	.310
7	3.548	.784	.406	.347	.230	.204	.170	.266
8	4.044	.784	.406	.346	.230	.204	.170	.223
9	5.098	.784	.405	.346	.230	.205	.170	.115
10	6.138	.783	.405	.346	.230	.204	.170	.115
11	8.166	.785	.405	.347	.230	.204	.169	.115
12	9.172	.786	.405	.347	.230	.204	.169	.115
13	9.611	.785	.405	.347	.230	.204	.169	.115
14	9.168	.786	.405	.347	.230	.204	.169	.115
15	6.139	.785	.406	.346	.230	.205	.170	.115
16	4.049	.787	.407	.347	.232	.205	.170	.222
17	3.020	.786	.408	.347	.231	.203	.184	.311
18	2.029	.794	.408	.346	.418	.439	.446	.465
19	.999	1.006	1.007	1.004	1.003	1.001	1.001	1.001

		Sidewall static pressures, $p/p_{t,j}$					
		Row 3					
		x/x_t					
Point	$p_{t,j}/p_\infty$	0.791	1.011	1.286	1.560	2.220	2.769
1	1.001	1.005	.997	.998	.998	.995	.997
2	1.585	.803	.587	.299	.369	.571	.622
3	1.851	.802	.587	.299	.295	.509	.531
4	1.997	.804	.584	.299	.262	.482	.494
5	2.578	.799	.584	.300	.262	.219	.369
6	3.031	.798	.584	.300	.262	.163	.344
7	3.548	.800	.583	.300	.261	.163	.256
8	4.044	.799	.583	.300	.261	.163	.189
9	5.098	.798	.583	.300	.260	.163	.131
10	6.138	.799	.583	.299	.260	.163	.130
11	8.166	.799	.584	.300	.260	.162	.127
12	9.172	.798	.584	.299	.260	.162	.126
13	9.611	.799	.584	.299	.260	.162	.126
14	9.168	.798	.584	.299	.260	.162	.126
15	6.139	.799	.583	.300	.261	.163	.130
16	4.049	.798	.584	.301	.262	.164	.163
17	3.020	.797	.585	.302	.262	.164	.347
18	2.029	.801	.587	.300	.262	.473	.486
19	.999	.996	.999	1.001	1.001	1.004	1.002

TABLE IV.- COMPUTER PRINTOUT OF RATIO OF INTERNAL STATIC PRESSURE TO JET TOTAL PRESSURE FOR SINGLE-RAMP EXPANSION NOZZLES

(a) Configuration SR1

Upper flap static pressures, $p/p_{t,j}$

		Row 1						Row 2				
		$x/x_{t,u}$						$x/x_{t,u}$				
Point	$p_{t,j}/p_\infty$	0.888	1.008	1.129	1.250	1.449	1.691	0.888	1.008	1.129	1.250	1.449
1	.999	1.003	1.000	1.003	1.000	.998	1.001	1.000	1.000	.999	1.037	1.000
2	1.496	.794	.449	.510	.549	.627	.691	.788	.426	.506	.588	.640
3	2.542	.797	.238	.260	.241	.452	.497	.779	.246	.271	.266	.479
4	3.503	.793	.237	.261	.241	.226	.453	.778	.245	.272	.257	.231
5	4.237	.791	.236	.260	.240	.225	.193	.778	.245	.271	.253	.231
6	5.146	.792	.235	.259	.240	.225	.193	.778	.243	.270	.247	.230
7	6.185	.790	.234	.259	.239	.225	.193	.777	.243	.269	.238	.230
8	6.683	.790	.234	.259	.239	.225	.193	.778	.242	.269	.238	.230
9	7.244	.789	.234	.258	.238	.224	.193	.776	.241	.269	.238	.230
10	9.482	.786	.232	.257	.238	.224	.192	.776	.240	.266	.239	.229
11	10.423	.785	.232	.257	.238	.224	.192	.776	.239	.264	.239	.229
12	9.429	.785	.232	.257	.238	.224	.192	.775	.239	.265	.239	.229
13	6.685	.788	.233	.258	.239	.225	.193	.778	.242	.269	.238	.230
14	4.219	.788	.236	.260	.240	.226	.194	.778	.244	.271	.237	.232
15	2.491	.793	.238	.256	.240	.462	.489	.781	.244	.271	.237	.486
16	1.061	.999	.999	.997	1.000	1.001	.998	1.002	1.000	1.000	.983	1.000

Lower flap static pressures, $p/p_{t,j}$

		Row 1				Row 2			
		$x/x_{t,l}$				$x/x_{t,l}$			
Point	$p_{t,j}/p_\infty$	0.881	1.001	1.079	1.168	0.881	1.001	1.079	1.168
1	.999	.998	1.001	.999	.999	1.003	1.001	1.000	1.003
2	1.490	.845	.538	.452	.609	.843	.535	.453	.613
3	2.542	.842	.532	.426	.332	.846	.532	.429	.335
4	3.503	.841	.531	.425	.332	.846	.531	.429	.334
5	4.237	.843	.530	.424	.332	.844	.530	.428	.333
6	5.146	.843	.530	.425	.332	.846	.530	.428	.332
7	6.185	.842	.529	.425	.332	.845	.530	.427	.332
8	6.683	.843	.529	.424	.333	.845	.530	.427	.332
9	7.244	.842	.529	.424	.332	.844	.529	.427	.332
10	9.482	.840	.528	.424	.332	.842	.528	.426	.331
11	10.423	.838	.528	.424	.332	.841	.528	.425	.331
12	9.429	.839	.527	.423	.332	.841	.527	.425	.331
13	6.685	.842	.528	.425	.333	.844	.528	.426	.332
14	4.219	.843	.529	.425	.334	.843	.529	.428	.333
15	2.491	.843	.530	.427	.334	.845	.531	.429	.333
16	1.061	1.000	.997	1.000	1.001	1.000	1.000	1.000	.997

TABLE IV.- Continued

(a) Concluded

		Sidewall static pressures, $p/p_{t,j}$										
		Row 1							Row 2			
		$x/x_{t,u}$							$x/x_{t,u}$			
Point	$p_{t,j}/p_\infty$	0.888	1.008	1.129	1.250	1.371	1.510	1.691	1.250	1.371	1.510	1.691
1	.999	1.002	1.005	.999	.999	.997	1.001	.998	.999	1.001	.998	1.001
2	1.490	.731	.610	.488	.613	.640	.666	.672	.568	.614	.656	.682
3	2.542	.566	.597	.324	.215	.365	.445	.420	.236	.386	.482	.482
4	3.503	.503	.595	.325	.215	.190	.282	.340	.238	.223	.211	.420
5	4.237	.473	.596	.325	.215	.181	.210	.251	.238	.223	.210	.226
6	5.146	.448	.594	.325	.215	.181	.150	.205	.239	.223	.211	.175
7	6.185	.427	.594	.325	.214	.181	.121	.164	.238	.223	.210	.174
8	6.683	.420	.594	.325	.214	.181	.121	.150	.238	.223	.210	.175
9	7.244	.414	.594	.325	.214	.180	.121	.136	.238	.222	.210	.175
10	9.482	.391	.595	.325	.213	.180	.121	.088	.237	.221	.208	.172
11	10.423	.384	.595	.325	.213	.179	.121	.088	.237	.221	.209	.172
12	9.429	.391	.593	.325	.213	.180	.121	.088	.237	.221	.209	.171
13	6.685	.420	.593	.326	.215	.181	.121	.149	.239	.222	.210	.172
14	4.219	.473	.592	.326	.216	.182	.210	.259	.240	.223	.210	.225
15	2.491	.569	.593	.326	.215	.373	.453	.429	.237	.391	.491	.484
16	1.001	.997	.994	1.000	1.001	1.004	.999	1.002	1.001	.998	1.002	.999

TABLE IV.- Continued

(b) Configuration SR2

		Upper flap static pressures, $p/p_{t,j}$										
		Row 1						Row 2				
		$x/x_{t,u}$						$x/x_{t,u}$				
Point	$p_{t,j}/p_\infty$	0.888	1.008	1.129	1.250	1.449	1.691	0.888	1.008	1.129	1.250	1.449
1	1.001	1.000	.998	1.001	1.000	.999	1.002	.997	.999	.999	.999	.997
2	1.527	.793	.435	.498	.535	.612	.672	.785	.393	.500	.552	.630
3	2.547	.795	.238	.258	.240	.451	.496	.777	.245	.270	.251	.472
4	3.549	.792	.237	.260	.240	.224	.450	.776	.245	.272	.247	.231
5	4.233	.789	.236	.259	.239	.225	.197	.776	.244	.271	.246	.231
6	5.092	.791	.235	.259	.239	.225	.194	.776	.243	.271	.245	.230
7	6.267	.789	.234	.258	.239	.224	.195	.776	.242	.269	.244	.231
8	6.708	.789	.234	.258	.238	.224	.194	.777	.242	.269	.244	.230
9	7.280	.788	.234	.258	.238	.224	.195	.776	.242	.268	.244	.230
10	9.381	.788	.233	.257	.238	.224	.193	.777	.241	.267	.244	.230
11	10.338	.787	.232	.257	.238	.224	.193	.778	.241	.266	.244	.230
12	9.333	.787	.232	.257	.238	.224	.194	.778	.241	.267	.244	.230
13	6.679	.789	.233	.258	.239	.225	.194	.778	.242	.270	.245	.231
14	4.196	.788	.236	.259	.240	.226	.209	.778	.245	.271	.247	.232
15	2.499	.794	.237	.256	.240	.459	.488	.781	.244	.270	.252	.479
16	1.000	1.000	1.000	.999	1.000	1.000	.997	1.003	1.000	1.000	1.001	1.001

		Lower flap static pressures, $p/p_{t,j}$							
		Row 1				Row 2			
		$x/x_{t,l}$				$x/x_{t,l}$			
Point	$p_{t,j}/p_\infty$	0.881	1.001	1.079	1.168	0.881	1.001	1.079	1.168
1	1.001	.992	.998	1.000	.998	1.001	.998	.999	1.000
2	1.527	.844	.535	.446	.584	.843	.533	.441	.592
3	2.547	.839	.530	.426	.332	.845	.530	.427	.333
4	3.549	.838	.528	.425	.332	.845	.529	.427	.332
5	4.233	.839	.528	.424	.331	.842	.528	.426	.332
6	5.092	.839	.529	.424	.332	.845	.528	.426	.331
7	6.207	.839	.528	.425	.332	.844	.528	.426	.332
8	6.706	.840	.528	.424	.332	.844	.528	.426	.331
9	7.280	.841	.528	.425	.332	.844	.528	.426	.331
10	9.381	.841	.529	.425	.332	.843	.528	.426	.331
11	10.338	.840	.529	.425	.333	.843	.529	.426	.332
12	9.333	.841	.529	.425	.333	.843	.528	.426	.331
13	6.679	.842	.529	.425	.333	.844	.529	.427	.331
14	4.196	.844	.529	.426	.333	.842	.529	.428	.333
15	2.499	.843	.531	.426	.334	.844	.531	.429	.334
16	1.000	1.009	1.002	1.000	1.001	1.001	1.002	1.002	1.000

TABLE IV.- Continued

(b) Concluded

		Sidewall static pressures, $p/p_{t,j}$							
		Row 1					Row 2		
		$x/x_{t,u}$					$x/x_{t,u}$		
Point	$p_{t,j}/p_\infty$	0.888	1.008	1.129	1.250	1.329	1.250	1.371	1.510
1	1.001	.999	.999	.997	.998	.994	.998	.995	.999
2	1.527	.721	.604	.433	.606	.634	.559	.600	.648
3	2.547	.565	.597	.324	.215	.331	.235	.394	.433
4	3.549	.501	.597	.325	.215	.201	.237	.220	.267
5	4.233	.473	.597	.325	.215	.190	.237	.222	.220
6	5.092	.450	.596	.325	.215	.190	.237	.222	.209
7	6.207	.428	.596	.325	.214	.190	.237	.222	.208
8	6.766	.420	.596	.325	.214	.190	.237	.222	.207
9	7.280	.413	.596	.325	.214	.190	.237	.221	.207
10	9.381	.394	.597	.326	.214	.189	.236	.221	.207
11	10.338	.387	.597	.326	.214	.189	.237	.221	.207
12	9.333	.394	.597	.326	.214	.189	.236	.221	.207
13	6.679	.421	.596	.327	.215	.191	.237	.222	.208
14	4.196	.475	.596	.327	.216	.192	.238	.223	.222
15	2.499	.570	.597	.327	.216	.339	.236	.404	.439
16	1.000	1.002	.999	1.002	1.001	1.005	1.002	1.005	1.001

TABLE IV.- Continued

(c) Configuration SR3

Upper flap static pressures, $p/p_{t,j}$

Point	$p_{t,j}/p_\infty$	Row 1, $x/x_{t,u}$ = 0.888	1.008	1.129	1.250	1.449	1.691	Row 2, $x/x_{t,u}$ = 0.888	1.008	1.129	1.250	1.449
1	1.001	.998	.998	.999	.998	.999	.998	.996	.999	.998	1.000	.998
2	1.490	.792	.482	.543	.590	.656	.687	.786	.452	.543	.628	.669
3	2.541	.794	.237	.257	.240	.459	.475	.777	.243	.269	.359	.440
4	3.535	.791	.236	.260	.239	.224	.460	.776	.243	.271	.248	.301
5	4.197	.789	.236	.260	.239	.225	.306	.776	.243	.270	.246	.255
6	5.069	.790	.235	.259	.239	.225	.195	.776	.240	.270	.245	.214
7	6.128	.789	.234	.259	.238	.225	.194	.776	.240	.269	.244	.176
8	6.715	.789	.233	.258	.238	.224	.194	.777	.241	.268	.244	.159
9	7.298	.787	.233	.258	.238	.224	.194	.776	.239	.268	.243	.145
10	9.425	.786	.232	.257	.238	.223	.194	.776	.238	.266	.243	.117
11	10.361	.786	.232	.257	.238	.224	.194	.776	.239	.265	.243	.116
12	9.444	.785	.232	.257	.238	.223	.194	.776	.238	.266	.243	.117
13	6.681	.788	.233	.258	.239	.225	.195	.778	.241	.269	.244	.160
14	4.201	.788	.236	.259	.240	.226	.793	.778	.244	.271	.246	.255
15	2.532	.794	.238	.257	.241	.461	.476	.781	.244	.270	.248	.443
16	1.000	.999	1.003	1.001	1.001	1.001	1.003	1.003	1.003	1.002	1.000	1.002

Lower flap static pressures, $p/p_{t,j}$

Point	$p_{t,j}/p_\infty$	Row 1, $x/x_{t,l}$ = 0.881	1.001	1.079	1.168	Row 2, $x/x_{t,l}$ = 0.881	1.001	1.079	1.168
1	1.001	.997	.998	.998	.999	.999	.998	.999	.997
2	1.490	.843	.540	.523	.620	.841	.536	.533	.630
3	2.541	.839	.530	.425	.332	.845	.530	.428	.333
4	3.535	.839	.530	.424	.332	.844	.529	.427	.332
5	4.197	.839	.529	.425	.332	.842	.528	.426	.332
6	5.069	.839	.529	.424	.332	.844	.527	.426	.331
7	6.128	.839	.529	.424	.332	.843	.528	.427	.331
8	6.715	.841	.529	.424	.332	.844	.528	.427	.331
9	7.298	.841	.528	.424	.332	.843	.528	.426	.331
10	9.425	.840	.528	.424	.332	.842	.528	.426	.331
11	10.361	.838	.529	.425	.333	.841	.528	.426	.331
12	9.444	.839	.528	.424	.332	.841	.527	.426	.331
13	6.681	.842	.529	.425	.333	.844	.528	.427	.332
14	4.201	.842	.529	.425	.334	.842	.529	.428	.333
15	2.532	.843	.532	.427	.335	.845	.531	.429	.334
16	1.000	1.004	1.001	1.001	1.003	1.000	1.001	1.001	1.001

TABLE IV.- Continued

(c) Concluded

		Sidewall static pressures, $p/p_{t,j}$				
		Row 1				Row 2
		$x/x_{t,u}$				$x/x_{t,u}$
Point	$p_{t,j}/p_\infty$	0.888	1.008	1.129	1.190	1.190
1	1.001	.998	1.001	.997	.998	.997
2	1.490	.730	.612	.573	.628	.582
3	2.541	.565	.593	.318	.261	.253
4	3.535	.501	.591	.318	.260	.250
5	4.197	.474	.590	.317	.259	.250
6	5.069	.450	.589	.317	.259	.250
7	6.128	.429	.589	.317	.259	.249
8	6.715	.420	.589	.317	.258	.249
9	7.298	.412	.589	.317	.258	.249
10	9.425	.392	.589	.317	.257	.248
11	10.361	.386	.589	.317	.257	.248
12	9.444	.392	.588	.317	.257	.248
13	6.681	.420	.589	.319	.259	.250
14	4.201	.475	.589	.320	.261	.252
15	2.532	.567	.592	.321	.262	.255
16	1.000	1.002	.999	1.003	1.002	1.003

TABLE IV.- Continued

(d) Configuration SR4

		Upper flap static pressures, $p/p_{t,j}$										
		Row 1						Row 2				
		$x/x_{t,u}$						$x/x_{t,u}$				
Point	$p_{t,j}/p_\infty$	0.888	1.008	1.129	1.250	1.449	1.691	0.888	1.008	1.129	1.250	1.449
1	1.000	.999	.998	1.000	.999	.999	1.000	.997	.999	1.000	.999	.998
2	1.510	.792	.440	.502	.540	.620	.679	.786	.400	.506	.558	.635
3	2.546	.795	.237	.258	.240	.451	.496	.778	.246	.270	.251	.476
4	3.510	.792	.236	.259	.240	.224	.454	.777	.245	.271	.247	.232
5	4.222	.789	.236	.260	.240	.225	.195	.777	.245	.271	.246	.231
6	5.069	.791	.235	.259	.240	.226	.195	.777	.244	.270	.245	.230
7	6.196	.789	.235	.259	.239	.225	.195	.777	.243	.269	.245	.230
8	6.676	.789	.234	.258	.239	.225	.194	.777	.243	.268	.245	.230
9	7.279	.788	.234	.258	.239	.224	.194	.777	.241	.268	.244	.230
10	9.394	.787	.233	.258	.238	.224	.195	.778	.240	.266	.244	.229
11	10.315	.788	.232	.257	.238	.224	.195	.777	.240	.265	.244	.229
12	9.381	.787	.232	.257	.239	.224	.195	.777	.240	.265	.244	.229
13	6.682	.788	.233	.258	.239	.225	.196	.778	.241	.269	.245	.231
14	4.227	.789	.236	.259	.240	.226	.195	.778	.243	.271	.246	.231
15	2.526	.793	.237	.256	.240	.453	.494	.780	.244	.270	.251	.479
16	1.000	1.000	1.001	.998	1.000	1.001	.998	1.004	1.002	1.001	1.001	1.000

		Lower flap static pressures, $p/p_{t,j}$							
		Row 1				Row 2			
		$x/x_{t,l}$				$x/x_{t,l}$			
Point	$p_{t,j}/p_\infty$	0.881	1.001	1.079	1.168	0.881	1.001	1.079	1.168
1	1.000	.990	.998	1.000	.999	1.000	.996	.999	1.000
2	1.510	.843	.536	.449	.507	.842	.531	.444	.602
3	2.546	.840	.530	.425	.332	.844	.529	.428	.332
4	3.510	.841	.530	.425	.332	.844	.528	.427	.331
5	4.222	.840	.529	.424	.332	.842	.528	.426	.331
6	5.069	.841	.529	.424	.332	.845	.527	.426	.330
7	6.196	.841	.528	.424	.332	.844	.528	.426	.331
8	6.676	.842	.529	.424	.333	.844	.528	.426	.330
9	7.279	.843	.529	.425	.332	.843	.528	.426	.330
10	9.394	.841	.529	.425	.333	.843	.528	.427	.330
11	10.315	.841	.529	.425	.333	.842	.528	.427	.331
12	9.381	.841	.529	.425	.333	.843	.528	.427	.330
13	6.682	.842	.529	.425	.334	.844	.528	.427	.331
14	4.227	.842	.529	.424	.334	.842	.528	.427	.332
15	2.526	.844	.531	.426	.334	.844	.530	.429	.333
16	1.000	1.009	1.002	1.001	1.001	1.000	1.002	1.001	.999

TABLE IV.- Continued

(d) Concluded

		Sidewall static pressures, $p/p_{t,j}$								
		Row 1					Row 2			
		$x/x_{t,u}$					$x/x_{t,u}$			
Point	$p_{t,j}/p_{\infty}$	0.888	1.008	1.129	1.250	1.371	1.250	1.371	1.510	1.630
1	1.000	.999	1.001	.997	.998	.995	.998	.997	.998	.999
2	1.510	.724	.604	.453	.606	.644	.564	.608	.651	.673
3	2.546	.564	.596	.323	.214	.344	.235	.395	.463	.462
4	3.510	.502	.597	.324	.214	.261	.236	.224	.276	.365
5	4.222	.473	.596	.324	.214	.191	.237	.223	.211	.239
6	5.069	.450	.596	.324	.214	.182	.237	.222	.210	.193
7	6.196	.428	.596	.325	.213	.182	.237	.222	.210	.187
8	6.676	.420	.596	.325	.213	.182	.237	.222	.209	.186
9	7.279	.413	.596	.325	.213	.181	.237	.221	.209	.186
10	9.394	.393	.597	.325	.213	.181	.237	.220	.209	.187
11	10.315	.386	.598	.326	.213	.181	.237	.220	.209	.187
12	9.381	.393	.597	.326	.213	.181	.237	.220	.209	.187
13	6.682	.420	.598	.326	.214	.182	.238	.221	.210	.187
14	4.227	.473	.596	.326	.215	.192	.238	.222	.211	.239
15	2.526	.567	.596	.326	.215	.349	.236	.398	.466	.464
16	1.000	1.001	1.000	1.002	1.001	1.005	1.001	1.005	1.000	1.000

TABLE IV.- Continued

(e) Configuration SR5

		Upper flap static pressures, $p/p_{t,j}$										
		Row 1						Row 2				
		$x/x_{t,u}$						$x/x_{t,u}$				
Point	$p_{t,j}/p_\infty$	0.888	1.008	1.129	1.250	1.449	1.691	0.888	1.008	1.129	1.250	1.449
0	.999	.998	1.000	1.003	1.002	1.001	1.004	1.005	1.000	1.002	1.002	1.005
1	1.517	.798	.462	.513	.548	.631	.684	.792	.448	.511	.564	.672
2	2.483	.796	.240	.259	.240	.468	.479	.782	.249	.271	.256	.466
3	3.520	.794	.239	.261	.241	.225	.464	.779	.248	.273	.248	.331
4	4.168	.795	.238	.260	.240	.226	.321	.778	.248	.272	.247	.260
5	5.115	.793	.237	.260	.240	.226	.194	.778	.246	.272	.246	.224
6	6.174	.791	.236	.259	.239	.225	.195	.778	.245	.270	.245	.215
7	6.674	.791	.235	.259	.239	.225	.196	.779	.244	.269	.245	.214
8	7.271	.792	.235	.259	.238	.224	.196	.778	.244	.269	.245	.213
9	9.371	.788	.233	.257	.238	.224	.194	.777	.241	.266	.244	.211
10	10.241	.789	.233	.257	.238	.224	.194	.777	.241	.266	.244	.211
11	9.318	.787	.233	.257	.237	.224	.194	.777	.241	.266	.244	.211
12	6.715	.791	.234	.258	.238	.225	.194	.778	.242	.268	.245	.213
13	4.159	.794	.237	.259	.240	.226	.321	.778	.246	.272	.247	.260
14	2.503	.796	.239	.257	.238	.464	.478	.779	.246	.270	.253	.465
15	1.002	1.001	1.000	.996	.997	.998	.996	.995	1.000	.998	.997	.995

		Lower flap static pressures, $p/p_{t,j}$							
		Row 2				Row 1			
		$x/x_{t,l}$				$x/x_{t,l}$			
Point	$p_{t,j}/p_\infty$	0.881	1.001	1.079	1.168	0.881	1.001	1.079	1.168
0	.999	.985	1.003	1.001	1.002	1.002	1.000	1.002	1.002
1	1.517	.843	.539	.450	.603	.846	.540	.464	.613
2	2.483	.837	.533	.426	.333	.847	.532	.431	.335
3	3.520	.836	.529	.425	.333	.847	.530	.428	.335
4	4.168	.836	.529	.424	.332	.844	.529	.428	.333
5	5.115	.835	.528	.425	.332	.846	.528	.428	.332
6	6.174	.835	.528	.425	.332	.846	.528	.427	.332
7	6.674	.835	.528	.425	.333	.846	.528	.428	.331
8	7.271	.835	.528	.425	.333	.845	.528	.427	.331
9	9.371	.833	.528	.425	.333	.843	.528	.427	.331
10	10.241	.833	.528	.425	.333	.843	.528	.427	.331
11	9.318	.833	.527	.425	.333	.843	.527	.426	.330
12	6.715	.836	.528	.425	.334	.846	.528	.428	.331
13	4.159	.839	.529	.425	.334	.844	.528	.429	.333
14	2.503	.841	.532	.427	.334	.846	.531	.430	.334
15	1.002	1.01*	.998	.998	1.000	.997	.999	.999	.997

TABLE IV.- Concluded

(e) Concluded

		Sidewall static pressures, $p/p_{t,j}$						
		Row 1				Row 2		
		$x/x_{t,u}$				$x/x_{t,u}$		
Point	$p_{t,j}/p_\infty$	0.888	1.008	1.129	1.190	1.190	1.250	1.371
0	.999	1.002	1.003	1.000	1.000	1.000	.998	1.002
1	1.517	.725	.612	.513	.603	.551	.571	.630
2	2.463	.574	.597	.326	.261	.252	.359	.414
3	3.520	.503	.596	.326	.261	.252	.239	.286
4	4.166	.476	.595	.326	.260	.252	.238	.241
5	5.115	.450	.595	.326	.260	.251	.239	.220
6	6.174	.429	.596	.326	.259	.251	.239	.215
7	6.674	.422	.596	.327	.260	.251	.239	.214
8	7.271	.413	.596	.327	.259	.250	.238	.213
9	9.371	.393	.597	.327	.259	.248	.237	.212
10	10.241	.387	.597	.327	.259	.248	.237	.212
11	9.318	.393	.596	.327	.259	.249	.237	.212
12	6.715	.420	.596	.328	.260	.250	.239	.214
13	4.159	.476	.594	.328	.261	.252	.240	.241
14	2.503	.571	.595	.328	.262	.253	.352	.410
15	1.002	.998	.996	1.000	1.000	1.001	1.002	.999

APPENDIX

TABLE V.- COMPUTER PRINTOUT OF RATIO OF INTERNAL STATIC PRESSURE TO JET TOTAL PRESSURE FOR WEDGE NOZZLES

(a) Configuration W1

		Flap static pressure, $p/p_{t,j}$									
		Row 1					Row 2				
		x/x_t					x/x_t				
Point	$p_{t,j}/p_\infty$	0.851	0.954	1.012	1.056	1.076	0.851	0.954	1.012	1.056	1.076
1	1.000	1.002	.998	1.001	1.000	1.000	1.000	.998	.997	1.005	1.017
2	1.516	.939	.805	.573	.531	.[illegible]	.599	.542	.572	.[illegible]	.[illegible]
3	1.999	.938	.808	.572	.381	.[illegible]	.400	.380	.573	.804	.[illegible]
4	3.014	.936	.807	.572	.382	.[illegible]	.311	.384	.571	.[illegible]	.[illegible]
5	3.487	.937	.804	.573	.382	.310	.312	.381	.571	.[illegible]	.[illegible]
6	4.009	.934	.805	.572	.382	.311	.313	.383	.571	.[illegible]	.[illegible]
7	4.551	.936	.806	.572	.383	.[illegible]	.313	.383	.571	.[illegible]	.[illegible]
8	5.542	.935	.806	.572	.384	.[illegible]	.314	.385	.572	.[illegible]	.[illegible]
9	7.184	.935	.805	.572	.384	.[illegible]	.316	.385	.572	.[illegible]	.[illegible]
10	8.736	.936	.804	.573	.385	.310	.316	.387	.573	.804	.939
11	10.120	.936	.805	.574	.386	.311	.319	.[illegible]	.575	.[illegible]	.939
12	8.689	.936	.805	.573	.386	.311	.[illegible]	.[illegible]	.575	.801	.935
13	5.547	.936	.809	.573	.385	.310	.[illegible]	.387	.575	.799	.930
14	4.013	.934	.808	.572	.384	.311	.[illegible]	.[illegible]	.574	.796	.926
15	3.001	.934	.811	.573	.384	.311	.314	.[illegible]	.574	.795	.925
16	2.009	.935	.813	.573	.383	.[illegible]	.[illegible]	.[illegible]	.576	.796	.923
17	1.000	.996	1.005	.998	1.000	.999	1.000	.999	1.003	.804	.981

		Sidewall static pressure, $p/p_{t,j}$				
		x/x_t				
Point	$p_{t,j}/p_\infty$	0.886	1.035	1.264	1.430	1.601
1	1.000	1.000	1.000	1.000	.999	1.000
2	1.516	.907	.476	.[illegible]	.671	.[illegible]
3	1.999	.910	.416	.[illegible]	.510	.[illegible]
4	3.014	.911	.418	.[illegible]	.343	.[illegible]
5	3.487	.910	.417	.[illegible]	.284	.311
6	4.009	.911	.418	.[illegible]	.272	.[illegible]
7	4.551	.910	.417	.157	.300	.[illegible]
8	5.542	.910	.419	.107	.187	.241
9	7.184	.910	.419	.078	.081	.174
10	8.736	.909	.420	.079	.069	.126
11	10.120	.909	.421	.079	.074	.097
12	8.689	.909	.421	.079	.070	.127
13	5.547	.909	.420	.106	.192	.243
14	4.013	.910	.419	.196	.280	.254
15	3.001	.910	.418	.353	.346	.330
16	2.009	.908	.416	.513	.509	.511
17	1.000	1.002	1.000	1.000	1.001	1.000

APPENDIX

TABLE V.- Continued

(a) Concluded

		Wedge static pressure, $p/p_{t,j}$									
		Row 1									
		x/x_t									
Point	$p_{t,j}/p_\infty$	0.817	0.920	1.012	1.029	1.082	1.158	1.251	1.396	1.567	1.737
1	1.000	.998	1.000	1.000	1.000	.999	1.000	.999	0.000	1.000	1.000
2	1.516	.936	.893	.415	.466	.578	.582	.684	0.000	.676	.680
3	1.999	.940	.889	.356	.274	.284	.518	.519	0.000	.522	.524
4	3.014	.940	.892	.360	.274	.284	.283	.388	0.000	.355	.378
5	3.487	.939	.890	.363	.275	.284	.153	.329	0.000	.364	.289
6	4.069	.940	.890	.363	.274	.285	.154	.190	0.000	.212	.284
7	4.551	.939	.889	.362	.272	.224	.154	.091	0.000	.153	.312
8	5.542	.939	.890	.361	.272	.224	.155	.092	0.000	.315	.114
9	7.164	.938	.888	.359	.270	.225	.156	.093	0.000	.149	.199
10	8.736	.938	.888	.358	.270	.224	.156	.093	0.000	.097	.143
11	10.120	.938	.888	.358	.269	.224	.157	.094	0.000	.087	.109
12	8.689	.937	.886	.358	.270	.225	.157	.094	0.000	.097	.144
13	5.547	.938	.892	.362	.272	.227	.157	.093	0.000	.324	.114
14	4.013	.939	.891	.364	.273	.226	.155	.191	0.000	.211	.299
15	3.001	.939	.892	.359	.273	.226	.294	.384	0.000	.358	.380
16	2.469	.938	.889	.354	.273	.287	.511	.519	0.000	.520	.522
17	1.000	1.039	.995	1.000	1.000	1.002	1.000	1.000	0.000	1.000	1.044

		Row 2					Row 3				
		x/x_t					x/x_t				
Point	$p_{t,j}/p_\infty$	0.920	1.029	1.251	1.396	1.737	0.920	1.029	1.251	1.396	1.737
1	1.000	1.004	.999	.998	.998	.999	.996	.999	1.001	.998	1.000
2	1.516	.897	.454	.665	.677	.664	.889	.466	.[illegible]	.682	.677
3	1.999	.898	.260	.512	.512	.506	.883	.260	.510	.521	.519
4	3.014	.898	.260	.380	.340	.347	.880	.264	.[illegible]	.334	.372
5	3.487	.896	.263	.337	.270	.301	.880	.265	.330	.282	.277
6	4.069	.893	.264	.217	.324	.273	.877	.269	.301	.358	.286
7	4.551	.893	.264	.089	.323	.257	.879	.265	.[illegible]	.363	.304
8	5.542	.892	.262	.090	.182	.153	.879	.268	.[illegible]	.161	.112
9	7.164	.890	.261	.091	.096	.160	.879	.269	.095	.115	.200
10	8.736	.889	.261	.092	.042	.123	.878	.269	.096	.087	.143
11	10.120	.889	.261	.092	.041	.107	.879	.269	.097	.048	.117
12	8.689	.888	.262	.092	.042	.123	.879	.269	.097	.087	.145
13	5.547	.890	.263	.091	.183	.155	.880	.268	.095	.158	.113
14	4.013	.889	.264	.213	.329	.277	.879	.269	.197	.370	.303
15	3.001	.890	.263	.387	.347	.350	.881	.266	.390	.341	.377
16	2.469	.893	.259	.518	.341	.304	.885	.263	.519	.521	.517
17	1.000	.891	1.001	1.002	1.001	1.030	1.002	1.001	.999	1.002	1.040

TABLE V. - Continued

(b) Configuration W2

		Flap static pressure, $p/p_{t,j}$									
		Row 1					Row 2				
		x/x_t					x/x_t				
Point	$p_{t,j}/p_\infty$	0.851	0.954	1.012	1.056	1.076	0.851	0.954	1.012	1.056	1.076
1	1.000	1.006	1.005	1.003	1.002	1.002	1.001	1.001	1.002	1.317	1.327
2	1.542	.939	.807	.575	.419	.597	.408	.526	.578	.812	.954
3	1.988	.936	.803	.575	.382	.405	.408	.383	.577	.807	.946
4	3.017	.936	.800	.574	.382	.309	.317	.384	.573	.805	.945
5	3.921	.937	.795	.572	.383	.309	.313	.382	.572	.804	.943
6	4.835	.935	.796	.573	.382	.309	.314	.384	.573	.805	.944
7	4.550	.936	.795	.572	.383	.309	.314	.385	.573	.805	.942
8	5.596	.936	.790	.572	.384	.309	.314	.386	.573	.805	.942
9	7.223	.936	.782	.572	.385	.309	.317	.386	.573	.803	.940
10	8.839	.935	.780	.572	.385	.309	.317	.387	.574	.805	.939
11	9.983	.936	.780	.572	.386	.310	.318	.388	.575	.804	.938
12	8.743	.935	.780	.572	.386	.310	.317	.386	.574	.802	.935
13	5.604	.935	.791	.577	.386	.309	.316	.385	.573	.799	.929
14	4.046	.934	.796	.572	.385	.310	.316	.383	.574	.798	.925
15	3.004	.934	.799	.577	.384	.310	.314	.385	.574	.796	.922
16	2.066	.934	.801	.577	.383	.370	.391	.382	.575	.794	.918
17	1.000	.993	.996	.996	.997	.999	1.000	.996	.997	.997	.971

		Sidewall static pressure, $p/p_{t,j}$				
		x/x_t				
Point	$p_{t,j}/p_\infty$	0.886	1.012	1.089	1.226	1.430
1	1.000	1.002	1.005	1.000	1.002	1.000
2	1.512	.908	.536	.650	.663	.670
3	1.988	.910	.529	.518	.504	.512
4	3.017	.912	.530	.387	.332	.344
5	3.921	.911	.530	.240	.285	.282
6	4.835	.912	.530	.1[illegible]	.249	.272
7	4.550	.911	.529	.1[illegible]	.221	.297
8	5.596	.911	.530	.120	.179	.170
9	7.223	.911	.529	.089	.139	.079
10	8.839	.909	.529	.084	.113	.088
11	9.983	.910	.529	.088	.105	.088
12	8.743	.909	.528	.088	.114	.088
13	5.604	.910	.527	.119	.179	.151
14	4.046	.910	.528	.196	.247	.277
15	3.004	.910	.525	.370	.333	.346
16	2.066	.908	.523	.514	.496	.510
17	1.000	.999	.995	1.000	.999	1.001

TABLE V.- Continued

(b) Concluded

Wedge static pressure, $p/p_{t,j}$

Row 1

Point	$p_{t,j}/p_\infty$	x/x_t 0.817	0.920	1.012	1.029	1.082	1.158	1.251	1.396	1.567	1.737
1	1.000	1.000	.997	1.003	1.004	1.002	1.000	1.003	1.000	.996	1.000
2	1.512	.941	.892	.392	.466	.504	.568	.682	0.000	.478	.683
3	1.488	.942	.887	.355	.272	.309	.525	.522	0.000	.524	.527
4	3.617	.942	.892	.383	.275	.226	.249	.389	0.000	.355	.386
5	3.521	.940	.889	.365	.275	.227	.159	.322	0.000	.372	.272
6	4.635	.941	.890	.384	.275	.227	.153	.194	0.000	.211	.209
7	4.556	.940	.888	.367	.273	.227	.154	.091	0.000	.152	.324
8	5.546	.940	.890	.360	.274	.226	.155	.092	0.000	.339	.441
9	7.223	.938	.888	.356	.270	.225	.158	.093	0.000	.142	.490
10	8.839	.938	.888	.355	.269	.224	.156	.094	0.000	.101	.137
11	9.983	.939	.888	.354	.268	.223	.159	.094	0.000	.091	.115
12	8.743	.937	.889	.354	.268	.223	.156	.094	0.000	.102	.140
13	5.664	.939	.891	.358	.270	.226	.156	.092	0.000	.351	.113
14	4.046	.940	.892	.362	.272	.226	.155	.175	0.000	.210	.334
15	3.064	.941	.893	.357	.272	.225	.280	.391	0.000	.305	.389
16	2.666	.941	.889	.351	.270	.290	.520	.518	0.000	.521	.523
17	1.000	1.000	1.001	.997	.995	.998	.999	.996	0.000	1.001	1.000

Row 2

Point	$p_{t,j}/p_\infty$	x/x_t 0.920	1.029	1.251	1.396	1.737
1	1.000	1.001	1.002	1.001	1.000	1.002
2	1.512	.895	.450	.670	.679	.669
3	1.488	.894	.260	.514	.518	.512
4	3.617	.894	.260	.378	.345	.351
5	3.521	.893	.263	.330	.269	.305
6	4.633	.894	.264	.209	.317	.269
7	4.550	.894	.264	.089	.331	.240
8	5.546	.893	.263	.089	.173	.189
9	7.223	.891	.262	.090	.097	.165
10	8.839	.889	.262	.091	.043	.123
11	9.983	.888	.261	.091	.041	.106
12	8.743	.889	.262	.091	.045	.124
13	5.664	.890	.263	.090	.107	.195
14	4.046	.890	.263	.187	.337	.270
15	3.064	.892	.258	.383	.354	.353
16	2.666	.893	.258	.513	.512	.507
17	1.000	.998	.998	.999	1.000	.998

Row 3

Point	$p_{t,j}/p_\infty$	x/x_t 0.920	1.029	1.251	1.396	1.737
1	1.000	1.000	1.002	1.003	1.000	1.000
2	1.512	.890	.478	.667	.688	.679
3	1.488	.891	.261	.524	.524	.522
4	3.617	.896	.266	.395	.337	.384
5	3.521	.895	.263	.323	.278	.284
6	4.633	.892	.268	.195	.384	.264
7	4.550	.894	.265	.097	.384	.316
8	5.546	.893	.265	.095	.174	.111
9	7.223	.892	.263	.094	.114	.192
10	8.839	.890	.262	.093	.094	.139
11	9.983	.889	.261	.093	.091	.116
12	8.743	.890	.261	.093	.095	.142
13	5.664	.893	.264	.095	.151	.113
14	4.046	.892	.264	.176	.342	.333
15	3.064	.895	.263	.309	.343	.385
16	2.666	.897	.259	.519	.521	.518
17	1.000	.997	.998	.999	1.000	1.000

TABLE V.- Continued

(c) Configuration W3

		Flap static pressure, $p/p_{t,j}$									
		Row 1					Row 2				
		x/x_t					x/x_t				
Point	$p_{t,j}/p_\infty$	0.817	0.920	1.044	1.158	1.260	0.817	0.920	1.044	1.158	1.260
1	.999	1.006	1.003	1.007	1.003	1.004	1.002	1.004	1.002	1.005	1.002
2	1.522	.947	.918	.593	.357	.638	.947	.912	.588	.362	.638
3	2.065	.945	.914	.592	.355	.481	.947	.909	.589	.361	.410
4	3.623	.942	.912	.591	.357	.284	.945	.905	.586	.362	.289
5	3.526	.943	.912	.590	.355	.284	.946	.907	.586	.361	.290
6	4.632	.941	.912	.590	.355	.282	.944	.908	.587	.360	.290
7	4.560	.942	.913	.590	.354	.280	.944	.906	.586	.360	.288
8	5.615	.941	.911	.589	.354	.278	.944	.906	.586	.358	.285
9	7.187	.940	.910	.589	.353	.274	.943	.907	.587	.357	.286
10	8.832	.939	.908	.589	.352	.272	.941	.903	.588	.356	.295
11	10.242	.939	.909	.590	.353	.270	.941	.905	.588	.355	.295
12	8.801	.937	.906	.589	.352	.271	.939	.904	.588	.355	.293
13	5.611	.939	.911	.590	.355	.274	.942	.906	.589	.358	.288
14	4.055	.940	.913	.591	.356	.279	.943	.907	.591	.360	.289
15	3.624	.940	.912	.590	.357	.286	.944	.904	.589	.362	.294
16	2.000	.941	.915	.590	.354	.480	.945	.906	.591	.361	.474
17	1.001	.993	.999	.997	.998	.998	.998	.998	.998	.998	.998

		Sidewall static pressure, $p/p_{t,j}$				
		x/x_t				
Point	$p_{t,j}/p_\infty$	0.886	1.035	1.264	1.430	1.601
1	.999	1.000	1.000	1.003	1.001	1.001
2	1.522	.918	.566	.647	.664	.666
3	2.065	.919	.567	.478	.508	.511
4	3.623	.920	.567	.302	.359	.362
5	3.526	.921	.566	.301	.318	.284
6	4.632	.920	.565	.297	.229	.270
7	4.560	.920	.564	.295	.192	.267
8	5.615	.920	.564	.291	.157	.195
9	7.187	.919	.561	.283	.112	.121
10	8.832	.916	.559	.272	.093	.086
11	10.242	.915	.557	.261	.087	.070
12	8.801	.915	.556	.261	.090	.085
13	5.611	.917	.559	.264	.162	.198
14	4.055	.918	.561	.267	.235	.277
15	3.624	.918	.561	.267	.357	.372
16	2.000	.917	.560	.479	.511	.513
17	1.001	1.000	.994	.997	.999	1.000

TABLE V.- Continued

(c) Concluded

		Wedge static pressure, $p/p_{t,j}$									
		Row 1									
		x/x_t									
Point	$p_{t,j}/p_\infty$	0.817	0.920	1.012	1.029	1.082	1.158	1.251	1.396	1.567	1.737
1	.999	.999	1.036	1.011	1.006	1.003	1.003	1.000	1.001	1.000	1.001
2	1.522	.947	.916	.473	.413	.426	.432	.447	.478	.673	.677
3	2.665	.946	.905	.477	.412	.425	.330	.488	.527	.522	.522
4	3.023	.945	.907	.483	.409	.426	.334	.765	.485	.431	.325
5	3.566	.945	.906	.478	.408	.425	.333	.764	.339	.259	.350
6	4.032	.944	.905	.474	.407	.424	.332	.764	.291	.311	.216
7	4.560	.943	.903	.472	.406	.423	.331	.763	.179	.309	.230
8	5.615	.942	.905	.469	.405	.423	.329	.763	.145	.177	.317
9	7.167	.941	.902	.464	.404	.423	.327	.763	.146	.092	.243
10	8.632	.939	.899	.459	.400	.421	.323	.763	.149	.051	.138
11	10.242	.938	.897	.455	.397	.421	.320	.764	.150	.049	.095
12	8.661	.937	.897	.456	.398	.421	.322	.764	.149	.049	.095
13	5.611	.940	.903	.461	.402	.423	.328	.766	.147	.183	.331
14	4.655	.943	.904	.468	.403	.427	.331	.767	.229	.340	.203
15	3.624	.943	.905	.472	.404	.427	.332	.766	.471	.409	.317
16	2.060	.945	.930	.465	.406	.424	.327	.498	.529	.525	.523
17	1.001	1.000	.998	.988	.992	.997	.998	.999	.999	1.000	.999

		Row 2					Row 3				
		x/x_t					x/x_t				
Point	$p_{t,j}/p_\infty$	0.920	1.029	1.251	1.396	1.737	0.920	1.029	1.251	1.396	1.737
1	.999	1.000	1.001	1.003	.997	1.001	1.001	1.005	1.004	1.001	1.000
2	1.522	.910	.393	.641	.665	.663	.905	.396	.650	.674	.673
3	2.665	.911	.392	.482	.510	.535	.898	.394	.492	.523	.515
4	3.023	.910	.397	.266	.383	.337	.895	.396	.268	.450	.317
5	3.526	.913	.397	.264	.315	.307	.898	.398	.268	.327	.379
6	4.032	.909	.396	.264	.231	.260	.894	.397	.267	.234	.211
7	4.560	.908	.395	.264	.181	.212	.894	.396	.266	.182	.229
8	5.615	.907	.394	.261	.135	.231	.895	.394	.265	.151	.306
9	7.167	.905	.394	.261	.131	.174	.894	.397	.265	.147	.232
10	8.632	.902	.390	.260	.130	.144	.891	.393	.266	.146	.095
11	10.242	.901	.388	.260	.132	.110	.891	.395	.269	.147	.095
12	8.661	.900	.389	.261	.133	.135	.890	.396	.267	.148	.136
13	5.611	.904	.390	.263	.141	.232	.893	.399	.267	.155	.326
14	4.655	.906	.393	.265	.221	.248	.894	.401	.268	.224	.201
15	3.624	.907	.393	.266	.403	.336	.895	.403	.268	.457	.309
16	2.060	.908	.386	.481	.512	.507	.899	.398	.500	.524	.517
17	1.001	.999	.998	.997	1.001	.998	.998	.995	.995	.999	.999

APPENDIX

TABLE V.- Continued

(d) Configuration W4

		Flap static pressure, $p/p_{t,j}$									
		Row 1					Row 2				
		x/x_t					x/x_t				
Point	$p_{t,j}/p_\infty$	0.817	0.920	1.044	1.158	1.260	0.817	0.920	1.044	1.158	1.260
1	.999	1.006	1.005	1.001	1.003	1.003	1.001	1.006	1.003	1.002	1.003
2	1.483	.950	.971	.593	.364	.655	.949	.922	.588	.342	.666
3	2.015	.947	.929	.591	.355	.479	.945	.910	.588	.341	.471
4	2.993	.942	.913	.590	.357	.281	.945	.906	.585	.342	.314
5	3.512	.943	.914	.589	.356	.281	.946	.907	.585	.342	.312
6	4.042	.941	.915	.590	.356	.279	.944	.908	.586	.340	.311
7	4.616	.942	.917	.589	.355	.279	.944	.907	.586	.340	.301
8	5.602	.941	.913	.589	.354	.275	.943	.906	.586	.339	.291
9	7.237	.941	.911	.589	.353	.272	.942	.907	.586	.338	.285
10	8.856	.940	.913	.590	.353	.270	.942	.904	.586	.336	.274
11	9.996	.939	.913	.591	.354	.267	.941	.905	.590	.335	.271
12	8.815	.939	.908	.590	.354	.268	.941	.904	.589	.335	.273
13	5.546	.939	.911	.591	.355	.272	.941	.906	.588	.338	.278
14	4.024	.938	.912	.591	.356	.275	.943	.906	.589	.340	.281
15	2.999	.938	.910	.591	.357	.275	.943	.904	.588	.342	.285
16	2.011	.943	.913	.591	.353	.477	.943	.904	.586	.340	.487
17	1.001	.994	.994	.997	.997	.994	.999	.998	.997	.998	.997

		Sidewall static pressure, $p/p_{t,j}$				
		x/x_t				
Point	$p_{t,j}/p_\infty$	0.886	1.012	1.089	1.226	1.430
1	.999	1.003	1.004	1.003	1.000	1.000
2	1.483	.920	.658	.435	.809	.683
3	2.015	.921	.651	.433	.347	.506
4	2.993	.922	.649	.433	.241	.357
5	3.512	.920	.648	.433	.241	.324
6	4.042	.921	.648	.433	.239	.238
7	4.616	.921	.647	.432	.238	.198
8	5.602	.920	.647	.431	.237	.163
9	7.237	.919	.645	.431	.235	.112
10	8.856	.917	.644	.430	.234	.090
11	9.996	.918	.642	.430	.232	.092
12	8.815	.916	.641	.430	.232	.092
13	5.546	.917	.641	.431	.234	.163
14	4.024	.917	.641	.431	.236	.237
15	2.999	.918	.640	.432	.238	.360
16	2.011	.914	.641	.427	.318	.509
17	1.001	.997	.994	.998	.999	1.000

TABLE V.- Continued

(d) Concluded

		Wedge static pressure, $p/p_{t,j}$									
		Row 1									
		x/x_t									
Point	$p_{t,j}/p_\infty$	0.817	0.920	1.012	1.029	1.082	1.158	1.251	1.396	1.567	1.737
1	.999	1.001	.998	1.004	1.004	1.001	1.000	1.000	0.000	.999	1.001
2	1.483	.952	.905	.479	.443	.427	.475	.664	0.000	.688	.694
3	2.015	.951	.901	.476	.442	.426	.328	.445	0.000	.519	.519
4	2.993	.947	.904	.481	.469	.427	.333	.266	0.000	.446	.337
5	3.512	.949	.902	.479	.468	.429	.332	.265	0.000	.259	.387
6	4.042	.946	.903	.477	.466	.424	.332	.265	0.000	.325	.206
7	4.616	.944	.901	.475	.406	.425	.331	.265	0.000	.265	.232
8	5.662	.943	.903	.472	.465	.424	.329	.264	0.000	.190	.316
9	7.237	.942	.901	.468	.403	.423	.326	.263	0.000	.264	.237
10	8.856	.940	.894	.464	.394	.422	.323	.264	0.000	.056	.134
11	9.996	.938	.897	.459	.396	.422	.319	.265	0.000	.049	.094
12	8.813	.938	.898	.459	.396	.422	.321	.265	0.000	.049	.096
13	5.596	.940	.902	.464	.460	.424	.326	.265	0.000	.192	.337
14	4.054	.943	.903	.467	.462	.425	.329	.267	0.000	.344	.260
15	2.999	.944	.905	.471	.402	.427	.331	.269	0.000	.424	.317
16	2.011	.947	.901	.485	.402	.425	.324	.496	0.000	.522	.520
17	1.001	.998	1.002	.995	.995	.998	.999	.999	0.000	1.001	.994

		Row 2					Row 3				
		x/x_t					x/x_t				
Point	$p_{t,j}/p_\infty$	0.920	1.029	1.251	1.396	1.737	0.920	1.029	1.251	1.396	1.737
1	.999	.998	1.002	1.002	1.000	1.001	1.000	1.004	1.002	1.000	1.000
2	1.483	.913	.395	.652	.684	.642	.909	.397	.665	.689	.690
3	2.015	.913	.394	.478	.510	.505	.900	.396	.485	.520	.512
4	2.993	.910	.397	.266	.401	.358	.898	.399	.267	.444	.330
5	3.512	.908	.396	.264	.328	.309	.897	.394	.267	.330	.367
6	4.042	.908	.396	.264	.227	.270	.898	.397	.266	.232	.209
7	4.616	.909	.395	.263	.189	.219	.897	.394	.265	.178	.231
8	5.662	.907	.393	.261	.137	.207	.898	.394	.265	.152	.308
9	7.237	.905	.391	.259	.138	.150	.896	.391	.265	.148	.240
10	8.856	.903	.388	.258	.138	.114	.894	.388	.266	.147	.098
11	9.996	.899	.386	.256	.137	.100	.891	.384	.268	.147	.099
12	8.815	.900	.386	.257	.138	.113	.892	.385	.268	.149	.135
13	5.596	.902	.389	.260	.141	.216	.894	.388	.267	.156	.329
14	4.054	.903	.391	.261	.221	.267	.894	.395	.267	.225	.201
15	2.999	.905	.391	.262	.413	.351	.896	.397	.267	.450	.311
16	2.011	.906	.387	.478	.513	.505	.898	.397	.493	.522	.514
17	1.001	1.000	.996	.996	1.000	.997	.898	.995	.994	1.000	.998

TABLE V.- Continued

(e) Configuration W4(G20)

		Upper flap static pressures, $p/p_{t,j}$					Lower flap static pressures, $p/p_{t,j}$				
				x/x_t					x/x_t		
Point	$p_{t,j}/p_\infty$	0.749	0.880	1.045	1.143	1.245	0.778	0.936	1.041	1.140	1.255
1	.999	1.003	.997	1.001	1.002	1.002	1.001	1.006	1.001	1.002	1.002
2	1.514	.949	.934	.570	.355	.437	.950	.901	.598	.374	.434
3	2.010	.949	.934	.569	.353	.477	.949	.893	.594	.374	.475
4	3.043	.947	.931	.568	.357	.275	.949	.895	.594	.374	.279
5	3.517	.948	.932	.568	.356	.275	.950	.869	.594	.377	.279
6	4.072	.947	.931	.568	.356	.274	.949	.890	.594	.376	.279
7	4.561	.947	.930	.568	.355	.274	.948	.887	.595	.376	.277
8	5.619	.947	.931	.568	.355	.273	.949	.889	.594	.376	.276
9	7.177	.948	.931	.569	.355	.272	.948	.889	.598	.376	.276
10	9.258	.946	.930	.569	.355	.272	.948	.888	.596	.376	.276
11	7.154	.949	.932	.569	.355	.273	.948	.889	.596	.376	.277
12	5.667	.948	.932	.569	.356	.273	.949	.890	.596	.376	.277
13	4.050	.947	.933	.569	.356	.275	.949	.890	.598	.377	.279
14	3.014	.947	.933	.569	.357	.275	.950	.841	.596	.379	.279
15	1.990	.948	.932	.568	.352	.481	.950	.887	.598	.373	.479
16	1.061	.995	1.001	.999	.997	.999	1.000	.994	1.000	.998	.998

		Sidewall static pressures, $p/p_{t,j}$									
		Row 1					Row 2				
				x/x_t					x/x_t		
Point	$p_{t,j}/p_\infty$	0.890	1.034	1.144	1.264	1.440	0.890	1.034	1.144	1.264	1.440
1	.999	1.002	1.001	1.001	1.001	1.000	1.001	1.001	1.000	1.000	.999
2	1.514	.916	.536	.496	.626	.668	.911	.580	.346	.645	.671
3	2.010	.916	.535	.341	.483	.509	.914	.557	.345	.479	.512
4	3.043	.917	.533	.342	.261	.342	.912	.551	.348	.263	.339
5	3.517	.917	.535	.342	.260	.333	.915	.551	.347	.260	.333
6	4.072	.917	.534	.341	.261	.239	.914	.550	.347	.258	.246
7	4.561	.917	.534	.341	.260	.199	.916	.550	.347	.258	.204
8	5.619	.916	.534	.340	.259	.153	.914	.549	.347	.257	.157
9	7.177	.916	.535	.340	.259	.109	.914	.552	.346	.257	.112
10	9.258	.914	.535	.338	.258	.083	.911	.553	.346	.256	.085
11	7.154	.916	.534	.340	.258	.109	.913	.552	.347	.257	.112
12	5.667	.916	.534	.341	.259	.153	.915	.551	.348	.258	.158
13	4.050	.917	.535	.343	.261	.242	.915	.551	.349	.259	.250
14	3.614	.915	.535	.344	.262	.342	.914	.551	.349	.264	.341
15	1.990	.914	.534	.347	.490	.516	.912	.555	.346	.487	.517
16	1.001	.998	.999	1.000	1.000	.999	.998	1.000	1.000	1.000	1.001

APPENDIX

TABLE V.- Concluded

(e) Concluded

		Wedge static pressures, $p/p_{t,j}$									
		Row 1									
		x/x_t									
Point	$p_{t,j}/p_\infty$	0.817	0.920	1.012	1.029	1.082	1.158	1.251	1.396	1.567	1.737
1	.999	1.002	.997	1.003	1.001	1.001	1.001	1.000	1.000	1.001	1.001
2	1.514	.947	.902	.474	.462	.421	.449	.651	.679	.676	.682
3	2.010	.944	.898	.473	.403	.421	.325	.505	.425	.521	.520
4	3.043	.943	.902	.477	.401	.424	.330	.766	.469	.404	.301
5	3.517	.943	.899	.476	.401	.423	.329	.265	.332	.245	.395
6	4.072	.942	.901	.475	.400	.422	.330	.766	.718	.336	.207
7	4.561	.941	.899	.473	.400	.423	.329	.266	.164	.303	.226
8	5.619	.940	.901	.471	.400	.422	.328	.265	.140	.185	.327
9	7.177	.940	.900	.470	.399	.423	.328	.265	.141	.084	.246
10	9.258	.938	.899	.467	.398	.423	.327	.266	.140	.057	.123
11	7.154	.940	.900	.469	.399	.424	.329	.266	.141	.085	.247
12	5.607	.940	.903	.471	.400	.424	.330	.266	.140	.185	.327
13	4.050	.941	.904	.474	.401	.424	.331	.767	.271	.334	.210
14	3.014	.942	.906	.475	.402	.426	.331	.268	.467	.429	.316
15	1.990	.943	.902	.470	.403	.423	.325	.517	.531	.526	.525
16	1.001	.999	1.003	.998	1.000	.999	.999	1.000	1.000	1.000	.999

		Row 2					Row 3				
		x/x_t					x/x_t				
Point	$p_{t,j}/p_\infty$	0.920	1.029	1.251	1.396	1.737	0.920	1.029	1.251	1.396	1.737
1	.999	.997	1.004	.999	1.001	1.001	1.003	1.003	1.000	1.001	1.000
2	1.514	.905	.404	.614	.678	.667	.907	.397	.651	.675	.676
3	2.010	.907	.402	.482	.520	.505	.901	.393	.508	.519	.513
4	3.043	.907	.398	.255	.426	.346	.898	.395	.269	.447	.301
5	3.517	.908	.401	.256	.333	.310	.899	.396	.271	.330	.405
6	4.072	.906	.402	.256	.234	.264	.899	.397	.270	.226	.200
7	4.561	.907	.401	.255	.178	.216	.901	.396	.271	.173	.218
8	5.619	.905	.400	.255	.134	.212	.899	.395	.270	.147	.301
9	7.177	.905	.400	.255	.132	.151	.902	.395	.270	.142	.232
10	9.258	.901	.399	.254	.129	.109	.900	.395	.269	.137	.078
11	7.154	.904	.399	.255	.131	.153	.901	.395	.269	.142	.233
12	5.607	.906	.400	.255	.136	.212	.901	.395	.270	.147	.300
13	4.050	.907	.400	.257	.235	.265	.901	.397	.271	.228	.204
14	3.014	.908	.396	.257	.425	.354	.900	.394	.270	.445	.315
15	1.996	.910	.398	.491	.525	.510	.900	.397	.521	.524	.518
16	1.001	1.002	.996	1.000	.999	.999	.996	.998	.999	.999	1.000

REFERENCES

1. Schmeer, James W.; Lauer, Rodney F., Jr.; and Berrier, Bobby L.: Performance of Blow-in-Door Ejector Nozzles Installed on a Twin-Jet Variable-Wing-Sweep Fighter Airplane Model. NASA TM X-1383, 1967.

2. Reubush, David E.; and Mercer, Charles E.: Effects of Nozzle Interfairing Modifications on Longitudinal Aerodynamic Characteristics of a Twin-Jet, Variable-Wing-Sweep Fighter Model. NASA TN D-7817, 1975.

3. Maiden, Donald L.; and Berrier, Bobby L.: Effect of Airframe Modifications on Longitudinal Aerodynamic Characteristics of a Fixed-Wing, Twin-Jet Fighter Airplane Model. NASA TM X-2523, 1972.

4. Maiden, Donald L.; and Petit, John E.: Investigation of Two-Dimensional Wedge Exhaust Nozzles for Advanced Aircraft. J. Aircr., vol. 13, no. 10, Oct. 1976, pp. 809-816.

5. Martens, Richard E.: F-15 Nozzle/Afterbody Integration. J. Aircr., vol. 13, no. 5, May 1976, pp. 327-333.

6. Capone, Francis J.: Summary of Propulsive-Lift Research in the Langley 16-Ft Transonic Tunnel. J. Aircr., vol. 13, no. 10, Oct. 1976, pp. 803-808.

7. Hiley, P. E.; Wallace, H. W.; and Booz, D. E.: Nonaxisymmetric Nozzles Installed in Advanced Fighter Aircraft. J. Aircr., vol. 13, no. 12, Dec. 1976, pp. 1000-1006.

8. Sedgwick, T. E.: Investigation of Nonaxisymmetric Two-Dimensional Nozzles Installed in Twin-Engine Tactical Aircraft. AIAA Paper No. 75-1319, Sept.-Oct. 1975.

9. Berrier, Bobby L.; Palcza, J. Lawrence; and Richey, G. Keith: Nonaxisymmetric Nozzle Technology Program - An Overview. AIAA Paper 77-1225, Aug. 1977.

10. F-15 2-D Nozzle System Integration Study. Volume I - Technical Report. NASA CR-145295, 1978.

11. Stevens, H. L.: F-15/Nonaxisymmetric Nozzle System Integration Study Support Program. NASA CR-135252, 1978.

12. Bergman, D.; Mace, J. L.; and Thayer, E. B.: Non-Axisymmetric Nozzle Concepts for an F-111 Test Bed. AIAA Paper No. 77-841, July 1977.

13. Wasson, H. R.; and Hall, G. R.: Results of a Feasibility Study to Add Canards and ADEN Nozzle to the YF-17. AIAA Paper 77-1227, Aug. 1977.

14. Capone, Francis J.: Static Performance of Five Twin-Engine Nonaxisymmetric Nozzles With Vectoring and Reversing Capability. NASA TP-1224, 1978.

15. Lander, J. A.; and Palcza, J. Lawrence: Exhaust Nozzle Deflector Systems for V/STOL Fighter Aircraft. AIAA Paper No. 74-1169, Oct. 1974.

16. Lander, J. A.; Nash, D. O.; and Palcza, J. Lawrence: Augmented Deflector Exhaust Nozzle (ADEN) Design for Future Fighters. AIAA Paper No. 75-1318, Sept.-Oct. 1975.

17. Nash, D. O.; Wakeman, T. G.; and Palcza, J. L.: Structural and Cooling Aspects of the ADEN Nonaxisymmetric Exhaust Nozzle. Paper No. 77-GT-110, American Soc. Mech. Eng., Mar. 1977.

18. Schnell, W. C.; Grossman, R. L.; and Hoff, G. E.: Comparison of Non-Axisymmetric & Axisymmetric Nozzles Installed on a V/STOL Fighter Model. [Preprint] 770983, Soc. Automot. Eng., Nov. 1977.

19. Maiden, Donald L.: Performance of an Isolated Two-Dimensional Variable-Geometry Wedge Nozzle With Translating Shroud and Collapsing Wedge at Speeds Up to Mach 2.01. NASA TN D-7906, 1975.

20. Maiden, Donald L.: Performance of an Isolated Two-Dimensional Wedge Nozzle With Fixed Cowl and Variable Wedge Centerbody at Mach Numbers Up to 2.01. NASA TN D-8218, 1976.

21. Capone, Francis J.; and Maiden, Donald L.: Performance of Twin Two-Dimensional Wedge Nozzles Including Thrust Vectoring and Reversing Effects at Speeds Up to Mach 2.20. NASA TN D-8449, 1977.

22. Goetz, Gerald F.; Young, John H.; and Palcza, J. Lawrence: A Two-Dimensional Airframe Integrated Nozzle Design With Inflight Thrust Vectoring and Reversing Capabilities for Advanced Fighter Aircraft. AIAA Paper No. 76-626, July 1976.

23. Pendergraft, O. C.: Comparison of Axisymmetric and Nonaxisymmetric Nozzles Installed on the F-15 Configuration. AIAA Paper No. 77-842, July 1977.

24. Carson, George T., Jr.; and Mason, Mary L.: Experimental and Analytical Investigation of a Nonaxisymmetric Wedge Nozzle at Static Conditions. NASA TP-1188, 1978.

25. Berrier, B. L.; and Re, R. J.: A Review of Thrust-Vectoring Schemes for Fighter Aircraft. AIAA Paper No. 78-1023, July 1978.

26. Sutton, George P.: Rocket Propulsion Elements. Second Edition. John Wiley & Sons, Inc., c.1961.

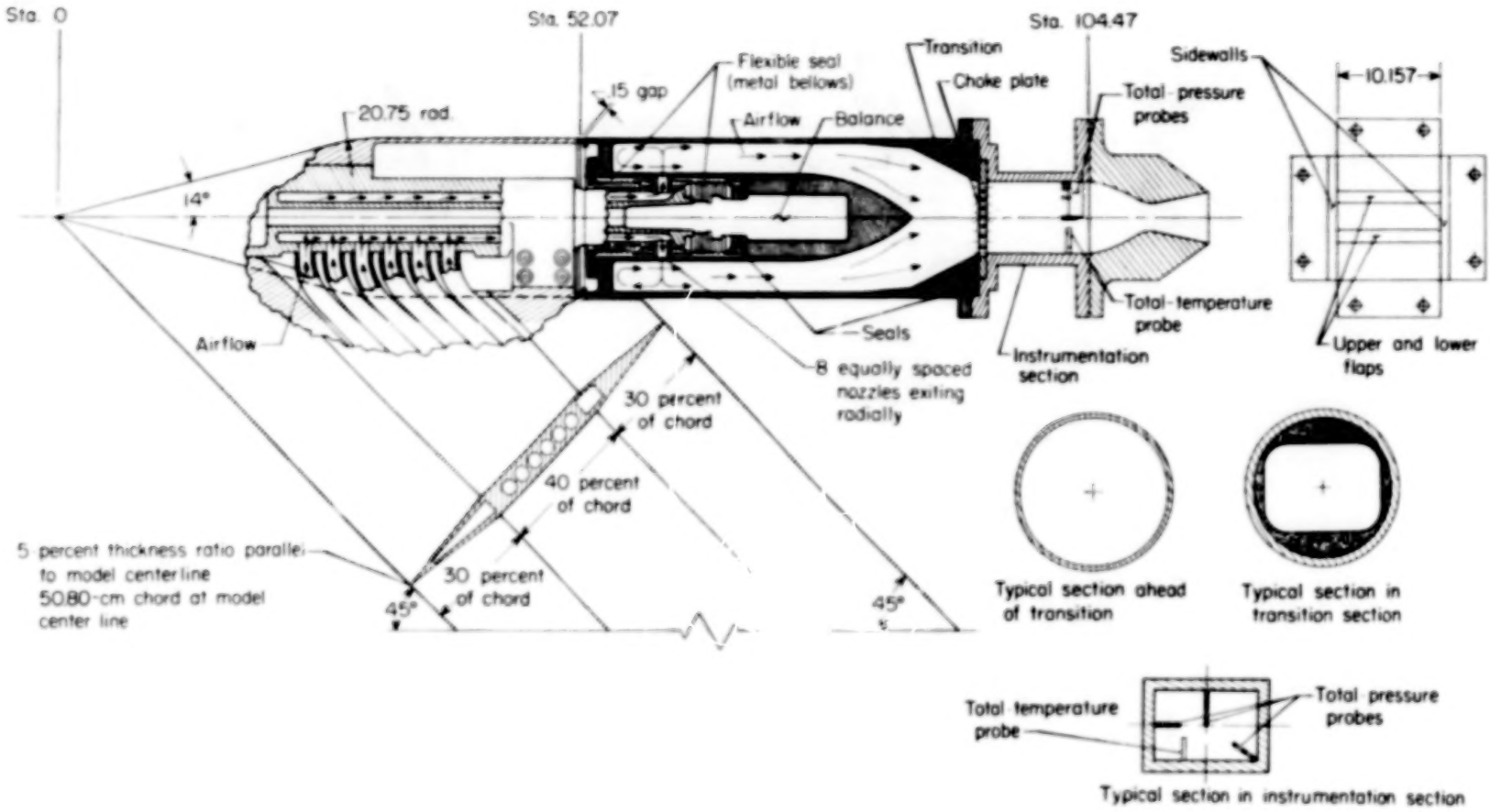

Figure 1.- Sketch of air-powered nacelle model with typical nozzle configuration installed. All dimensions are in centimeters unless otherwise noted.

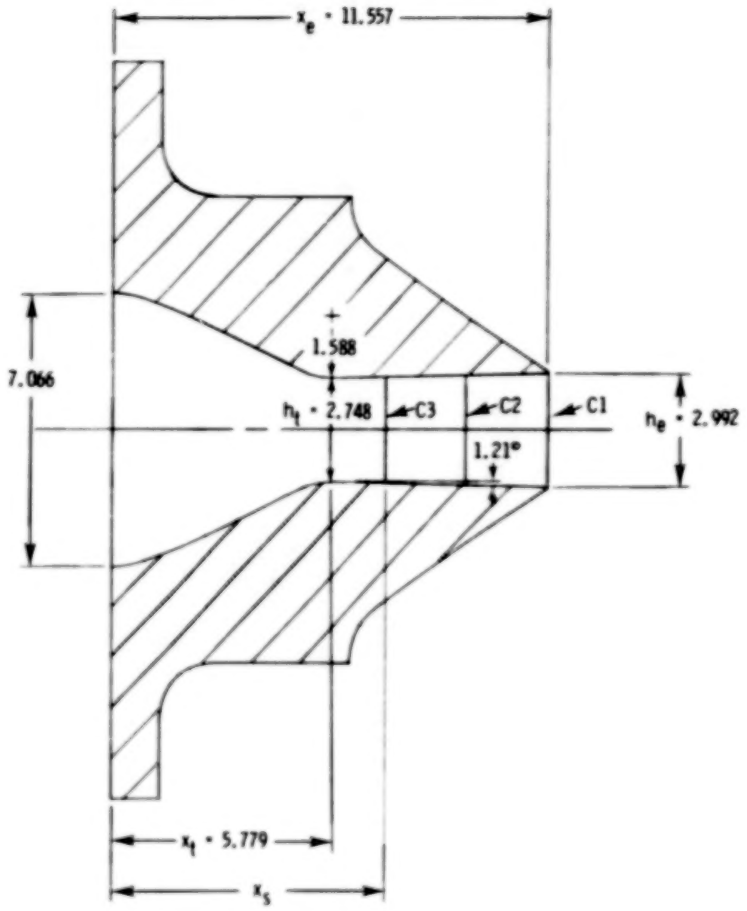

Configuration	A_t, cm^2	A_e, cm^2	p, deg.	A_e/A_t	AR	x_s
C1	27.911	30.390	1.21	1.089	3.696	11.557
C2	↓	↓	↓	↓	↓	9.398
C3	↓	↓	↓	↓	↓	7.239

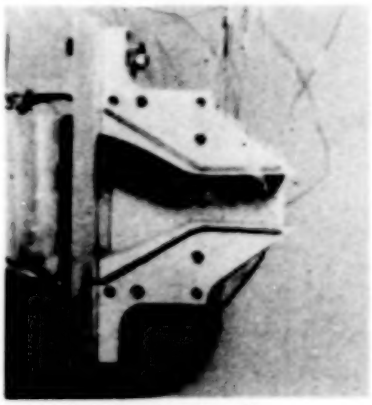

Configuration C1

Configuration C2

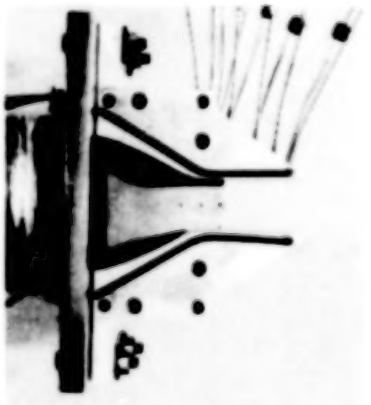

Configuration C3

L-79-155

(a) Configurations C1, C2, and C3.

Figure 2.- Sketches and photographs of nonaxisymmetric convergent-divergent nozzle configurations showing important dimensions. All dimensions are in centimeters unless otherwise noted.

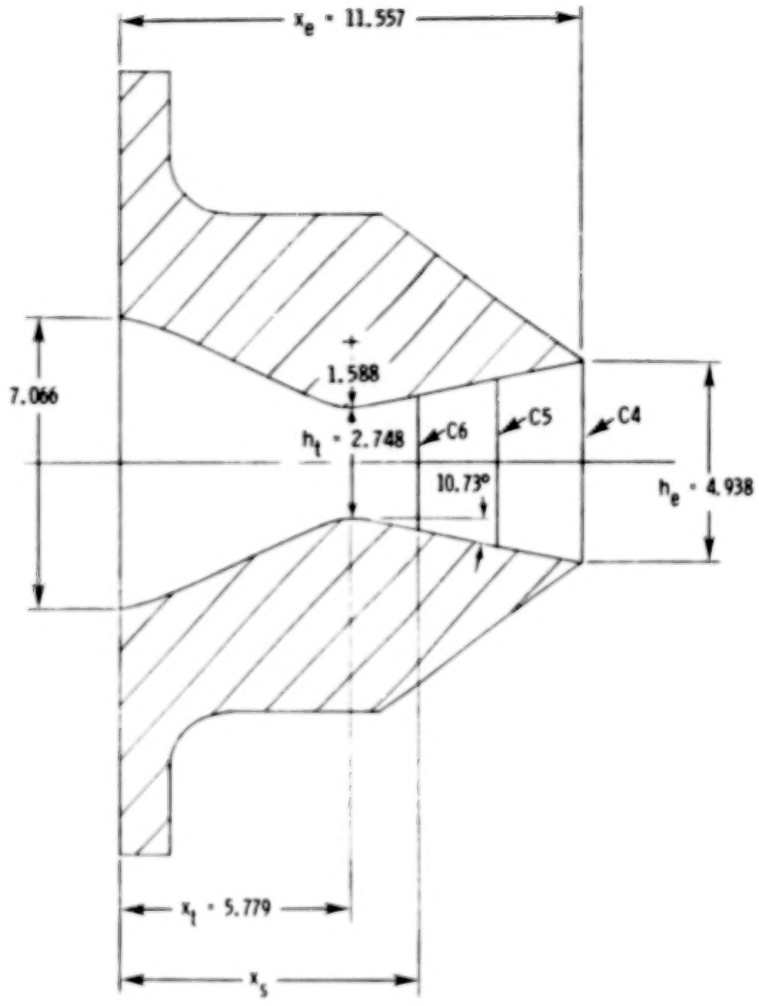

Configuration	A_t, cm^2	A_e, cm^2	ø, deg.	A_e/A_t	AR	x_s
C4	27.911	50.155	10.73	1.797	3.696	11.557
C5	↓	↓	↓	↓	↓	9.398
C6						7.239

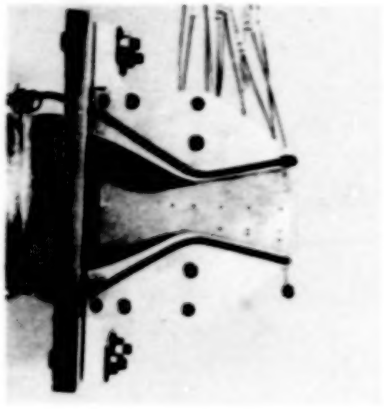

Configuration C4

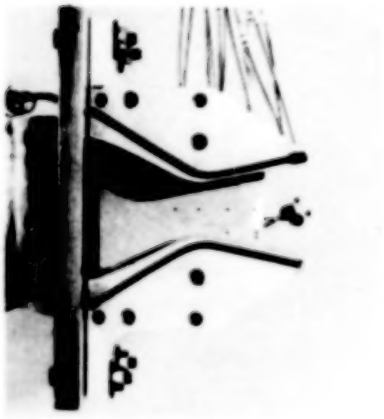

Configuration C5

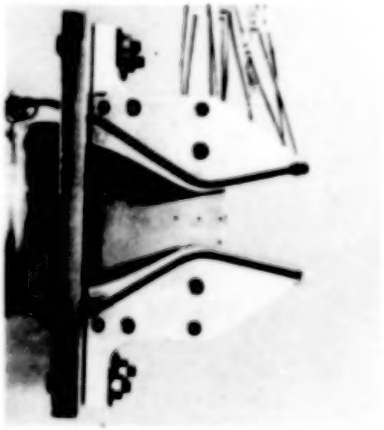

Configuration C6

L-79-156

(b) Configurations C4, C5, and C6.

Figure 2.- Continued.

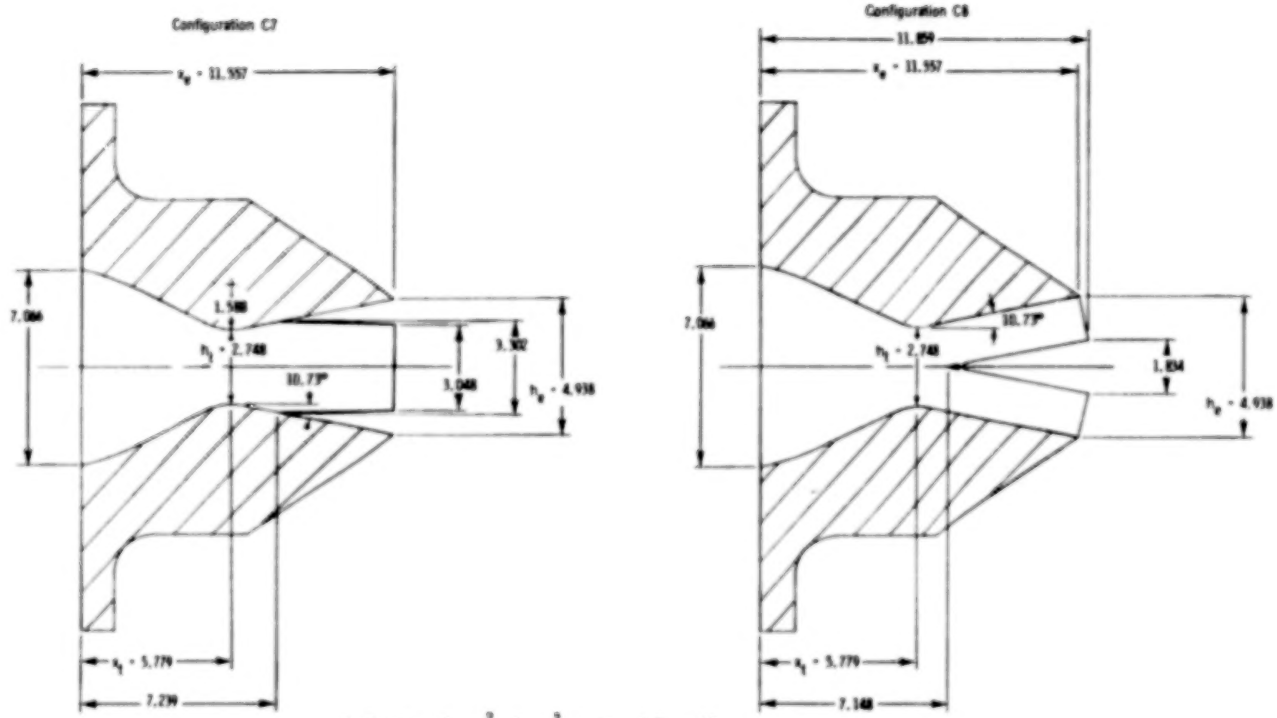

Configuration	A_t, cm^2	A_p, cm^2	β, deg	A_p/A_t	AR
C7	↓	50.155	10.77	1.797	3.696
C8	↓	↓	↓	↓	↓

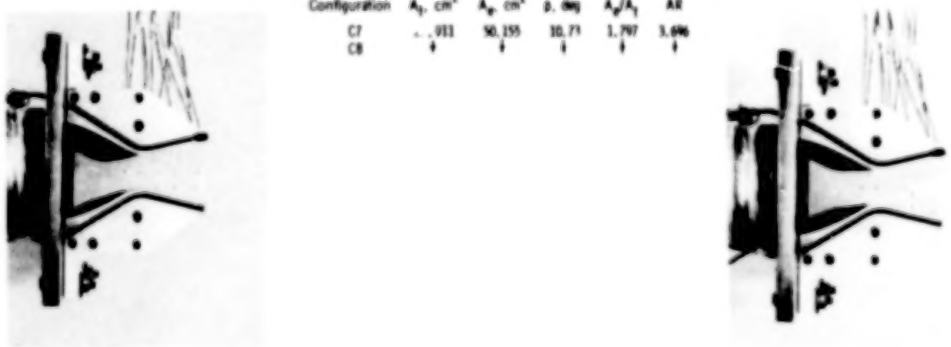

L-79-157

(c) Configurations C7 and C8.

Figure 2.- Continued.

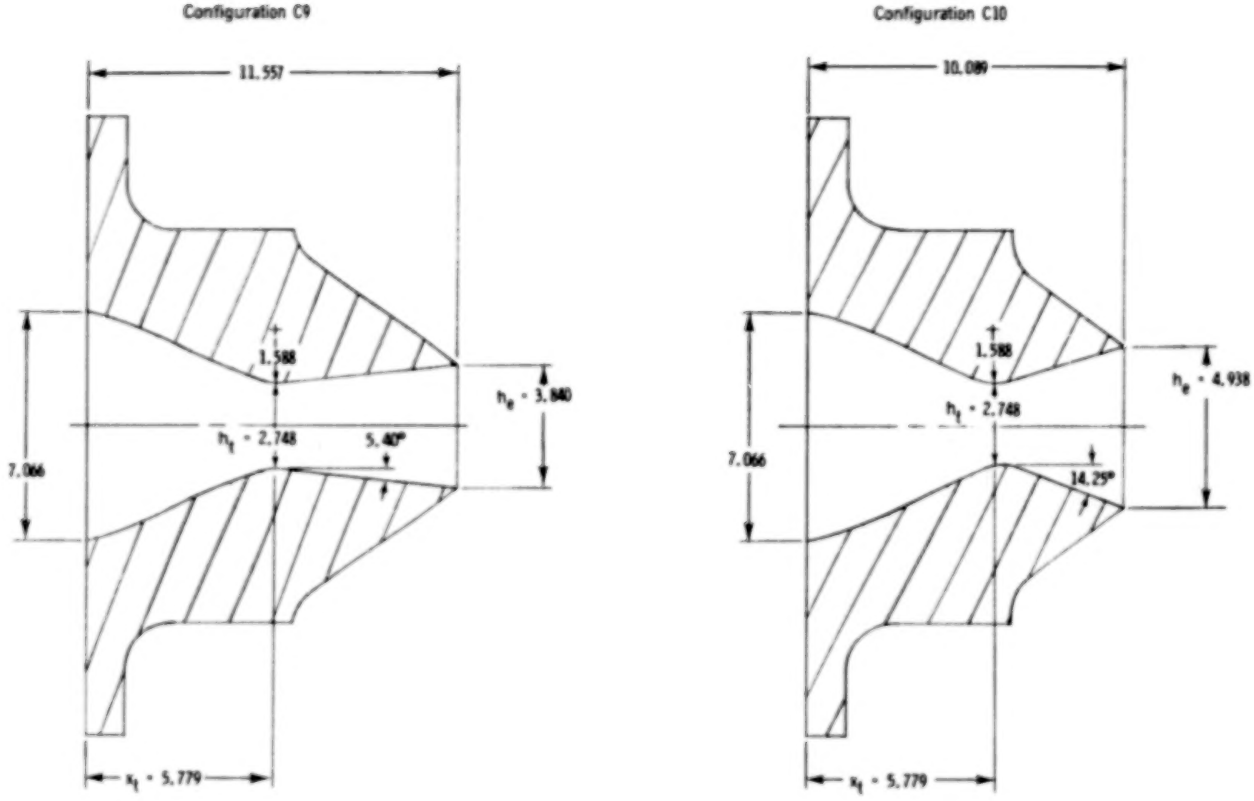

Configuration	A_t, cm^2	A_e, cm^2	ρ, deg	A_e/A_t	AR
C9	27.911	39.003	5.40	1.397	3.696
C10	↓	50.155	14.25	1.797	↓

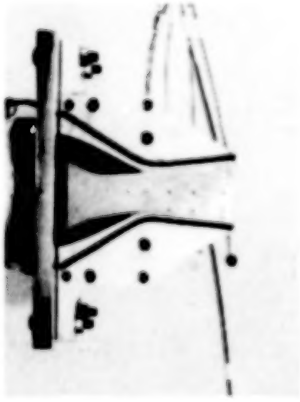

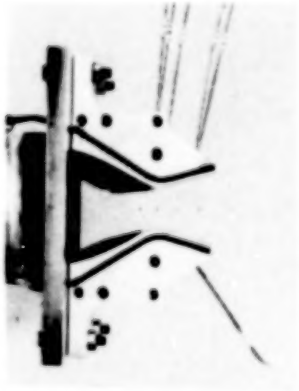

L-79-158

(d) Configurations C9 and C10.

Figure 2.- Continued.

Configuration C11

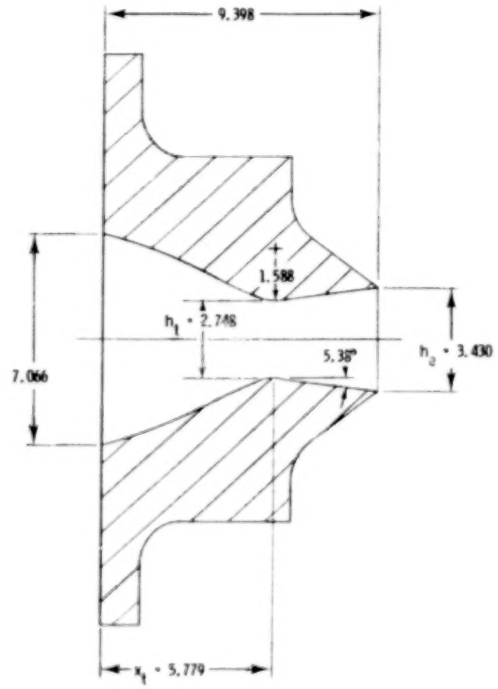

Configurations C12 and C13

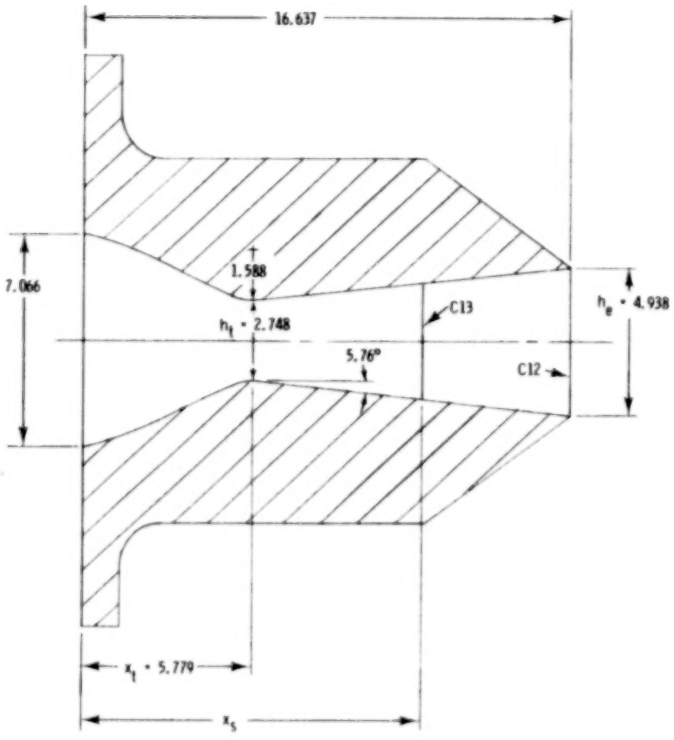

Configuration	A_t, cm^2	A_e, cm^2	ρ, deg	A_e/A_t	AR	x_s
C11	27.911	34.839	5.38	1.248	3.696	9.398
C12	↓	50.155	5.76	1.797	↓	16.637
C13	↓	↓	↓	↓	↓	11.557

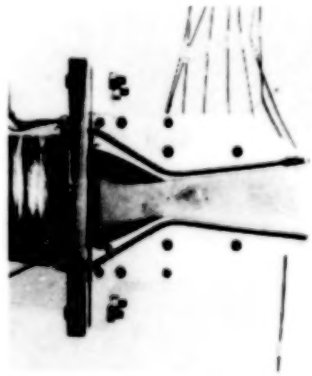

Configuration C12

L-79-159

(e) Configurations C11, C12, and C13.

Figure 2.- Concluded.

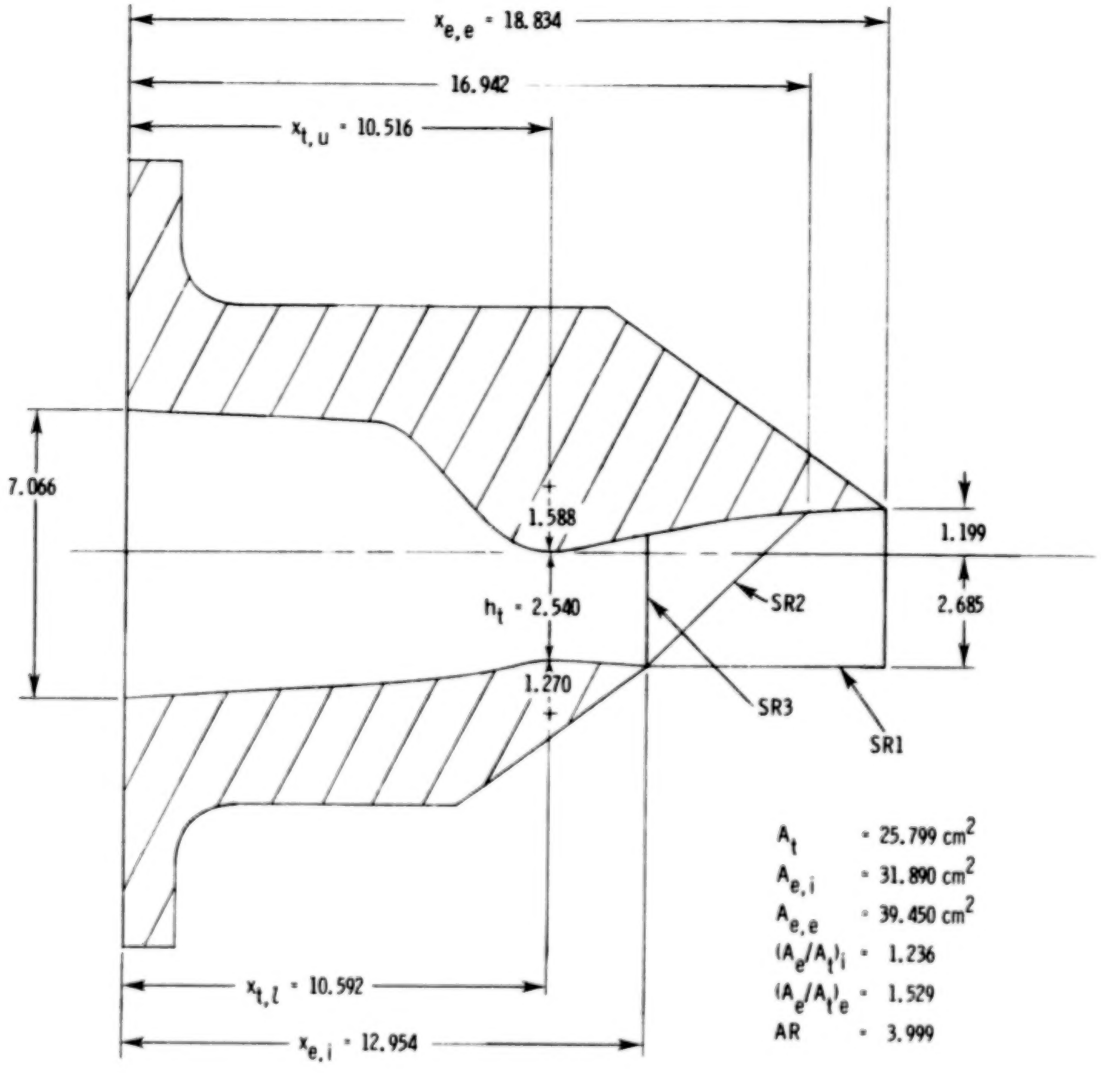

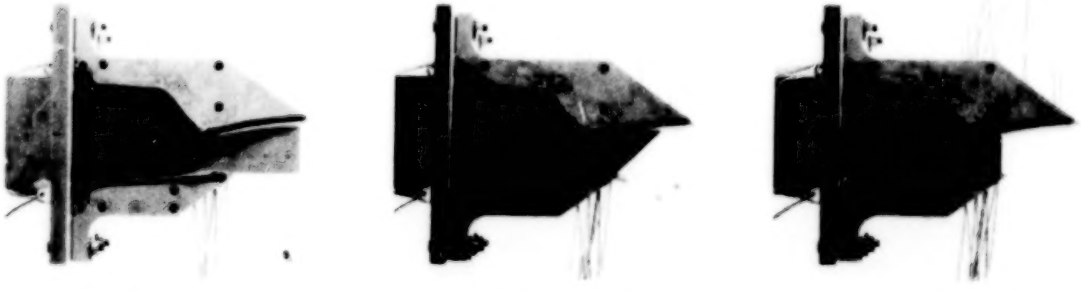

Configuration SR1 Configuration SR2 Configuration SR3

L-79-160

(a) Configurations SR1, SR2, and SR3.

Figure 3.- Sketches and photographs of single-ramp expansion nozzle configurations showing important dimensions. All dimensions are in centimeters unless otherwise noted.

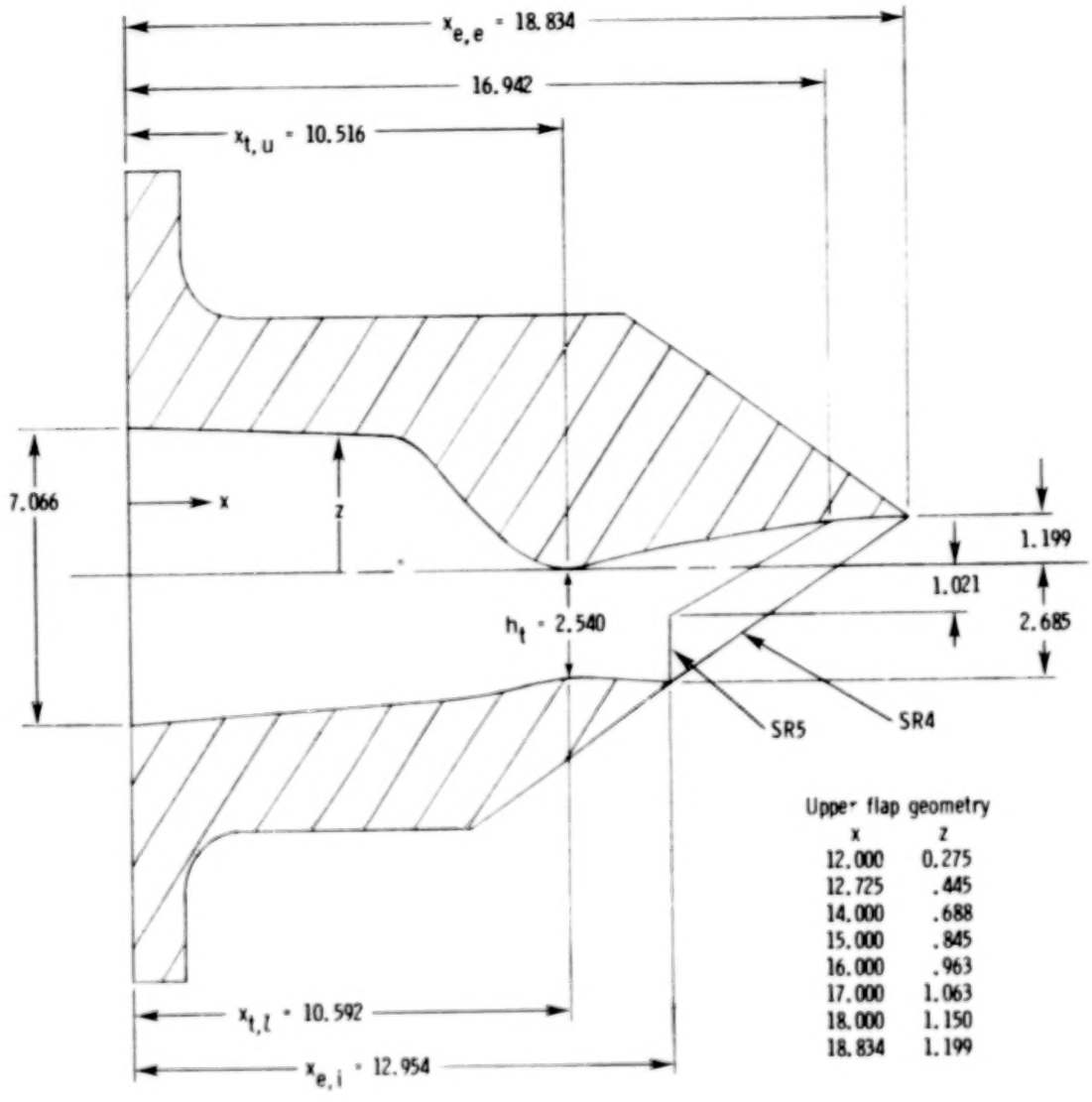

Upper flap geometry

x	z
12.000	0.275
12.725	.445
14.000	.688
15.000	.845
16.000	.963
17.000	1.063
18.000	1.150
18.834	1.199

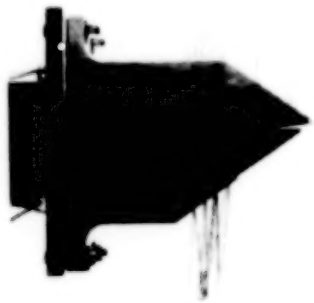

Configuration SR4

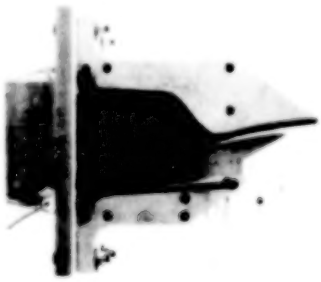

Configuration SR5

A_t = 25.799 cm^2
$A_{e,i}$ = 31.890 cm^2
$A_{e,e}$ = 39.450 cm^2
$(A_e/A_t)_i$ = 1.236
$(A_e/A_t)_e$ = 1.529
AR = 3.999

L-79-161

(b) Configurations SR4 and SR5.

Figure 3.- Concluded.

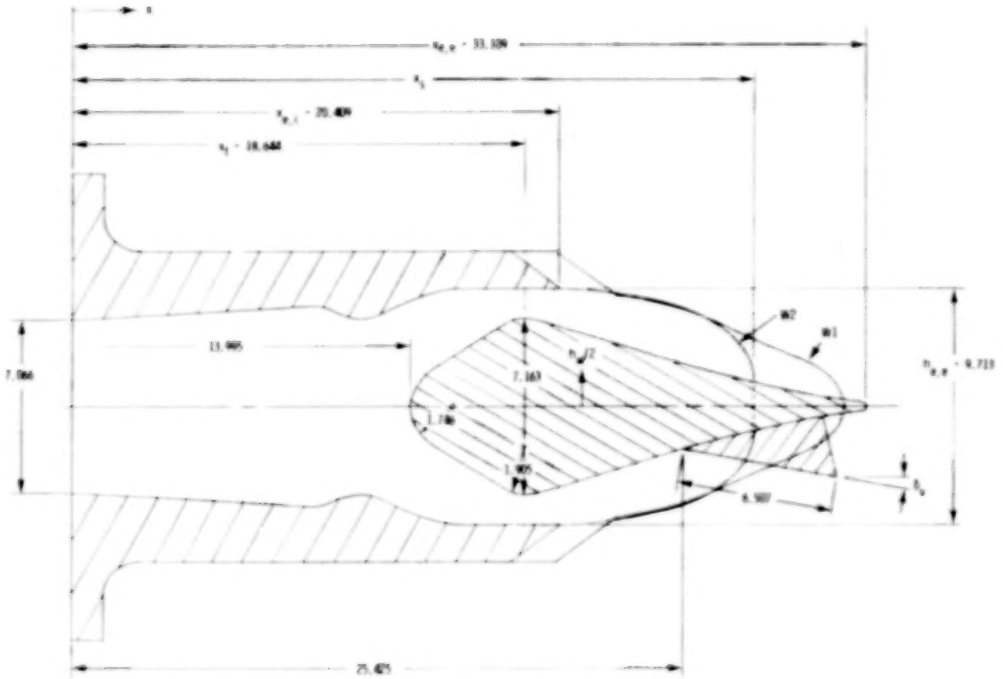

Wedge coordinates

x	$h_w/2$
13.995	0.000
16.535	2.900
18.077	3.561
19.177	3.536
20.168	3.325
21.750	2.825
23.330	2.329
25.500	1.548
27.965	1.067
30.500	0.600
33.109	0.000

Configuration	A_3, cm^2	$A_{e,f}$, cm^2	$A_{e,p}$, cm^2	$(A_p/A_3)_i$	$(A_p/A_3)_p$	AR	x_3, cm	δ_v, deg
W1	25.900	31.598	98.695	1.229	1.809	3.981	32.207	off
W1V5								5
W1V10								10
W1V20								20
W2							28.473	off

Configuration W1

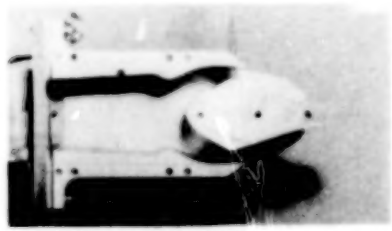
Configuration W2

L-79-162

(a) Configurations W1 and W2 with and without vector flap.

Figure 4.- Sketches and photographs of wedge nozzle configurations showing important dimensions. All dimensions are in centimeters unless otherwise noted.

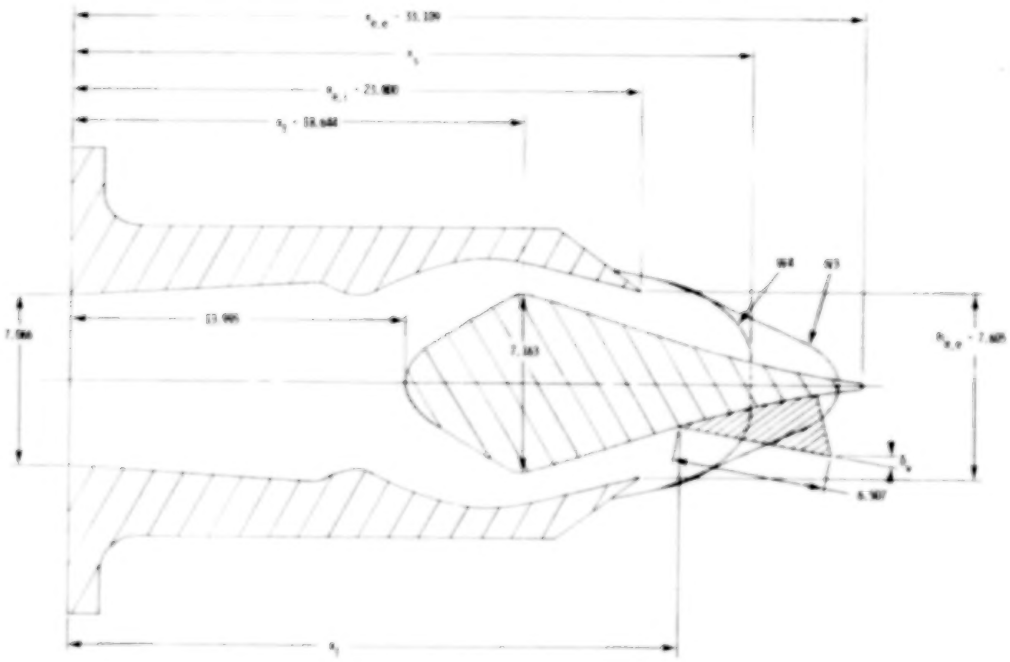

Wedge coordinates identical to W1 and W2

Configuration	A_j, cm^2	$A_{x,i}$, cm^2	$A_{x,e}$, cm^2	$(A_x/A_j)_i$	$(A_x/A_j)_e$	AR	x_v, cm	x_v, cm	δ_v, deg
W3	25.900	31.999	77.284	1.235	2.985	3.983	32.207		
W3V5								25.425	5
W3V10									10
W3V20									20
W4							78.473		
W4V5								25.425	5
W4V10									10
W4V20									20
W4FV5								23.467	3.5

Configuration W3

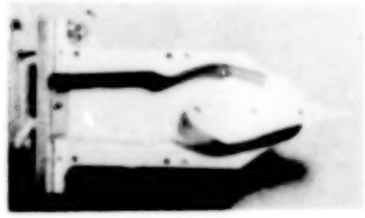

Configuration W4

L-79-163

(b) Configurations W3 and W4 with and without vector flap.

Figure 4.- Continued.

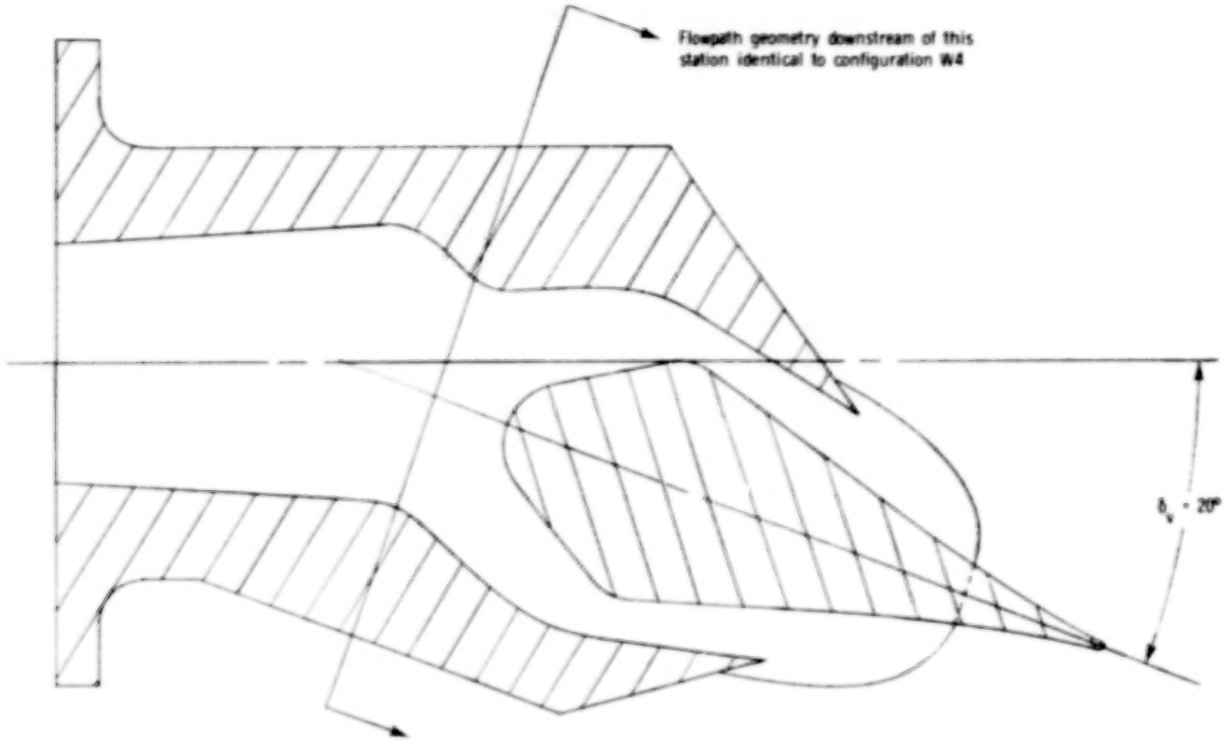

Configuration W4G20

L-79-164

(c) Gimbal configuration W4(G20).

Figure 4.- Concluded.

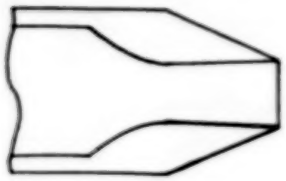

A_e/A_t = 1.089, AR = 3.696, ρ = 1.21°

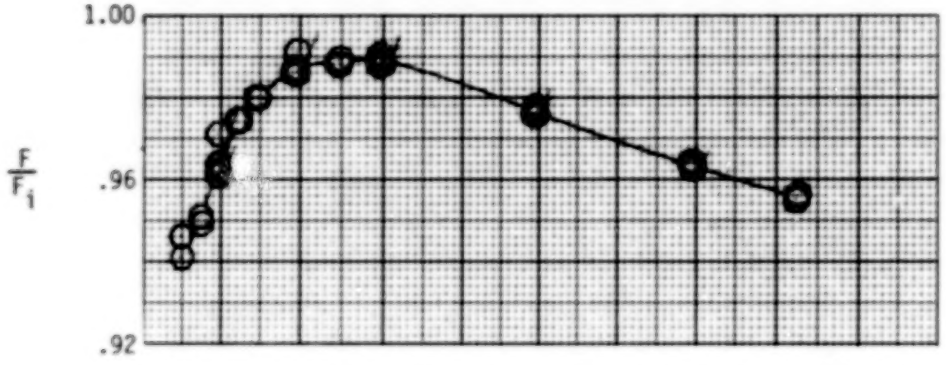

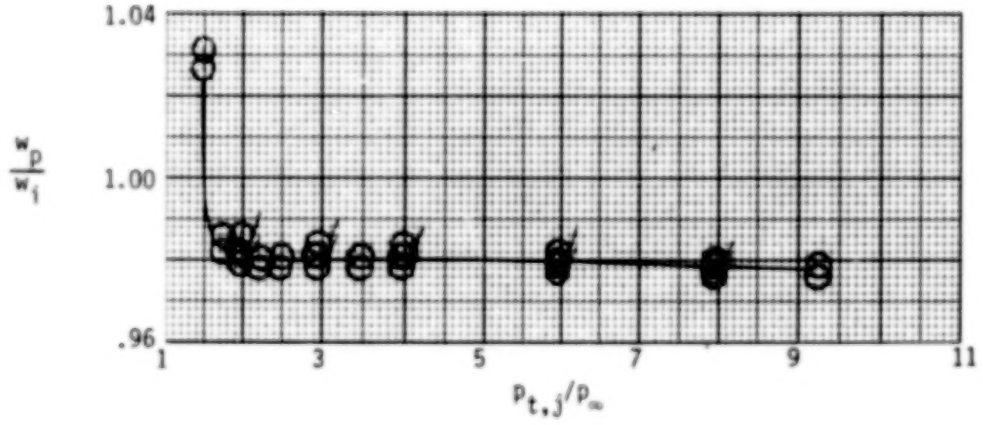

(a) Configuration C1.

Figure 5.- Variation of nozzle thrust ratio and discharge coefficient with nozzle pressure ratio for 2-D convergent-divergent nozzles. Flagged symbols indicate data taken as nozzle pressure ratio was decreasing.

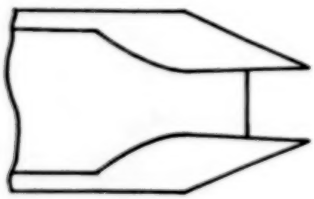

A_e/A_t = 1.089, AR = 3.696, ρ = 1.21°

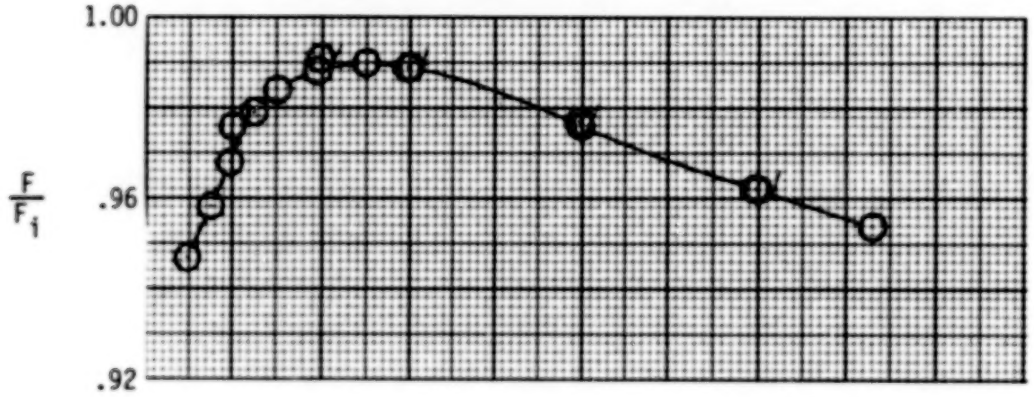

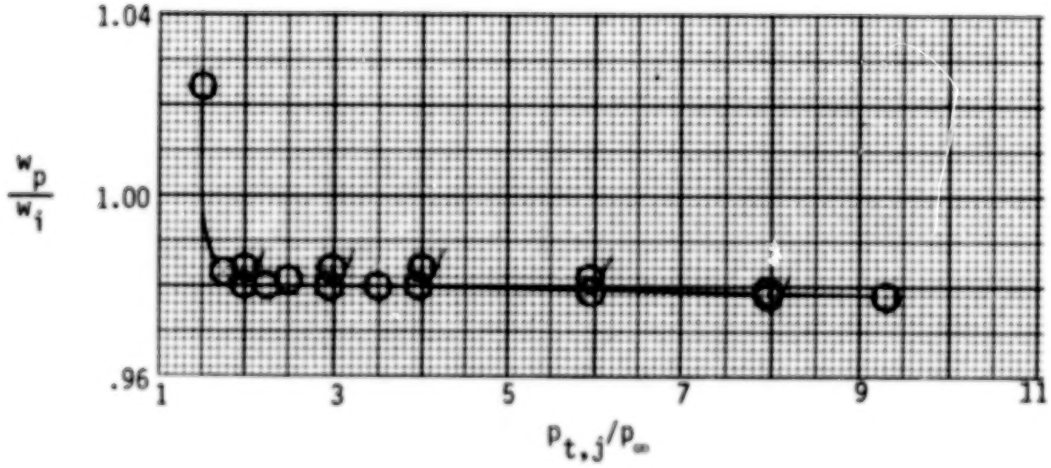

(b) Configuration C2.

Figure 5.- Continued.

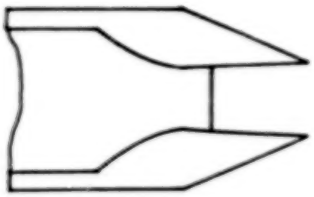

A_e/A_t = 1.089, AR = 3.696, ρ = 1.21°

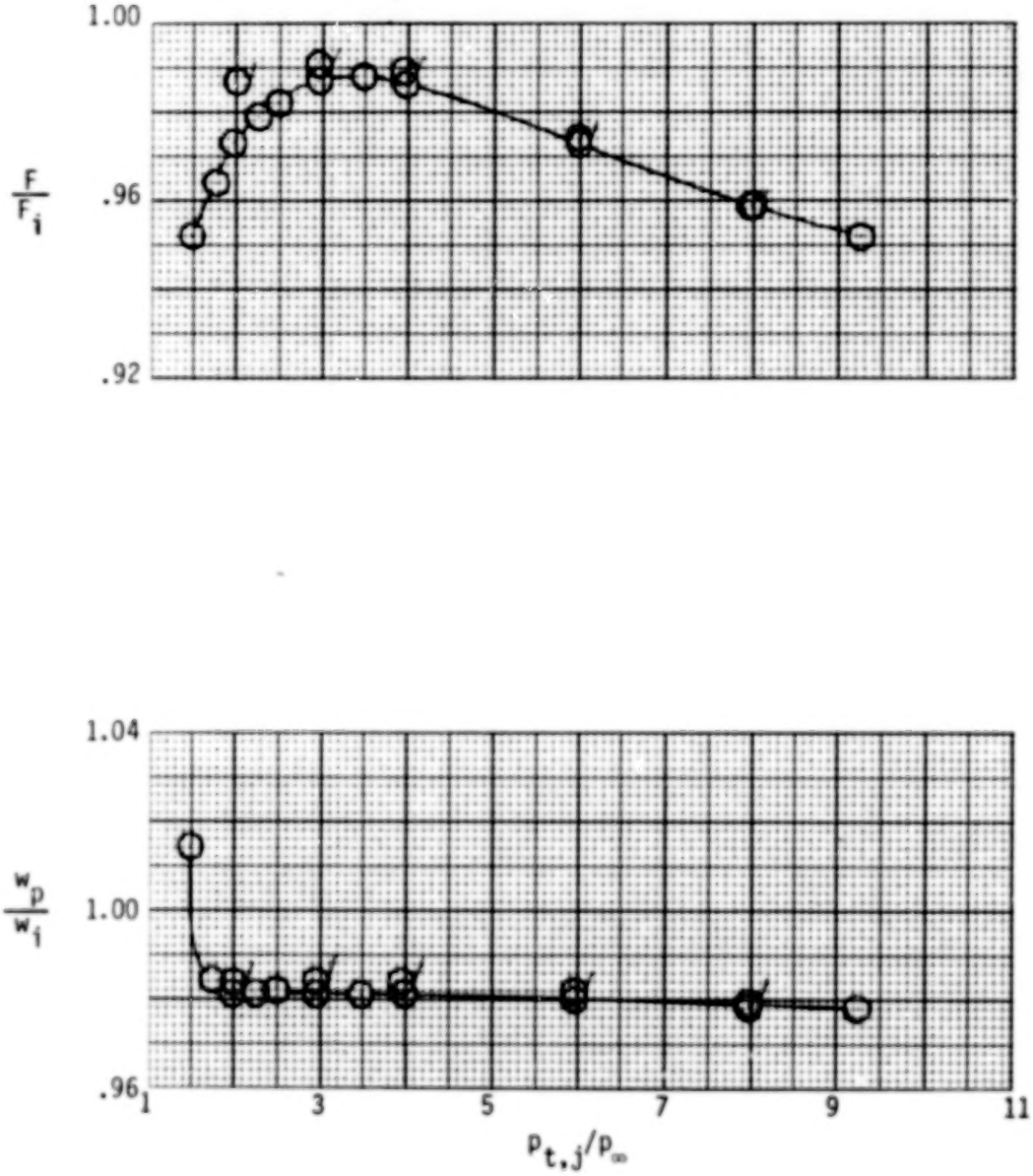

(c) Configuration C3.

Figure 5.- Continued.

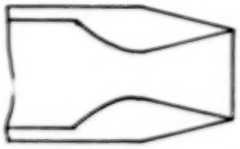

A_e/A_t = 1.797, AR = 3.696, ρ = 10.73°

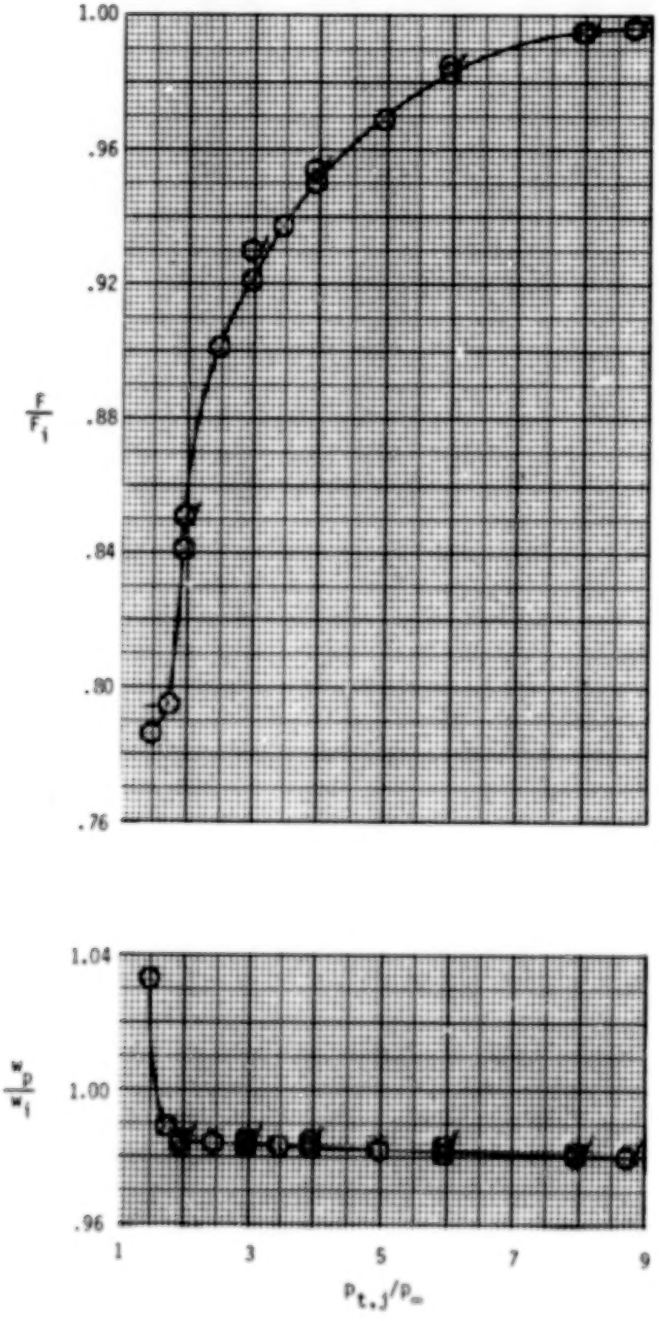

(d) Configuration C4.

Figure 5.- Continued.

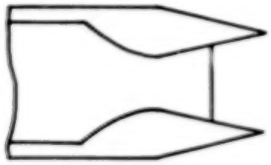

A_e/A_t = 1.797, AR = 3.696, ρ = 10.73°

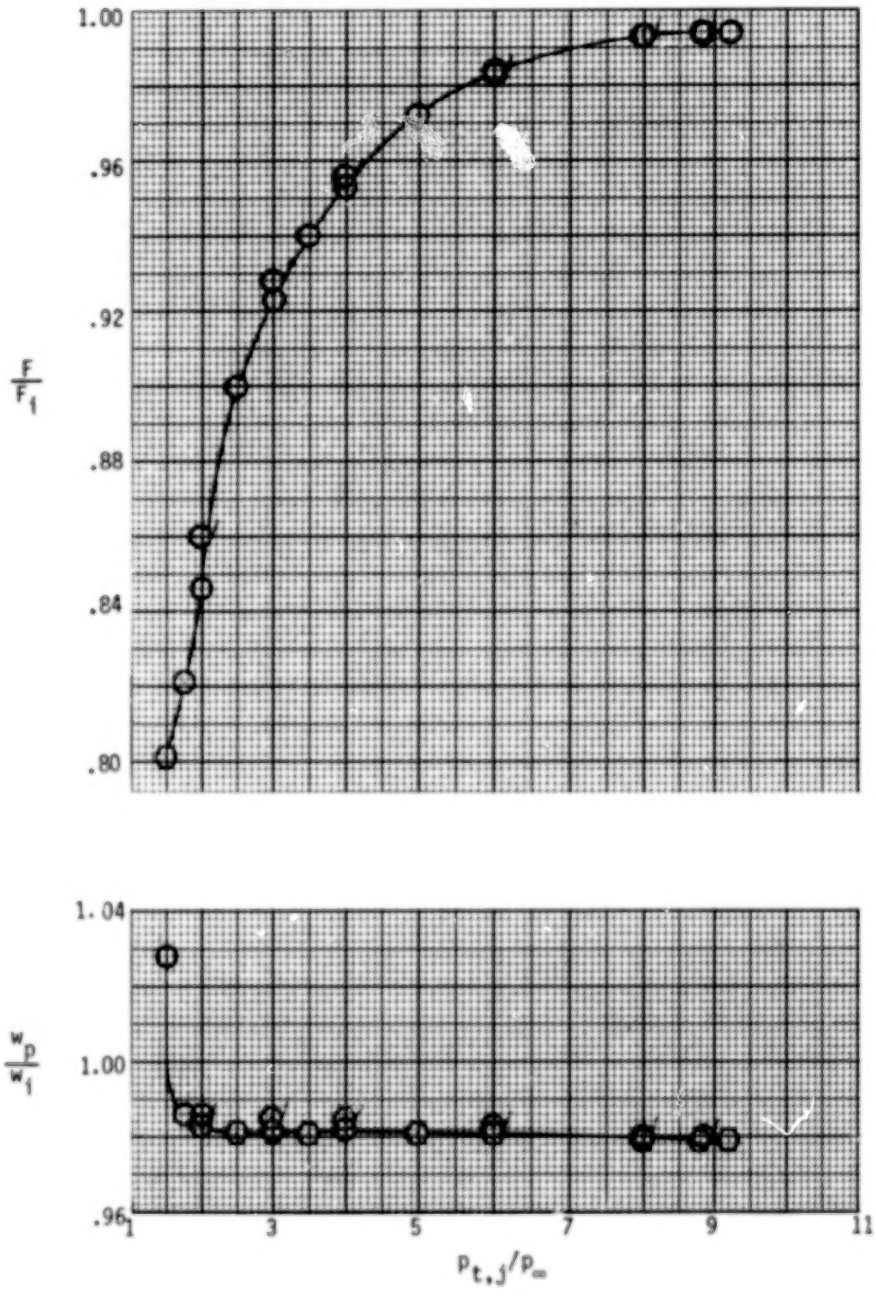

(e) Configuration C5.

Figure 5.- Continued.

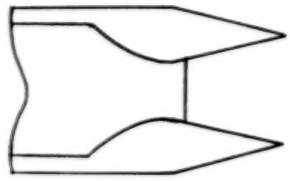

A_e/A_t = 1.797, AR = 3.696, ρ = 10.73°

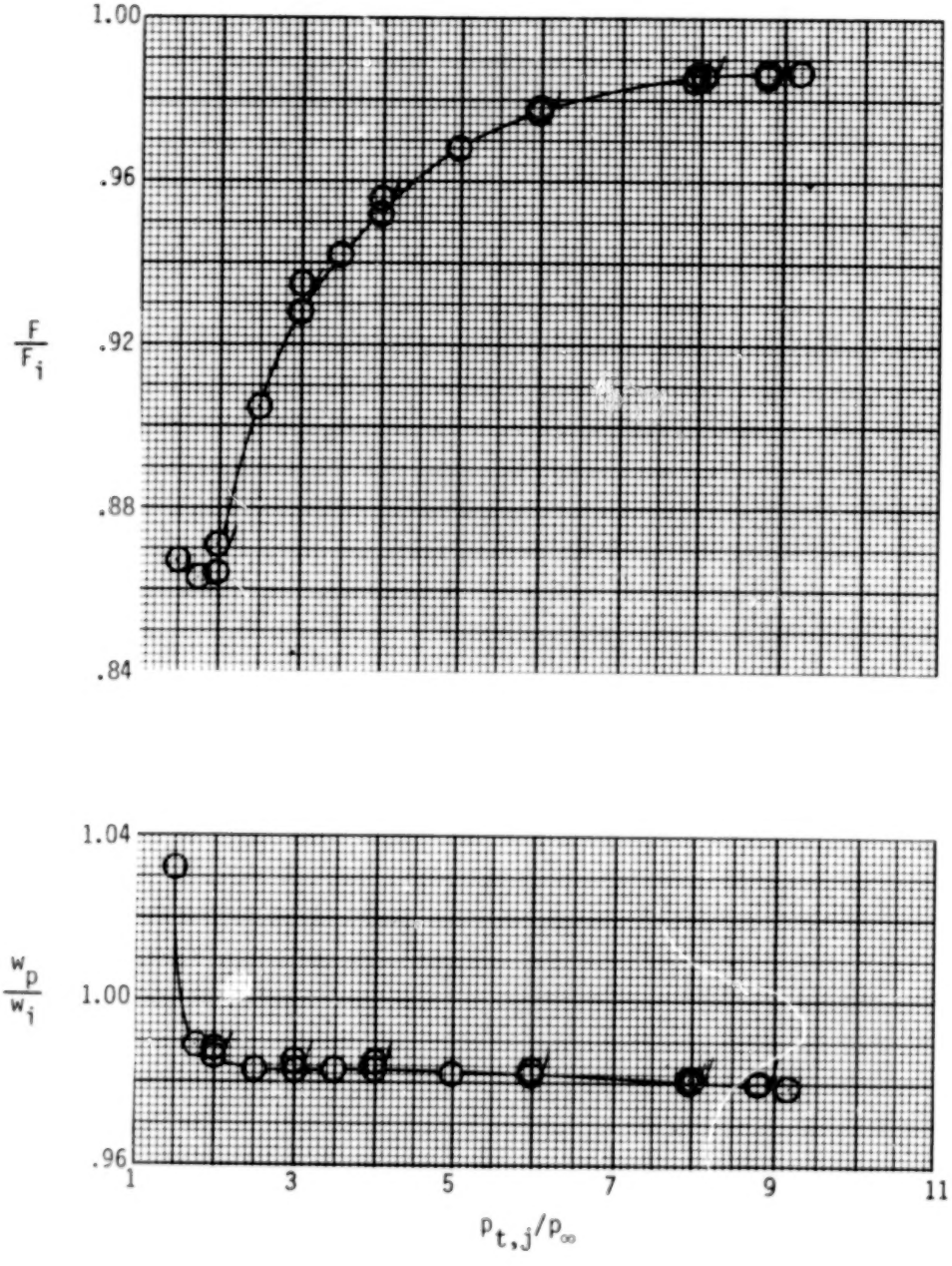

(f) Configuration C6.

Figure 5.- Continued.

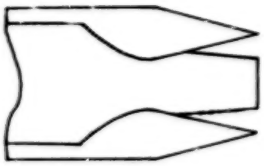

A_e/A_t = 1.797, AR = 3.696, ρ = 10.73°

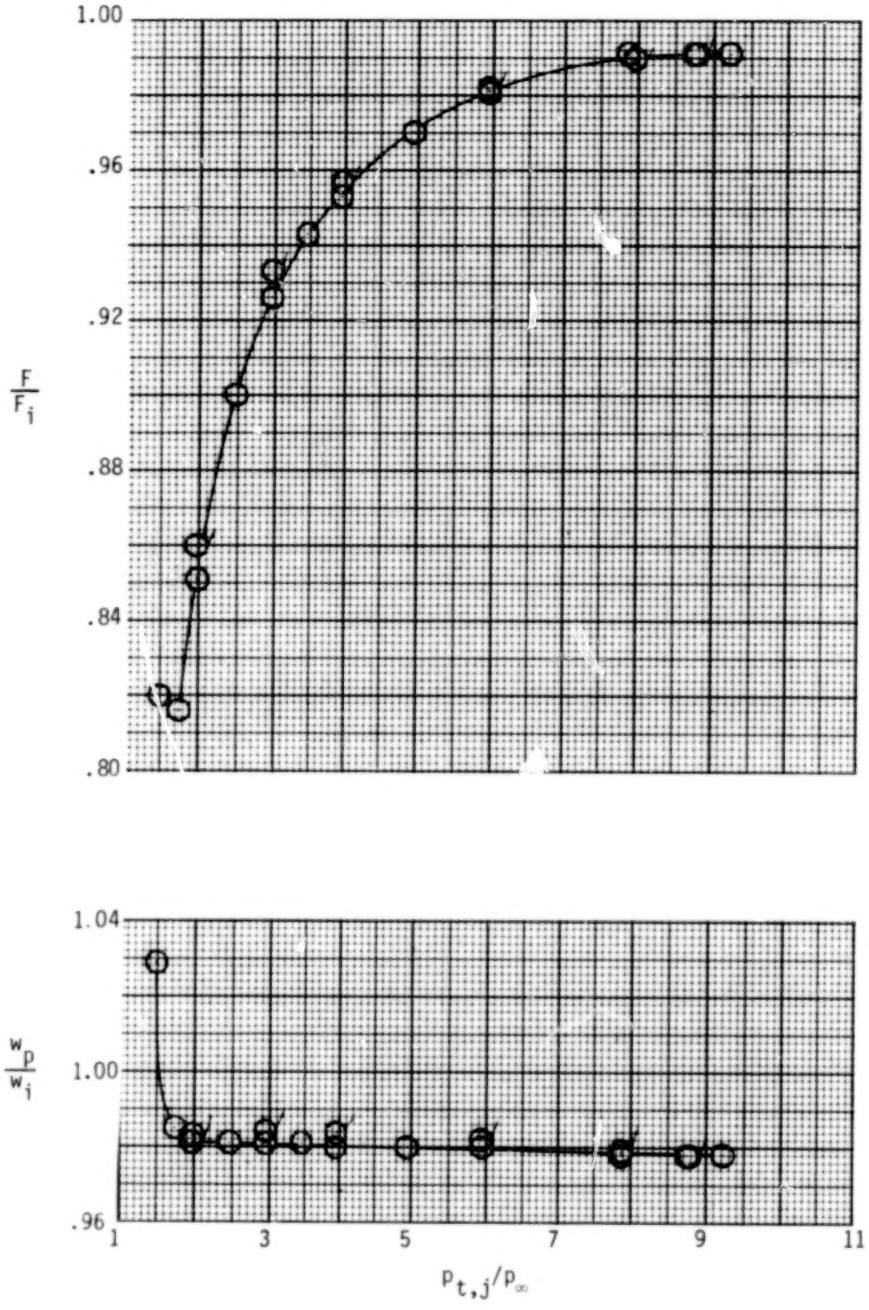

(g) Configuration C7.

Figure 5.- Continued.

A_e/A_t = 1.797, AR = 3.696, ρ = 10.73°

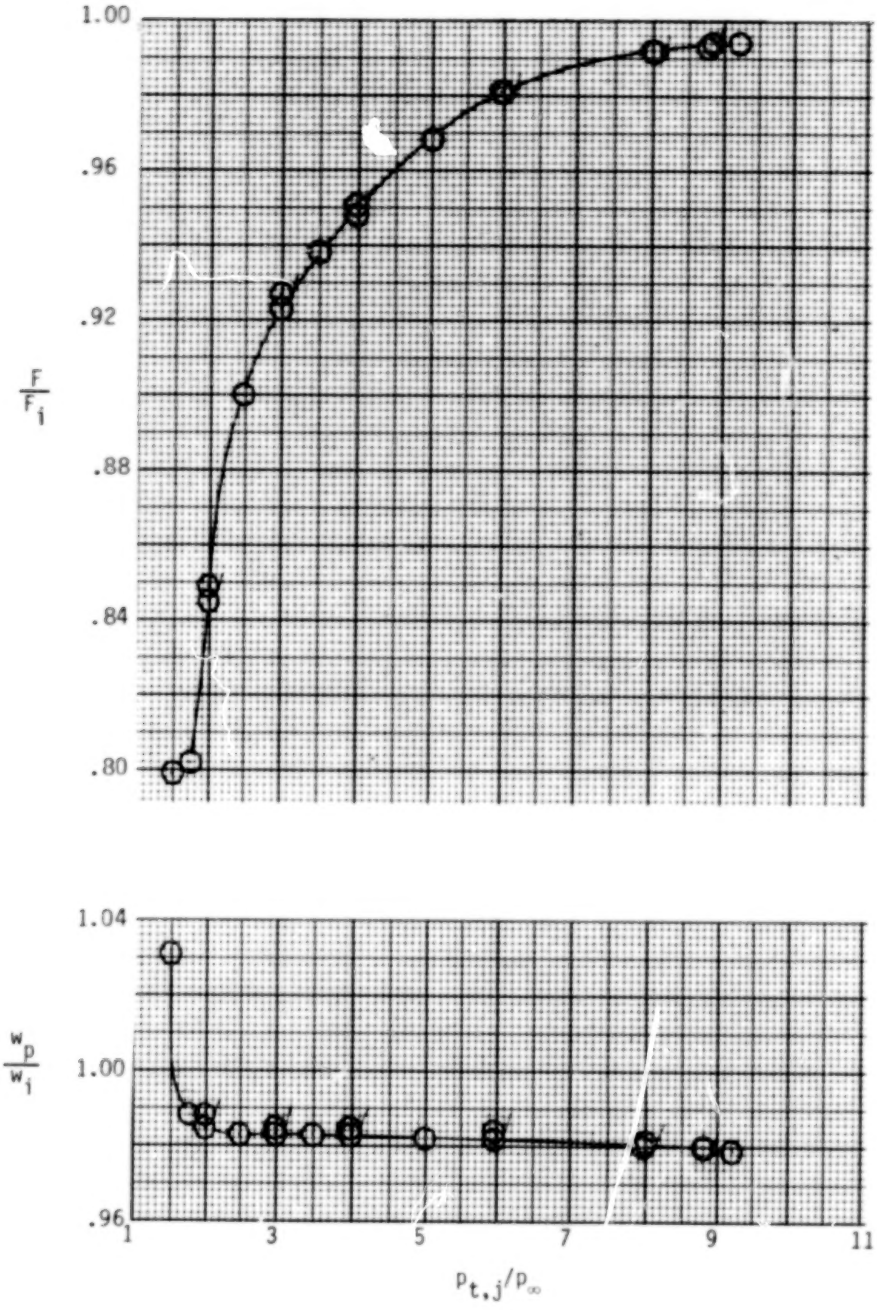

(h) Configuration C8.

Figure 5.- Continued.

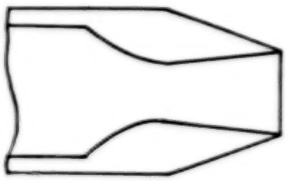

A_e/A_t = 1.397, AR = 3.696, ρ = 5.40°

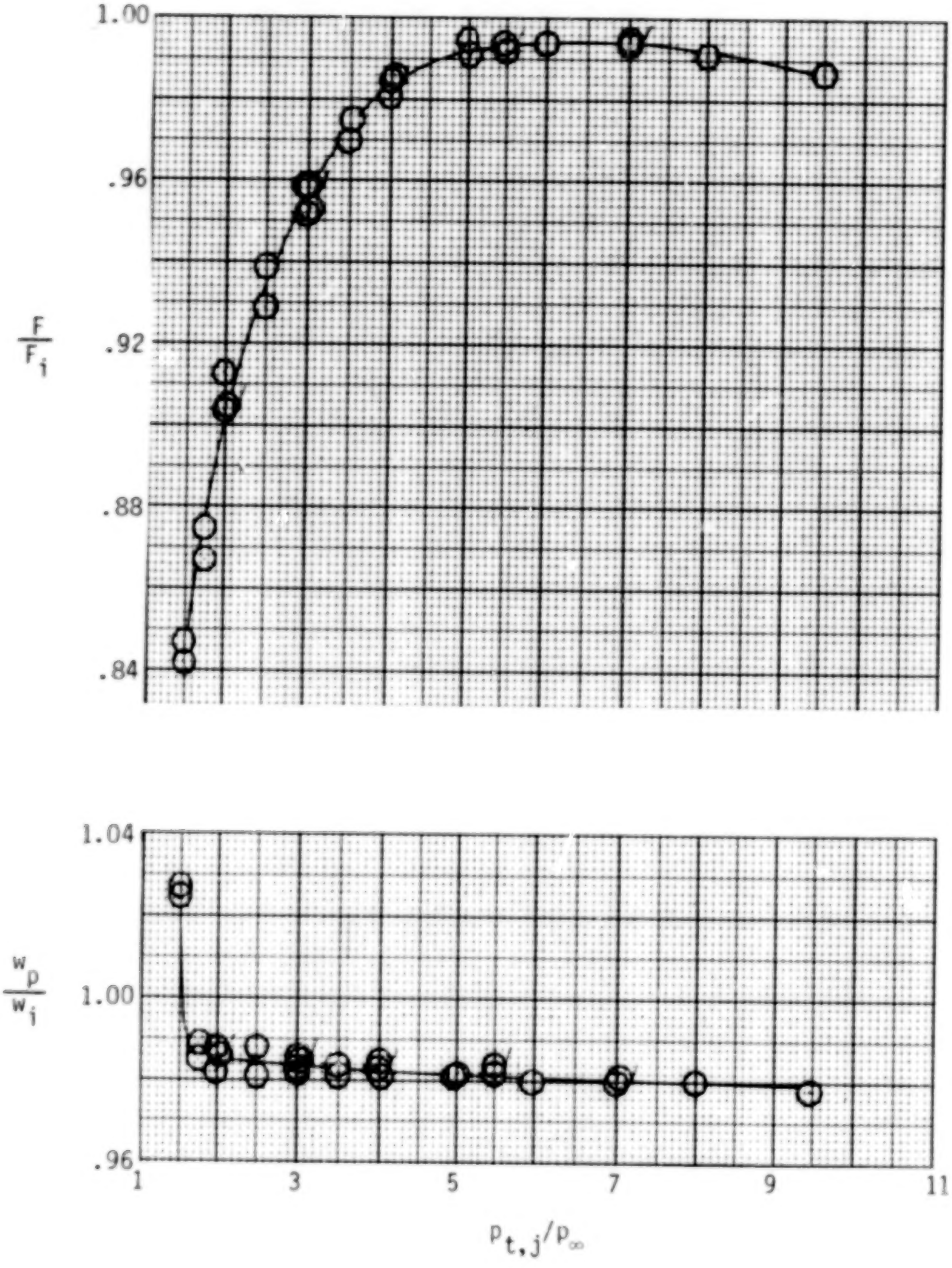

(i) Configuration C9.

Figure 5.- Continued.

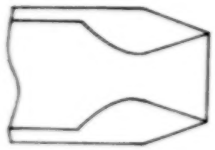

A_e/A_t = 1.797, AR = 3.696, ϕ = 14.25°

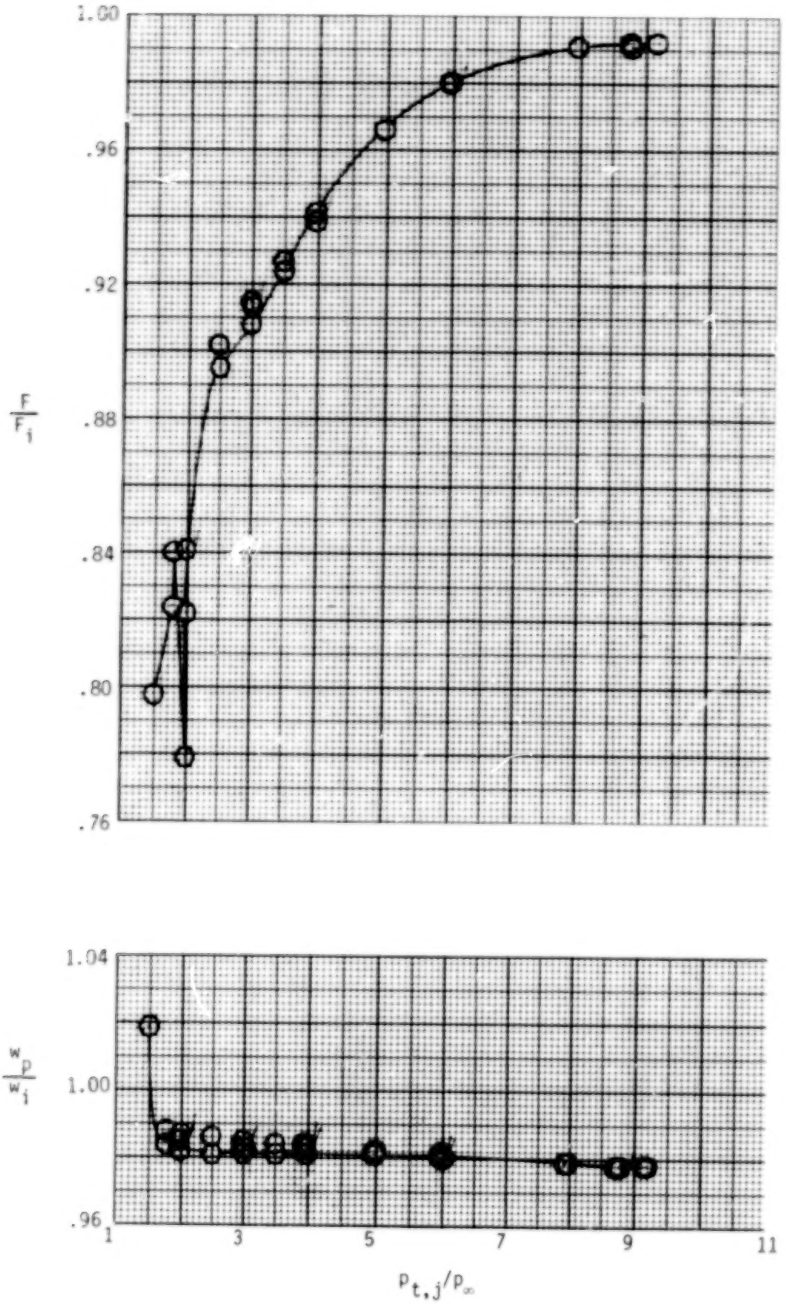

(j) Configuration C10.

Figure 5.- Continued.

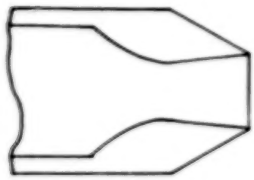

A_e/A_t = 1.248, AR = 3.696, ρ = 5.38°

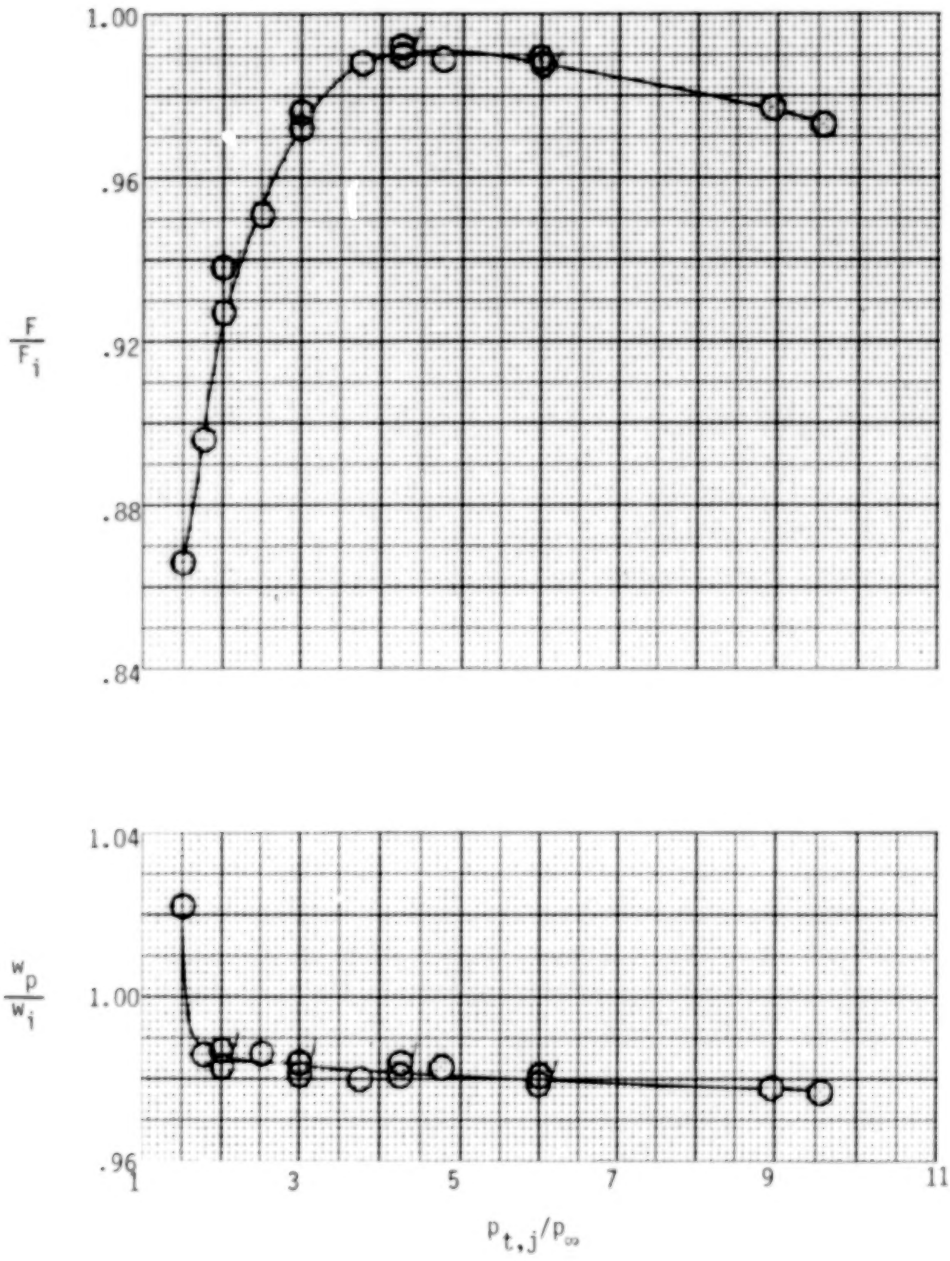

(k) Configuration C11.

Figure 5.- Continued.

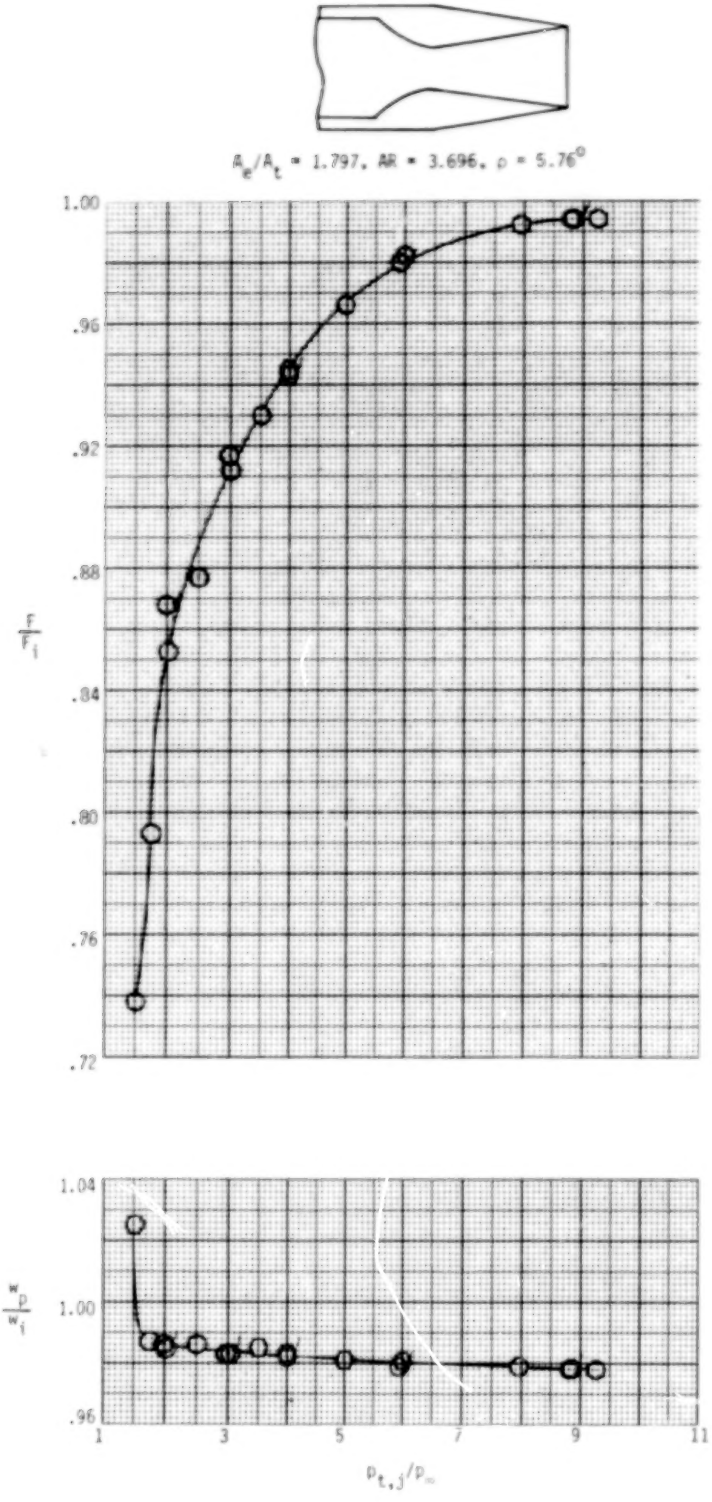

(1) Configuration C12.

Figure 5.- Continued.

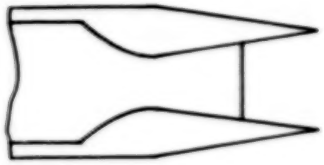

A_e/A_t = 1.797, AR = 3.696, ρ = 5.76°

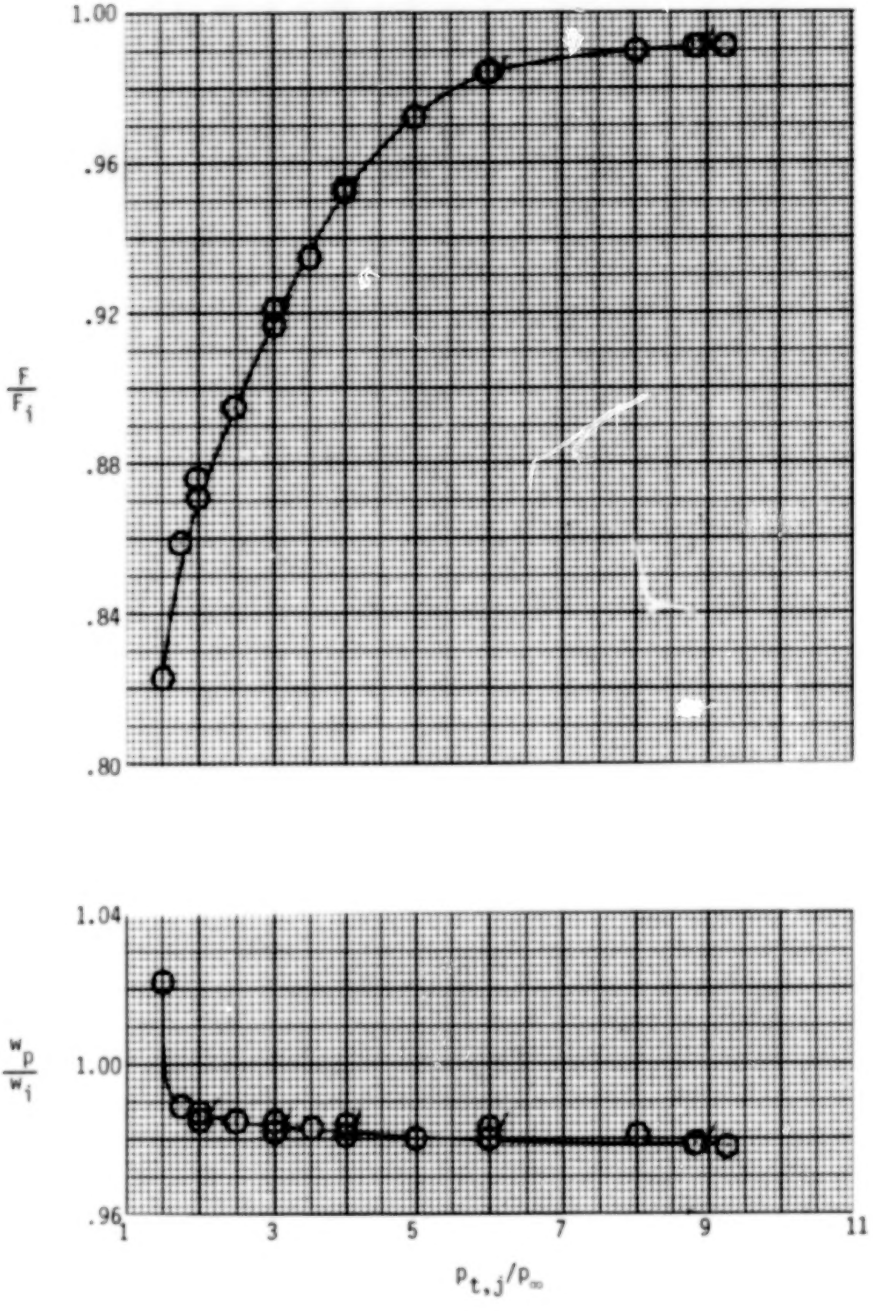

(m) Configuration C13.

Figure 5.- Concluded.

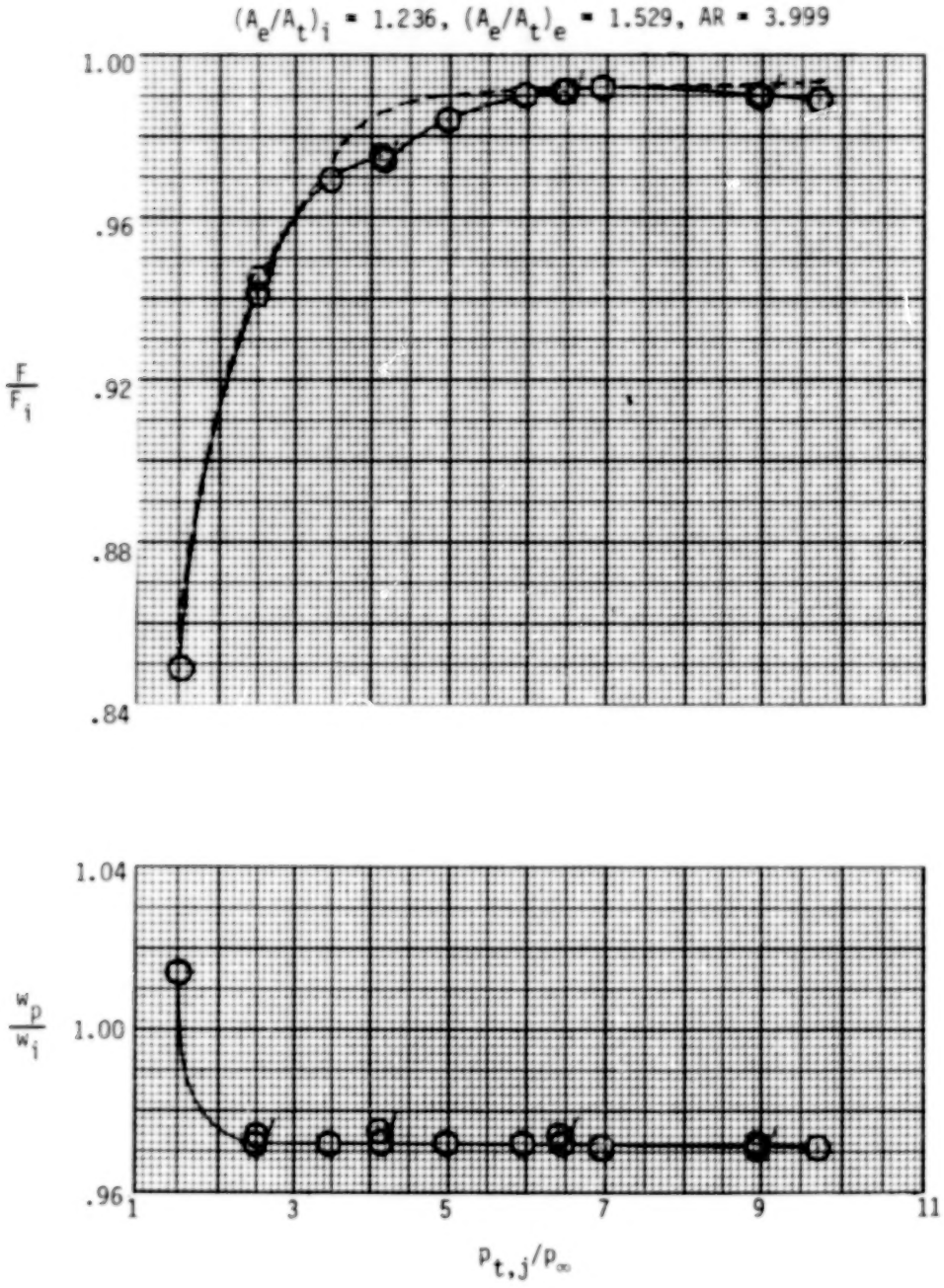

(a) Configuration SR1.

Figure 6.- Variation of nozzle thrust ratio and discharge coefficient with nozzle pressure ratio for single-ramp expansion nozzles. Flagged symbols indicate data taken as nozzle pressure ratio was decreasing. Dashed line indicates values of resultant gross thrust ratio F_r/F_i.

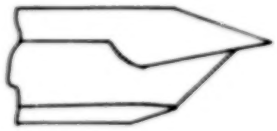

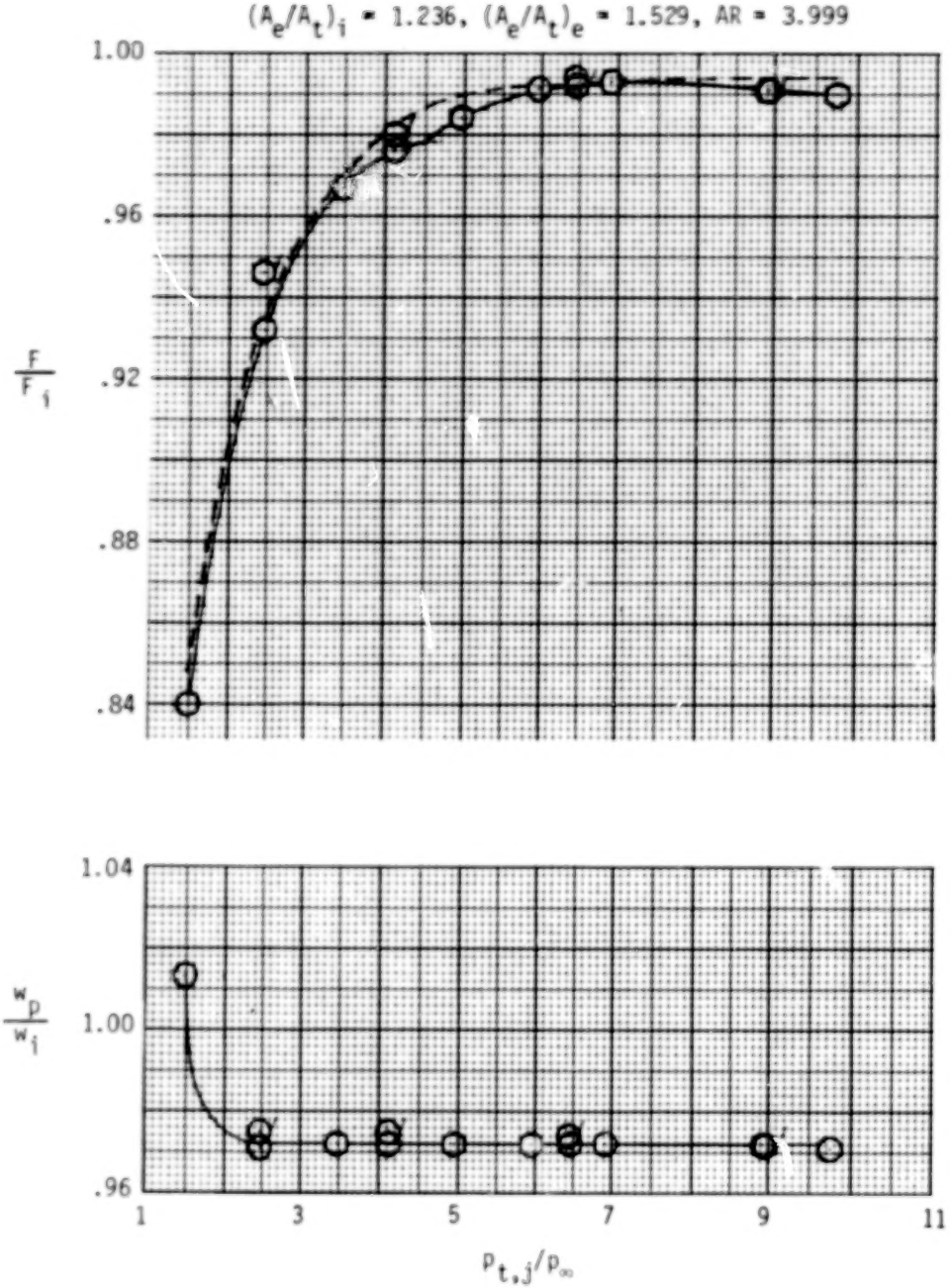

(b) Configuration SR2.

Figure 6.- Continued.

$(A_e/A_t)_i$ = 1.236, $(A_e/A_t)_e$ = 1.529, AR = 3.999

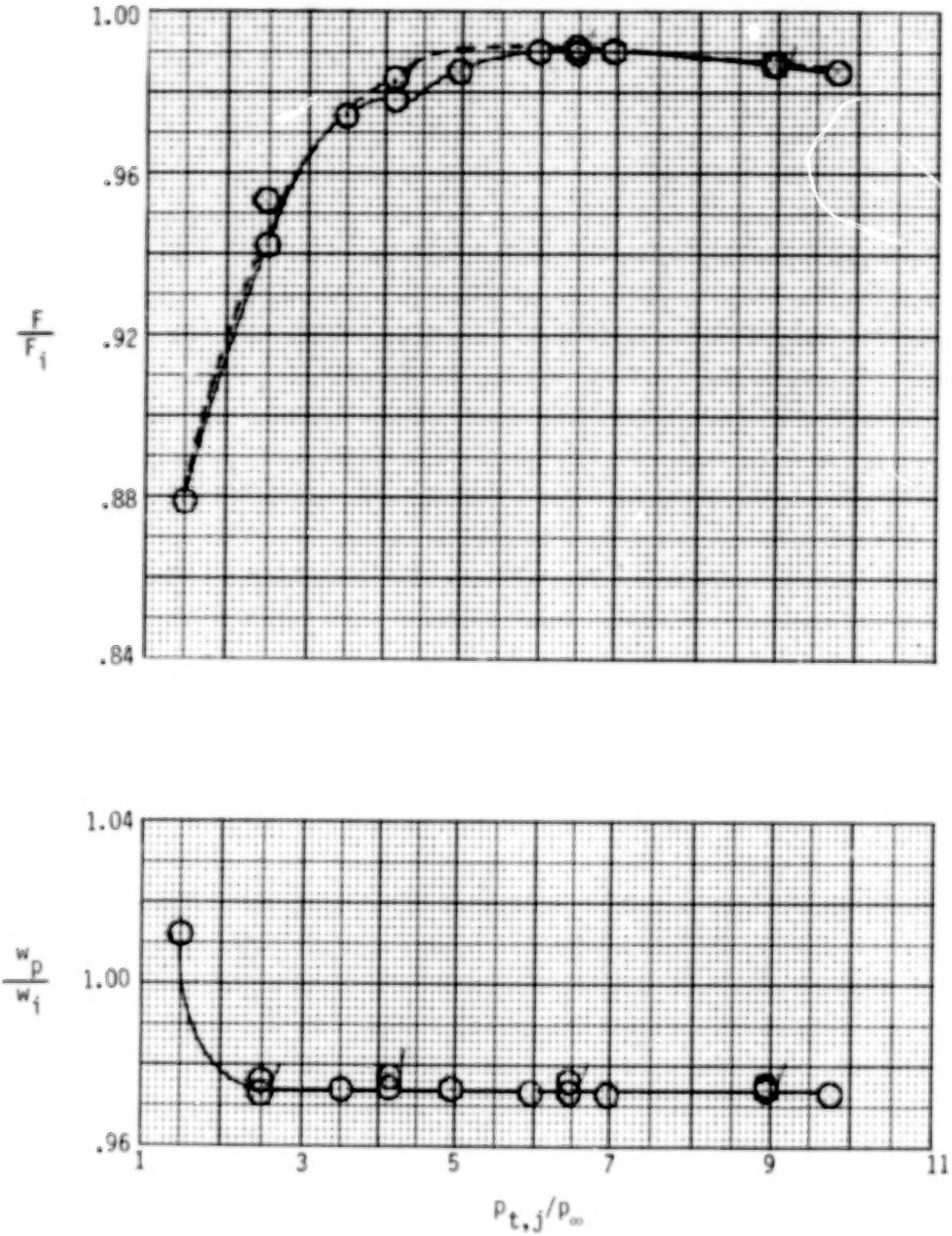

(c) Configuration SR3.

Figure 6.- Continued.

$(A_e/A_t)_i$ = 1.236, $(A_e/A_t)_e$ = 1.529, AR = 3.999

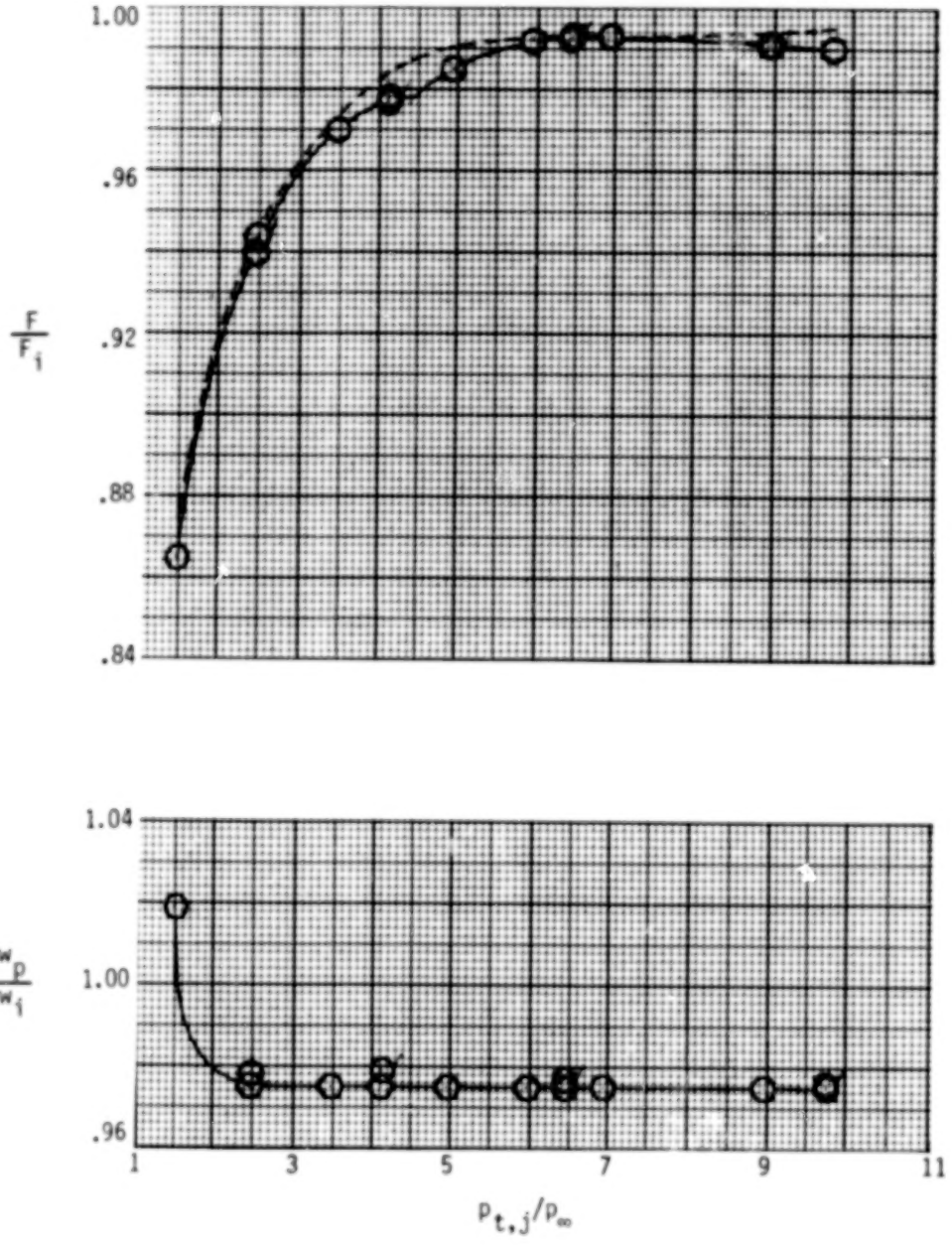

(d) Configuration SR4.

Figure 6.- Continued.

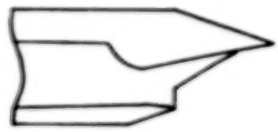

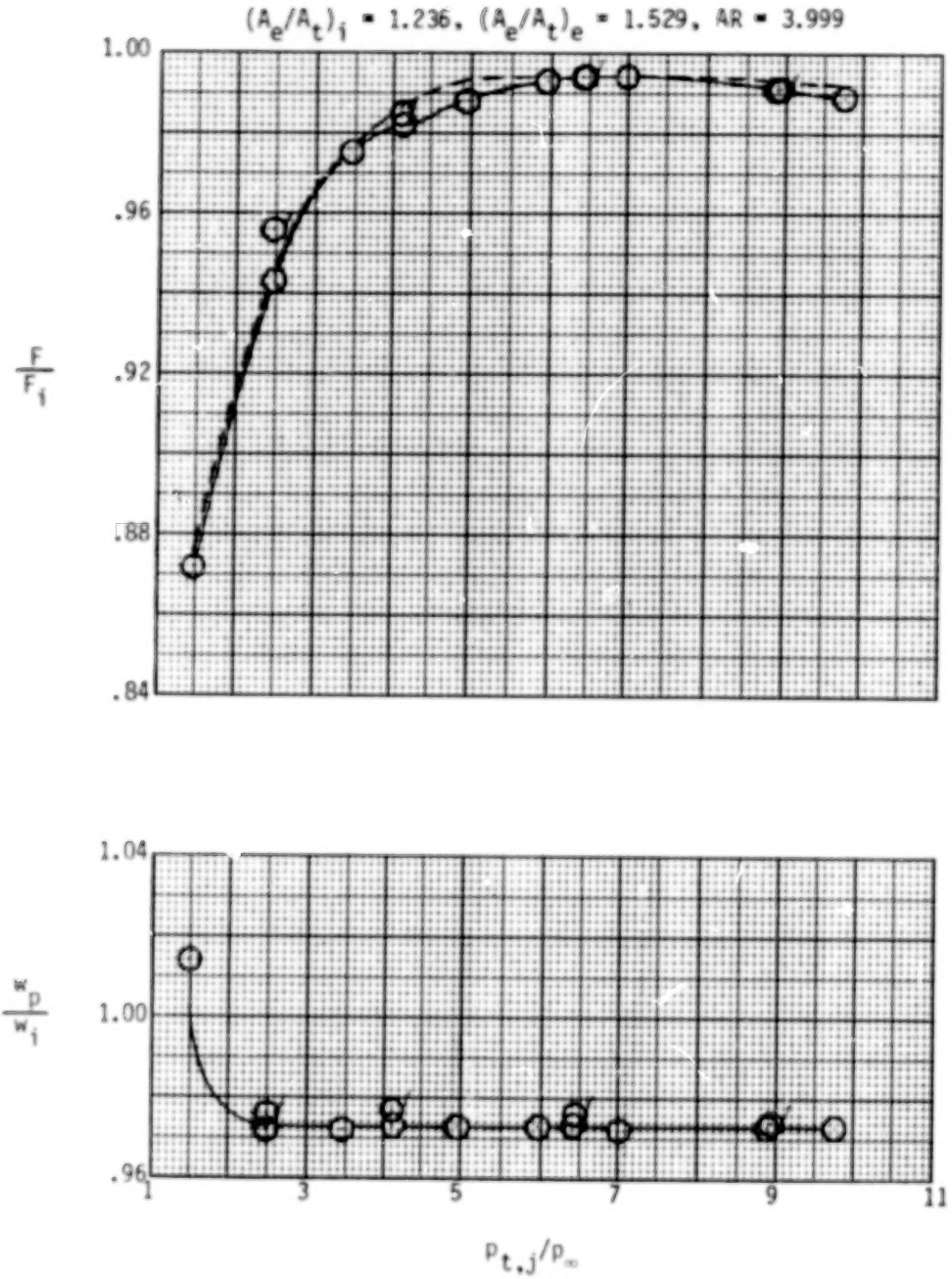

(e) Configuration SR5.

Figure 6.- Concluded.

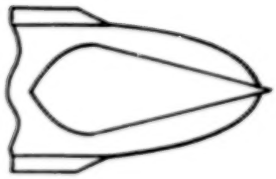

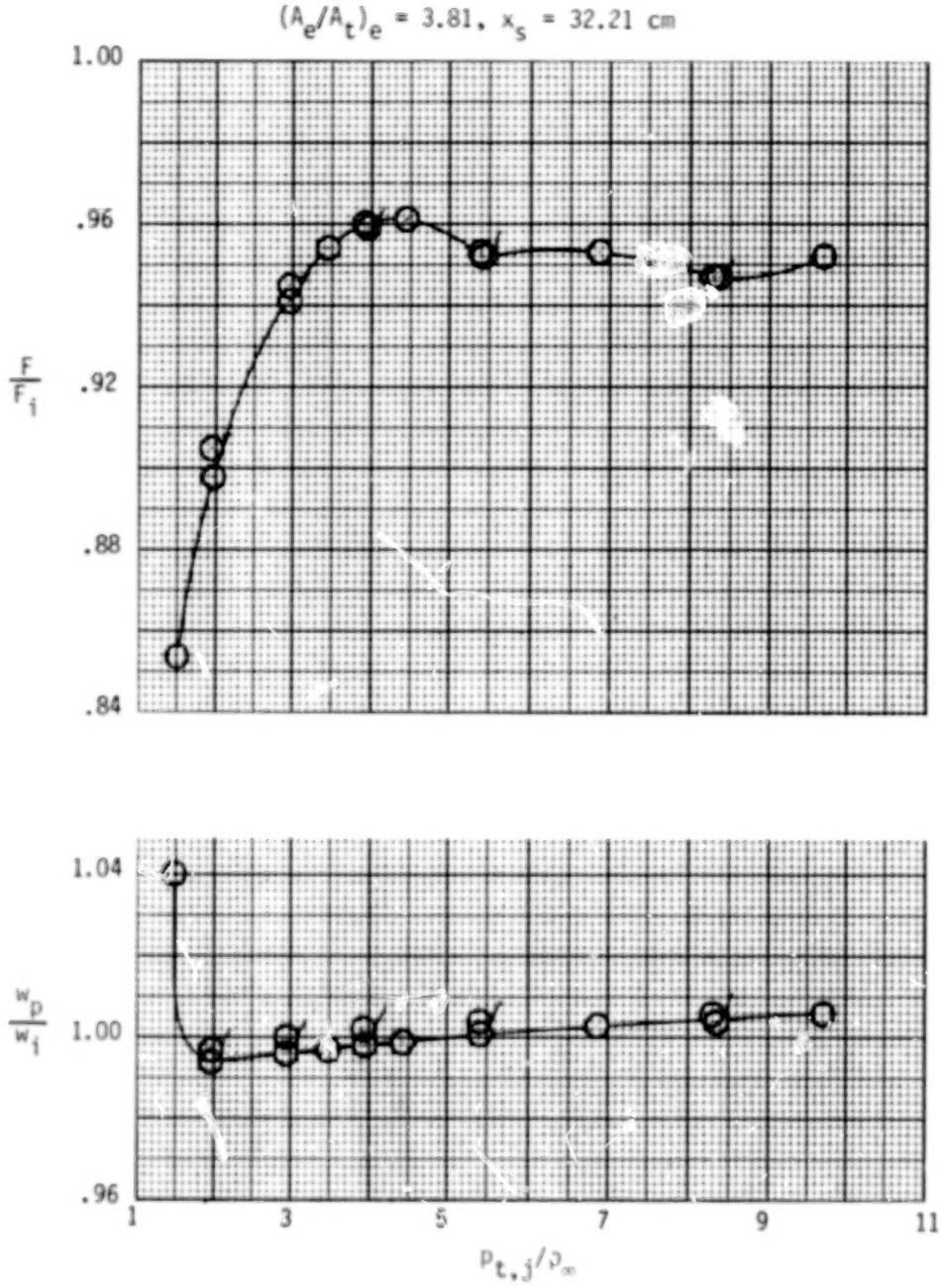

(a) Configuration W1.

Figure 7.- Variation of nozzle thrust ratio and discharge coefficient with nozzle pressure ratio for wedge nozzles. Dashed line indicates resultant thrust ratio (F_r/F_i) and flagged symbols indicate data taken as nozzle pressure ratio was decreasing. AR = 3.983; $(A_e/A_t)_i$ = 1.22.

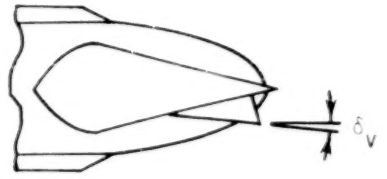

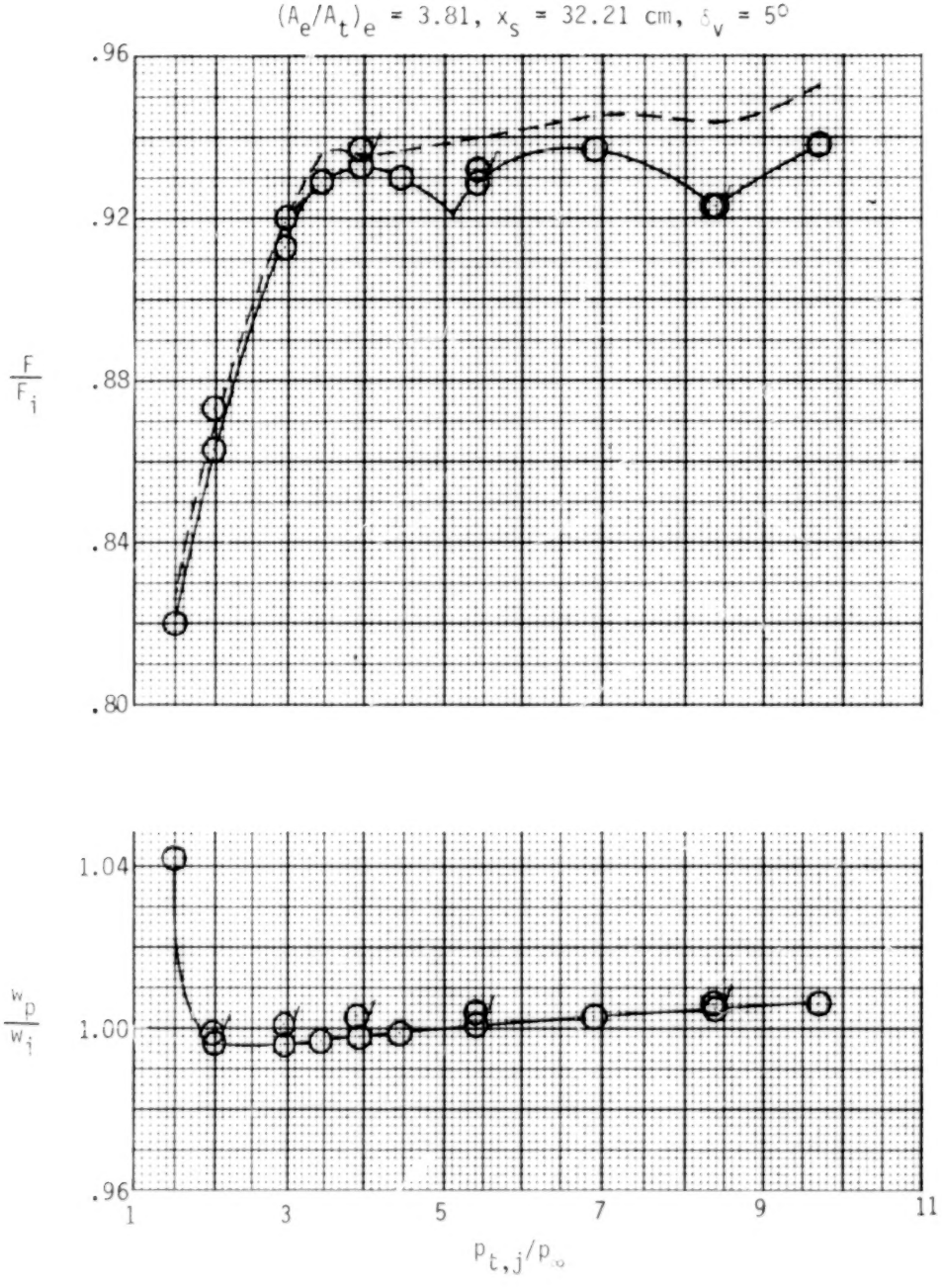

(b) Configuration W1(V5).

Figure 7.- Continued.

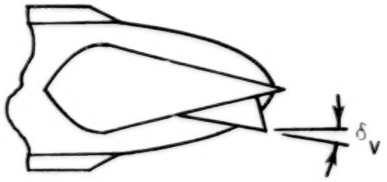

$(A_e/A_t)_e$ = 3.81, x_s = 32.21 cm, δ_v = 10°

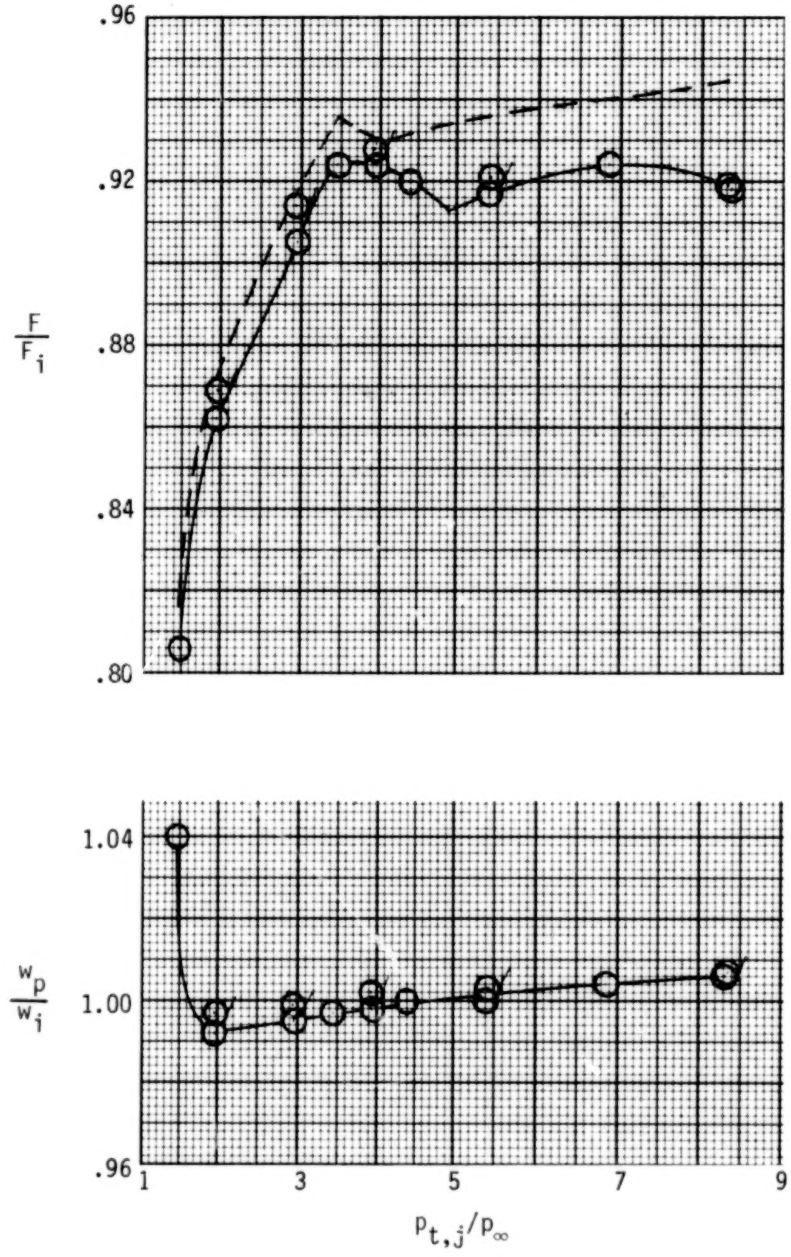

(c) Configuration W1(V10).

Figure 7.- Continued.

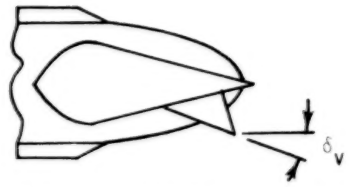

$(A_e/A_t)_e$ = 3.81, x_s = 32.21 cm, δ_v = 20°

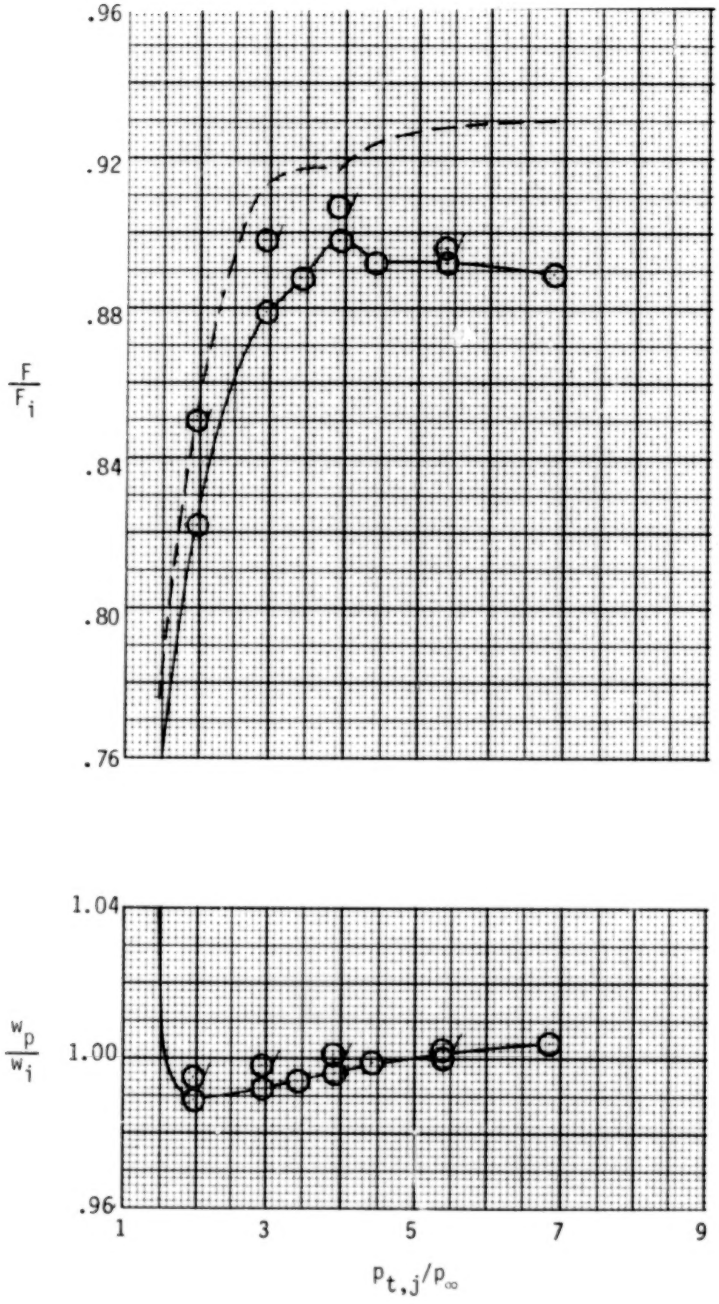

(d) Configuration W1(V20).

Figure 7.- Continued.

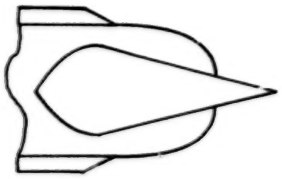

$(A_e/A_t)_e$ = 3.81, x_s = 28.47 cm

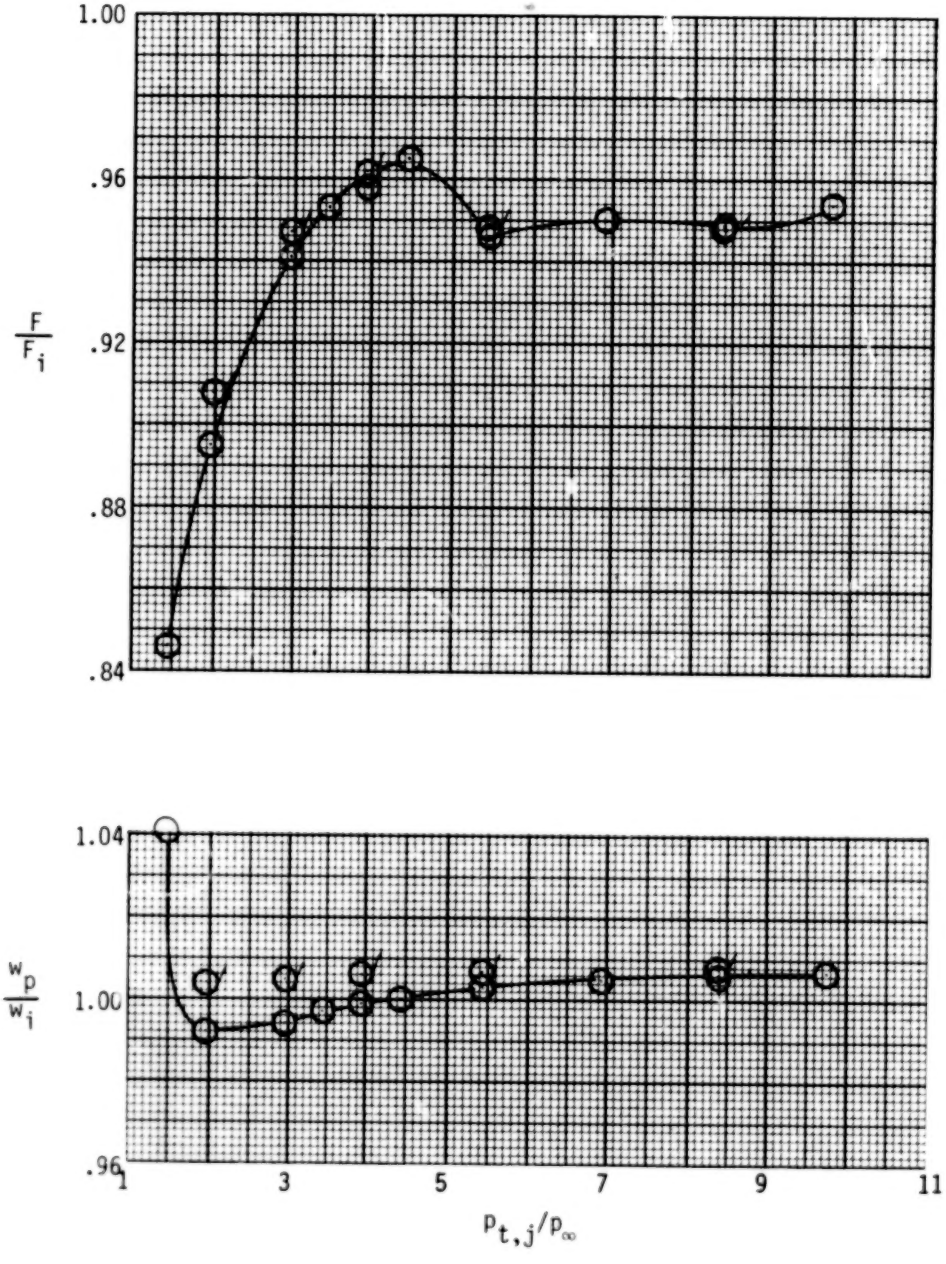

(e) Configuration W2.

Figure 7.- Continued.

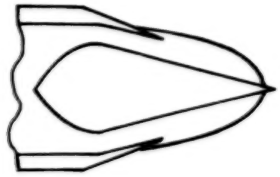

$(A_e/A_t)_e$ = 2.98, x_s = 32.21 cm

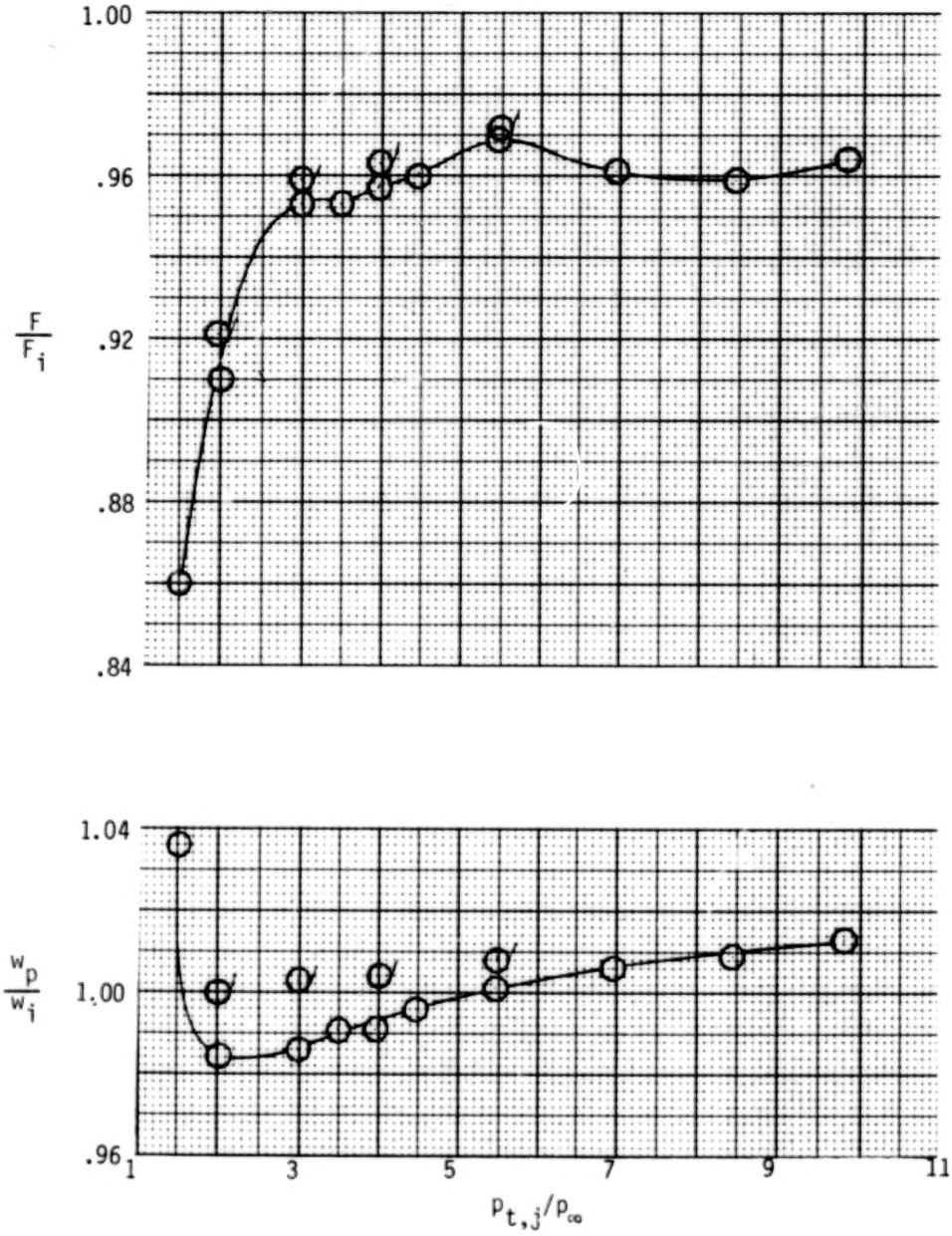

(f) Configuration W3.

Figure 7.- Continued.

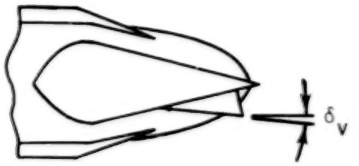

$(A_e/A_t)_e$ = 2.98, x_s = 32.21 cm, δ_v = 5°

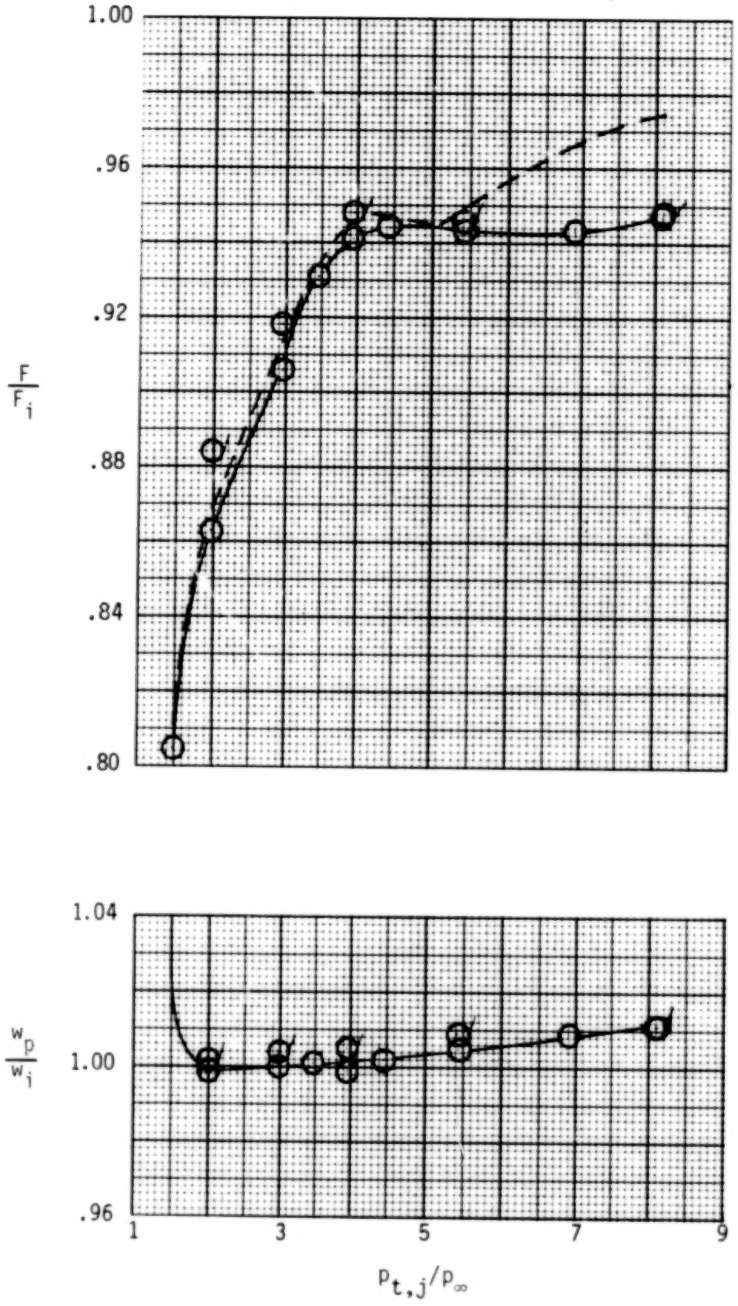

(g) Configuration W3(V5).

Figure 7.- Continued.

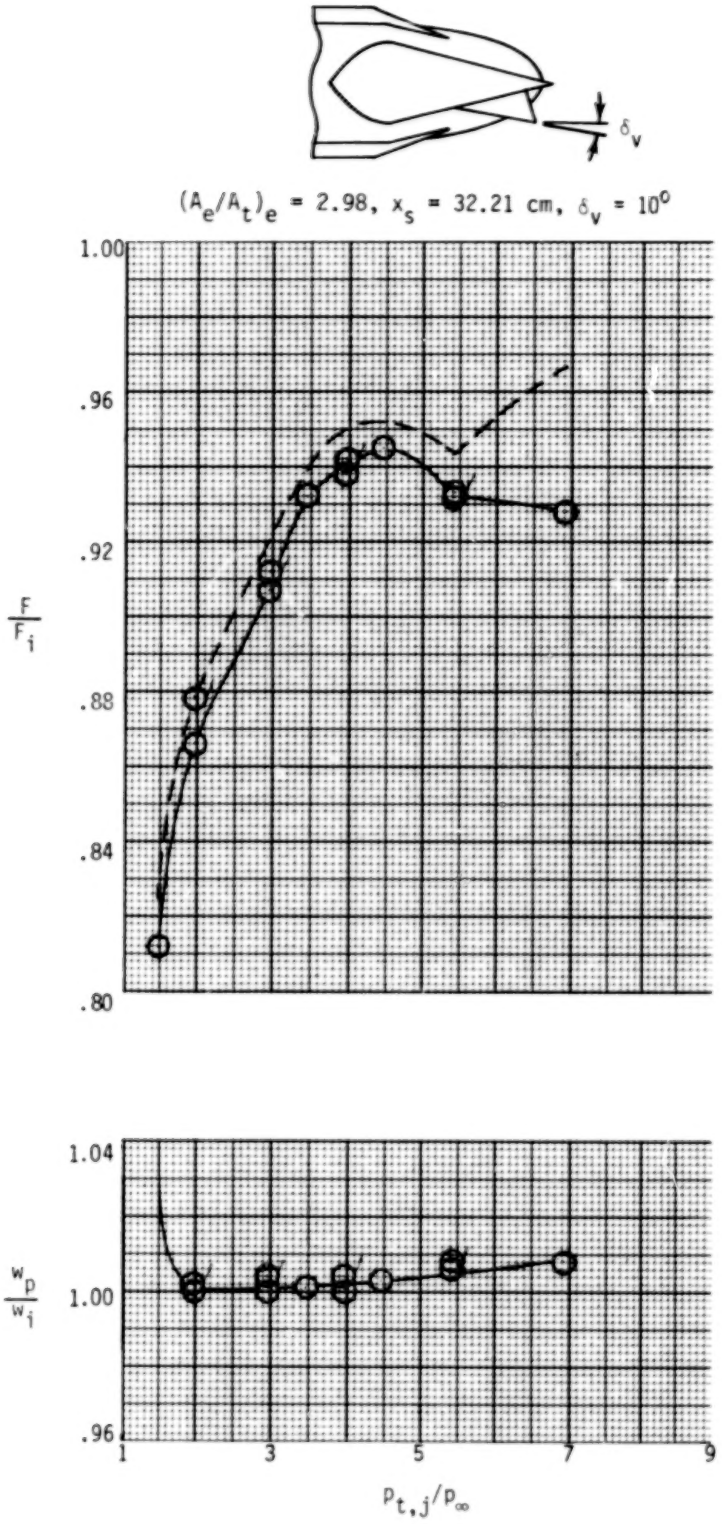

(h) Configuration W3(V10).

Figure 7.- Continued.

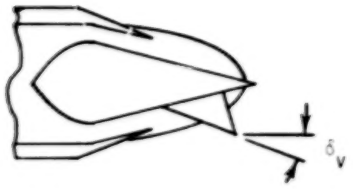

$(A_e/A_t)_e$ = 2.98, x_s = 32.21 cm, δ_v = 20°

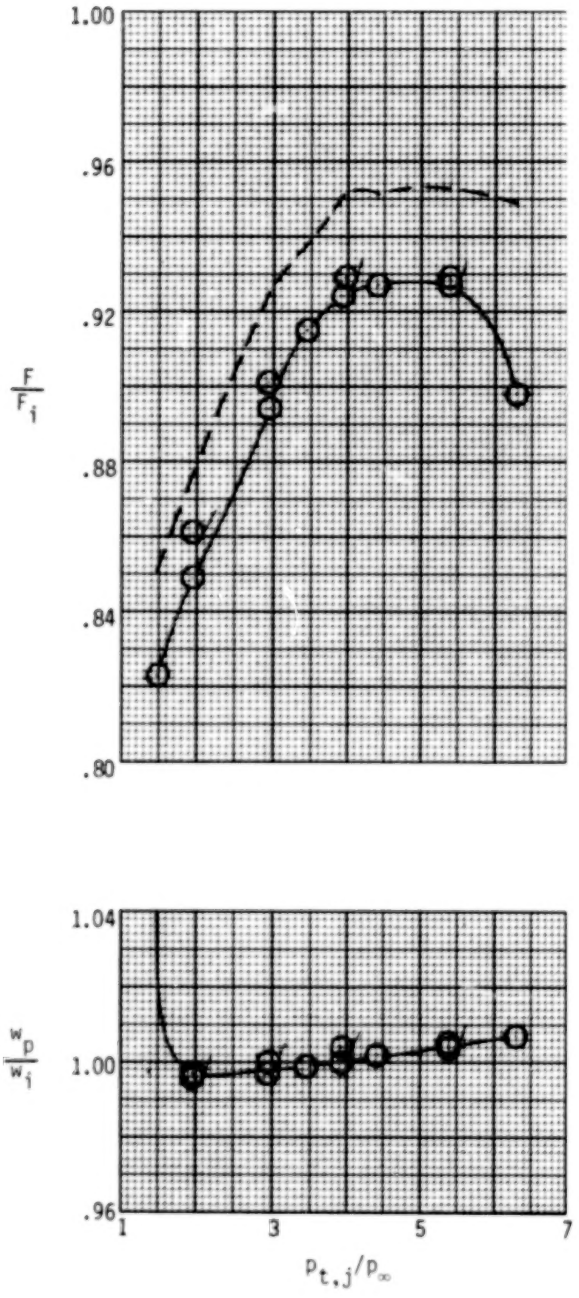

(i) Configuration W3(V20).

Figure 7.- Continued.

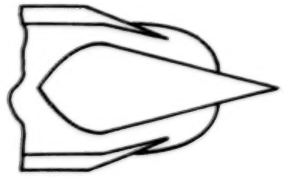

$(A_e/A_t)_e$ = 2.98, x_s = 28.47 cm

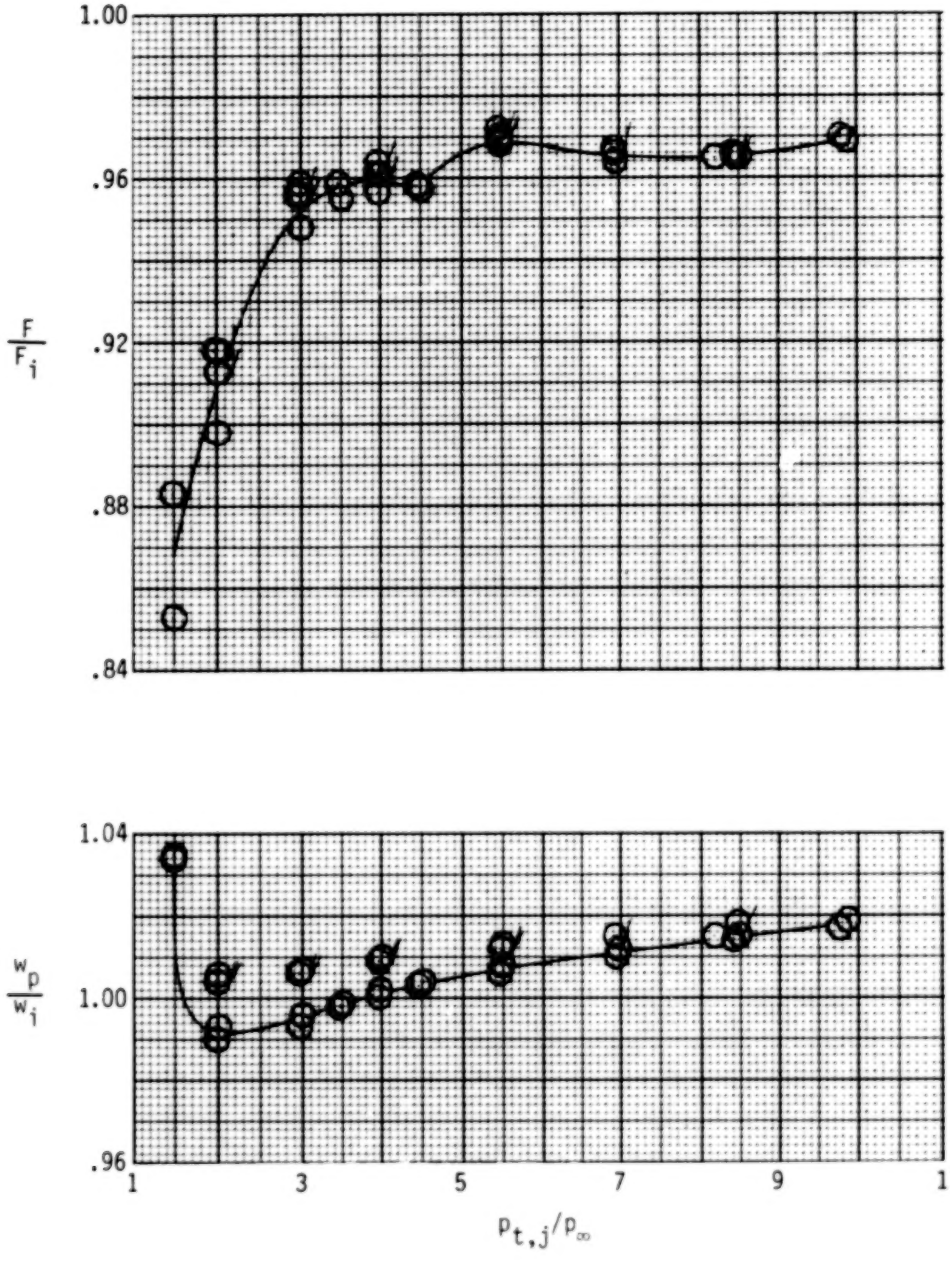

(j) Configuration W4.

Figure 7.- Continued.

$(A_e/A_t)_e$ = 2.98, x_s = 28.47 cm, δ_v = 5°

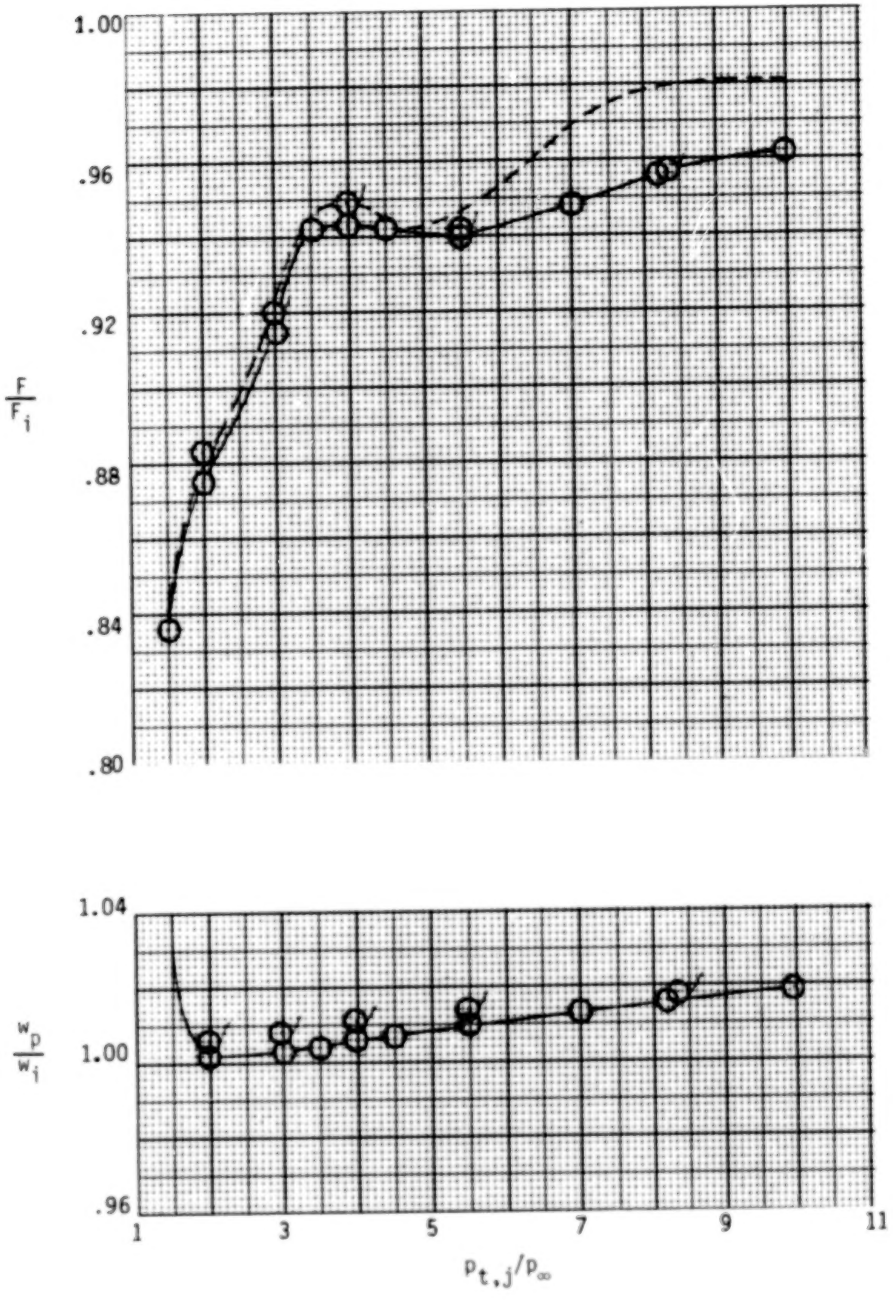

(k) Configuration W4(V5).

Figure 7.- Continued.

$(A_e/A_t)_e$ = 2.98, x_s = 28.47 cm, δ_v = 3.5°(forward flap)

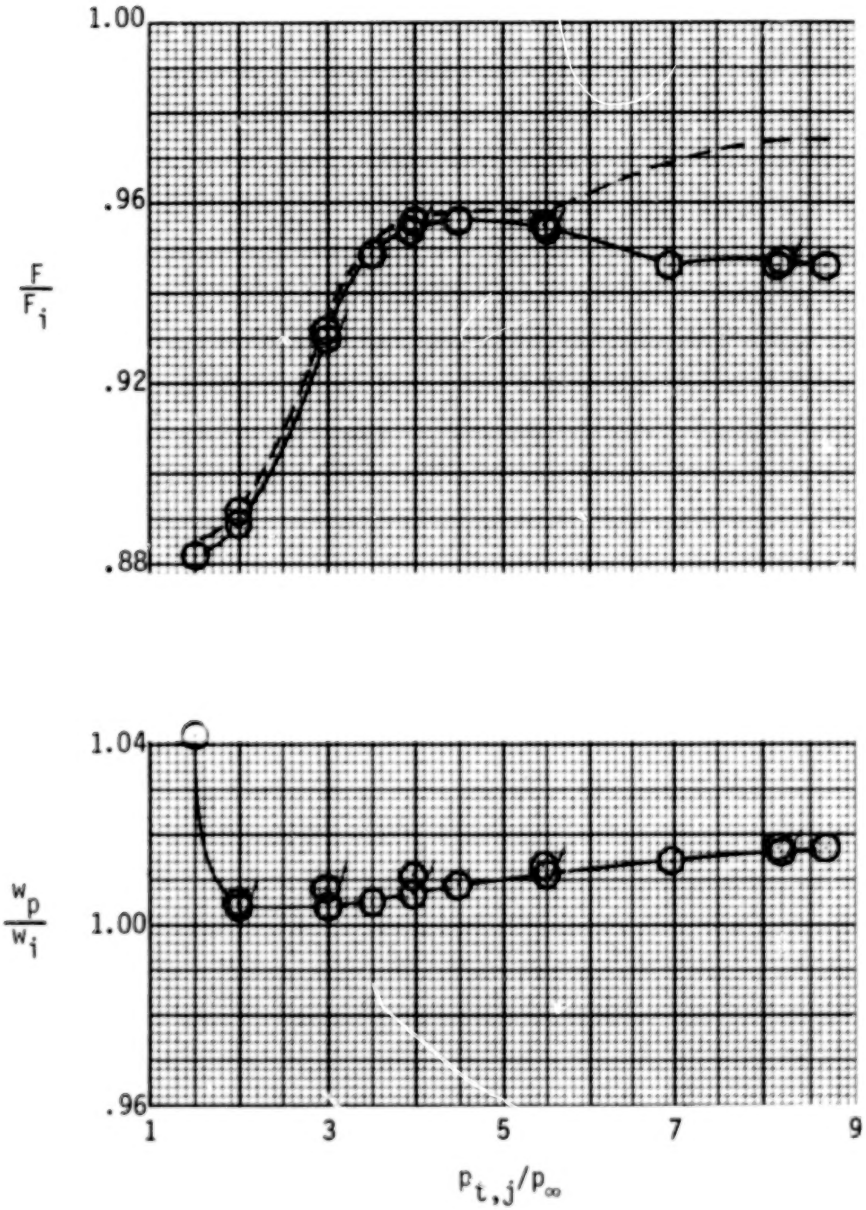

(1) Configuration W4(FV5).

Figure 7.- Continued.

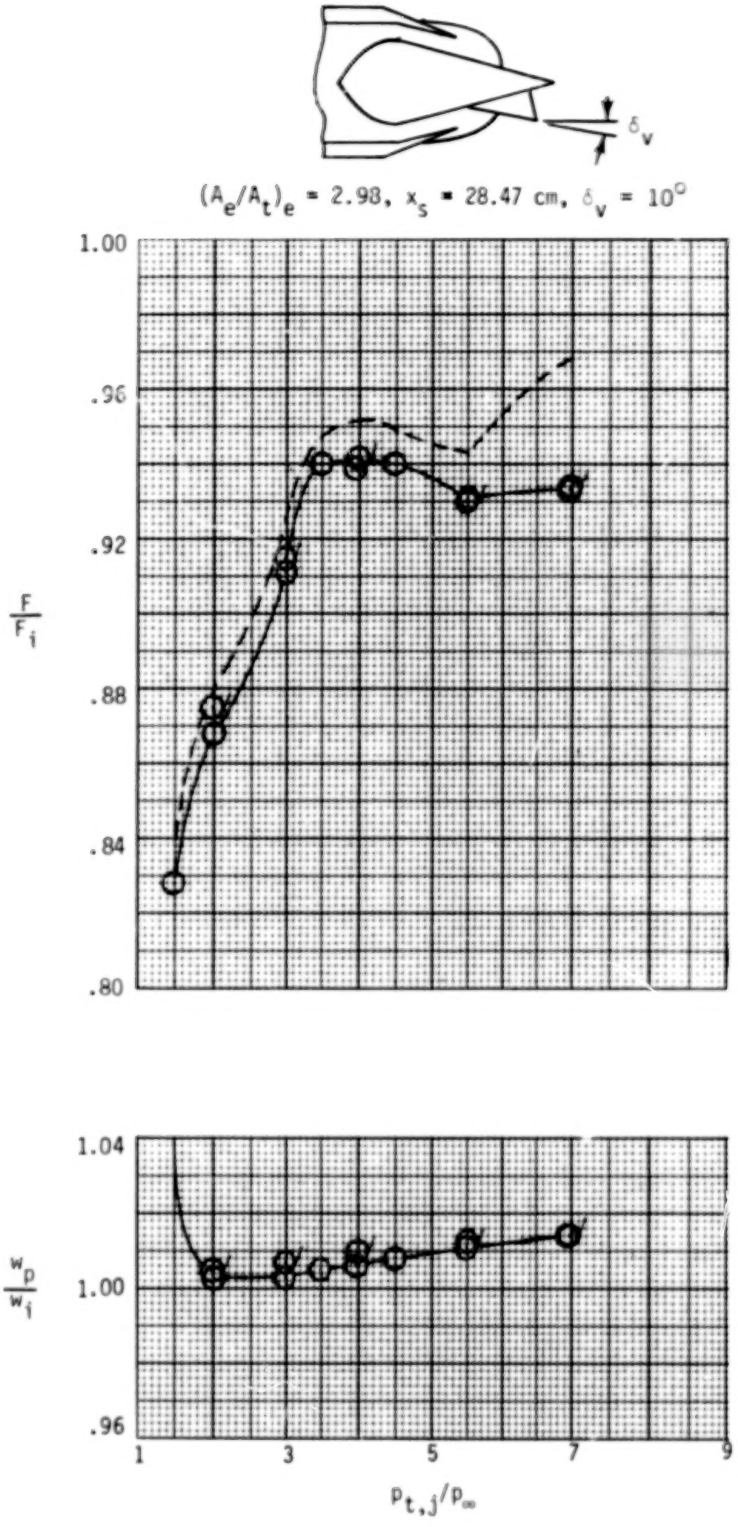

(m) Configuration W4(V10).

Figure 7.- Continued.

$(A_e/A_t)_e$ = 2.98, x_s = 28.47 cm, δ_v = 20°

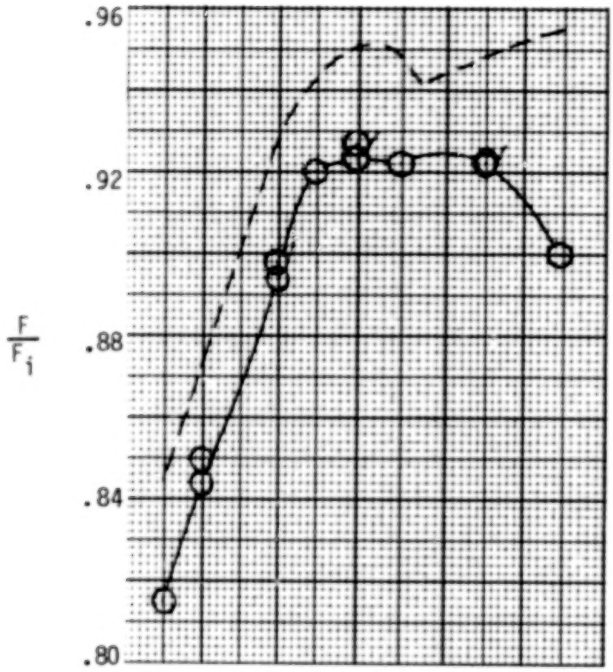

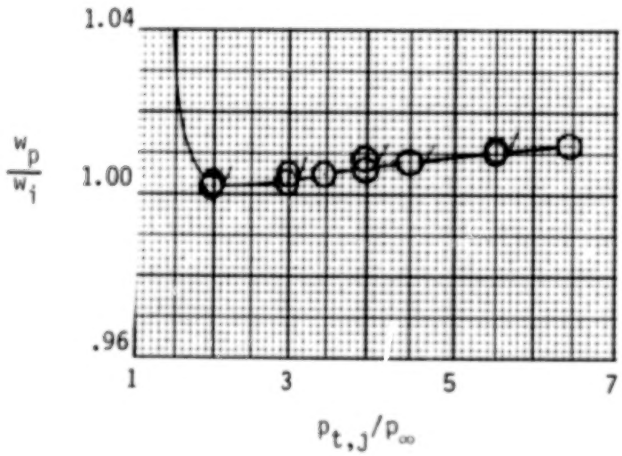

(n) Configuration W4(V20).

Figure 7.- Continued.

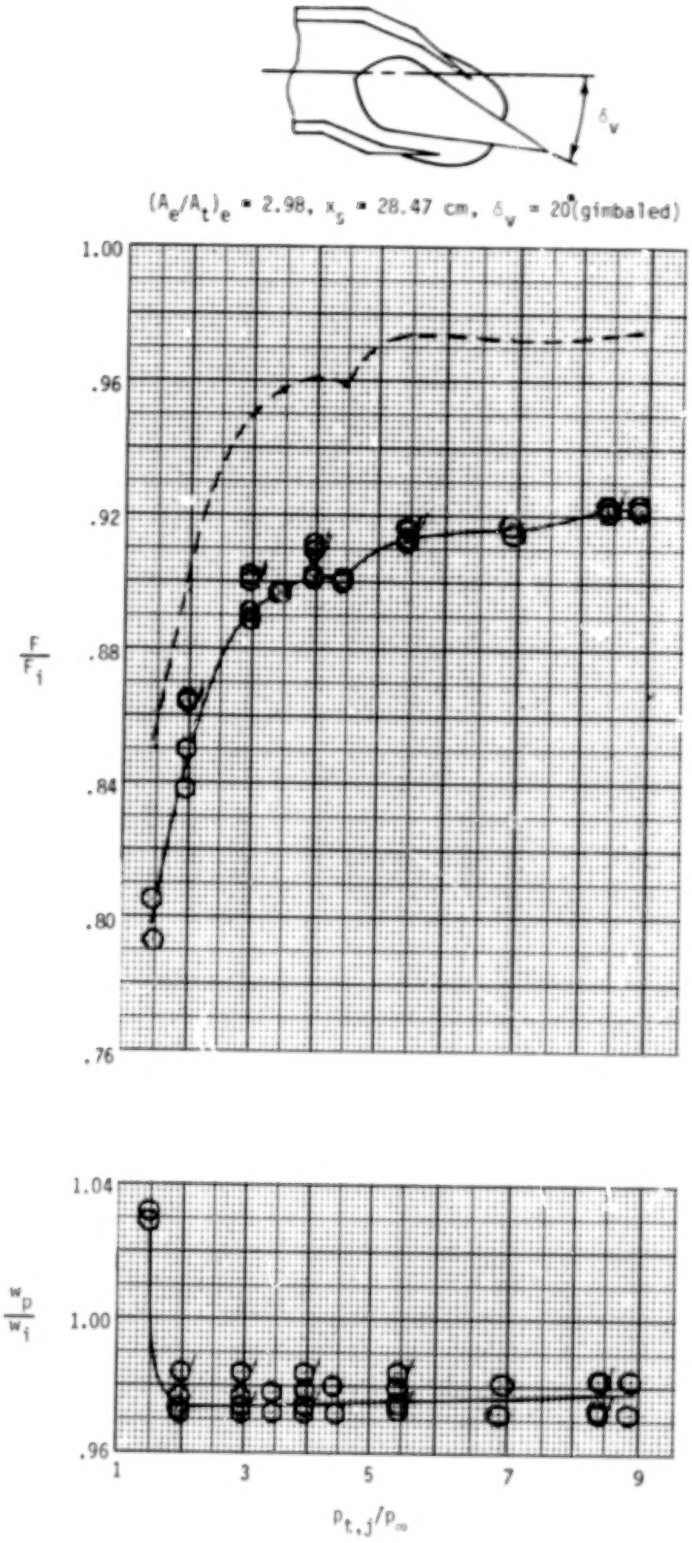

(o) Configuration W4(G20).

Figure 7.- Concluded.

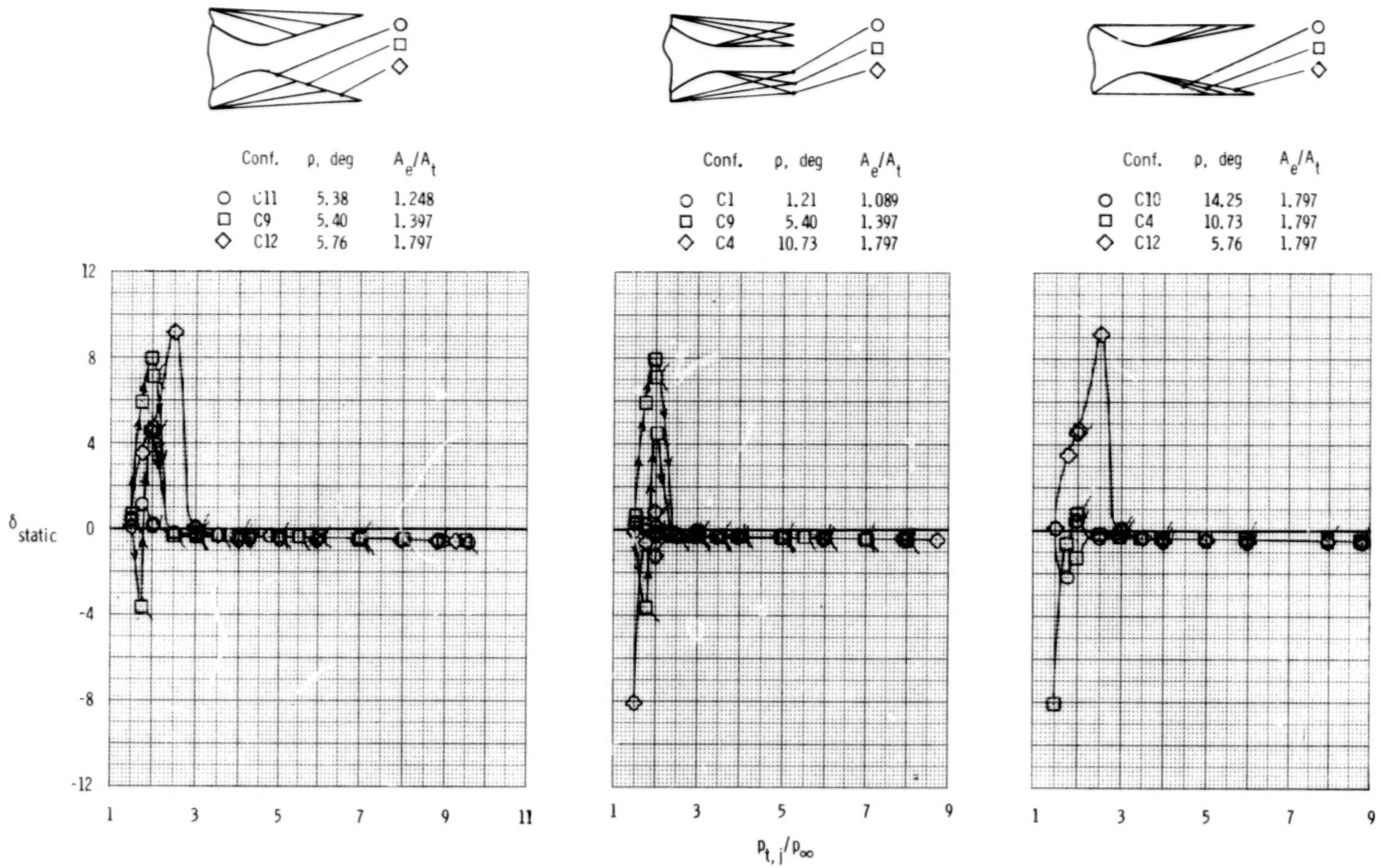

(a) Effect of expansion ratio, flap length, and divergence angle.

Figure 8.- Effect of nozzle geometric parameters on resultant thrust vector angle of nonaxisymmetric convergent-divergent nozzles. Flagged symbols indicate data taken as nozzle pressure ratio was decreasing and tailed symbols indicate repeat runs.

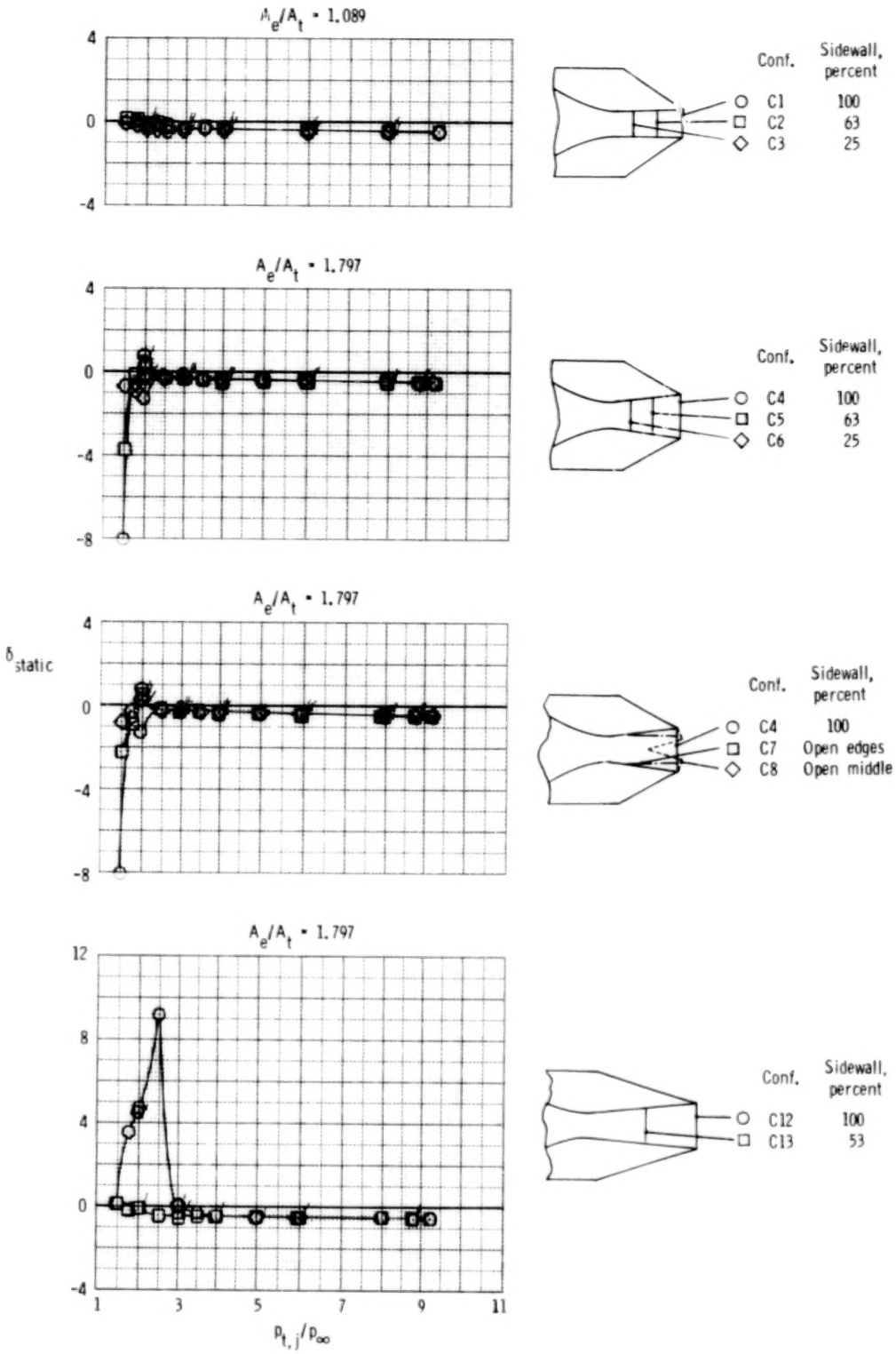

(b) Effect of sidewall length, AR = 3.696.

Figure 8.- Concluded.

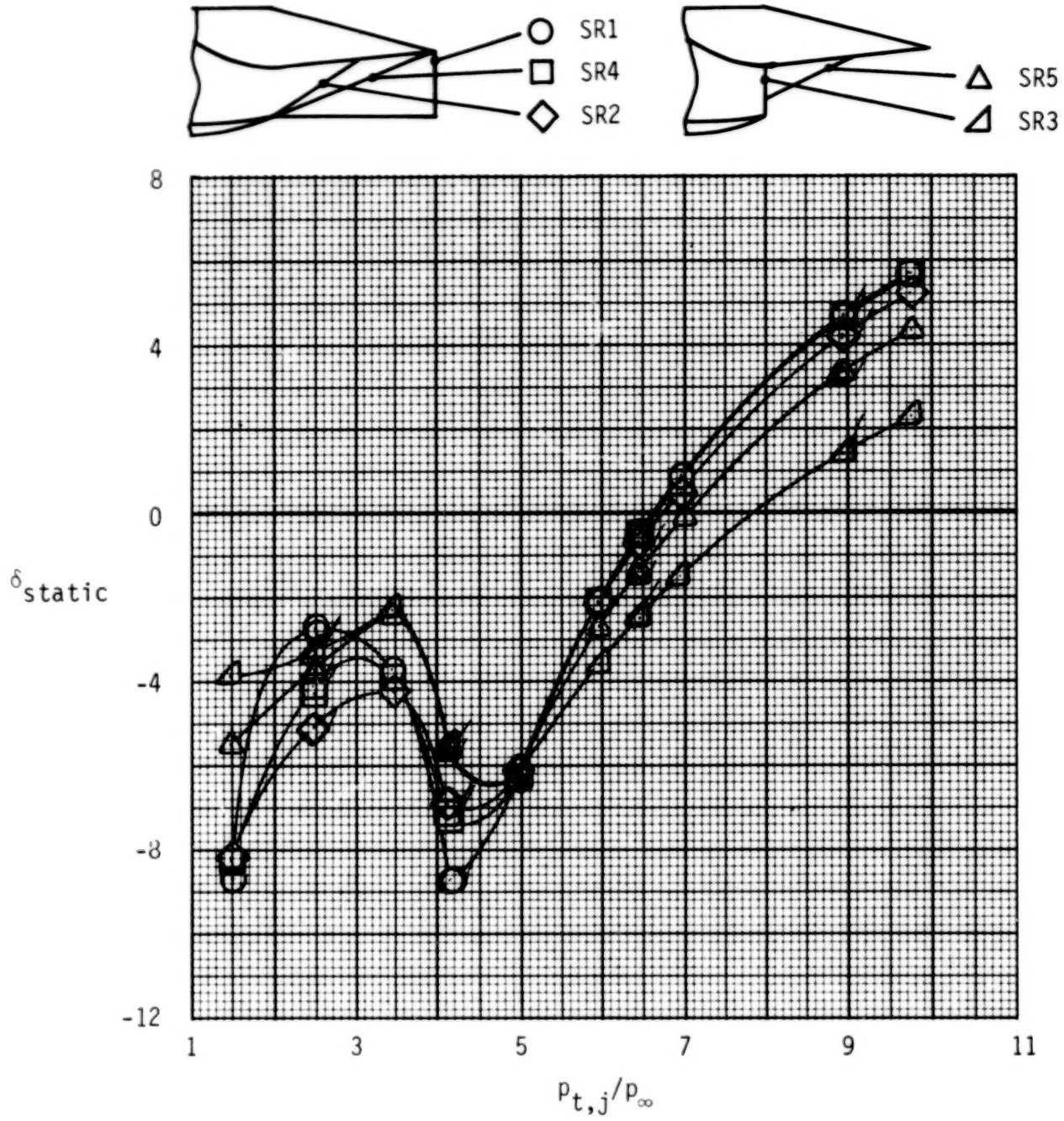

Figure 9.- Effect of sidewall geometry on resultant thrust vector angle of single-ramp expansion nozzle. Flagged symbols indicate data taken as nozzle pressure ratio was decreasing.

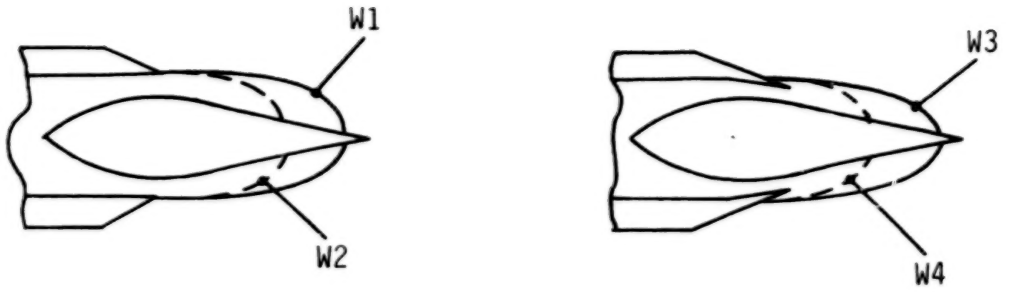

	Conf.	$(A_e/A_t)_e$	Sidewall
○	W1	3.809	Long
□	W2	3.809	Short
◇	W3	2.982	Long
△	W4	2.982	Short

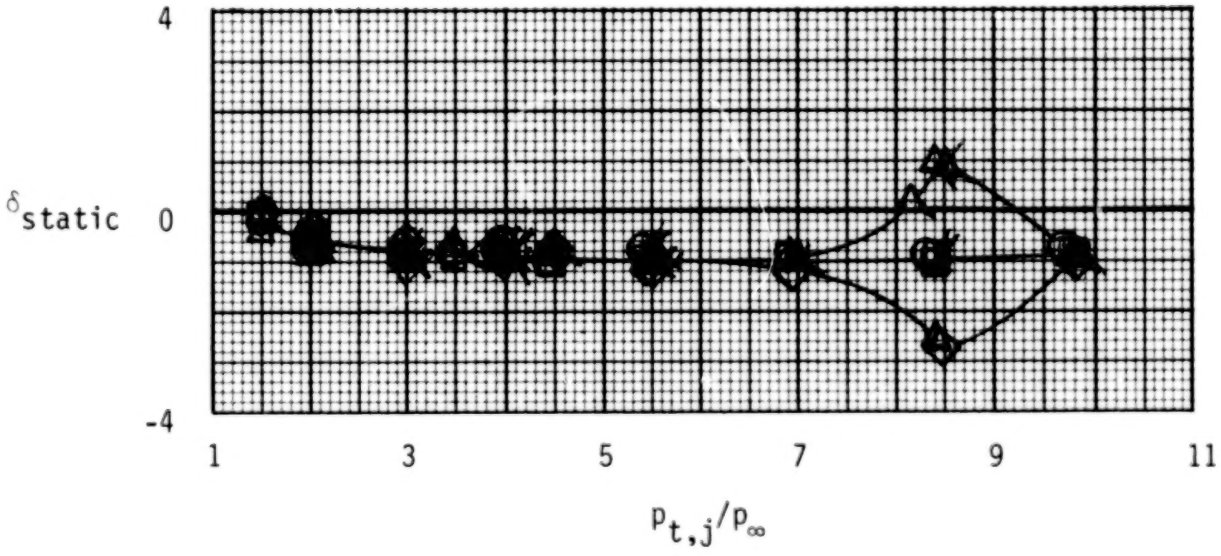

(a) Effect of external expansion ratio and sidewall length.

Figure 10.- Effect of several nozzle geometric parameters on the resultant thrust vector angle of wedge nozzles. Flagged symbols indicate data taken as nozzle pressure ratio was decreasing and tailed symbols indicate repeat runs.

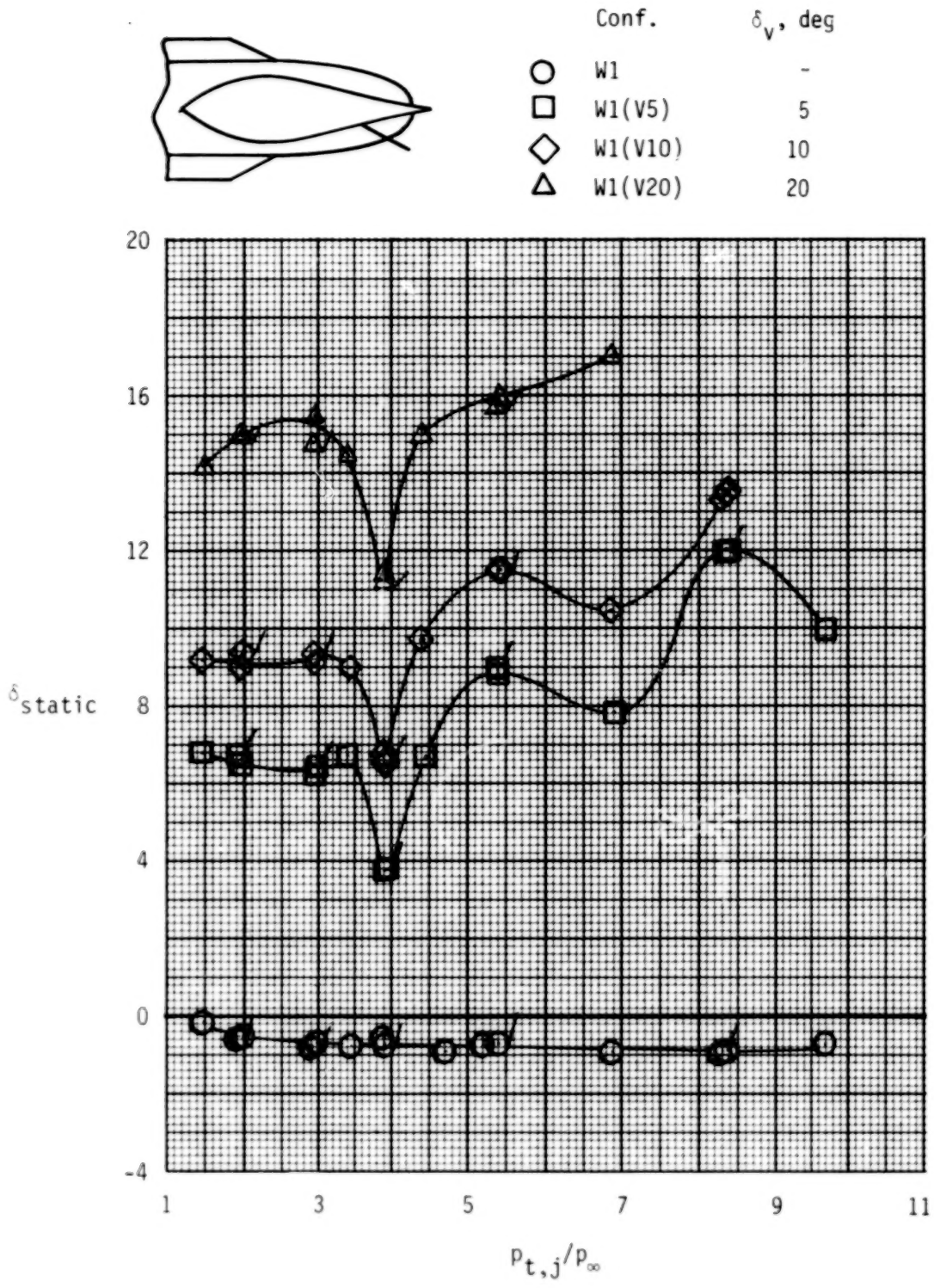

(b) Effect of vector angle. $(A_e/A_t)_e$ = 3.809; long sidewall.

Figure 10.- Continued.

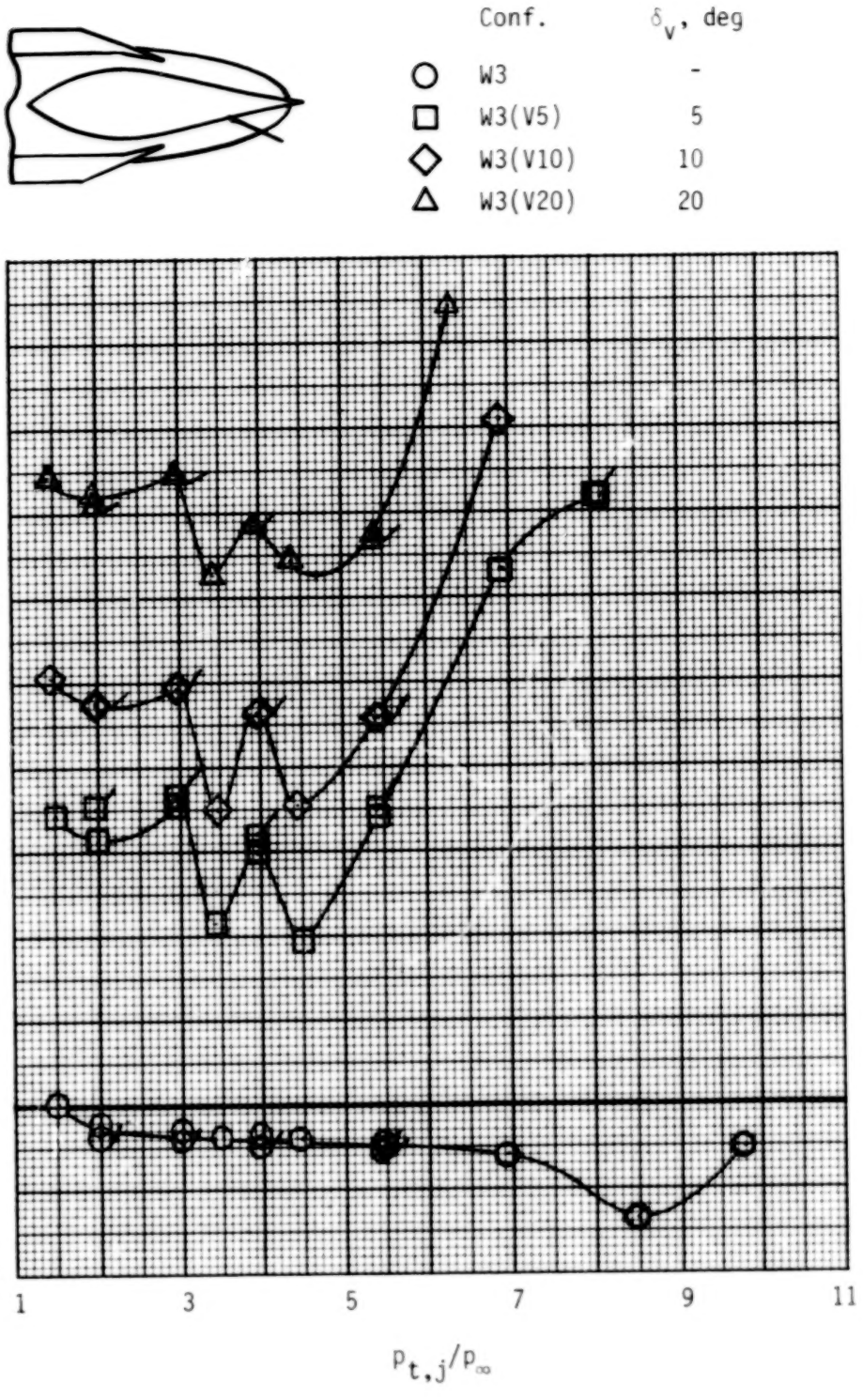

(c) Effect of vector angle. $(A_e/A_t)_e$ = 2.982; long sidewall.

Figure 10.- Continued.

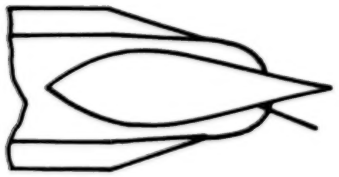

Conf.	δ_v, deg
W4	-
W4(V5)	5
W4(V10)	10
W4(V20)	20

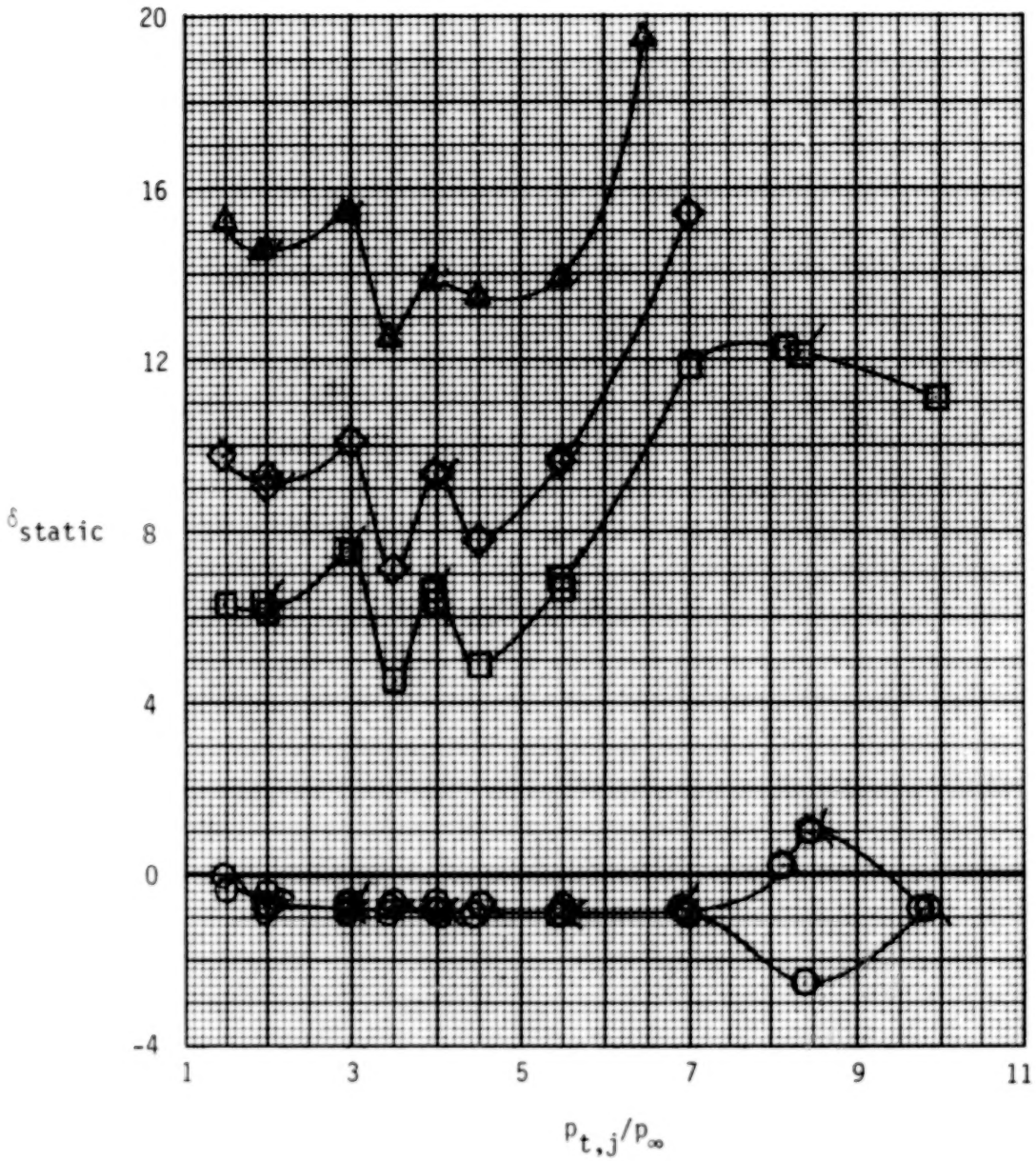

(d) Effect of vector angle. $(A_e/A_t)_e$ = 2.982; short sidewall.

Figure 10.- Continued.

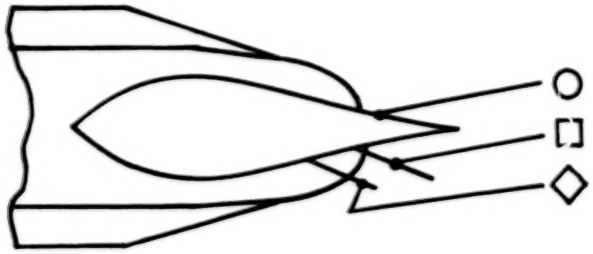

Conf.	δ_v, deg
W4	-
W4(V5)	5.0
W4(FV5)	3.5

(A_e/A_t) = 2.982, short sidewall

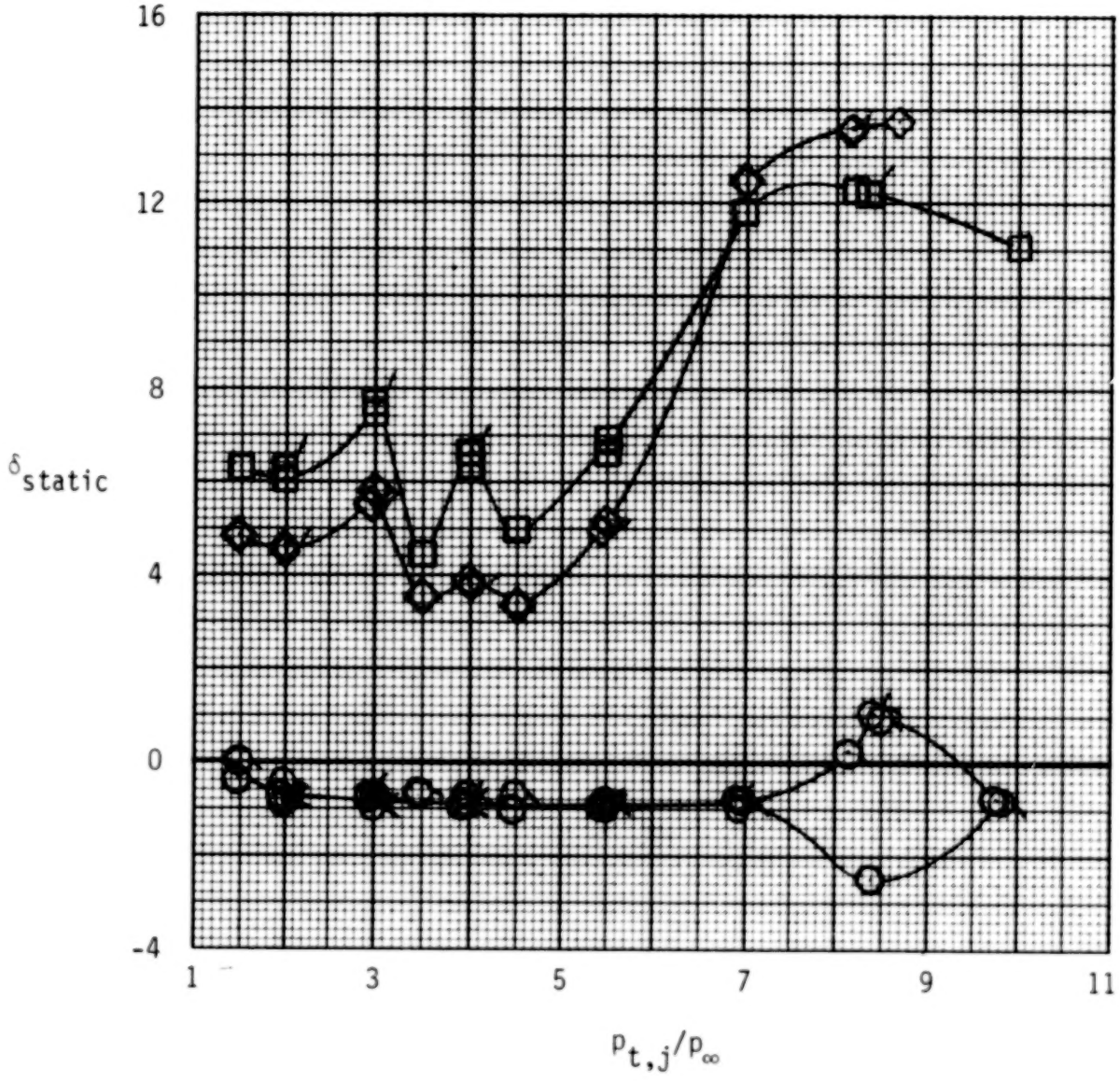

(e) Effect of vector flap location.

Figure 10.- Continued.

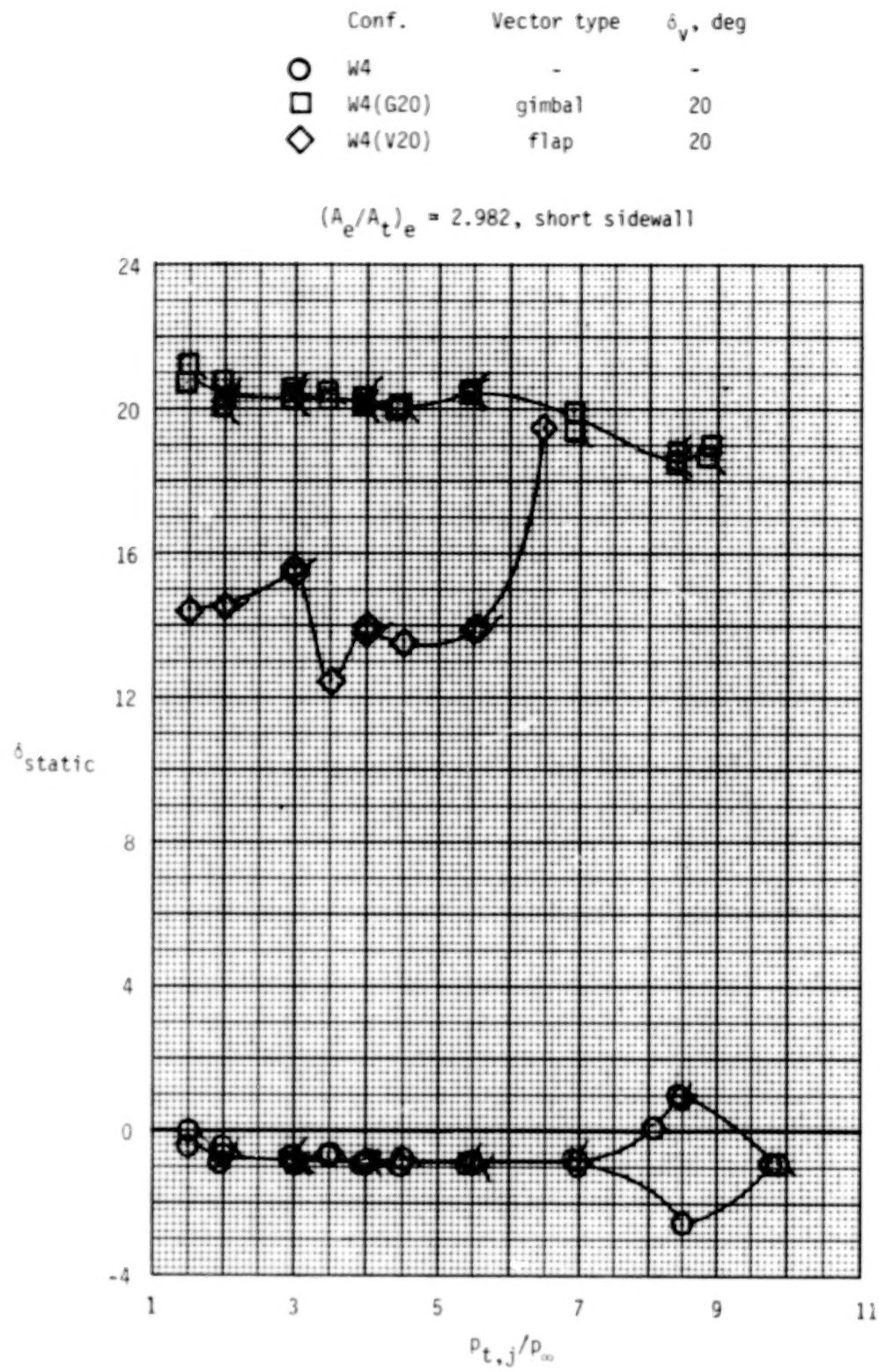

(f) Effect of vectoring type.

Figure 10.- Concluded.

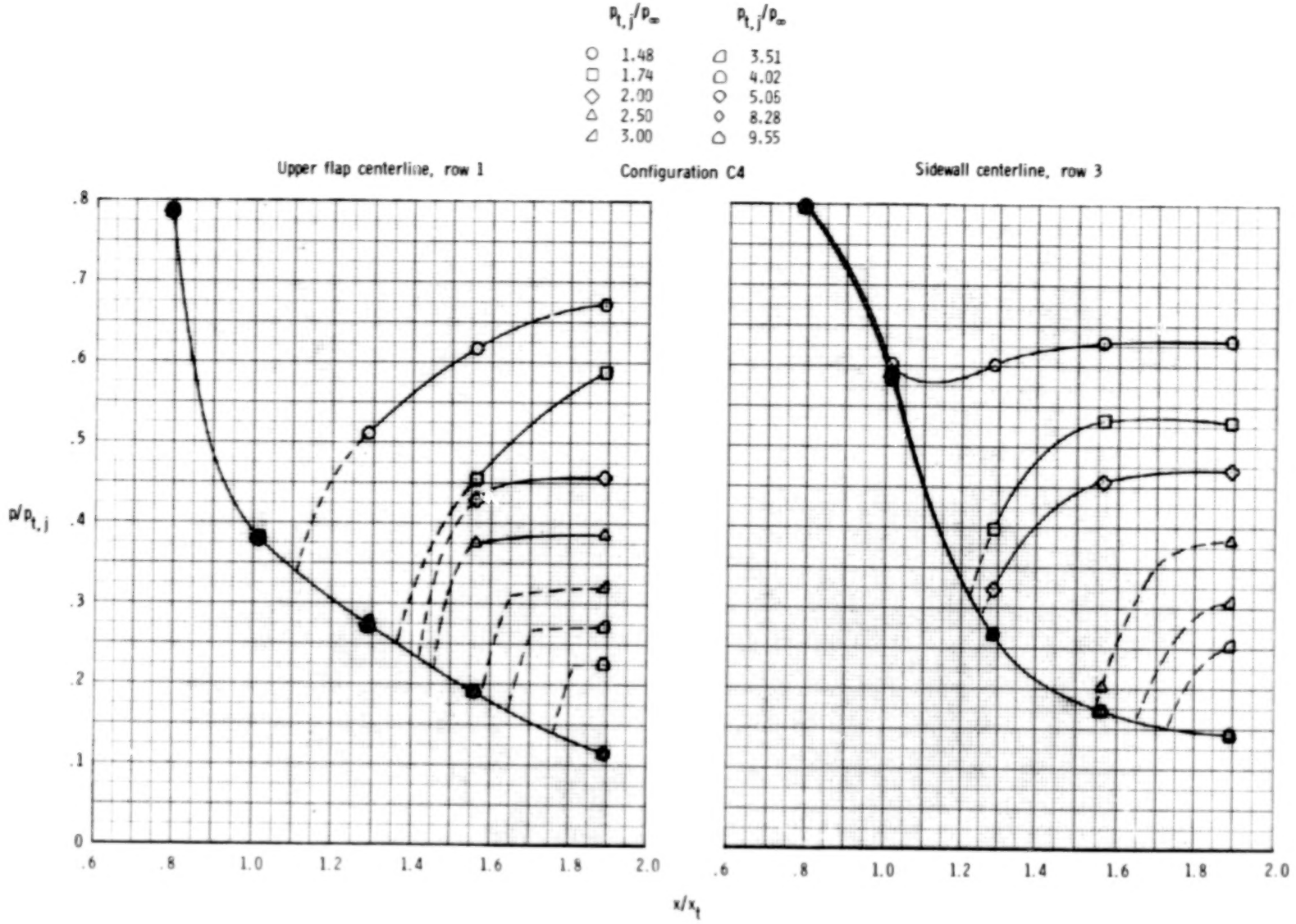

Figure 11.- Effect of nozzle pressure ratio on nonaxisymmetric convergent-divergent nozzle internal static-pressure distributions. Configuration C4; A_e/A_t = 1.797; full sidewall. Dashed lines indicate approximate fairing.

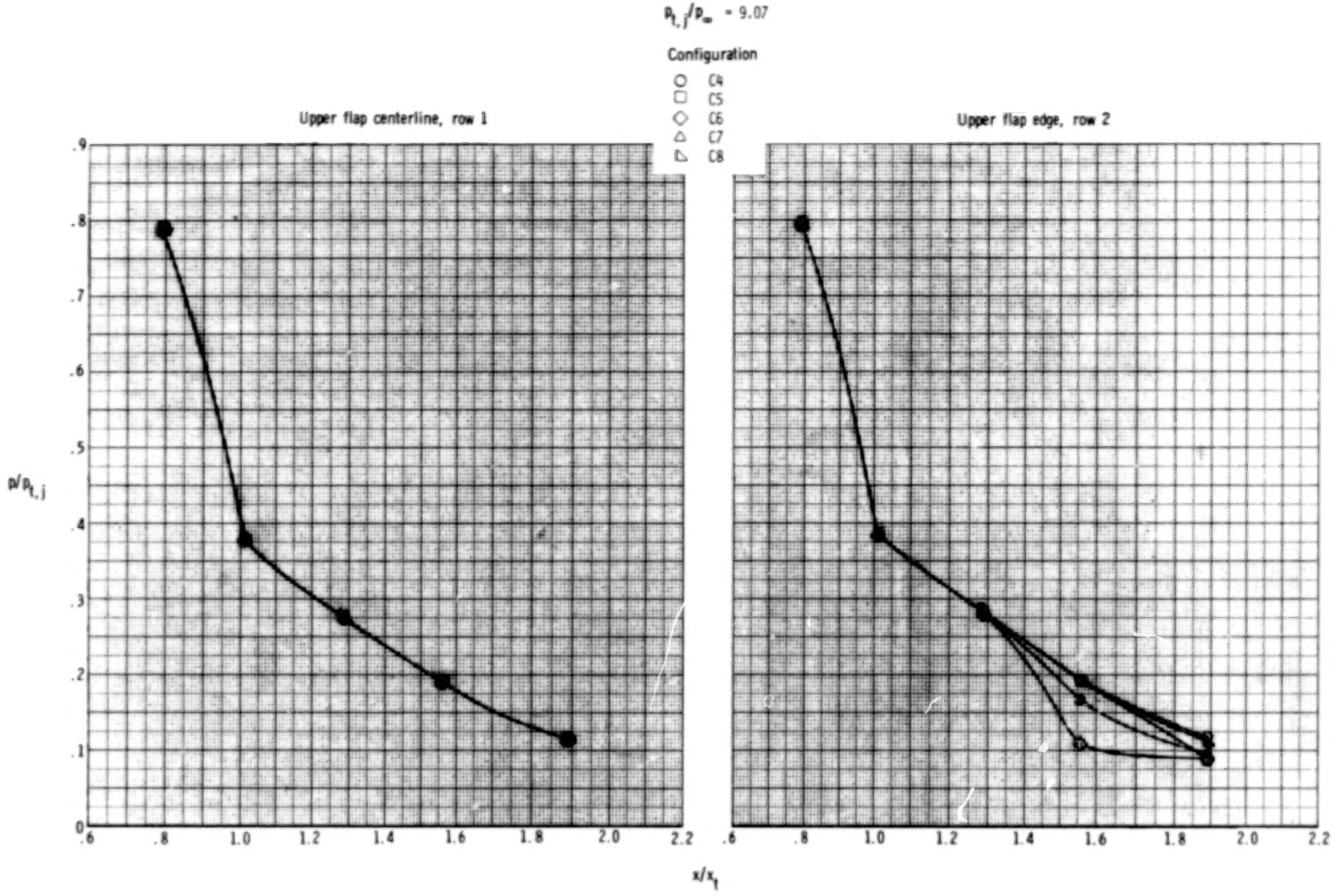

Figure 12.- Effect of sidewall geometry on nonaxisymmetric convergent-divergent nozzle internal-flap static-pressure distributions. A_e/A_t = 1.797.

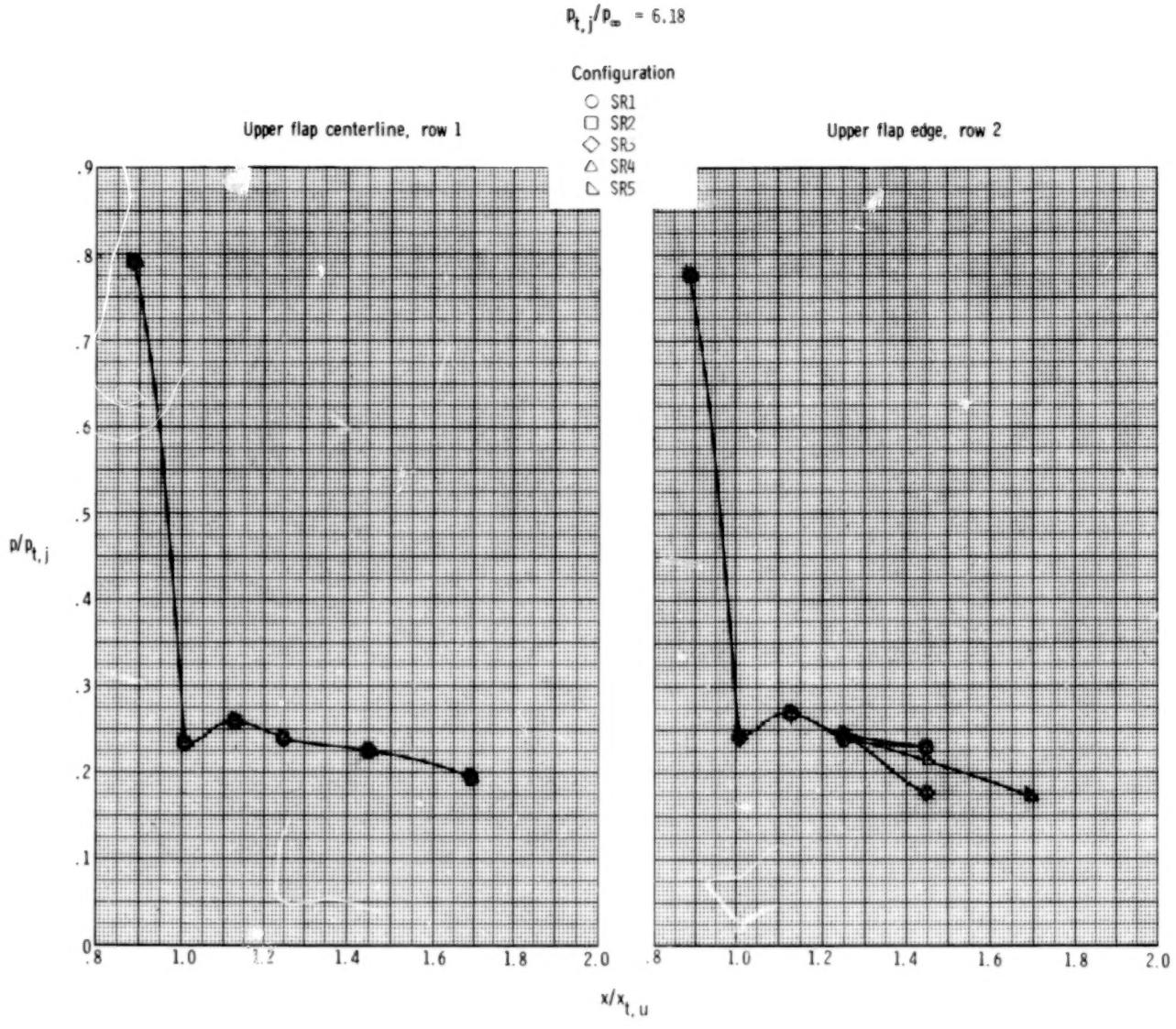

Figure 13.- Effect of sidewall geometry on single-ramp expansion nozzle static-pressure distributions. Upper flap.

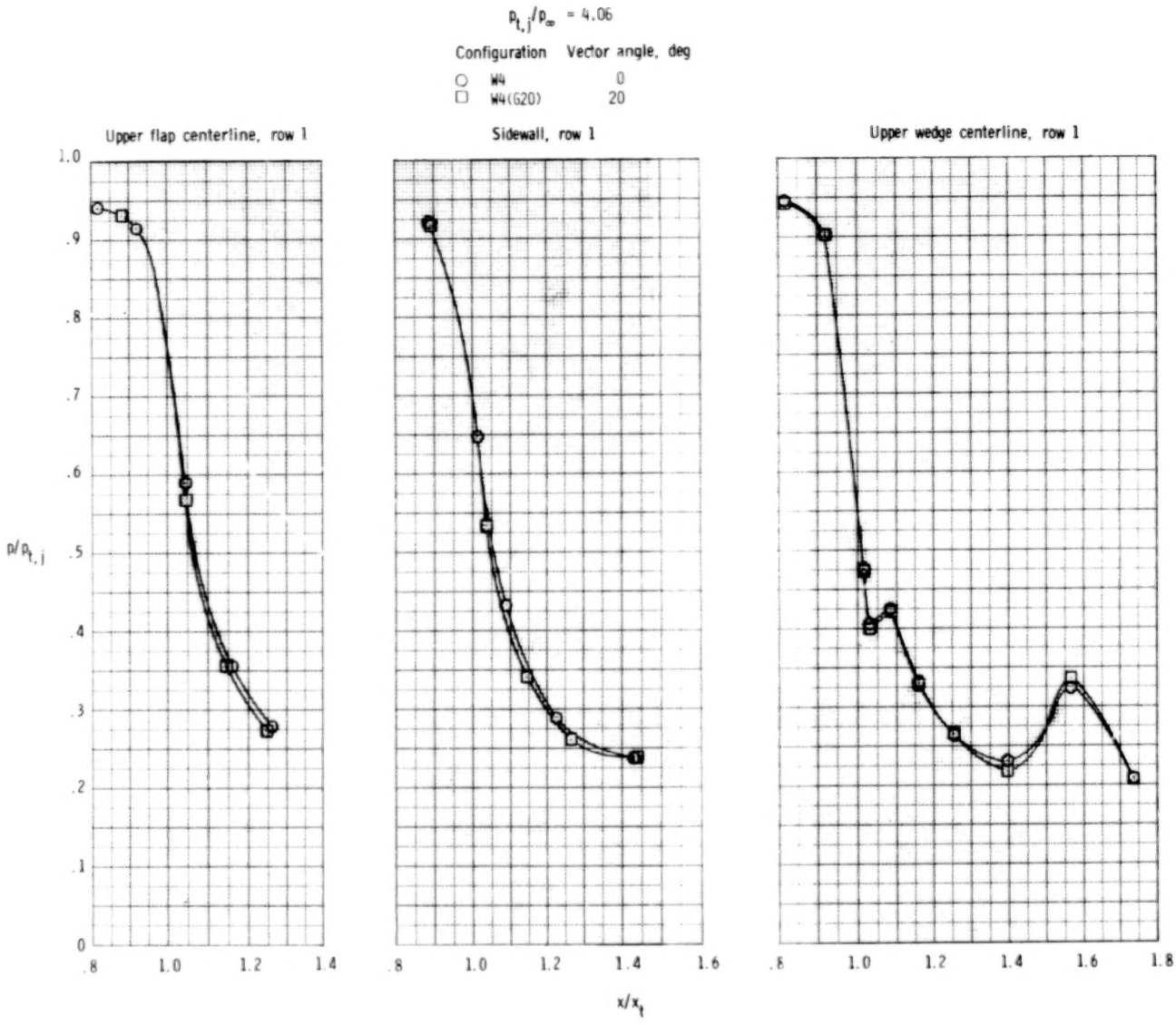

Figure 14.- Effect of gimbal vector angle on wedge nozzle internal pressure distributions. $(A_e/A_t)_e$ = 2.982; short sidewall.

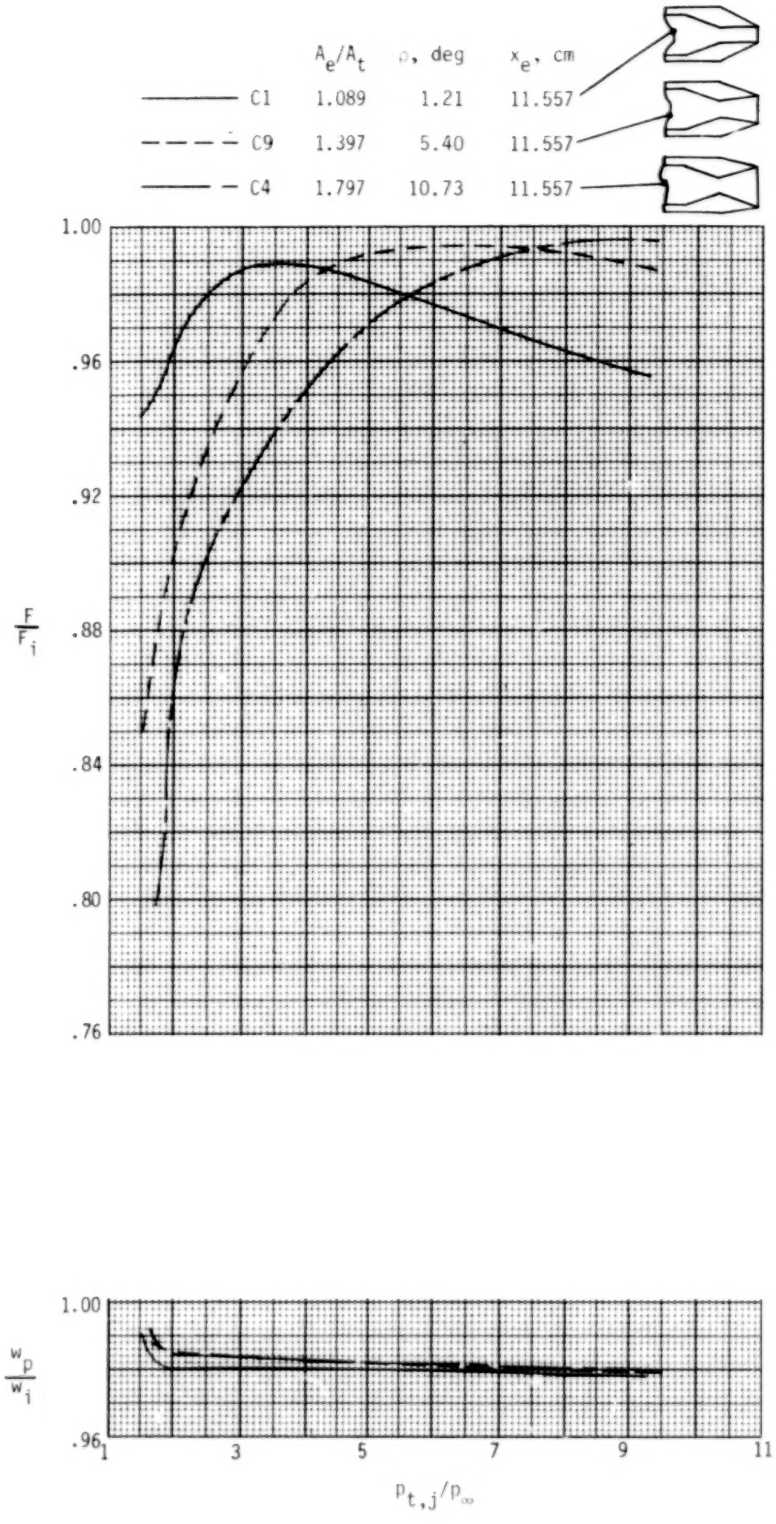

(a) Constant length; variable A_e/A_t and ρ.

Figure 15.- Effect of several nozzle design parameters on nozzle thrust ratio and discharge coefficient.

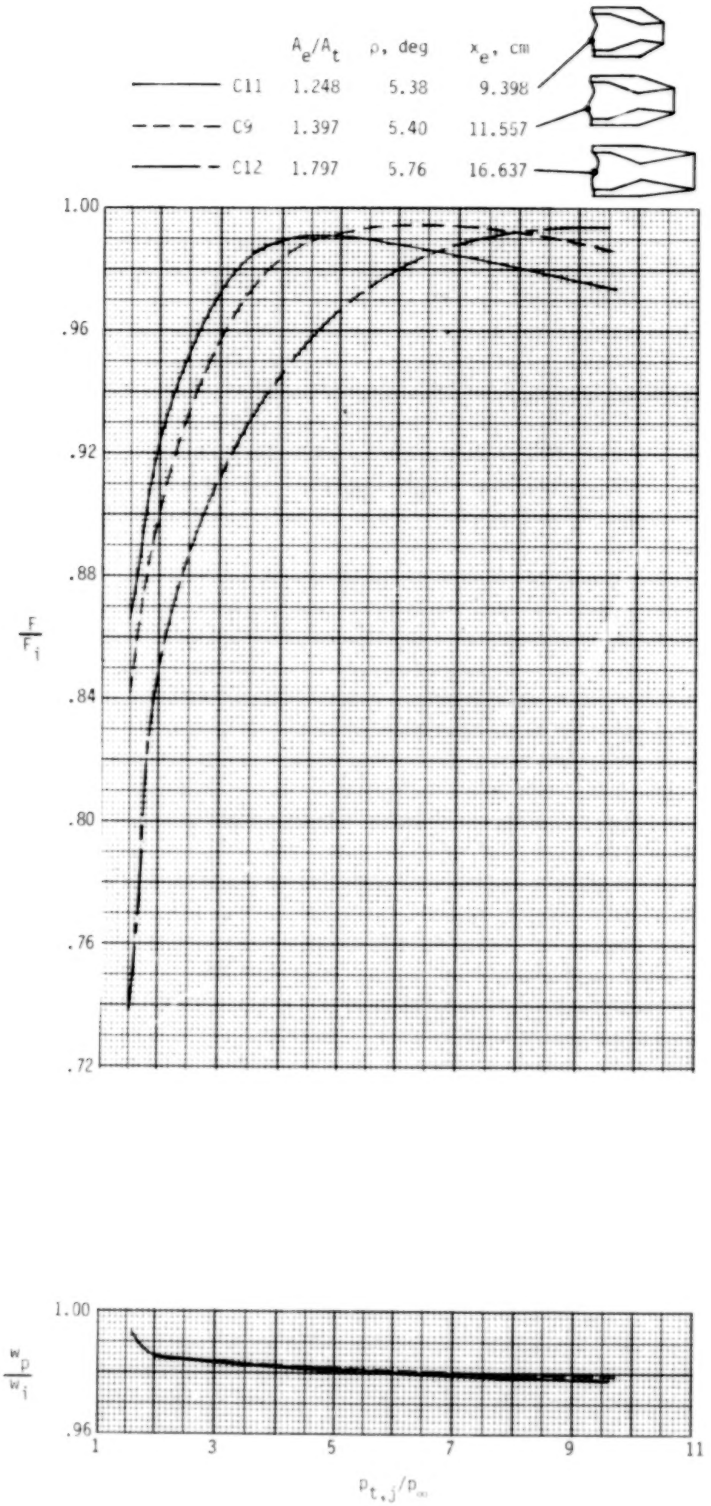

(b) Constant ρ; variable A_e/A_t and length.

Figure 15.- Continued.

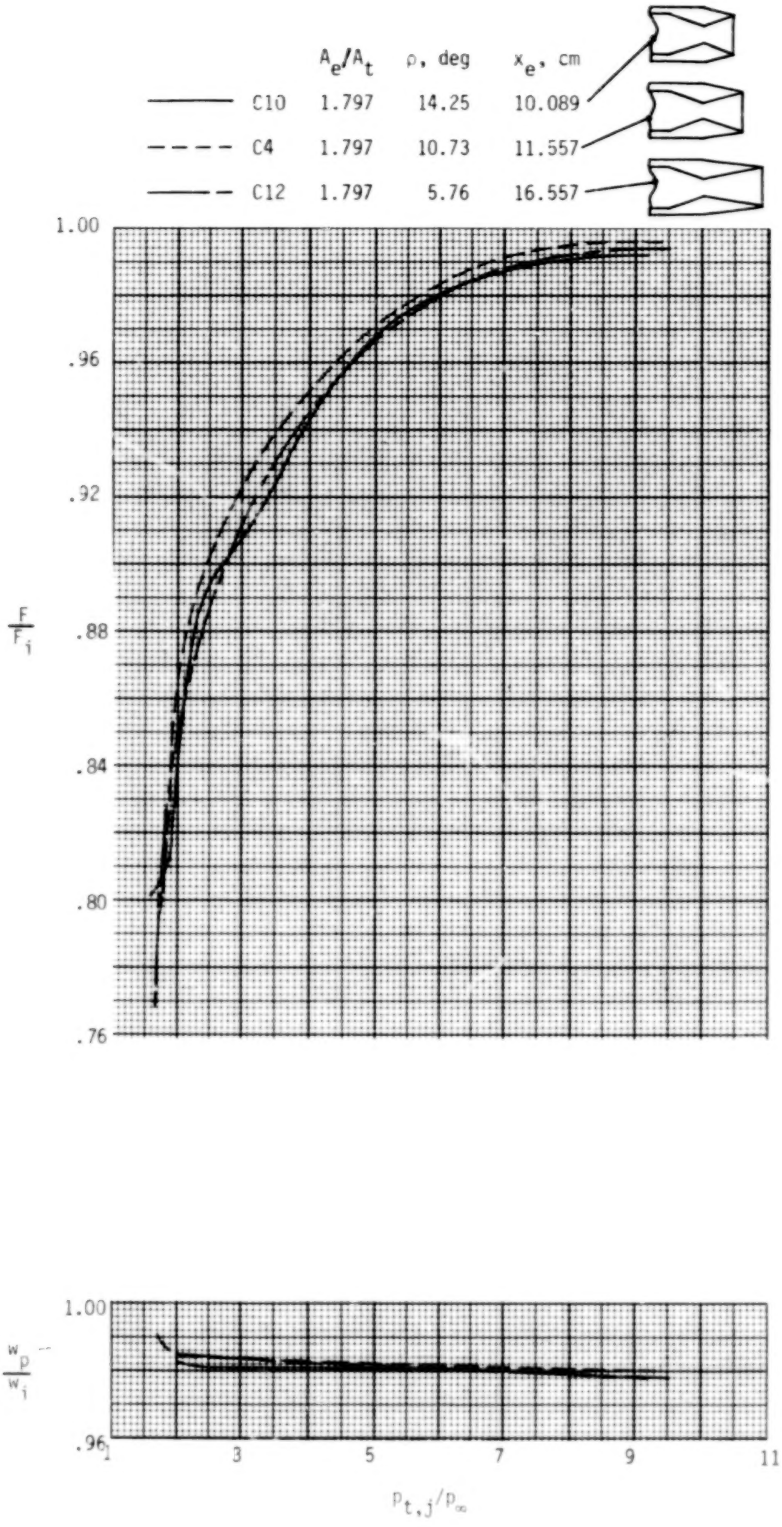

(c) Constant A_e/A_t; variable ρ and length.

Figure 15.- Concluded.

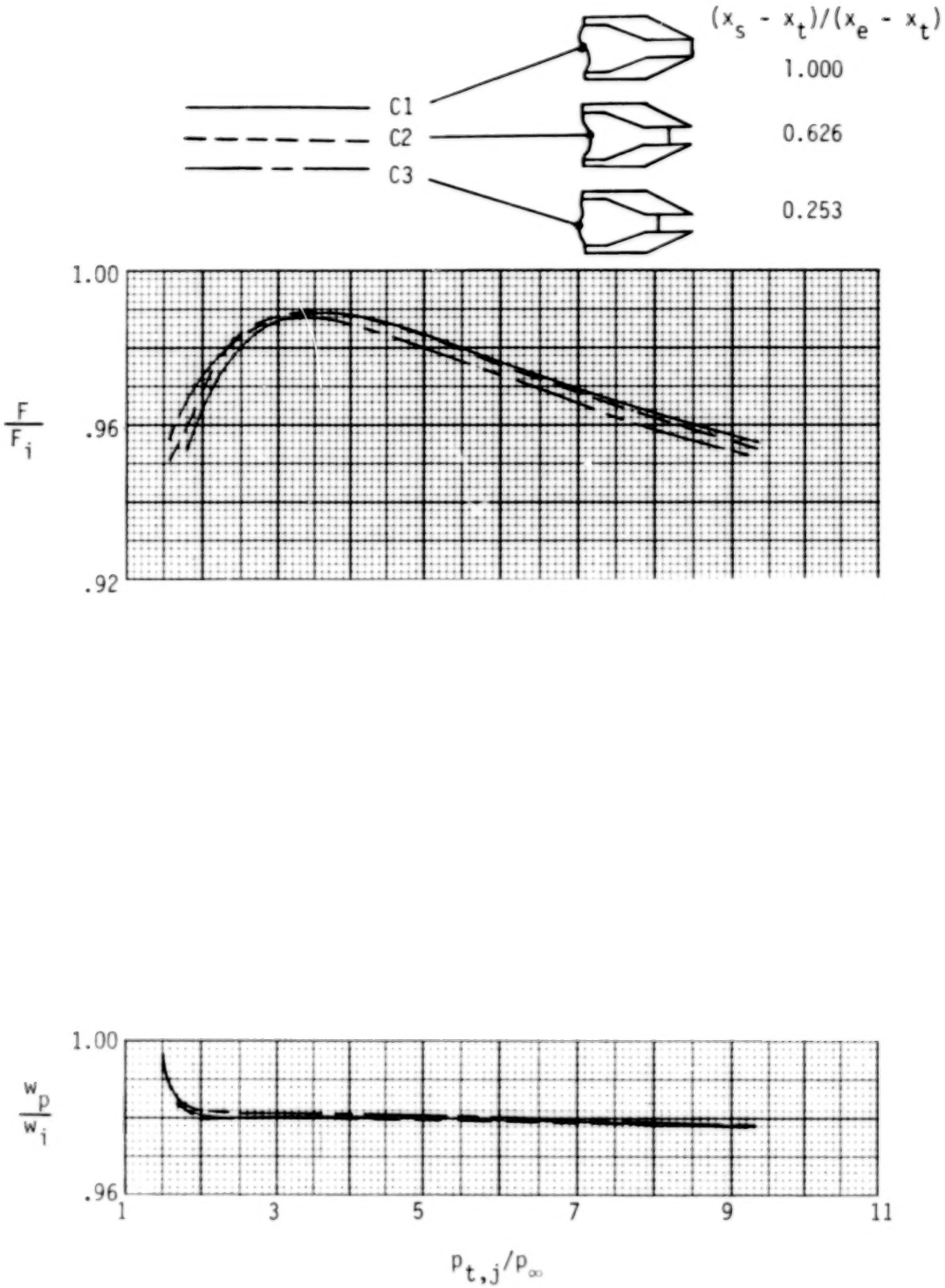

(a) A_e/A_t = 1.089; AR = 3.696; x_e = 11.557.

Figure 16.- Effect of sidewall length on nozzle thrust ratio and discharge coefficient.

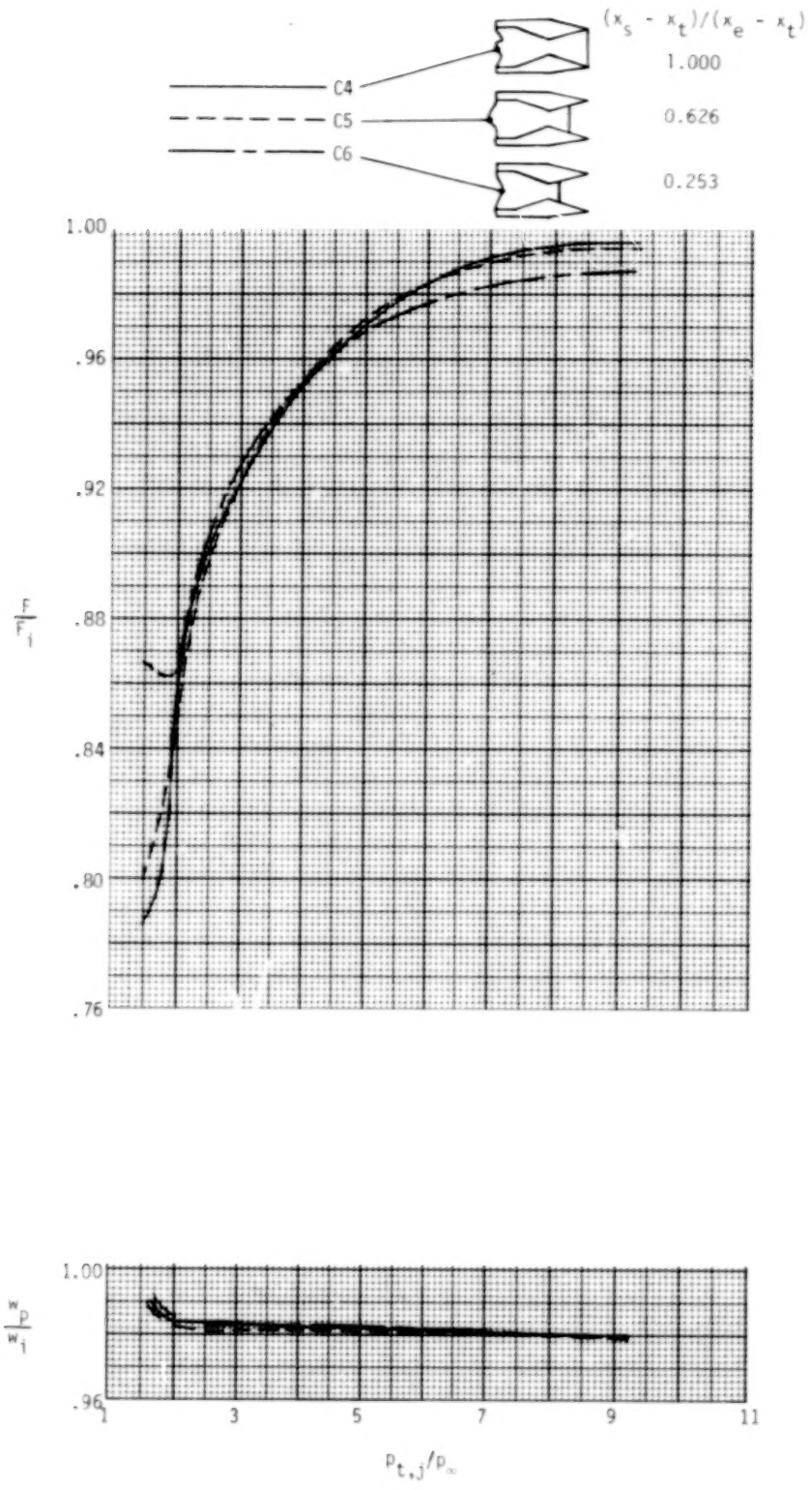

(b) A_e/A_t = 1.797; AR = 3.696; x_e = 11.557.

Figure 16.- Continued.

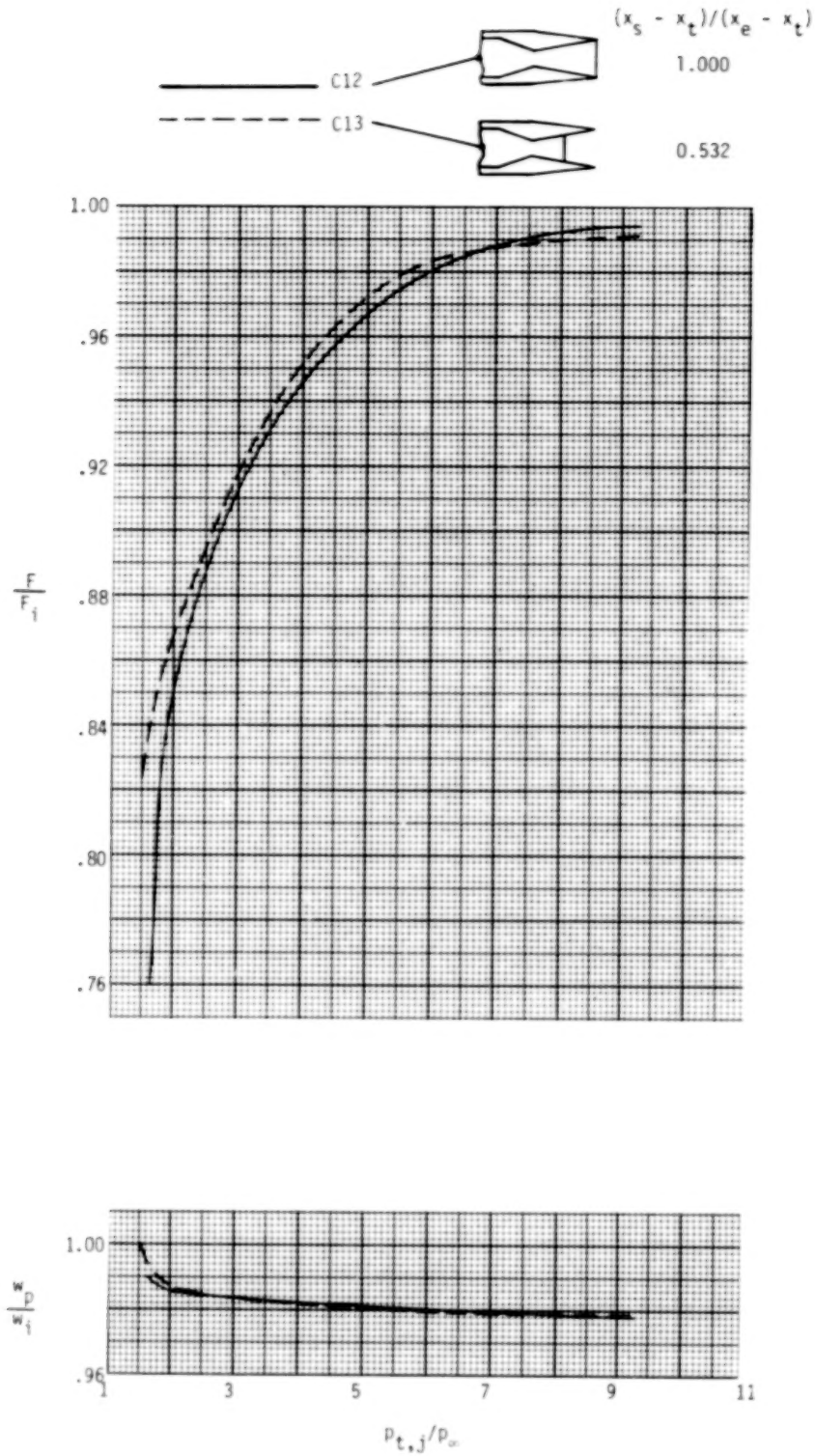

(c) A_e/A_t = 1.797; AR = 3.696; x_e = 16.637.

Figure 16.- Concluded.

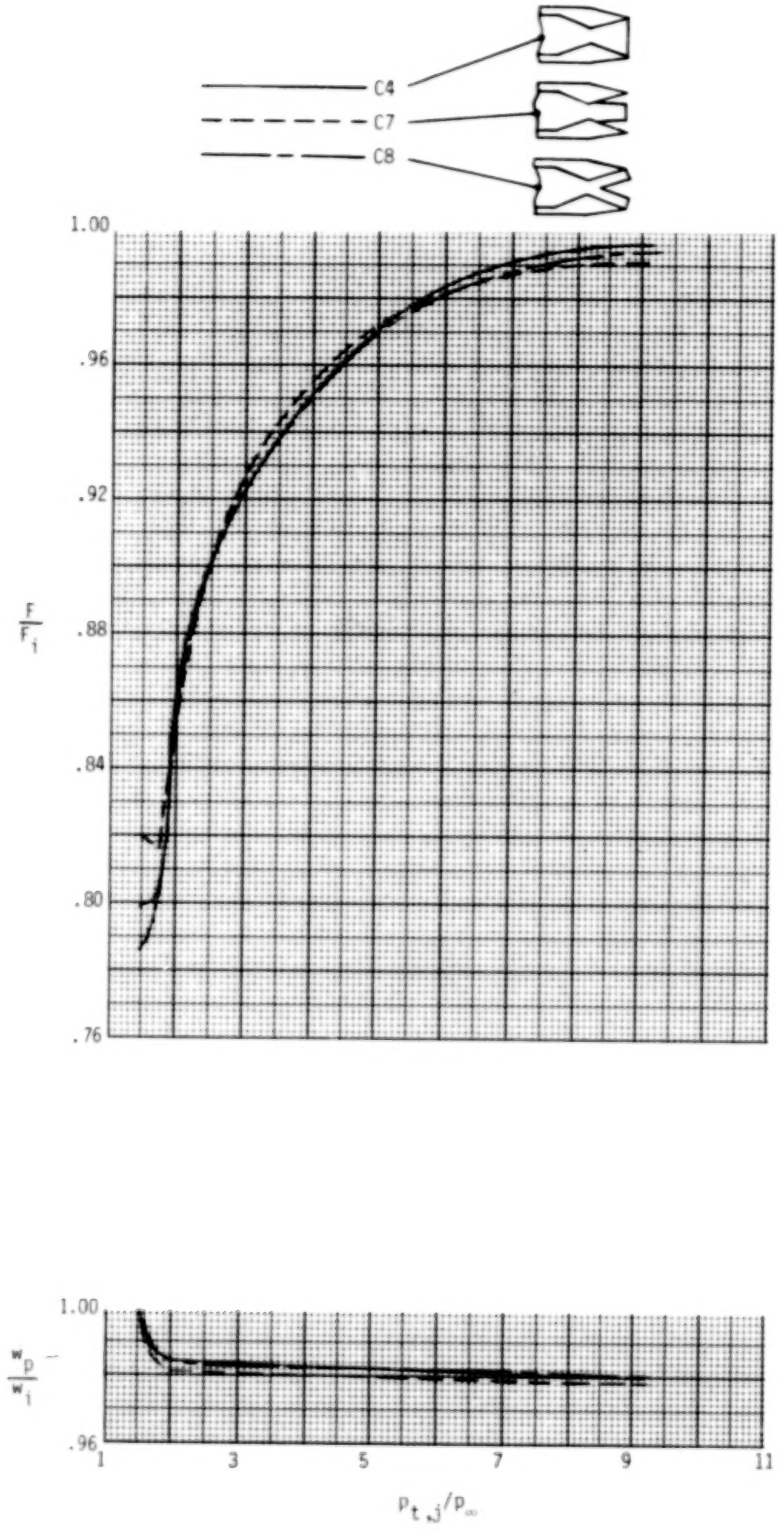

Figure 17.- Effect of sidewall geometry on nozzle thrust ratio and discharge coefficient. A_e/A_t = 1.797; AR = 3.696; x_e = 11.557.

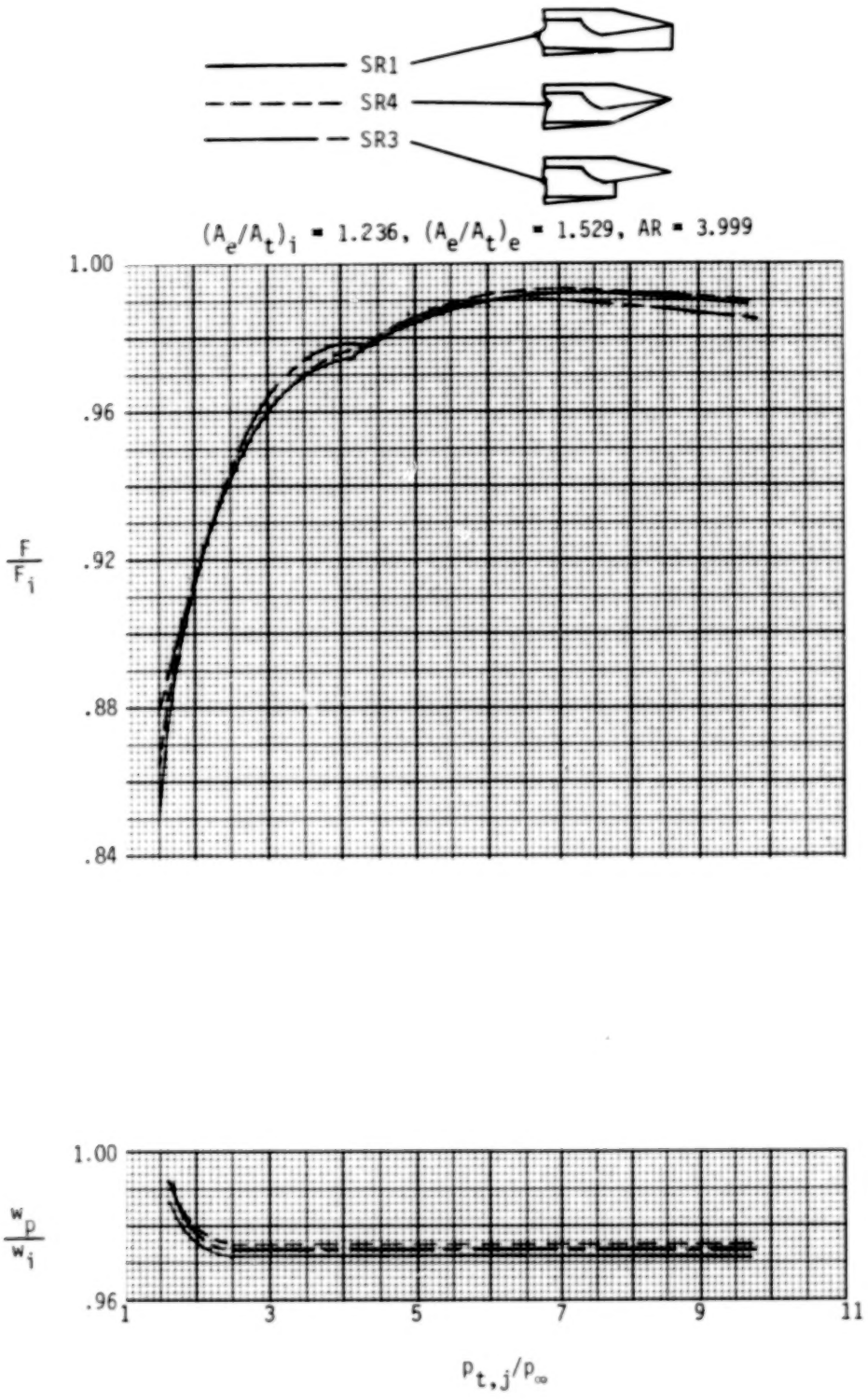

(a) Configurations SR1, SR3, and SR4.

Figure 18.- Effect of sidewall geometry on nozzle thrust ratio and discharge coefficient.

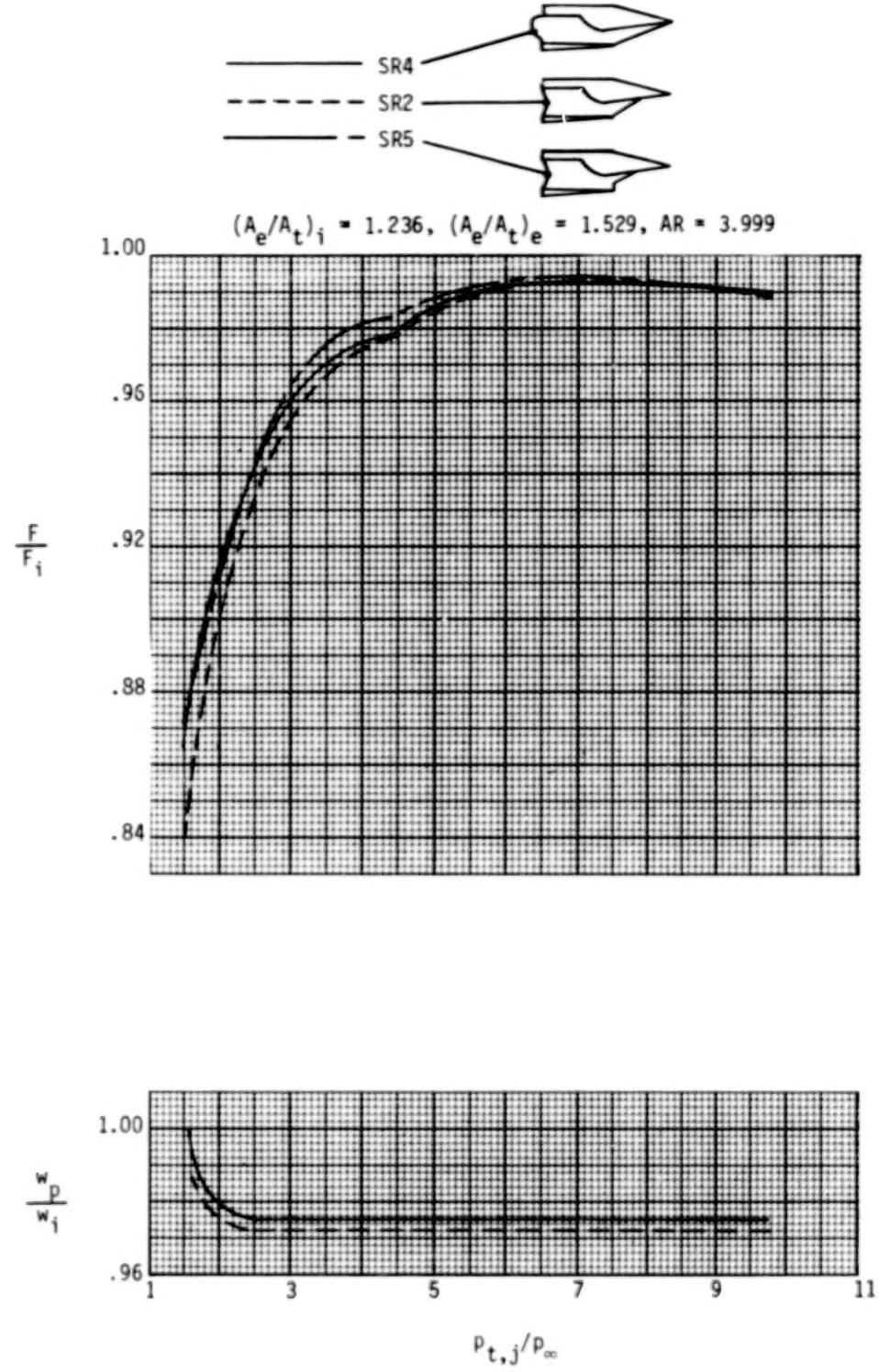

(b) Configurations SR2, SR4, and SR5.

Figure 18.- Concluded.

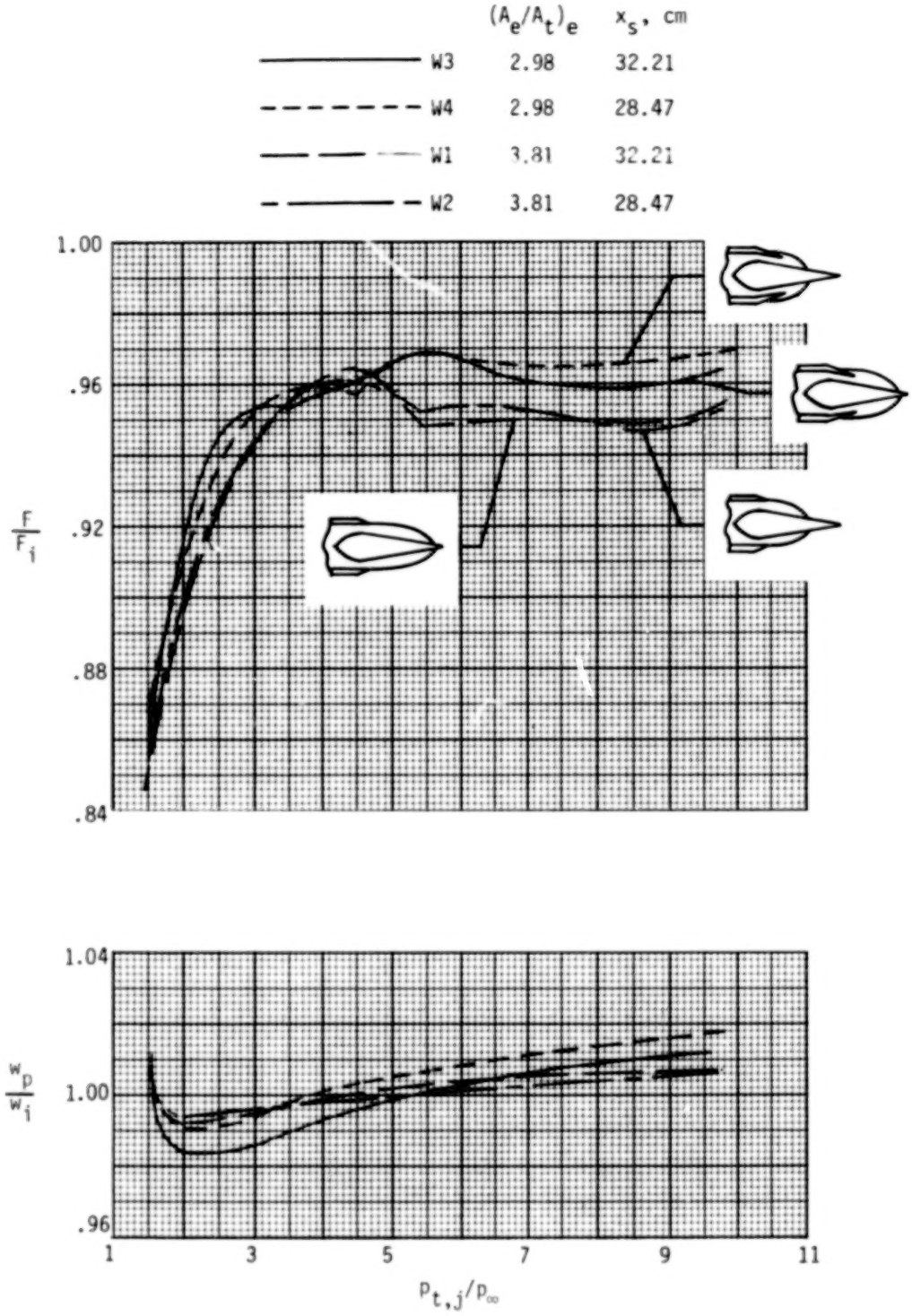

Figure 19.- Effect of external area ratio and sidewall length on nozzle thrust ratio and discharge coefficient.

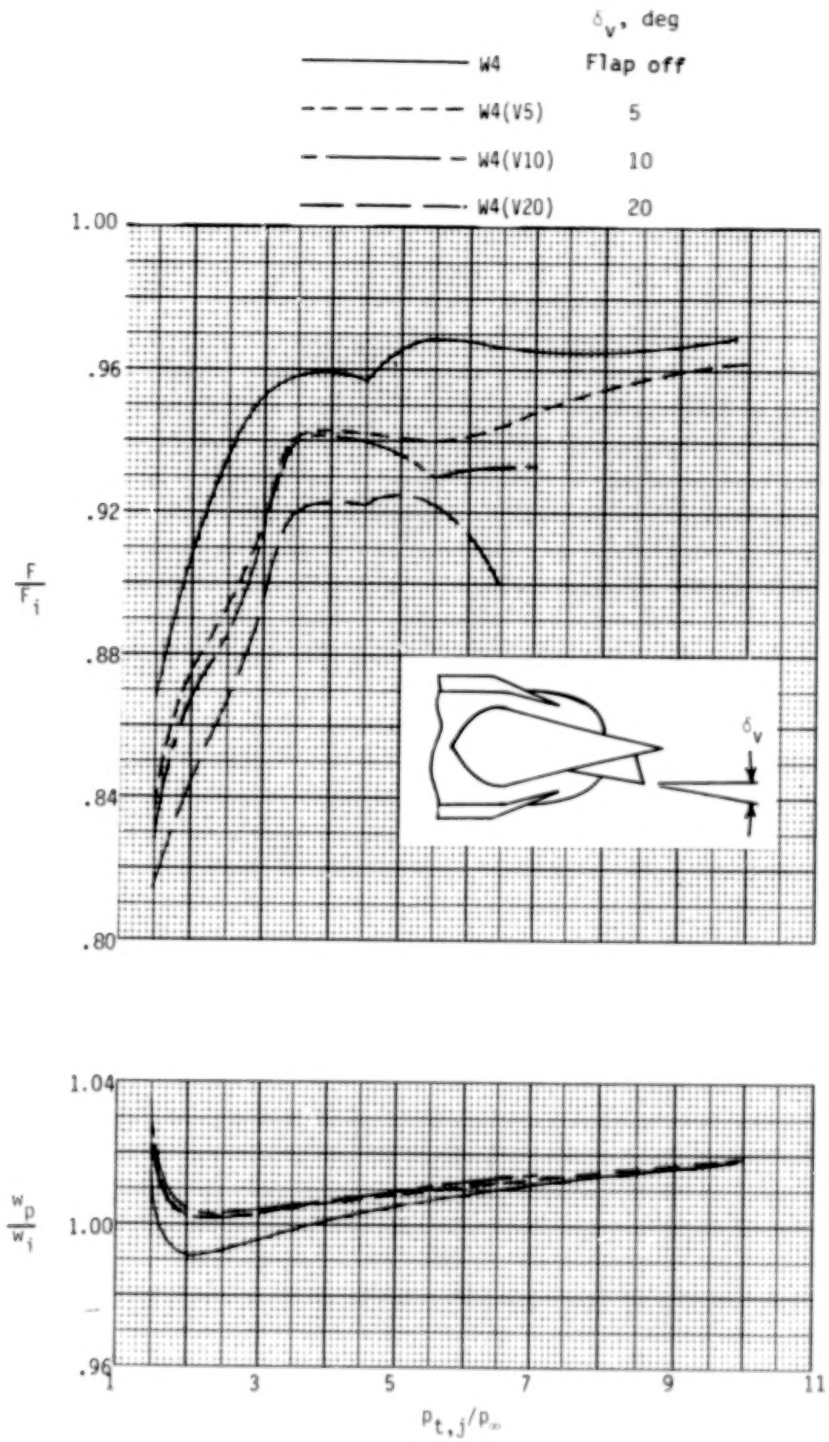

(a) $(A_e/A_t)_e = 2.98$; $x_s = 28.47$ cm.

Figure 20.- Effect of vector flap angle on nozzle thrust ratio and discharge coefficient.

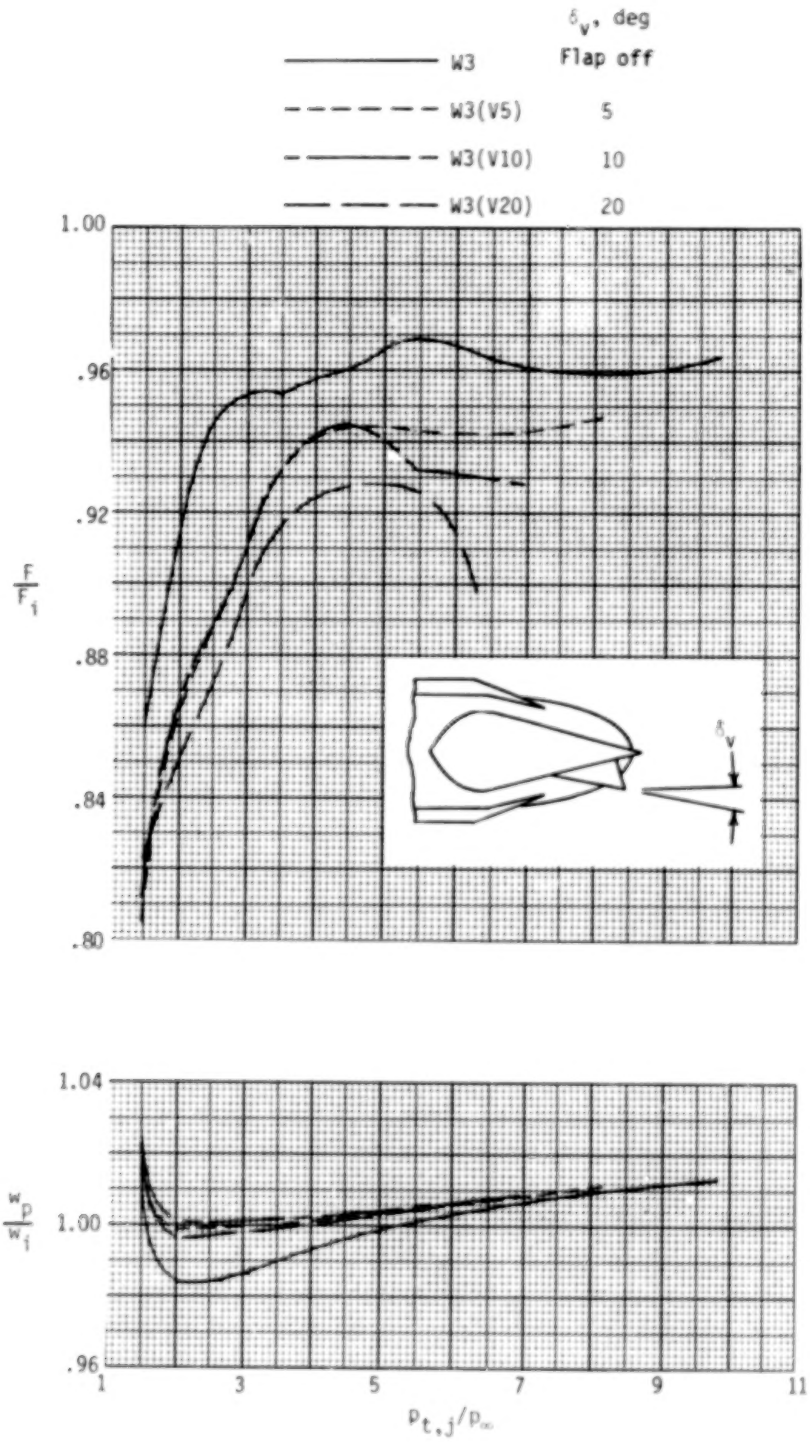

(b) $(A_e/A_t)_e = 2.98$; $x_s = 32.21$ cm.

Figure 20.- Continued.

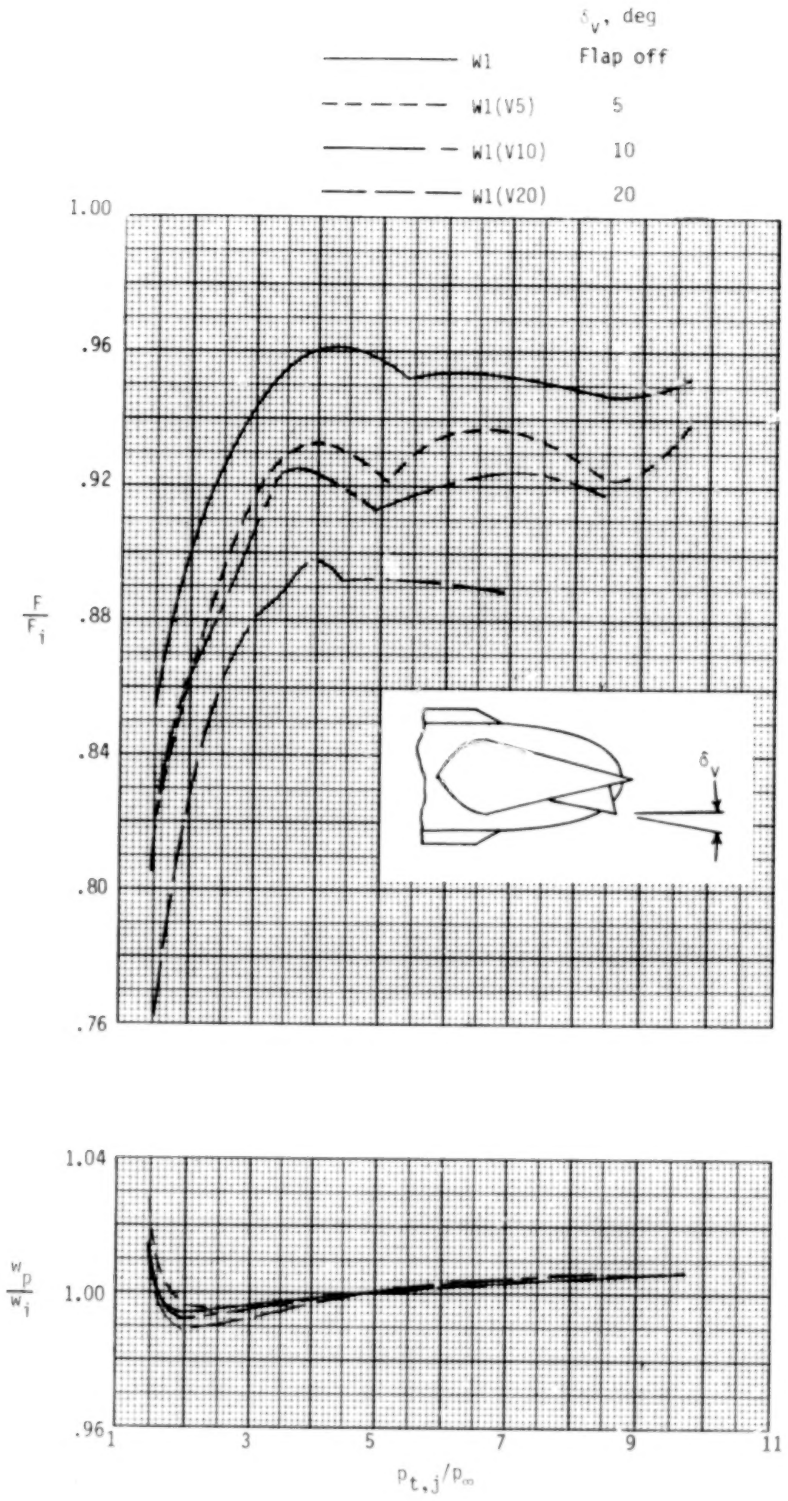

(c) $(A_e/A_t)_e = 3.81$; $x_s = 32.21$ cm.

Figure 20.- Concluded.

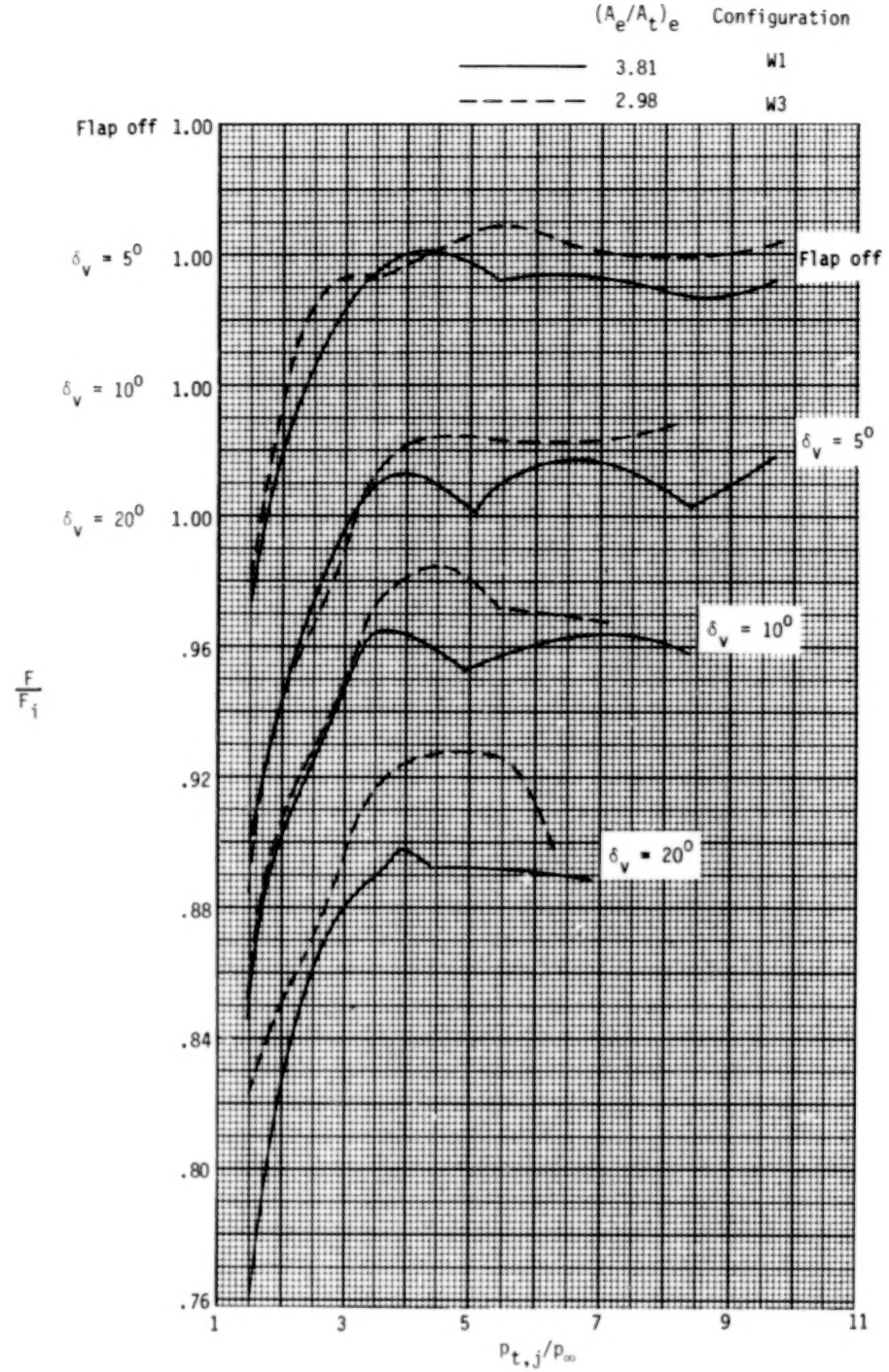

Figure 21.- Effect of expansion flap length (external-expansion ratio) on nozzle thrust ratio. x_s = 32.21 cm.

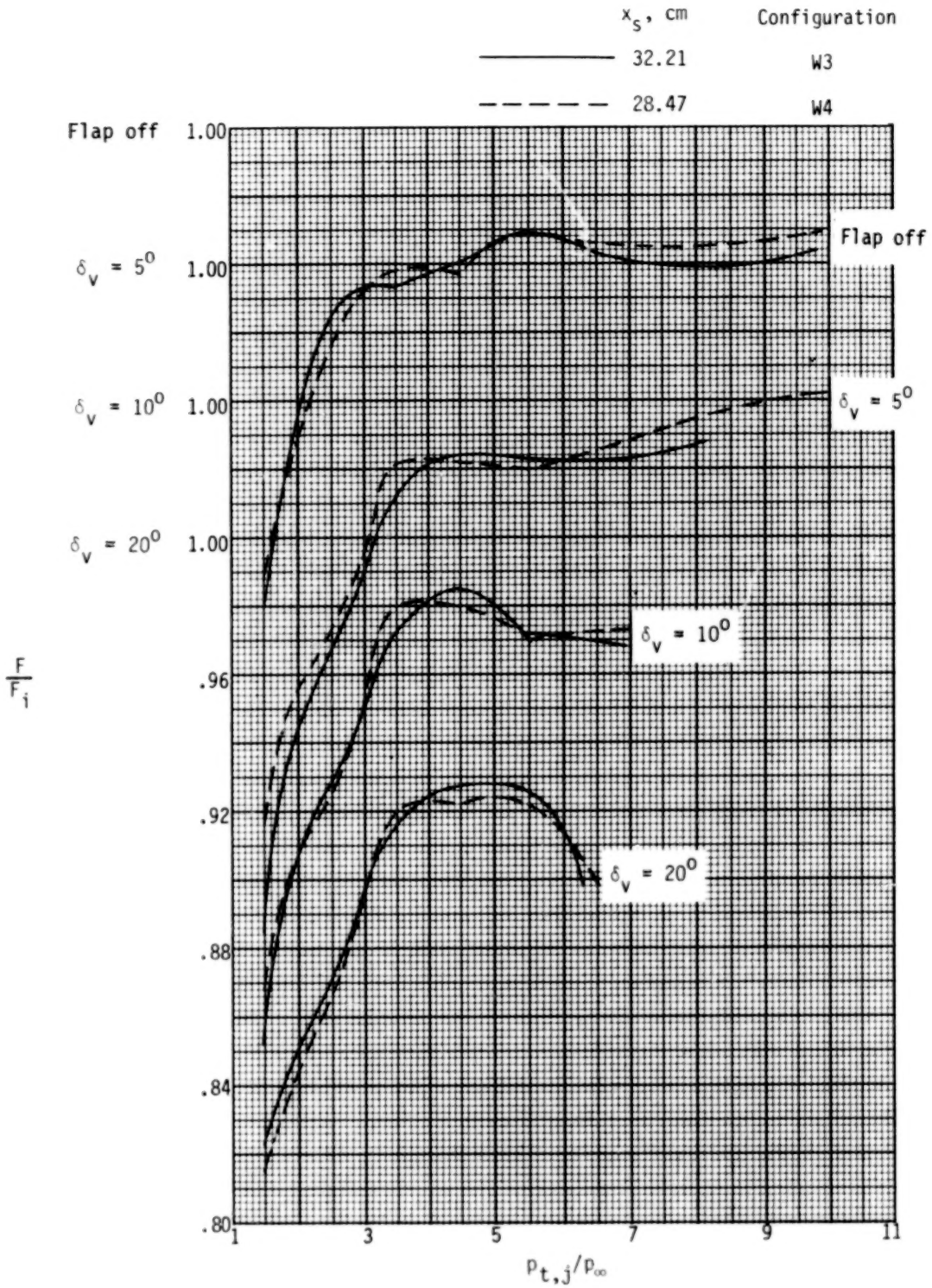

Figure 22.- Effect of sidewall length on nozzle thrust ratio. $(A_e/A_t)_e = 2.98$.

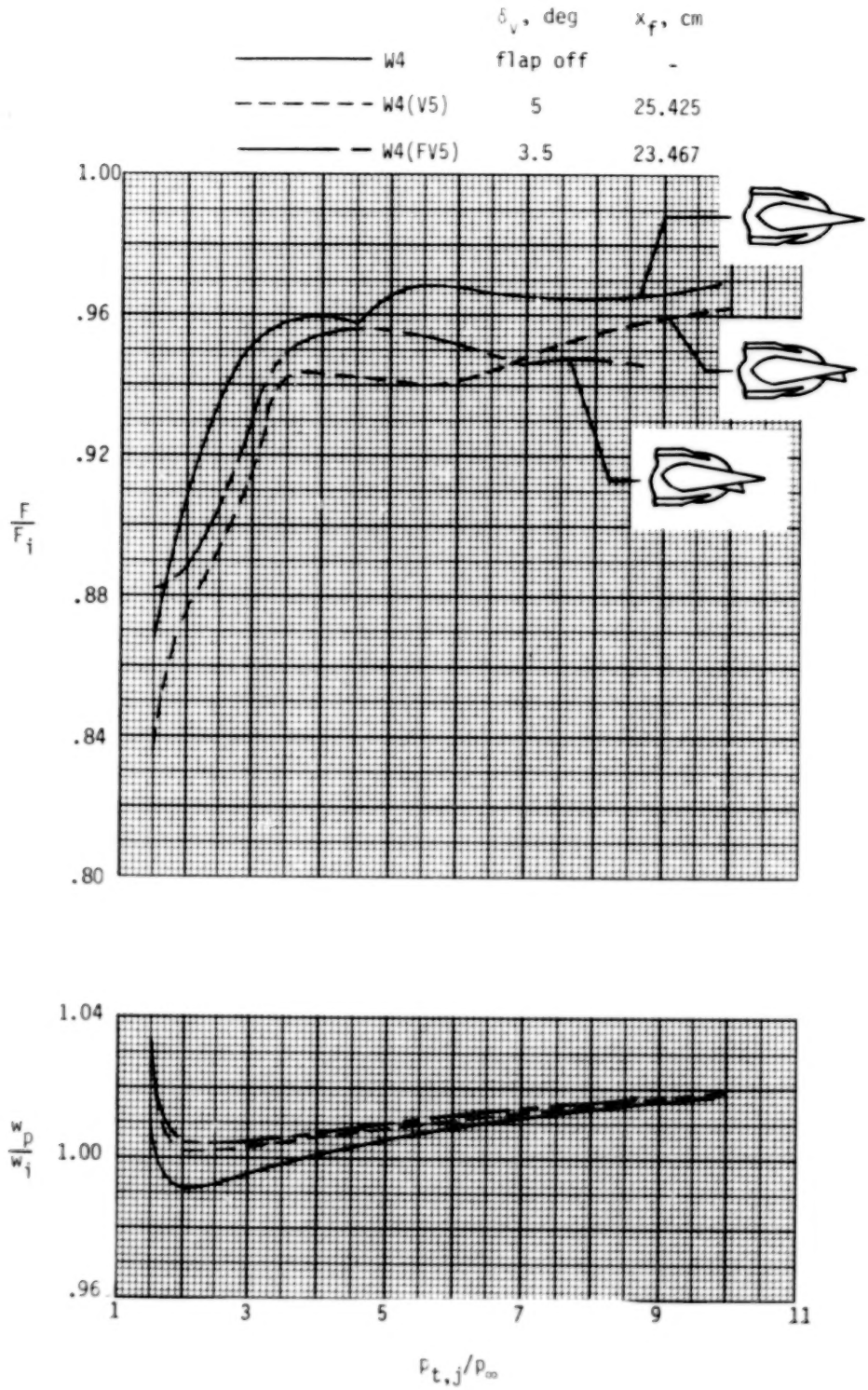

Figure 23.- Effect of vectoring flap location on nozzle thrust ratio and discharge coefficient. $(A_e/A_t)_e = 2.98$; $x_s = 28.47$ cm.

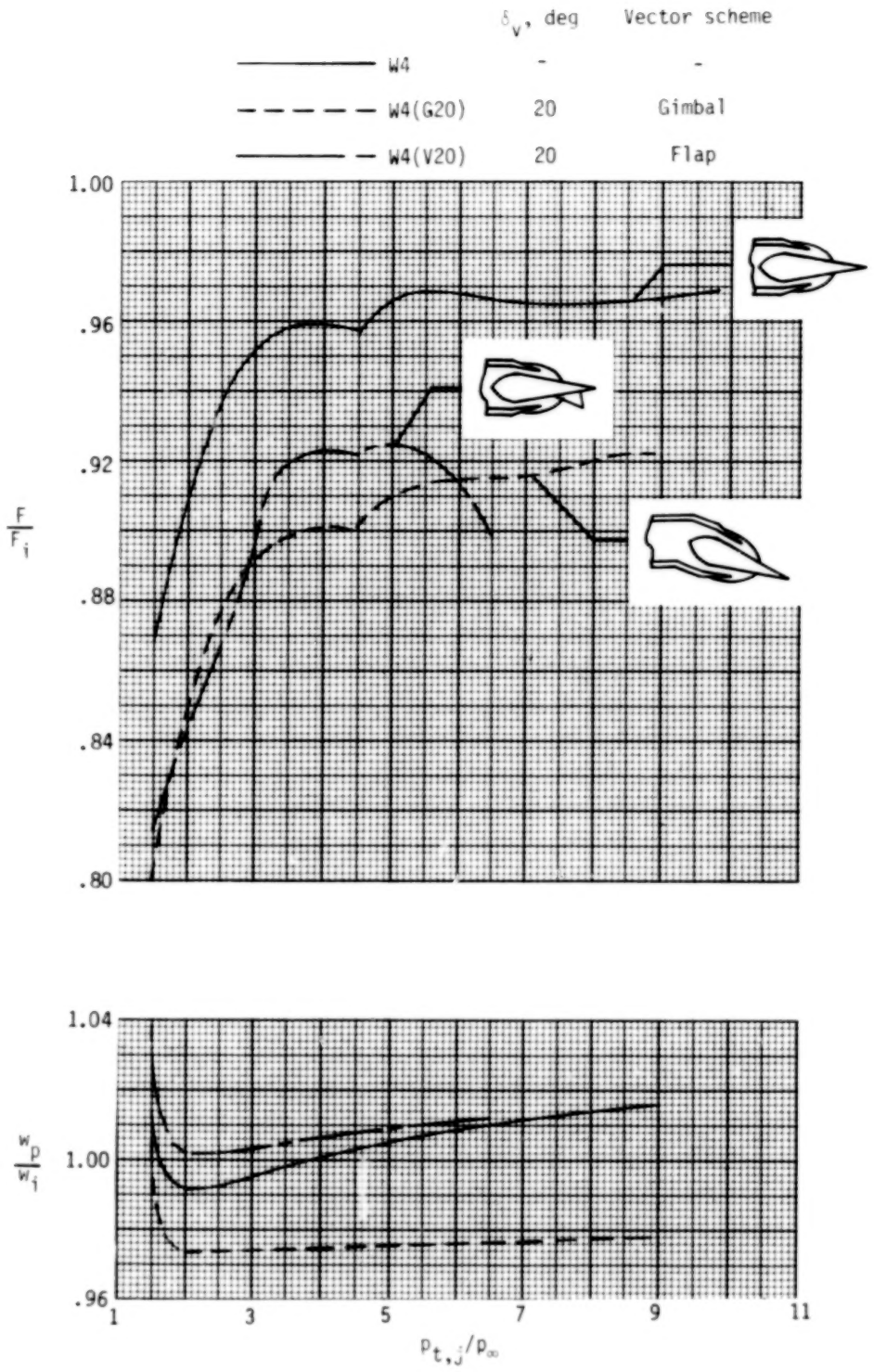

Figure 24.- Effect of wedge nozzle vectoring scheme on nozzle thrust ratio and discharge coefficient. $(A_e/A_t)_e = 2.98$; $x_s = 28.47$ cm.

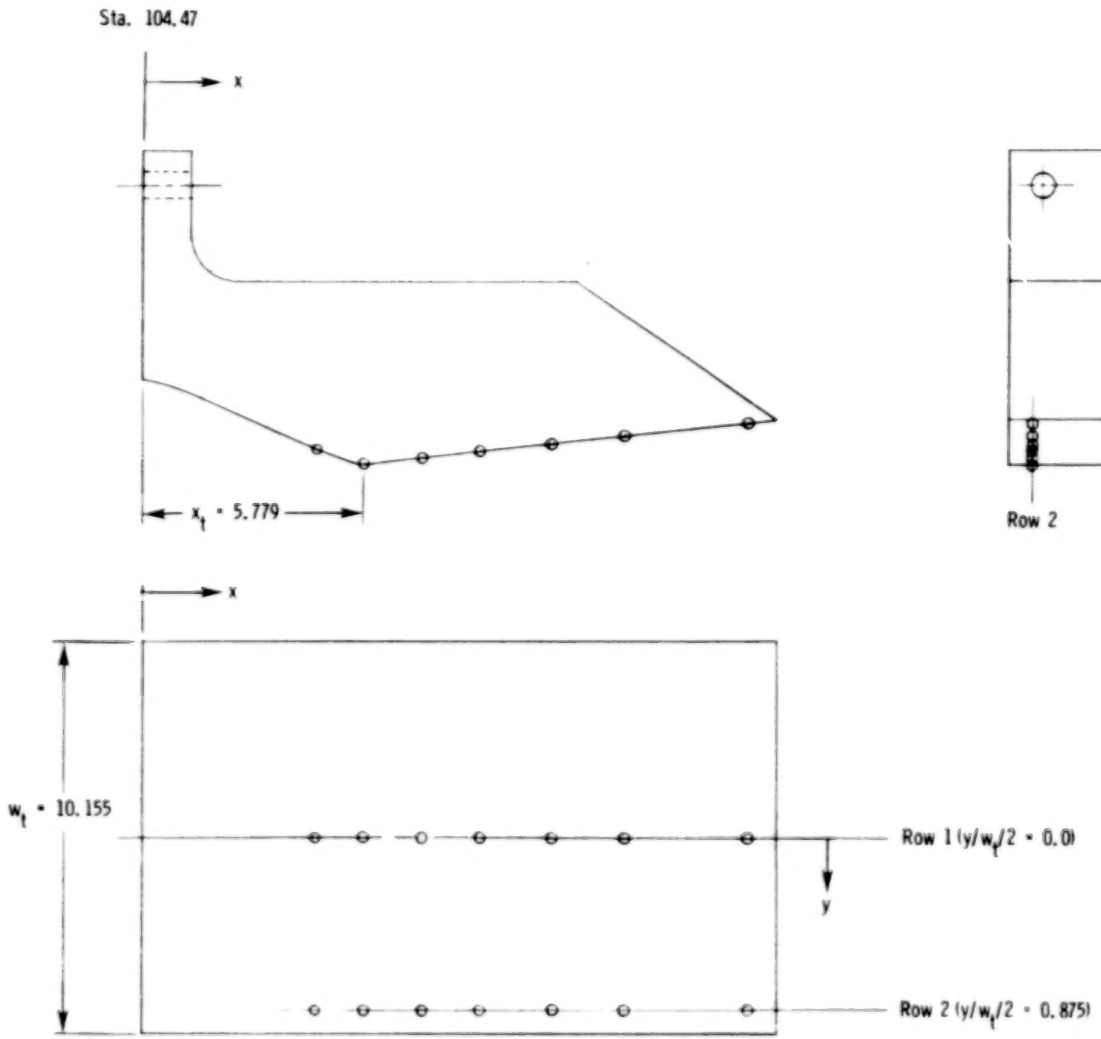

x/x_t	Configuration				
	C1 through C8		C9	C10, C11	C12
	Row 1	Row 2	Row 1	Row 1	Row 1
0.791	X	X	X	X	X
1.011	X	X	X	X	X
1.286	X	X	X	X	X
1.560	X	X	X	X	X
1.890	X	X	X		X
2.220					X
2.769					X

Typical nonaxisymmetric convergent-divergent nozzle flap

(a) Flap static-pressure instrumentation.

Figure 25.- Sketches of nonaxisymmetric convergent-divergent nozzle components showing internal static-pressure orifice locations. All dimensions are in centimeters unless otherwise noted.

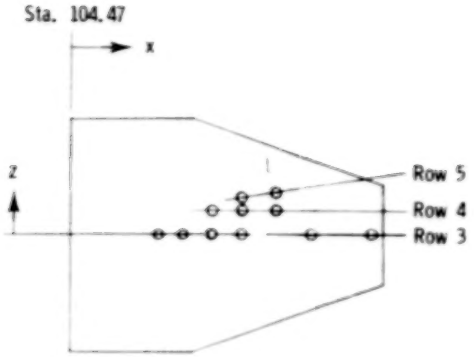

Typical nonaxisymmetric convergent-divergent nozzle sidewall

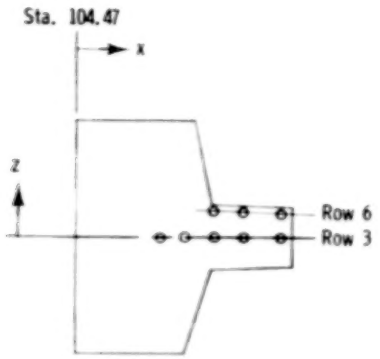

Configuration C7 sidewall

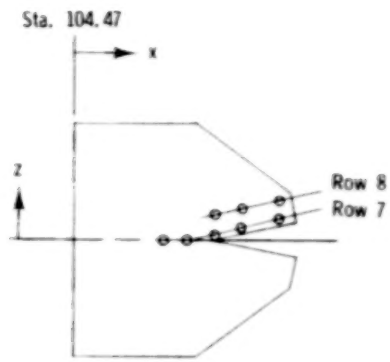

Configuration C8 sidewall

x/x_t	$z/h_t/2$													
	Configuration													
	C1, C4, C9			C2, C5, C11			C3, C6		C7		C8		C10	C12
	Row 3	Row 4	Row 5	Row 3	Row 4	Row 5	Row 3	Row 4	Row 3	Row 6	Row 7	Row 8	Row 3	Row 3
0.791	0.300	-	-	0.000	-	-	0.000	-	0.000	-	0.000	-	0.000	0.000
1.011	0.600	-	-	0.000	-	-	0.000	-	0.000	-	0.000	-	0.000	0.000
1.220	-	-	-	-	-	-	0.000	0.924	-	-	-	-	-	-
1.286	0.000	0.924	-	0.000	0.924	-	-	-	0.000	1.017	0.231	1.017	0.000	0.000
1.560	0.000	0.924	1.109	0.000	0.924	1.109	-	-	0.000	0.970	0.462	1.201	0.000	0.000
1.890	0.000	0.924	1.294	-	-	-	-	-	0.000	0.924	0.786	1.479	-	-
2.220	-	-	-	-	-	-	-	-	-	-	-	-	-	0.000
2.769	-	-	-	-	-	-	-	-	-	-	-	-	-	0.000

(b) Sidewall static-pressure instrumentation.

Figure 25.- Concluded.

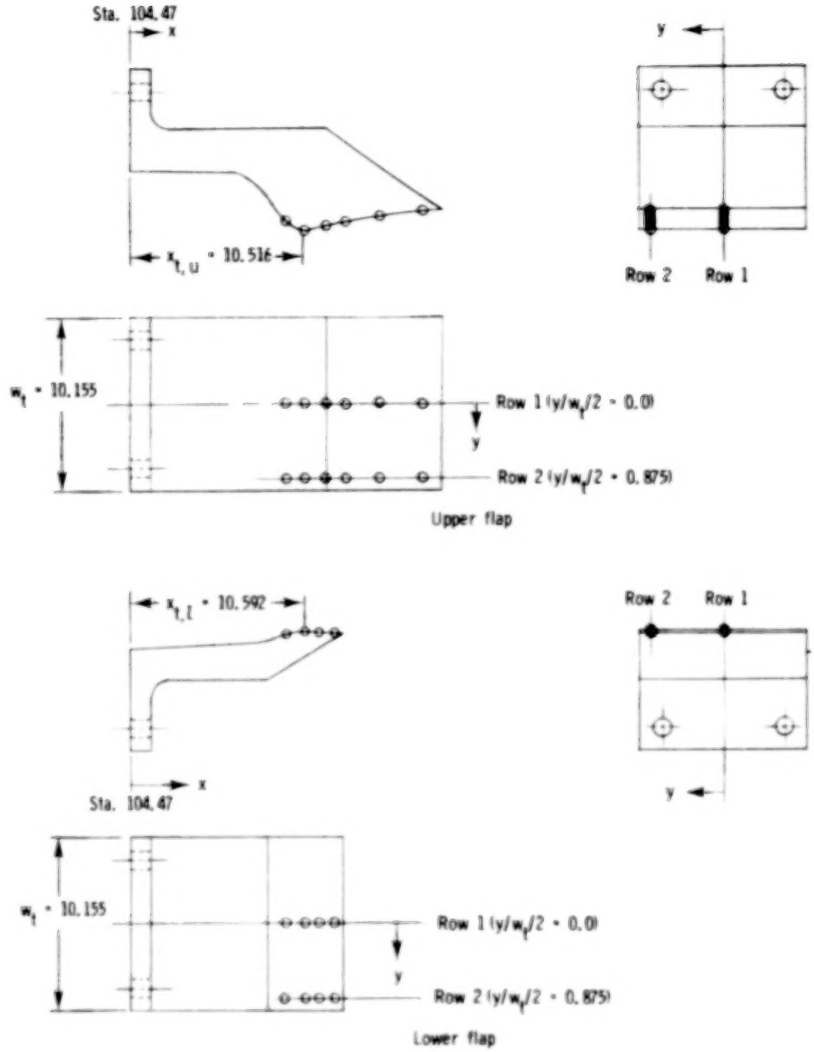

Upper flap		
Single-ramp expansion nozzle		
$x/x_{t,u}$	Row 1	Row 2
0.888	X	X
1.008	X	X
1.129	X	X
1.250	X	X
1.449	X	X
1.691	X	

Lower flap		
Single-ramp expansion nozzle		
$x/x_{t,l}$	Row 1	Row 2
0.881	X	X
1.001	X	X
1.079	X	X
1.168	X	X

(a) Flap static-pressure instrumentation.

Figure 26.- Sketches of single-ramp expansion nozzle components showing internal static-pressure orifice locations. All dimensions are in centimeters unless otherwise noted.

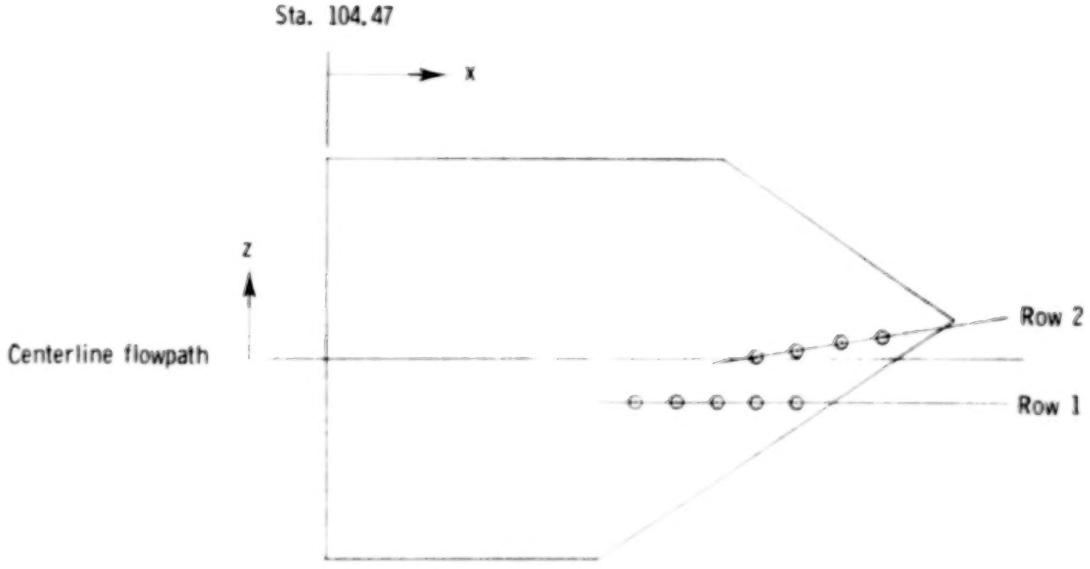

Typical single-ramp expansion nozzle sidewall

$x/x_{t,u}$	$z/h_t/2$									
	Configuration									
	SR1		SR2		SR3		SR4		SR5	
	Row 1	Row 2	Row 1	Row 2	Row 1	Row 2	Row 1	Row 2	Row 1	Row 2
0.888	-1.000	-	-1.000	-	-1.000	-	-1.000	-	-1.000	-
1.008	-1.000	-	-1.000	-	-1.000	-	-1.000	-	-1.000	-
1.129	-1.000	-	-1.000	-	-1.000	-	-1.000	-	-1.000	-
1.190	-	-	-	-	-1.000	0.000	-	-	-1.000	-0.050
1.250	-1.000	0.050	-1.000	0.050	-	-	-1.000	0.050	-	0.050
1.329	-	-	-1.000	-	-	-	-	-	-	-
1.371	-1.000	0.250	-	0.250	-	-	-1.000	0.250	-	0.250
1.510	-1.000	0.400	-	0.400	-	-	-	0.400	-	-
1.630	-	-	-	-	-	-	-	0.500	-	-
1.691	-1.000	0.500	-	-	-	-	-	-	-	-

(b) Sidewall static-pressure instrumentation.

Figure 26.- Concluded.

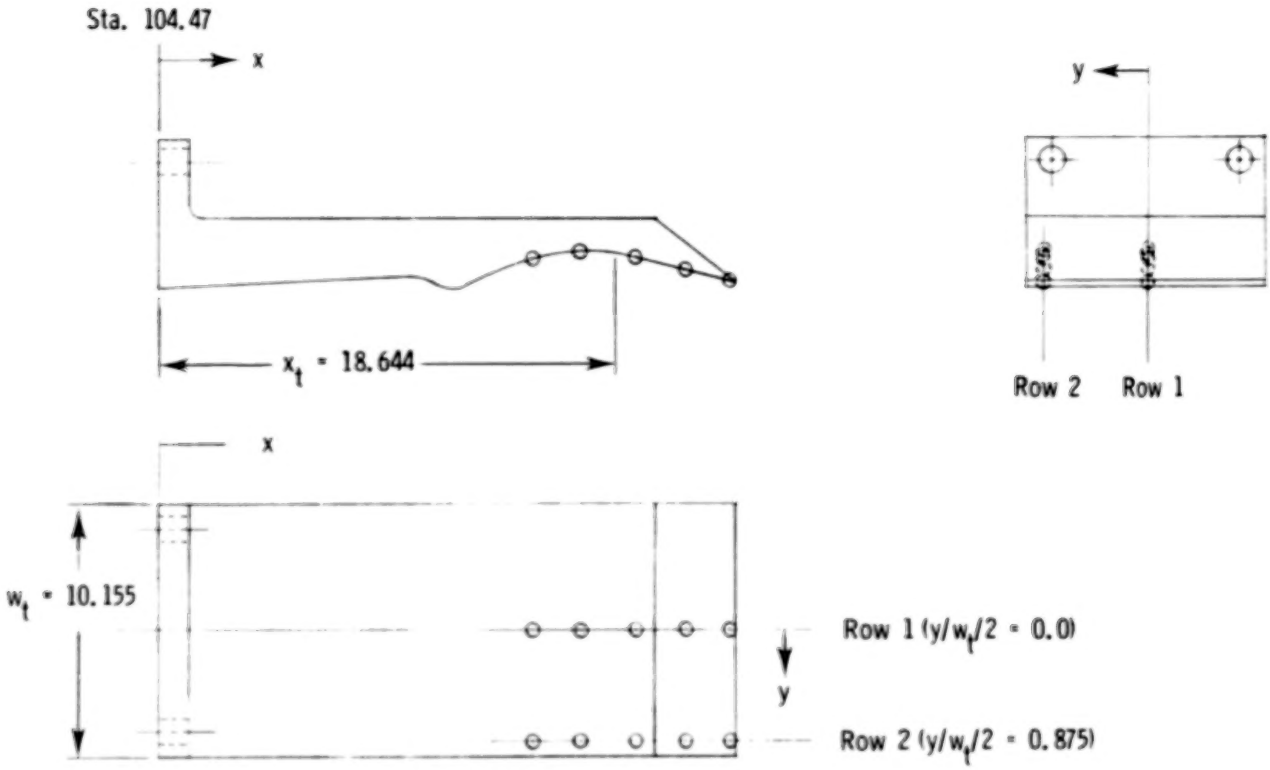

Typical wedge nozzle flap

x/x_t	Configuration			
	W1 and W2		W3 and W4	
	Row 1	Row 2	Row 1	Row 2
0.817			X	X
0.851	X	X		
0.920			X	X
0.954	X	X		
1.012	X	X		
1.044			X	X
1.056	X	X		
1.076	X	X		
1.158			X	X
1.260			X	X

(a) Unvectored flap static-pressure instrumentation.

Figure 27.- Sketches of wedge nozzle components showing internal static-pressure orifice locations. All dimensions are in centimeters unless otherwise noted.

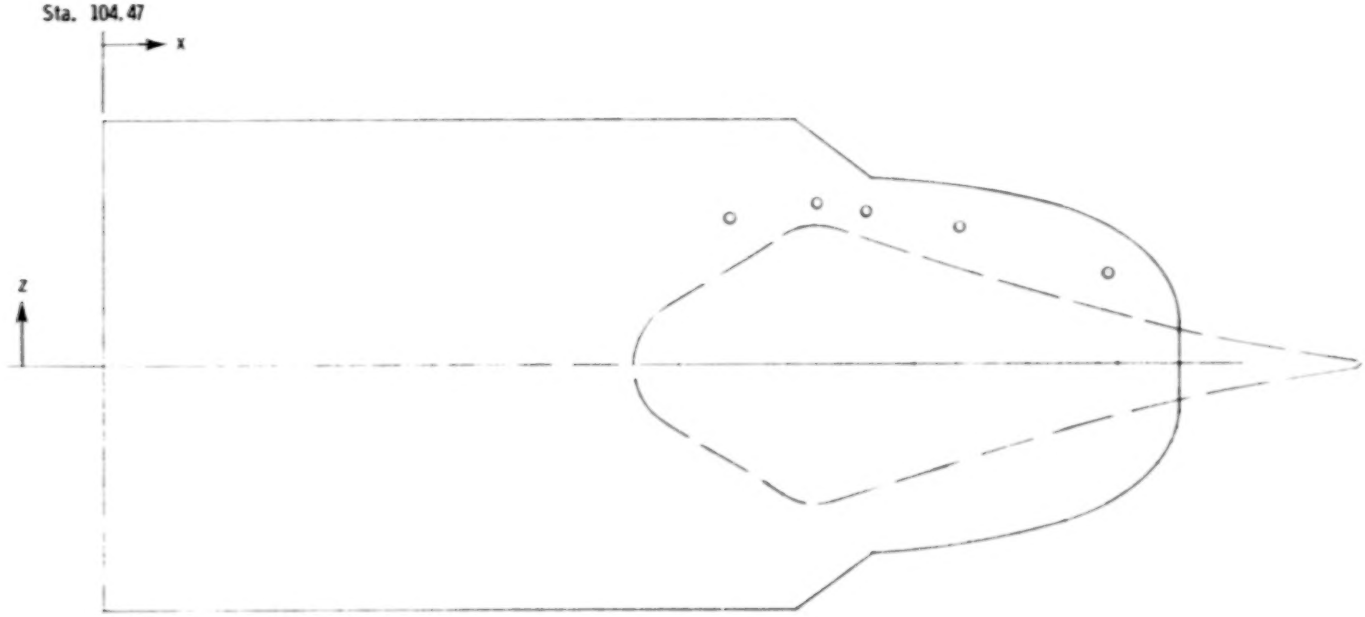

Typical wedge nozzle sidewall

x/x_t	$z/h_{w,max}/2$	
	Configuration	
	W1 and W3	W2 and W4
0.886	1.064	1.064
1.012	-	1.170
1.035	1.170	-
1.089	-	1.117
1.226	-	0.993
1.264	0.851	-
1.430	0.674	0.656
1.601	0.390	-

(b) Unvectored sidewall static-pressure instrumentation.

Figure 27.- Continued.

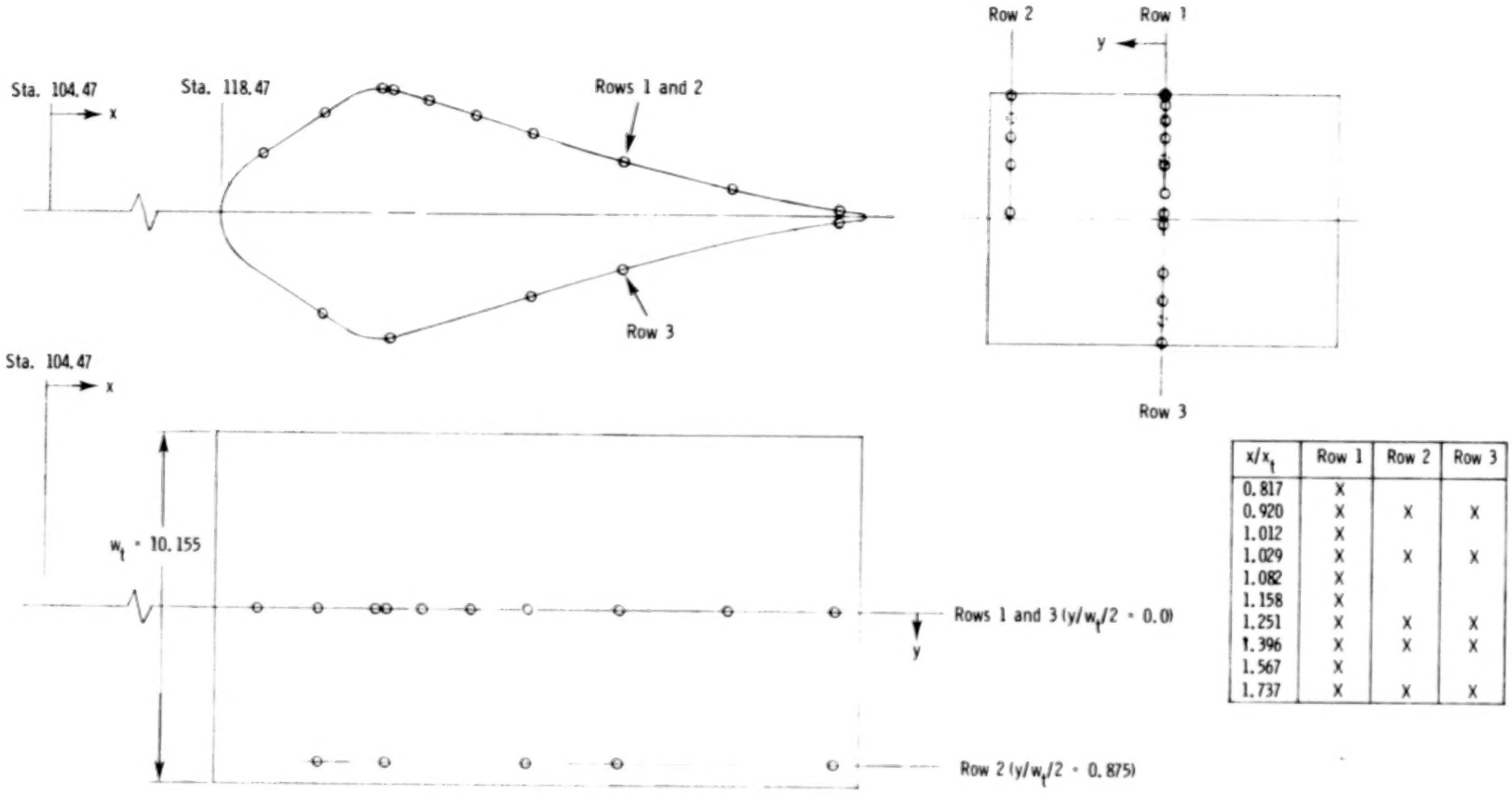

x/x_t	Row 1	Row 2	Row 3
0.817	X		
0.920	X	X	X
1.012	X		
1.029	X	X	X
1.082	X		
1.158	X		
1.251	X	X	X
1.396	X	X	X
1.567	X		
1.737	X	X	X

(c) Wedge static-pressure instrumentation. (Same wedge used for all configurations including W4(G20); pressures not measured with vector flap configurations.)

Figure 27.- Continued.

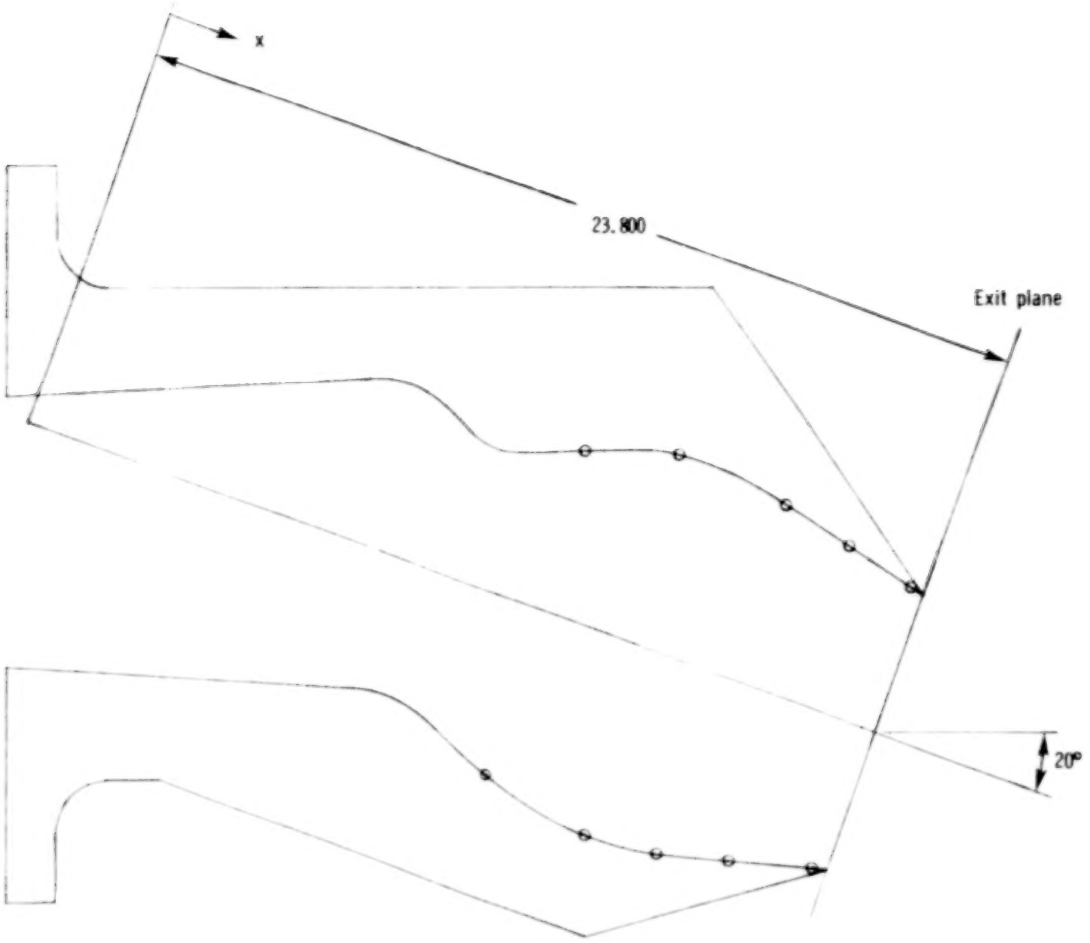

Upper flap: x/x_t = 0.749, 0.880, 1.045, 1.143, 1.245

Lower flap: x/x_t = 0.778, 0.936, 1.041, 1.140, 1.255

(d) Vectored flap static-pressure instrumentation.
All orifices on model centerline.

Figure 27.- Continued.

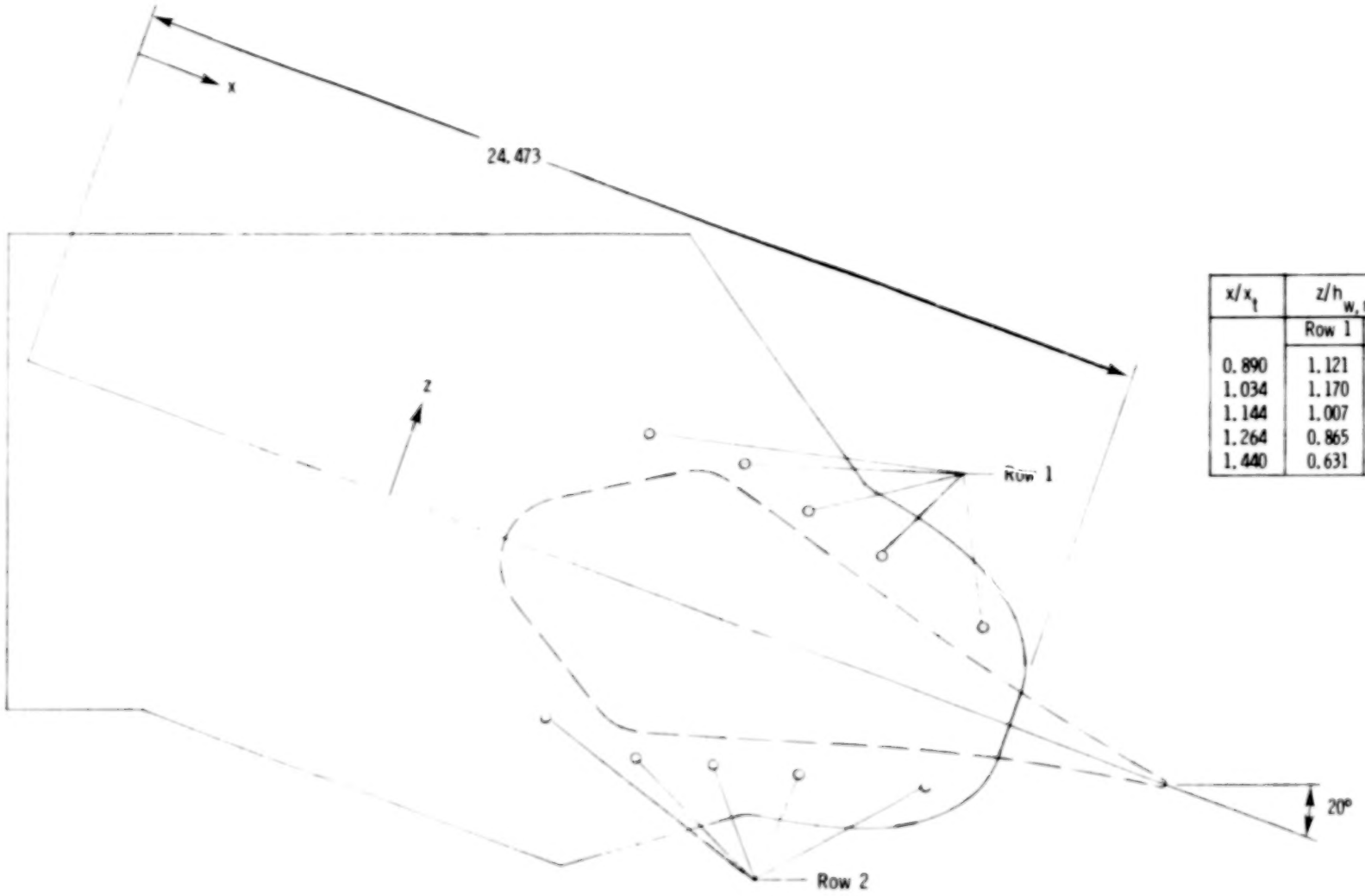

x/x_t	$z/h_{w,max}/2$	
	Row 1	Row 2
0.890	1.121	-1.121
1.034	1.170	-1.170
1.144	1.007	-1.007
1.264	0.865	-0.865
1.440	0.631	-0.631

(e) Vectored sidewall static-pressure instrumentation.

Figure 27.- Concluded.

1. Report No.	2. Government Accession No.	3. Recipient's Catalog No.
NASA TP-1468		

4. Title and Subtitle	5. Report Date
EFFECT OF SEVERAL GEOMETRIC PARAMETERS ON THE STATIC INTERNAL PERFORMANCE OF THREE NONAXISYMMETRIC NOZZLE CONCEPTS	July 1979
	6. Performing Organization Code
7. Author(s)	8. Performing Organization Report No.
Bobby L. Berrier and Richard J. Re	L-12810
	10. Work Unit No.
9. Performing Organization Name and Address	505-04-13-02
NASA Langley Research Center Hampton, VA 23665	11. Contract or Grant No.
	13. Type of Report and Period Covered
12. Sponsoring Agency Name and Address	Technical Paper
National Aeronautics and Space Administration Washington, DC 20546	14. Sponsoring Agency Code

15. Supplementary Notes

16. Abstract

An investigation has been conducted at static conditions in the static-test facility of the Langley 16-foot transonic tunnel. The effects of several geometric parameters on the internal performance of nonaxisymmetric convergent-divergent, single-ramp expansion, and wedge nozzles were investigated at nozzle pressure ratios up to approximately 10. In addition, two different thrust-vectoring schemes were investigated with the wedge nozzle.

The results of this investigation indicate that as with conventional round nozzles, peak nonaxisymmetric-nozzle internal performance occurs near the nozzle pressure ratio required for fully expanded exhaust flow. Nozzle sidewall length or area generally had little effect on the internal performance of the nozzles investigated.

17. Key Words (Suggested by Author(s))	18. Distribution Statement
Nonaxisymmetric nozzles Internal performance Static performance Gimbal vectoring	Unclassified - Unlimited Subject Category 02

19. Security Classif. (of this report)	20. Security Classif. (of this page)	21. No. of Pages	22. Price*
Unclassified	Unclassified	134	$7.25

* For sale by the National Technical Information Service, Springfield, Virginia 22161

NASA-Langley, 1979
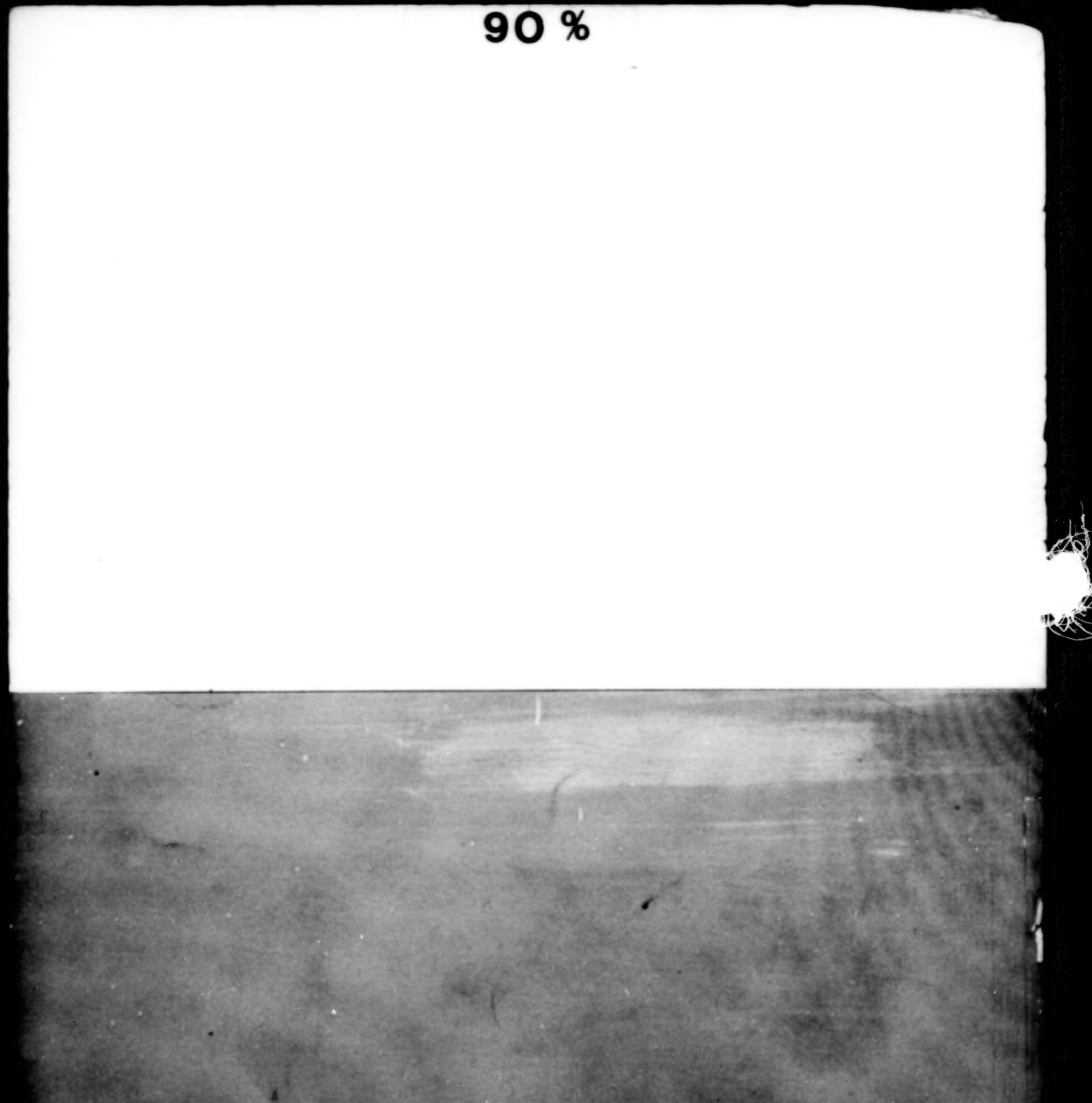
90 %